


For Reference

NOT TO BE TAKEN FROM THIS ROOM

Ex LIBRIS
UNIVERSITATIS
ALBERTAENSIS





Digitized by the Internet Archive
in 2022 with funding from
University of Alberta Library

<https://archive.org/details/Kollias1984>

THE UNIVERSITY OF ALBERTA

THREE DIMENSIONAL ANALYSIS OF HAMMER THROWING

by

C

IRAKLIS KOLLIAS

A THESIS

SUBMITTED TO THE FACULTY OF GRADUATE STUDIES AND RESEARCH
IN PARTIAL FULFILMENT OF THE REQUIREMENTS FOR THE DEGREE
OF DOCTOR OF PHILOSOPHY

DEPARTMENT OF PHYSICAL EDUCATION AND SPORT STUDIES

EDMONTON, ALBERTA

FALL 1984

DEDICATION

I T W A R A

στον πατέρα μου και στα αδελφια μου

to Isabelle

I T H A K A

When you set out for Ithaka
pray that your road's a long one,
full of adventure, full of discovery.
Laistrigonians, Cyclops, angry Poseidon
don't be scared of them:
you won't find things like that on your way
as long as your thoughts are exalted,
as long as a rare excitement
stirs your spirit and your body.
Laistrigonians, Cyclops, wild Poseidon
you won't encounter them
unless you bring them along inside you,
unless your soul raises them up in front of you.

Pray that your road's a long one.
May there be many a summer morning when
full of gratitude, full of joy
you come into harbors seen for the first time;
may you stop at Phoenician trading centers
and buy fine things,
mother of pearl and coral, amber and ebony,
sensual perfumes of every kind,
as many sensual perfumes as you can;
may you visit numerous Egyptian cities
to fill yourself with learning from the wise.

Keep Ithaka always in mind.
Arriving there is what you're destined for.
But don't hurry the journey at all.
Better if it goes on for years
so you're old by the time you reach the island,
wealthy with all you've gained on the way,
not expecting Ithaka to make you rich.
Ithaka gave you the marvelous journey.
Without her you wouldn't have set out.
She hasn't anything else to give.

And if you find her poor, Ithaka won't have fooled you.
Wise as you'll have become, and so experienced,
you'll have understood by then what an Ithaka means.

Kostas Kavafys

ABSTRACT

The purpose of this study was to develop techniques for analysis of the hammer throwing and to analyse the throwing technique of world caliber hammer throwers. The development of the techniques included testing of different versions of the DLT 3-D cinematographic method and the derivation of formulas, based on rigid body dynamics, for analysis of the kinematic and kinetic parameters involved in rotation of the human body.

The DLT was tested with and without mathematical models for image refinement and with calibration trees of different shape. A tree which was geometric in shape used with the basic DLT equations and with model IV for image refinement (Karara and Abdel Aziz, 1974) gave the best results of all the tests. The RMS error of the measured versus the simulated coordinates of the control point were found to be 0.24 cm. for the X-axis, 0.19 cm for the Y-axis and, 0.26 cm for the Z-axis. The method was also tested for areas outside the calibration tree. It was found that a well constructed tree with image refinement models can be used for calibrating areas of larger volume than the one covered by the calibration tree.

The hammer throwing data were collected during the 1982 European Championship, with the best throw of the three medalists being analysed. Lagrangian interpolation formulas were used for the time-match of the coordinates derived from the two films. The data were smoothed with digital filters.

It was found that the maximum velocity of the hammer occurred before the release point. None of the athletes achieved an optimal angle of release, while the closer to the optimal angle achieved by the winner could give him the gold medal with the same difference in throwing distance. The acceleration of the hammer was maximum in the last double support phase of the throw. It was the duration of the acceleration in this phase that was critical for a successful throw. Another parameter that characterised the analyzed athletes was their ability to increase the acceleration of the hammer during the single support phase of each turn or at least not to decrease it a great deal. This was accomplished by decreasing the moment of inertia of the body about the vertical axis. All athletes achieved faster single support phases than double support phases in all the turns. The latter was achieved by leaning backwards during the first half of the double support phase and by using the second half of this phase to initiate a fast rotation. The breaking of the horizontal movement in the last turn was critical for a successful throw. A relatively low center of mass of the body seemed to be appropriate for controlling the movement in all the turns. A tall and/or heavy athlete does not necessarily have advantages against a shorter and lighter athlete. The length of the hammer should be shortened in order for athletes to perform mechanically better throws.

ACKNOWLEDGEMENTS

The author wishes to express his acknowledgements to:

Dr. W. Bedingfield, his supervisor, for her patience, encouragment and assistance throughout the course of this study.

His committee members: Dr. R. Wilberg; Dr. J. Haddow; Dr. J. Kramer; Professor A. Grimer and Professor G. Simonyi for their assistance and suggestions.

All the people who positively interfered in the course of this study.

The Greek General Secretary of Sports for financial support.

A very special "Thank You" goes to Isabelle for all the understanding, patience, tolerance, support, help and consideration during the difficult times.

Table of Contents

Chapter	Page
I. INTRODUCTION	1
A. Purpose of the study	10
B. Limitations	10
C. Delimitations	11
D. Definition of terms	11
II. REVIEW OF RELATED LITERATURE.	14
A. Three-Dimensional Cinematographic Techniques. ..	14
Single Camera Technique.	14
Mirror Technique.	15
Stereometric Technique.	15
Multiple Cameras Technique.	16
B. Smoothing Techniques.	21
C. Hammer Throwing.	23
III. METHODS AND PROCEDURES	26
A. DLT Method	26
Validation of DLT Method	28
B. Hammer Throwing Analysis	33
Subjects	33
Data Collection	34
Data Reduction.	35
Analysis of Data.	40
IV. RESULTS AND DISCUSSION	53
A. Results of the DLT Tests.	53
B. Error Analysis	57
C. Kinematics and Kinetics of the Hammer.	59

D. Kinematics and Kinetics of the Body.	101
E. Kinematics and Kinetics of the System	129
F. Discussion of Hammer Throwing	163
V. SUMMARY AND CONCLUSIONS	169
Recommendations	175
BIBLIOGRAPHY	177
APPENDIX A	183
Description of the DLT Technique.	184
Solution of the Linear System	191
Image Refinement	192
Solution of the Non-Linear System	197
Simulation of the Spatial Coordinates	200
DLT Programs	202
APPENDIX B	230
Moments and Products of Inertia with respect to CMS	231
Moments and Products of Inertia of segments about their CM	232
Calculation of Direction Cosines of the Principal Axes	233
Angular Momentum of the System	237
Angular Velocity of the Segmental Principal Axes	239
Instantaneous Angular Velocity of the System	242
APPENDIX C	244
Radius of Curvature.	245
Center of Curvature.	248
APPENDIX D	251

C.P. Coordinates and Calibration	
Coefficients	251

LIST OF TABLES

Table	Page
1. World Record of the Hammer and Discus Throwing for 1950 to 1980.....	9
2. Mass, Height and Throwing Distance of the Analyzed Athletes.....	34
3. Anthropometric Data of the Segments.....	41
4. Principal Moments of Inertia of the Segments.....	45
5. RMS Differences of CP for the Second Tree.....	53
6. RMS Differences of CP for the Data Collection Tree.....	54
7. Simulated Coordinates and Distance of the Cameras from Origin with Different Models.....	55
8. Absolute Differences of two Digitizings for the Right Hip and the Hammer.....	58
9. Timing of Each Reference Instance.....	64
10. Contribution of Each Turn to the Maximum Velocity and Acceleration of the Hammer.....	73
11. Impulse Applied upon the Hammer in Each Phase.....	87

LIST OF FIGURES

Figure		Page
1.	Dimensions of the Hammer.....	5
2.	Hammer Throwing Circle.....	7
3.	Data Collection Calibration Tree.....	32
4.	Location of the Cameras.....	34
5.	Power Spectra of the Hammer (X-Axis), Subject 1.....	60
6.	Power Spectra of the Right Hip (X-Axis), Subject 1....	61
7.	Acceleration of the Hammer with Raw and Filtered Data, Subject 1.....	62
8.	Trajectory of the Hammer in the X-Y Plane, Subject 3.....	65
9.	Trajectory of the Hammer in the X-Z Plane, Subject 3.....	66
10.	Trajectory of the Hammer in the Y-Z Plane, Subject 3.....	67
11.	Radius of Curvature of the Hammer, Subject 1.....	68
12.	Radius of Curvature of the Hammer, Subject 2.....	69
13.	Radius of Curvature of the Hammer, Subject 3.....	70
14.	Angle of Radius of Curvature with Cable of the Hammer, Subject 1.....	72
15.	Linear Velocity of the Hammer, Subject 1.....	74
16.	Linear Velocity of the Hammer, Subject 2.....	75
17.	Linear Velocity of the Hammer, Subject 3.....	76
18.	Linear Acceleration of the Hammer, Subject 1.....	78
19.	Linear Acceleration of the Hammer, Subject 2.....	79
20.	Linear Acceleration of the Hammer, Subject 3.....	80
21.	Acceleration of the Hammer in the X, Y, Z Axes, Subject 1.....	82
22.	Tension in the Cable of the Hammer, Subject 1.....	84
23.	Tension in the Cable of the Hammer, Subject 2.....	85

24. Tension in the Cable of the Hammer, Subject 3.....	86
25. Moments of Inertia of the Hammer, Subject 1.....	88
26. Moments of Inertia of the Hammer, Subject 2.....	89
27. Moments of Inertia of the Hammer, Subject 3.....	90
28. Hammer - CMs Distance, Subject 1.....	91
29. Hammer - CMs Distance, Subject 2.....	92
30. Hammer - CMs Distance, Subject 3.....	93
31. Angular Momentum of the Hammer, Subject 1.....	95
32. Angular Momentum of the Hammer, Subject 2.....	96
33. Angular Momentum of the Hammer, Subject 3.....	97
34. Direction Angles of the Angular Momentum Vector of the Hammer, Subject 1.....	98
35. Direction Angles of the Angular Momentum Vector of the Hammer, Subject 2.....	99
36. Direction Angles of the Angular Momentum Vector of the Hammer, Subject 3.....	100
37. Trajectory of the CMb, in the X-Y Plane, Subject 1...	102
38. Trajectory of the CMb, in the X-Z Plane, Subject 1...	103
39. Trajectory of the CMb, in the Y-Z Plane, Subject 1...	104
40. Trajectory of the CMb, in the Y-Z Plane, Subject 2...	104
41. Radius of Curvature of the CMb, Subject 1.....	105
42. Radius of Curvature of the CMb, Subject 2.....	106
43. Radius of Curvature of the CMb, Subject 3.....	107
44. Linear Velocity of the CMb, Subject 1.....	109
45. Linear Velocity of the CMb, Subject 2.....	110
46. Velocity of the CMb in the X, Y, Z Axes, Subject 1...	111
47. Acceleration of the CMb in the X, Y, Z Axes, Subject 1.....	112
48. Acceleration of the CMb in the Z axis, Subject 1.....	114

49. Acceleration of the CMb in the Z axis, Subject 2.....	115
50. Acceleration of the CMb in the Z axis, Subject 3.....	116
51. Moments of Inertia of the Body about the CMs, Subject 3.....	117
52. Angular Momentum of the Body about the CMs, Subject 1.....	118
53. Angular Momentum of the Body about the CMs, Subject 2.....	119
54. Angular Momentum of the Body about the CMs, Subject 3.....	120
55. Direction Angles of the Angular Momentum Vector of the Body, Subject 1.....	122
56. Left Knee Angle, Subject 1.....	123
57. Left Knee Angle, Subject 2.....	124
58. Left Knee Angle, Subject 3.....	125
59. Hips - Shoulders Angle, Subject 1.....	127
60. Angles of Trunk with X, Y, Z Axes, Subject 1.....	128
61. Coordinates of the CMs, Subject 1.....	130
62. CMs Trajectory in the X-Y Plane, Subject 3.....	131
63. CMs Trajectory in the X-Z Plane, Subject 3.....	132
64. CMs Trajectory in the Y-Z Plane, Subject 3.....	133
65. Radius of Curvature of the CMs, Subject 1.....	134
66. Radius of Curvature of the CMs, Subject 2.....	135
67. Radius of Curvature of the CMs, Subject 3.....	136
68. Linear Velocity of the CMs, Subject 1.....	137
69. Linear Velocity of the CMs, Subject 2.....	138
70. Linear Velocity of the CMs, Subject 3.....	139
71. Velocity of the CMs in the X, Y, Z Axes, Subject 1.....	141
72. Velocity of the CMs in the X, Y, Z Axes, Subject 2.....	142

73. Velocity of the CMs in the X, Y, Z Axes, Subject 3.....	143
74. Acceleration of the CMs in the X, Y, Z Axes, Subject 1.....	144
75. Acceleration of the CMs in the X, Y, Z Axes, Subject 2.....	145
76. Acceleration of the CMs in the X, Y, Z Axes, Subject 3.....	146
77. Moments of Inertia of the system about its center of mass, Subject 1.....	147
78. Instantaneous Angular Velocity of the System, Subject 1.....	149
79. Instantaneous Angular Velocity of the System, Subject 2.....	150
80. Instantaneous Angular Velocity of the System, Subject 3.....	151
81. Angular Momentum of the System in the X, Y, Z Axes, Subject 1.....	152
82. Angular Momentum of the System in the X, Y, Z Axes, Subject 2.....	153
83. Angular Momentum of the System in the X, Y, Z Axes, Subject 3.....	154
84. External Torques of the System, Subject 1.....	155
85. Direction Angles of the Angular Momentum Vector of the System, Subject 1.....	157
86. Direction Angles of the Angular Momentum Vector of the System, Subject 2.....	158
87. Direction Angles of the Angular Momentum Vector of the System, Subject 3.....	159
88. Trajectories of the Angular Momentum Vector in the X-Y Plane.....	160
89. Total Kinetic Energy of the System, Subject 1.....	161
90. Kinetic Energy of Translation of the System, Subject 1.....	162

I. INTRODUCTION

Biomechanics of sport is a discipline which studies the mechanics of human motion under the special condition of sports. Its content can be grouped into four major areas.

1. Determination of the characteristics of an outstanding performer.
2. Detection of differences between performers.
3. Investigation of new techniques of performance.
4. Validation and supply of data for mathematical models of performance.

Biomechanists derive information about human motion mainly by means of: (a) Direct force measurements; (b) Electromyography; (c) Electrogoniometry; and (d) Cinematography. Direct attachments to the subject are required with methods (a), (b) and (c), while in (d) a camera can be placed a considerable distance from the subject ensuring no physical interference.

Cinematography has been a most useful tool for researchers in biomechanics and a most acceptable tool for subjects when data has to be collected in real life situations.

Most of human motion occurs in three-dimensional space rather than in a plane. However, film as a plane does not provide the analyst with information about the third dimension. Investigators in biomechanics have sought methods

of deriving three-dimensional coordinates of the body in motion by using films. In 1930, Bernstein introduced the use of a mirror in order to obtain a second image of the motion by using one camera. Since that time a variety of three-dimensional methods have been introduced. Within the last decade several investigators have drawn upon techniques from other disciplines in their attempts to resolve the problem.

Photogrammetry is a discipline in which the use of highly sophisticated metric cameras enable measurements based on the photogrammetric concept that the film, being a perfect plane, is a central projection of the object space. Assuming that the internal characteristics of the cameras are well known and by using a comparator and observations from different points, one can achieve spatial coordinates of a point in the object space. This is a normal photogrammetric procedure since the characteristics of the metric cameras are well known.

In 1971, the photogrammetrists Abdel-Aziz and Karara presented a technique called "*Direct Linear Transformation (DLT)*" with which one can achieve photogrammetric measurements by using non-metric cameras. This is a two-pass regression technique; a set of control points (calibration tree) in the object space is used to calculate the external and internal characteristics of the cameras. The calculated coefficients are used together with digitized coordinates of the points of interest to achieve the spatial coordinates of

the points.

Shapiro (1978), Walton (1981) and Miller et al (1980) tested the technique for biomechanical research and found the resulting measurements to be highly satisfactory. The calibration of the cameras in these studies was achieved by using a three dimensional calibration tree. In 1980, Woltring presented a technique in which calibration could be achieved by filming a plane grid with control points. The grid was rotated to different positions and filmed. These different positions of the grid offered a 3-D calibration tree. This method has the advantage of ease of construction, but it is difficult to have a large grid in rotation without deformation.

The relationship between the volume of the calibration tree and of the calibrated area has been of main concern among the researchers involved with DLT. To resolve this problem Dapena et al, (1981) presented a version of the DLT with which one can use a control object of unknown shape to calibrate large areas. Weak points of this technique included complexity in the calibration process, and failure to account for refinement of the image caused by lens distortion and film deformations. It is generally accepted that data collected with non-metric cameras encompasses errors caused by these factors (Shapiro 1978, Walton 1981 and Karara and Abdel-Aziz 1974). In 1974, Karara and Abdel-Aziz presented six mathematical models which when used together with the basic DLT model account for image

refinement. These models have not been utilized in previous biomechanics research.

Assuming that the body is a mechanical link system and if the coordinates of points of interest of the body can be accurately determined in 3-D space, one can use classical mechanics methods to investigate human motion.

Hammer throwing originally appeared as a hunting method, later as means of waging war as a weapon and finally, in todays "civilized world", as an Olympic event.

Despite its change in purpose, the movement pattern has remained basically the same. A heavy object mounted at the end of a stick, or a belt, or a string, is released after a few rotations in order to kill a dinosaur, to wound a Goliath, or to break the world record. According to Howard Payne,

"Hammer throwing as we know it today, has had a short history if we date it from 1887 when the Americans drew up rules setting the circle diameter at 7 feet., the hammer length at 4 ft. and the weight of the ball, chain and handle of the implement at 16 lb. However, if we include sledge hammers, shafted implements and wheel hubs, then we can go way back to trace the origins -some historians think to 2000 B.C. when at the Tailteann Games in Ireland the "Roth Cleas" or "wheel feat" was contested, ...",
(Payne 1969:9)

The specifications of today's Olympic event, according to Rules and By-Laws of the Canadian Track and Field Association, are presented below.

The hammer is composed of a sphere (the head) and a grip connected by a steel wire, as in Figure 1. The minimum weight of the hammer is 7.257 kg. and the complete length

must be between 117.5 and 121.5 cm. A glove can be worn by the athlete to protect his fingers while throwing.

The Head, must be spherical with a diameter between 102mm. and 130mm. It should be made from solid iron, or brass, or any metal not softer than brass, or a shell of such metal filled with lead or other solid materials. If a filling is used it must be inserted in such a manner that it is immovable and the distance of the centre of gravity from the centre of the sphere is less than 6mm.

The Grip must be triangular and may be either of single or double loop construction, but must be rigid and without hinging of any kind and so made that it cannot stretch appreciably while being thrown.

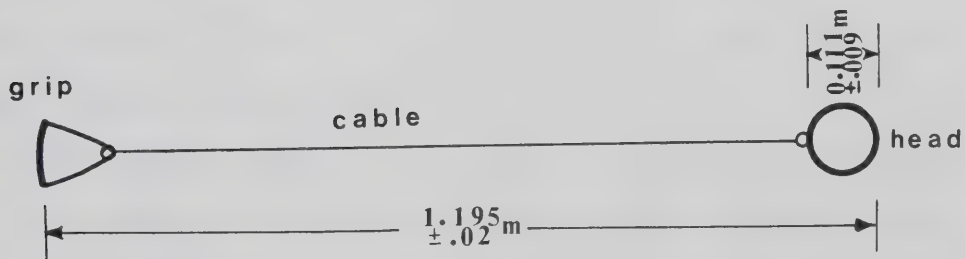


Figure 1: Dimensions of the Hammer

The Connection Wire must be a single unbroken and straight length of spring steel wire with a diameter no less

than 3mm. It may be looped at one or both ends as a means of attachment. The connections of the wire with the grip and the head shall be such that they do not increase the length of the hammer while it is being thrown.

The throwing circle must be made from concrete and have a slightly rough surface. The diameter of the circle must be 2.134 meters, and the throwing arc 40°. For protection purposes, a cage with certain specifications is required. Figure 2 is a schematic representation of the throwing circle and the protection cage.

The following is a description of a right-handed throwing technique. The athlete stands at the back of the circle with his feet almost parallel and facing the opposite direction of the throw. The gloved left hand is placed in the handle so that the grip rests along the middle phalanges of the fingers. The right hand is placed under the left. The athlete swings the hammer a few times around his head while his feet remain almost stationary. At the end of the last swing the thrower initiates a whole body turning action with his feet, rotating with his weight over his left foot. The gradually accelerated rotation carries him to the front of the circle after three or four turns and he uses the last turn to give the hammer a final large release velocity. The plane of the orbit of the hammer throughout is inclined at an angle so that an optimal angle of release can be achieved.

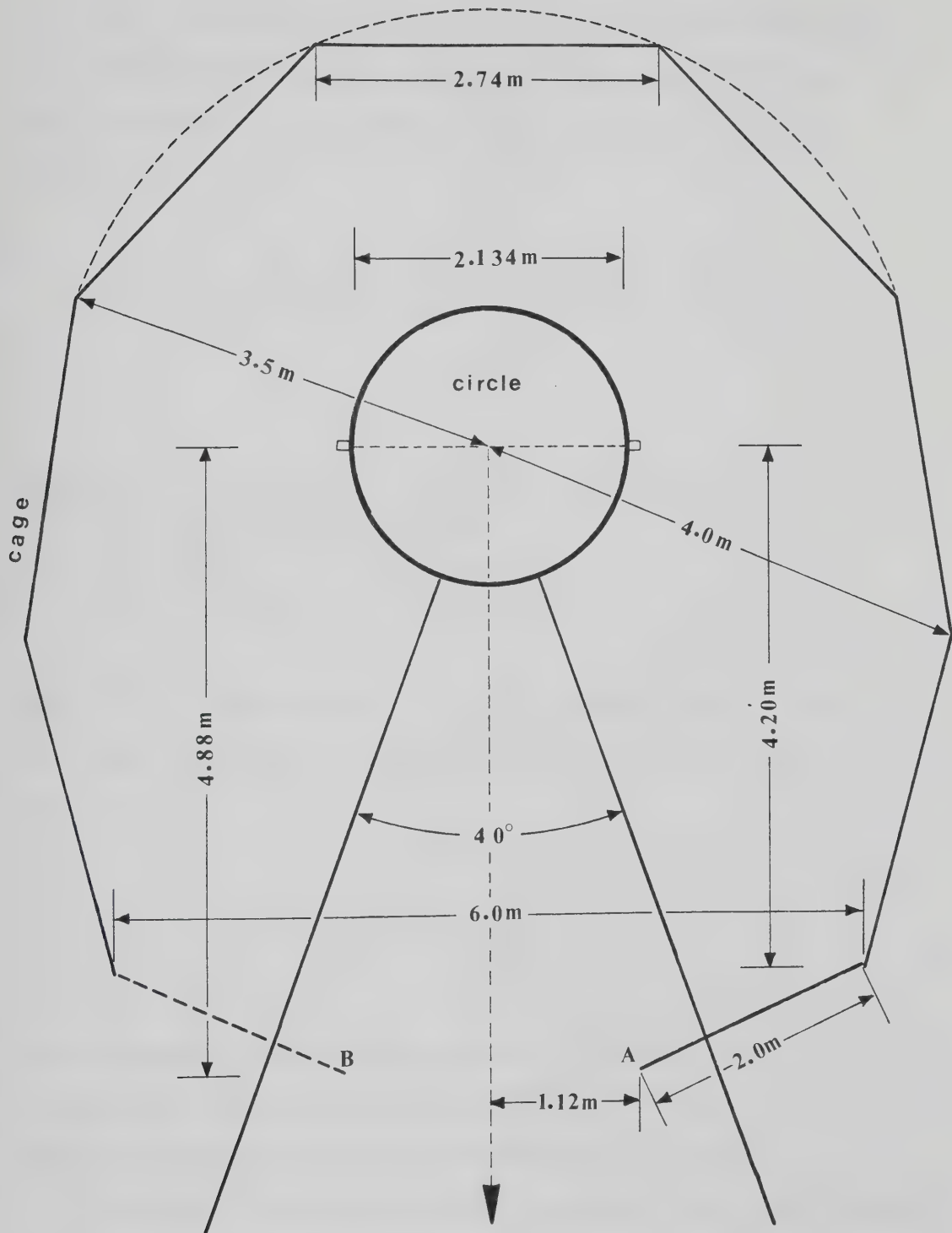


Figure 2: Hammer Throwing Circle

The hammer is a projectile and assuming negligible aerodynamic factors or Coriolis forces during flight, the final distance of a throw is given by the following equation.

$$L = \frac{U^2 \sin 2\theta + 2U \cos \theta (U^2 \sin^2 \theta + 2gh)^{1/2}}{2g} \quad (1)$$

where: L = Horizontal distance of the throw.
 U = Velocity of release.
 θ = Angle of release.
 h = Height of release.
 g = Acceleration due to gravity.

Also, by differentiating (1) with respect to θ , with constant velocity and height of release the distance L will be maximum if:

$$\sin^2 \theta = \frac{U^2}{2(U^2 + gh)} \quad (2)$$

Thus, assuming an optimal angle of release it is reasonable to consider the velocity of release as the most important factor affecting the final distance of a throw.

The world record for hammer throwing has shown greater improvement than the records for any other field event. This is mainly a result of continued improvement in technique. The world records in this event and in the discus throwing event for the last four decades are shown in Table 1.

TABLE 1WORLD RECORD OF HAMMER AND DISCUS THROWING
FOR 1950 TO 1980

<u>Year</u>	<u>Hammer</u>	<u>Discus</u>
1950	59.80m.	57.93m.
1960	70.33m.	60.46m.
1970	75.84m.	68.40m.
1980	81.80m.	71.12m.

Although the technique has been continuously evolving, there is limited literature available concerning the event. Publications which are available are almost entirely qualitative in nature. The lack of quantitative analysis may be a result of one or both of the following.

1. The lack of interest in the event by non-Europeans. In the last two decades, the event has been dominated by athletes from the U.S.S.R. The three medals in this event in the last three Olympic Games have been collected by athletes of that country.
2. Hammer throwing, a complex event, is basically a rotational movement, therefore, the value of a two-dimensional film analysis is questionable. The physical space required for this event increases its complexity. It is obvious that a controlled laboratory environment is not the best place for throwing the hammer.

The underlying responsibility of the sports biomechanist is to provide the coach and the athlete with

useful information about kinematic and kinetic parameters of the skill. The lack of such information about hammer throwing performance inspired this study.

A. Purpose of the study

The purpose of this study was to develop a method for analysis of hammer throwing and to analyze the technique of world caliber hammer throwers as it is performed in a competition. In order to develop the method for analysis, different versions of the DLT 3-D cinematographic method were tested. These tests included the basic DLT method with different mathematical models for image refinement, as well as different calibration trees for the derivation of the calibration coefficients. Rigid body dynamics were used for the derivation of the formulas to investigate the parameters for analysis. Temporal, kinematic, and kinetic parameters of (a) the hammer, (b) the athlete, and (c) the system, athlete plus hammer, were analysed.

A comparison between between the different subjects was made based on the analysed parameters.

B. Limitations

The conduct of the study was limited by the ability of the researcher to determine the location of selected body and object points, and also by the number of subjects.

C. Delimitations

The study was delimited to the three medalists of the 1982 European Championship, to a filming frame rate of 100 frames per second, to the motion of the hammer and the system after the preliminary swings.

D. Definition of terms

Calibration of an image is the process of determining a number of unique coefficients which when substituted into an equation or a set of equations define the object to image transformation.

Calibration coefficients are the unique numbers which when substituted into equations define the object to image transformation.

Calibration tree is a structure which provides a set of points (control points) with well known spatial coordinates and they are used for the calculation of the calibration coefficients.

Central projection is a mapping of points in which each point, its projection and the projection center are collinear.

Comparator is a precise optical instrument with viewing optics for obtaining coordinate pairs from a secondary image.

Digital filter is a set of algorithms which form an analytical tool for removing or isolating certain frequency components from a digital signal.

Digitizer coordinates are a pair of coordinates which describe the location of a point with respect to digitizer reference frame.

Digitizing board is a precise instrument which is used to obtain coordinate pairs of points from a film.

Direction cosines are a set of numbers which define the orientation of a vector in an orthogonal system of axes.

Direct Linear Transformation (DLT) is a two-pass linear

regression technique with which three dimensional coordinates of a point in space can be achieved by using films from different observations.

Double support is the phase of the throw when the athlete has both feet on ground.

Film deformation is the image deformation caused by changes in the geometry of the film. For example the lack of a perfect plane when the film is in the camera or projector.

Focal center is the point of the lens through which all the optical rays appear to pass.

Instantaneous Center of curvature is the center of the instantaneous circle described by the orbit of a point which traces a rotational motion.

Interpolation is a numerical method in which a function is evaluated at some point within a specified interval of the independent variable based on neighboring values of the dependent variable.

Least square technique is a numerical method in which the parameters of a mathematical model are determined by minimizing the sum of the square differences between the observed and modeled values of the dependent variable.

Lens distortion is the geometric distortion of an image caused by the imperfection of the lens.

Metric camera is a precision camera for recording photographic images in photogrammetry. Some of the characteristics of this camera are: A fixed focus; Symmetric lens with minimal optical distortion; The ability to hold the film flat; A diaphragm shutter located within the lens; A precisely calibrated inner chamber for which the parameters of interior orientation are known.

Newton's iterative method is a numerical analysis method to find the roots of an overdetermined system of non-linear equations.

Newton's method is a numerical analysis method for determining the roots of an equation.

Non-metric camera is a camera which does not meet the requirements of a metric camera.(see metric camera).

Overdetermined system of equations is a system of equations in which the number of equations exceeds the number

of unknowns.

Photogrammetry is science of obtaining measurements from films.

Precessional motion is the motion of a spinning top where, as the top rotates about its axis of rotation, the axis of rotation rotates about another axis (vertical). *Nutation* is the special case of precession when the angle of precession does not remain constant.

Radii of curvature is the distance from the point which traces a rotational motion to the instantaneous center of curvature.

Random error is an error which is created by the inconsistencies of the measurement process.

Single support is the phase of the turn in which the athlete has only one foot on the ground.

Spatial coordinates are a pair or triplet of numbers which define the location of a point with respect to a reference frame.

Systematic error is an error which is consistent in the data and caused from the malfunction of an instrument or a mathematical model.

II. REVIEW OF RELATED LITERATURE.

The review of literature related to this work is presented in the following sequence:

- 2.1 Three-dimensional cinematographic techniques.
- 2.2 Smoothing techniques.
- 2.3 Hammer throwing.

A. Three-Dimensional Cinematographic Techniques.

The techniques found in the literature can be divided into four basic groups:

1. Single camera technique.
2. Mirror technique.
3. Stereometric technique.
4. Multi-camera techniques.

Single Camera Technique.

Plagenhoef (1968) presented a method that utilized the real length of body-segments, the camera-to-plane of motion distance and the length of the segments as they appeared in the film in order to calculate the spatial coordinates of points by using trigonometric functions. The same technique has been used by Riley et al (1978). In their study, a simulated computer graphics method was used to determine the third coordinate. The techniques described above give a rough estimation of the third coordinate. In analysis of

single segment movements, the results can be reasonable, but the lack of accuracy is obvious in more complicated analyses.

Mirror Technique.

This sophisticated technique was introduced by the Russian physiologist Bernstein (1930). A plane mirror is placed in such a way that the object space plus its image in the mirror are recorded on the film. With this technique, a researcher can obtain two images from different points of view by using only one camera. Although the technique has the advantage of absolute synchronization of the two "cameras", it suffers from the disadvantages of: (a) small image, (b) mirror surface distortion and (c) it can be used only in a laboratory environment.

Stereometric Technique.

This technique is based on the same principles as those of binocular vision. The eyes, being approximatively 7 cm apart record an object from different angles. The two different images are reconstructed in the brain giving the impression of the space more than of a plane. In practice, two photogrammetric cameras are placed side by side with their optical axes parallel to one another. For the calculation of the X,Y,Z coordinates, standard equations have been derived. Ayoud et al (1970) were the first to suggest the application of this technique for obtaining

three dimensional spatial coordinates of human motion.

This technique requires photogrammetric cameras with well known internal characteristics. Such cameras are very expensive, and consequently the technique appears to be unrealistic for the standards of a biomechanics laboratory. Moreover, the fact that they are still cameras and that an external device is necessary in order to obtain a multiple image (e.g. stroboscope) limits the technique to laboratory environments.

Multiple Cameras Technique.

This technique employs more than one camera to record the motion, and different algorithms can be found in the literature to reconstruct the three dimensional coordinates of the body in motion.

Noble and Kelley (1969) used three cameras to determine the three dimensional coordinates of a moving ball describing the path of a right circular helix. Two cameras were placed in the horizontal plane, 90° out of phase with one another. The third camera was positioned directly above the apparatus. The timing of the films was synchronized by firing a flash bulb at the beginning of the filming. Each film gave two coordinates and by using different scale factors, the X,Y,Z coordinates were reconstructed. However, the errors presented by the authors (35% of the criterion value in acceleration) deem the appropriateness of this technique within biomechanical research questionable.

Anderson (1970) presented a method which utilized three cameras, one sighted along each of the three orthogonal axes X,Y,Z. The two cameras in the horizontal plane were used to calculate the X,Y,Z coordinates while the camera in the vertical axis was used to provide correction factors for perspective errors. This method necessitates the recording of each point by all three cameras.

Miller (1971) presented another technique which also utilized three cameras. The cameras were not placed on the three orthogonal axes, but instead, in a horizontal plane and 120° out of phase with each other. The intersection of the optical axes of the three cameras was used as the origin. Three targets were carefully positioned beyond the origin and aligned with the optical axis of each camera, providing reference coordinates of the origin. The space coordinates of the cameras and the distance between the lens nodal plane and the film plane inside the camera are required to use the algorithm for the reconstruction of the X,Y,Z coordinates of the filmed object. This technique has a general applicability and provides an exact analytical solution to the perspective problem. However, because it requires a specific placement of the cameras and of the targets, it is difficult to use in real life events and especially in a competition situation.

Bergemann (1974) emphasized the importance of camera placement to the production of accurate spatial coordinates. The two cameras were placed in the horizontal plane with

their optical axes intersecting at a common origin. For the placement of the cameras, standard surveying equipment was used. Equations were derived to calculate the position of several arbitrary points on a coordinate grid. A similar method was presented by Van Gheluwe (1974). Pensore et al (1976) have shown that it is no longer necessary for the optical axes to intersect, although a theodolite is required to obtain precise spatial information for the cameras and the reference points.

Van Gheluwe (1978) reported a technique involving camera placement in any position relative to the subject being filmed. The basic principle of the technique relies upon the explicit mathematical reconstruction of the position of the cameras in the space using the known life-sized coordinates and the image-coordinates of certain reference points. A steel tri-axial reference frame was placed in the filmed space to provide appropriate information for the calculation of the position and for orientation of the cameras. The accuracy of the presented results were within the acceptable limits. However, it is not known whether the points chosen for the reliability test were other than control points. Moreover the method does not account for image refinement from lens distortion or film deformation errors.

In 1971, Abdel-Aziz and Karara presented a method that allowed the use of non-metric cameras (cameras with unknown internal characteristics) in stereo-photogrammetry. This

method is the "Direct Linear Transformation" (DLT) method. The position and orientation of the cameras were derived through the use of control points in the space instead of a comparator. A minimum of six non-coplanar control points was required for the solution. Six mathematical models were presented by the same investigators (Karara et al, 1974) to refine the image from lens distortion and film deformation in non-metric photographs.

Shapiro (1978) tested the DLT method with high-speed cinematography. A "tree" with 48 control points was used to calibrate the cameras. It was found that the unknown spatial coordinates of a point can be located with an average error of $\pm 0.4\text{cm}$ for the X-axis, $\pm 0.5\text{cm}$ for the Y-axis and $\pm 0.5\text{cm}$ for the Z-axis. In a dynamic test the acceleration of a ball in free fall was found to yield between -9.5 to -10 m/s^2 .

In an extended investigation of the three dimensional problem, Walton (1981) arrived at the conclusion that the precision with which the object points were located with the DLT method, was adequate for most analyses of human motion. He suggested that accuracy of the measurements can be increased by using a redundant number of control points and, if possible, more than two cameras.

Miller et al (1980) presented the use of the DLT method together with a method for obtaining spatial kinematic parameters of segments of biomechanical systems.

The problem of producing accurate three dimensional coordinates has been of continuing interest. Virtually all

of the above studies validated their procedures by filming an artificial frame. Walton (1981), in one of his validation procedures, used the body landmarks of a trampolinist to calculate the acceleration of the C of M of the athlete due to gravity. He found that the largest error in any of the computed values for "g" was 1.58 m/s^2 . He also found that the mathematical model of the DLT solution with the image refinement model increased the accuracy of the measurements. He suggested that the data obtained through cinematography should be filtered to reduce inherent errors associated with film analysis.

Woltring (1980) tested the same technique. For a calibration tree, he used a 2-D plane with control points. The plane was rotated about an axis and was filmed in some specific angular positions. This technique can be very useful in a laboratory environment or for calibrating small areas, but it is difficult to find construction material which will not undergo deformation when the plane is of a large size and must be rotated.

A alteration of the DLT method was presented by Dapena et al (1981). With this method the use of a calibration tree is no longer necessary and the calibration of the cameras is achieved by the use of two calibration crosses and a set of vertical poles which are placed in the filming area. The authors validated this method by using a 24-point grid. The average Root Mean Square error of the measured versus the simulated coordinates of 15 points of the grid was 1.50cm

for the X-axis, 1.30cm for the Y-axis and 0.60cm for the Z-axis. This model did not account for the image refinement components and in a large filmed area the image deformations from the lens or the film itself would be expected to be large. Further, these investigators did not justify the deletion of 9 points of the tested grid (15 points of the grid out of 24 were used for the validation).

B. Smoothing Techniques.

Since there is always a certain amount of error associated with film analysis, it is necessary to use numerical methods which reduce this kind of error. There are several different methods of data smoothing utilized in biomechanics research. Early researchers used manual smoothing methods to draw smooth curves through successive data points (Miller and Nelson, 1973). Finite differences have been used to calculate first and second time derivatives of displacement data (Miller and Nelson, 1973). Plagenhoef (1973) used a polynomial approximation method to smooth film data. Using displacement data, he determined the coefficients of a polynomial which best fit the data points. The order of the polynomial could be altered depending on the regularity of displacement data. The polynomial was differentiated to obtain estimates of velocity and acceleration data.

Reinsch (1967) presented the use of spline functions to smooth experimental data. The use of cubic splines has been

widely accepted by biomechanics researchers and it has been reported that the acceleration values calculated by this method for film displacement data were more accurate than those derived from other methods in the past (Zernicke et al, 1975; MacLaughlin et al, 1976). To solve the problem of acceleration of the displacement-time data becoming zero at the knot points, Zernicke et al, (1976) suggested that three extra points at the beginning and at the end of each data set should be used.

The estimation of the degree of smoothing is an additional problem for the researcher. MacLaughlin et al (1976) suggested that the calculated average error in measurement of distances from film can be used for the estimation of the degree of smoothing. Further, Zernicke et al (1976) suggested the use of the resultant acceleration curve to alter the degree of smoothing.

A more recent smoothing method was reported by Pezzack et al (1977) and it is known as the digital filter method. They used a second order Butterworth low pass recursive filter to reduce the noise inherent in the signal of film data. The acceleration curve of a freely rotating arm was used to validate the accuracy of smoothing with this method. Finite differences and Chebyshev least squares polynomials were tested in the same experiment. An accelerometer was connected to the arm to provide a criterion acceleration curve. It was found that the digital filter followed by finite difference differentiation was the only method to

accurately reproduce the acceleration time curve recorded by the accelerometer. Spline functions were not tested in the above study. However in their discussion, the authors doubted that spline functions would give more accurate results than Chebyshev polynomials.

The aforementioned studies present methods for smoothing data in biomechanical research. However the question of whether a signal of certain frequency is a data signal or a noise signal remains unanswered and the estimation of the error inherent in data analysis remains a subjective consideration.

C. Hammer Throwing.

The first attempt to biomechanically analyse hammer throwing technique was by Lapp (1935). He found that the hammer accelerates when the athlete is in the double support phase and decelerates during the single support phase.

Samozvetov (1974), in a study of the acceleration of the hammer found that the duration of acceleration of the hammer was critical for a maximum distance throw. He also found that the acceleration phase corresponds to the double support phase of the thrower.

Kuznyetsov (1974) used wire tensors attached to the handle of the hammer to measure centripetal forces caused by the effort of the thrower to propel the hammer. This was used as a strength measurement method but results were not presented.

Dyson, (1977) claimed that, throwers can accelerate the hammer in the single support phase by pulling it downward. *"Vertical downward acceleration is achieved by permitting the body weight to drop just before the hammer head itself drops in its swings or turns. Here, therefore, the limiting factor to acceleration is the thrower's weight - which can be lowered with or without contact with the ground."* (Dyson, 1977). If this statement is correct then the weight of the athlete is another critical factor in hammer throwing.

Elmendorf (1978) studied the relationship of turn time and distance thrown. He found that turn time and distance do not have significant relationships in a three turn throw, but they are significantly related when the athlete uses four turns.

Ariel (1978) compared kinematic parameters of the six best throwers of the 1976 Olympic Games with those of an average group. He found that the average group had a longer turn time for each turn. He also found that the double support time of the Olympians was longer than those of the second group.

Dapena (1981) suggested that the tangential component of the wire pull force, rather than the tangential component of weight of the hammer force is mainly responsible for changes in the velocity of the hammer. He found that for a throw of 67.50 metres, the maximum total wire pull was 2750 Newtons.

The above studies have presented limited quantitative information about the hammer throwing technique. The need for further study is evident.

III. METHODS AND PROCEDURES

The methods and procedures utilized in the present study are described below. The DLT method was tested together with different calibration trees and the six mathematical models for image refinement presented by Karara and Abdel-Aziz in 1974. The model which gave the best results was used for the data collection and data reduction of hammer throwing. The digital filter method was used for the reduction of the noise (Pezzack et al (1977) and Winter (1979)). Rigid body dynamics methods were employed for the analysis of the hammer throwing technique.

A. DLT Method

The DLT is based on the basic theoretical concept of photogrammetry: the photograph, being a perfect plane, is a central projection of the object space. Analytical representation of the geometry of the technique can be found in Appendix A. It is normal photogrammetric practice to determine the transformation of coordinates from the secondary image to real life coordinates by careful calibration of the metric cameras and comparators. However, when non-metric cameras are used, an external calibration is required. For this purpose, a set of known points named control points (CP) are located in the object-space. If X , Y , Z are the spatial coordinates of a point in space and U ,

V its digitized coordinates, the transformation is obtained by utilizing the following equations named basic DLT equations:

$$U + \Delta U = \frac{L_1X + L_2Y + L_3Z + L_4}{L_9X + L_{10}Y + L_{11}Z + 1} \quad (3)$$

$$V + \Delta V = \frac{L_5X + L_6Y + L_7Z + L_8}{L_9X + L_{10}Y + L_{11}Z + 1} \quad (4)$$

where: X,Y,Z are the coordinates of the point in space.
 U,V are the digitized coordinates of the point.
 $L_i (i=1, \dots, 11)$ are coefficients named transformation coefficients.
 $\Delta U, \Delta V$ are image refinement components of lens distortion and film deformation.

A minimum number of six CP is required for the solution of a system of twelve equations and eleven unknowns. For better accuracy a redundant number of control points is advised. In this case an over-determined system of equations has to be solved and a least square method can be used. In order to calculate 3-D coordinates of a point, at least two observations (cameras) are needed.

Once the transformation coefficients of the two cameras have been determined and the digitized coordinates of a point in the object-space from both cameras are given, the DLT equations are used for the determination of the spatial coordinates of the point.

Six mathematical models have been given by Karara and Abdel-Aziz (1974) for the image refinement components

($\Delta U, \Delta V$). These models can be found in Appendix A. The first model does not change the form of the DLT equations, because the eleven basic coefficients account for the linear components of lens distortion and film deformation. When one of the left five models is used, the number of calibration coefficients and the minimum number of CP are increased as shown in Table 1, Appendix A. With utilization the models II to VI and with a redundant number of control points, the system of equations to be solved becomes an overdetermined system of non-linear equations.

Validation of DLT Method

The DLT method was tested by utilizing three different calibration trees and the five mathematical models for the image refinement. Two Photo-Sonic IPL phase-locked cameras were used for the filming in all the tests. An Angenieux 12-120 zoom lens was mounted on each camera.

A computer program was written in HPL language to calculate the DLT calibration coefficients and to simulate the spatial coordinates of the CP. The DLT basic equations without any image refinement component were used as a first step. The least square method presented by Scheid (1968, pp.375) was used to solve the overdetermined system of equations. As a second step, the five mathematical models for the image refinement were sequentially introduced to the DLT equations. The digitized coordinates of the center of the projected images were calculated and were used as the

point of symmetry of the frames. Based on these coordinates and the digitizer coordinates of the CP the position vector of each point was defined with respect to the point of symmetry. The overdetermined system of non-linear equations was solved by expressing the equations in truncated Taylor series and then by using Newton's iterative least squares method. The transformation coefficients derived in the first step were entered as initial values for the unknowns at the first iteration. In the first iteration the image refinement coefficients were assigned a value of zero. The computer program was set to attenuate the iterations when the sum of the absolute values of the residuals was smaller or equal to the criteria value of 10^{-10} , ($\Sigma R \leq 10^{-10}$), or when the system stopped converging. With the models II, III and IV the system satisfied the first criteria. With model V the system stopped converging when the criteria value was $\Sigma R \leq 10^{-9}$ and with model VI the system stopped converging when the value was $\Sigma R \leq 10^{-8}$. This might be a result of the least square method used for the solution and of the precision of the computer (over 18 unknowns, 68 equations and requested high precision).

The first tested tree was a 2-D frame with dimensions 2X2.5 m (Woltring, 1980). The tree was constructed of metal tubes. table-tennis balls were used as control points and the tree was filmed in different angular positions. The cameras were placed approximately 20m from the frame and 10m from each other. This particular disposition of the cameras

is not a critical factor in the accuracy of the results (Walton, 1981; Miller et al, 1980). The cameras were set to operate at a speed of 100 frames per second (fps). The measurement of the mean error was approximately 10 cm. This large error was probably caused by the deformation of the tree. These results indicated that, for calibration of large areas and with non-expensive materials, the use of a 2-D tree was not viable.

In March 1982 a new calibration tree, a steel frame with dimensions 2.5 x 2 x 2 m was tested. Thirty-five randomly distributed table-tennis balls were mounted within the frame by means of strings. The reference frame and a golf ball in free fall released from the top of the frame were filmed.

The overall Root Mean Square (RMS) differences of the X,Y,Z coordinates simulated by the DLT method with the five mathematical models and the measured coordinates were calculated. Refinement with model III gave slightly better results than the other models. ($\text{RMS}(X) = 1.12 \text{ cm.}$, $\text{RMS}(Y) = 1.09 \text{ cm.}$, $\text{RMS}(Z) = 0.81 \text{ cm.}$). All the models gave more accurate results for the Z-axis (vertical) than for the other axes. This might be a result of the perspective errors of the two cameras which affected the X and Y axes or the precision of the instruments used for measuring the coordinates of the points in the experimental session.

A golf ball in free fall was digitized in every frame of both films and the DLT equations together with Model III

for image refinement were used to simulate the X, Y, and Z coordinates of the ball. The time-displacement data of the ball were filtered with a second order double pass Butterworth recursive filter with a cut-off frequency of 8 Hz. A first central difference method, (Miller et al 1973) was used to calculate the acceleration of the ball. This was found to be between -9.5 m/s^2 and -10.2 m/s^2 . (Criterion value of gravity = -9.81 m/s^2).

The results of the above test were complementary to results of similar studies and were, therefore, satisfactory. Several decisions were made based on the above test. To improve the accuracy of the results derived with the DLT method, the cameras must be placed as far as possible from the object space to avoid perspective error. A pre-built calibration "tree" with precisely measured control points must be used. For better precision and faster measuring, the calibration tree should be geometric in shape. This can provide some CP which do not require actual measurement since the spatial coordinates can be calculated with respect to the coordinates of other points.

The third tested tree was the calibration tree used for the data collection of the hammer throwing and was an aluminium frame of $3 \times 3 \times 3 \text{ m}$ (Figure 3). It was made from 12 aluminium sticks with a square cross-section ($2.5 \times 2.5 \text{ cm.}$). The sticks were parallel or perpendicular to the horizontal. The aluminium sticks were chosen instead of other material because they are easy to transport, easy to work with, and

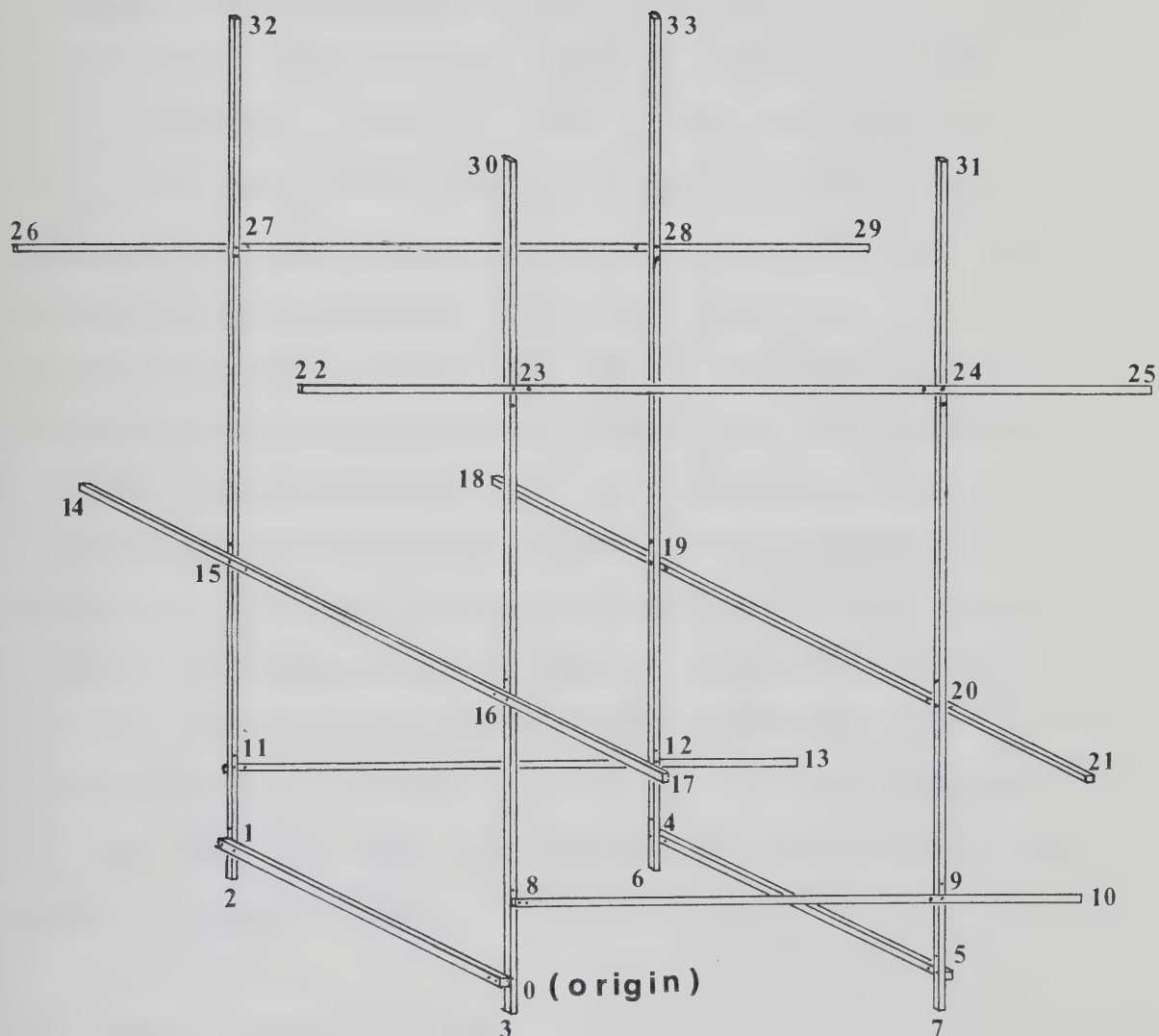


Figure 3: Data Collection Calibration Tree

because a three meter stick, when mounted by two points one meter from each end, presents no deformation. Rigid L-shape corners were used to improve the stability of the connections. The connections and the end points of the sticks provided a set of 33 CP plus one which was used as the space fixed origin. The coordinates of these points are presented in Appendix D. First, all the points were used to calculate the coefficients with each model and the X, Y, Z coordinates of all the points and the location of both cameras relative to the space fixed origin were simulated.

Second, 27 points were treated as control points and 6 points (points 28 to 33 in Figure 3) were treated as unknowns. The calibration coefficients were recalculated with all the models and the spatial coordinates of the control points and the unknowns were simulated. Model IV gave slightly smaller RMS differences for the 6 unknowns and it was chosen for the transformation of coordinates in the hammer throwing analysis.

B. Hammer Throwing Analysis

Subjects

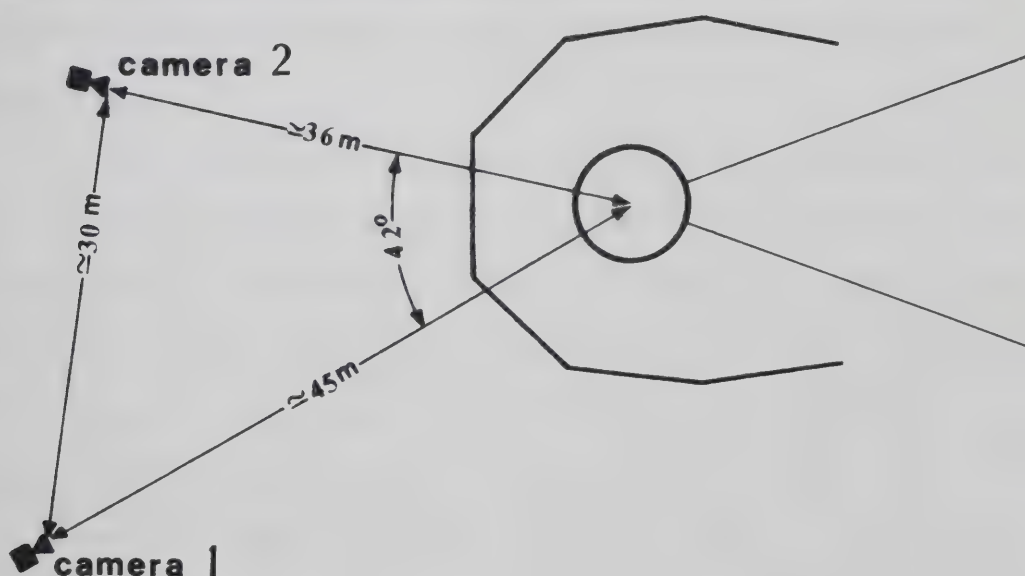
The three medalists of the 1982 European Championship were selected as subjects for this study and their best throw in this competition were analysed. The mass and height of each subject and the distance of the analyzed throws are presented in Table 2.

TABLE 2MASS, HEIGHT AND THROWING DISTANCE OF THE ANALYZED ATHLETES

Subject#	Mass(kg.)	Height(m.)	Distance(m.)
1	110	1.85	81.66
2	100	1.91	79.44
3	95	1.80	78.66

Data Collection

The data were collected in Athens, Greece, in September 1982 during the XIIIth European Athletics Championship. The location of the cameras can be seen in Figure 4. The cameras were set to an operating speed of 100 fps. (The actual frame rate was found to be 99 fps) An external light generator was used to flash a light inside each camera which was recorded on the side of the film. The frequency of this light was 10 Hz. The film was Kodak Ektachrome 2537, 100 ASA. The f stop was $f = 5.6$ and the exposure time was $1/1200$ second.

**Figure 4: Location of the Cameras**

After the cameras were set, the calibration tree (Figure 3) was placed in the throwing circle and filmed. The set-up and the filming of the calibration tree was finished before the competition started. A second check was made after the tree had been filmed. After the filming for calibration, the tree was dismounted and removed from the field.

Data Reduction.

The following hardware was used in the data reduction process: a) A Triad Model V/R-100 mirror projector which magnifies the projected frame; b) A Bendix digitizing board with dimensions 1.215 x 0.91 m. The precision of this board is ± 0.0254 cm; c) An HP 9864A digitizer; d) An HP 9825B desktop micro-computer with a RAM capacity of 64 K bytes. The film projector and the digitizing board were set parallel to each other and remained in the same position until the digitizing of the control points and the subjects was completed.

Each film with the control points was projected and each point was digitized three times with respect to the origin of the tree. The origin from each film was marked on the digitizing board to be used later for the digitizing of the subjects. The mean values of the U, V digitized coordinates of each control point were stored.

The DLT equations together with model IV for image refinement were used for the calculation of the calibration

coefficients. The following were the two equations which composed model IV for image refinement:

$$\begin{aligned}\Delta U = & a_1 + a_2U + a_3V + x(k_1r^2 + k_2r^4 + k_3r^6) \\ & + P_1(r^2 + 2x^2) + 2P_2xy\end{aligned}\quad (5)$$

$$\begin{aligned}\Delta V = & a_4 + a_5U + a_6V + y(k_1r^2 + k_2r^4 + k_3r^6) \\ & + P_2(r^2 + 2y^2) + 2P_1xy\end{aligned}\quad (6)$$

where: $\Delta U, \Delta V$ are image refinement components of lens distortion and film deformation;
 a_i ($i=1, \dots, 6$) are coefficients of film deformation;
 U, V are the digitized coordinates of the point;
 $x = U - U_s$ and $y = V - V_s$ with U_s & V_s the image coordinates of the point of symmetry;
 k_i ($i=1, \dots, 3$) are coefficients of symmetrical lens distortion;
 r is the length of the vector from the point of symmetry to the point under consideration;
 P_1, P_2 are coefficients of asymmetrical lens distortion.

Digitizing of the Subjects.

Nineteen points on the body of the athlete and on the hammer were digitized for each subject in each frame. The number of frames digitized for each subject was 155 for the first subject, 222 frames for the second subject and 194 for the third subject.

All the points were digitized with respect to the origin of the calibration tree.

Data Interpolation.

The light which was recorded on the sides of the films was used to check the timing of the digitized frames from both films. It was found that at the beginning of each run the slave camera had a delay running time with respect to

the master camera. In order to utilize these first frames interpolation polynomials were used to time-match the frames. A first interpolation was used to calculate the timing of the non-matched frames. A second interpolation was used to calculate the time-matched digitized coordinates of the second film. The interpolation formula was a cubic Lagrangian polynomial (Gerald 1980, p.174).

$$\begin{aligned}
 P(t) = & \frac{(t - t_2)(t - t_3)(t - t_4)}{(t_1 - t_2)(t_1 - t_3)(t_1 - t_4)} f(1) \\
 & + \frac{(t - t_1)(t - t_3)(t - t_4)}{(t_2 - t_1)(t_2 - t_3)(t_2 - t_4)} f(2) \\
 & + \frac{(t - t_1)(t - t_2)(t - t_4)}{(t_3 - t_1)(t_3 - t_2)(t_3 - t_4)} f(3) \\
 & + \frac{(t - t_1)(t - t_2)(t - t_3)}{(t_4 - t_1)(t_4 - t_2)(t_4 - t_3)} f(4)
 \end{aligned} \tag{7}$$

where: $P(t)$ is the time matched coordinate;
 t_1, t_2, t_3, t_4 are the times of the surrounding frames;
 $f(1), f(2), f(3), f(4)$ are the digitized coordinates of the same frames.

After the interpolation, the digitized coordinates of the points and the calibration coefficients of each camera were introduced into the system of equations composed by equations (3), (4), (5) and (6) for each camera and the spatial coordinates of the points were simulated.

Rotation and Translation of the Axes.

The spatial coordinates of all points for analysis were measured with respect to the origin of the calibration tree. The center of the throwing circle at ground level was chosen as the origin of the reference frame for analysis of the throws. The coordinates of this point with respect to the origin O of the calibration tree were $X = 73.75$, $Y = 73.75$ and $Z = -11.5$ cm. The general formula for this transformation was the following:

$$C_{i0'} = C_{i0} - C_0 \quad (8)$$

where: $C_{i0'}$ is the coordinate of the point of interest with respect to the new origin O' ;
 C_{i0} is the coordinate of the point with respect to the old origin O ;
 C_0 is the coordinate of the new origin O' with respect to the old origin O .

In order to present the direction of the positive Y axis as the direction of the throw the coordinates were rotated 95° about the Z -axis. The following matrix equation was used for the above rotation:

$$\begin{vmatrix} X' \\ Y' \\ Z' \end{vmatrix} = \begin{vmatrix} a_{11} & a_{12} & a_{13} \\ a_{21} & a_{22} & a_{23} \\ a_{31} & a_{32} & a_{33} \end{vmatrix} \begin{vmatrix} X \\ Y \\ Z \end{vmatrix} \quad (9)$$

where : X' , Y' , Z' are the coordinates of a point in the new coordinate system O' .
 X , Y , Z are the coordinates of the point in the old coordinate system O .

a_{i1} , a_{i2} , a_{i3} are the direction cosines of the X' axis ($i = 1$), Y' axis ($i = 2$) and Z' axis ($i = 3$) in the old coordinate system O' .

Calculation of Error and Data Smoothing.

The error involved in the data for the present study can be expressed as systematic and random error.

The systematic error is that error, inherent in the coordinates of any point, which is due to the DLT method including the model IV for image refinement. Six points of the calibration tree were treated as unknowns and the RMS differences of the measured versus the simulated coordinates of these points gave an estimation of the amount of error. Although the error due the DLT is a random error when the calibration coefficients are calculated, the final value is a systematic error in the transformation of the coordinates of each point for analysis.

The random error involved in the data was due to the digitizing process, that is the difficulty of detecting the exact position of the points of interest on the projected film. For the calculation of this error, a set of 7 frames was randomly selected and redigitized after the digitizing had finished.

A second order double pass Butterworth filter was used to reduce the error involved in the data for analysis. The data were expressed in Fourier series and the power spectra were plotted. After investigation of the power spectra plot the cut-off frequency was decided to be 9 Hz. for the hammer

kinematics and 6 Hz. for all the other analysis.

Analysis of Data.

The following is a presentation of the procedures undertaken for the analysis of the data.

Calculation of the Center of Mass.

The coordinates of the center of mass of the body of the athletes (CMB) and the system:athlete + hammer (CMS), were calculated by using the following equations:

$$Cb_j = \sum_{i=1}^{12} [P_{ij} - (P_i - D_{ij})q_i]m_i \quad (10)$$

$$Cs_j = (M * Cb_j + 7.257 * H_j)/(M + 7.257) \quad (11)$$

where : Cb_j and Cs_j are the coordinates of the CMB and CMS respectively in the j th frame;
 P_{ij} and D_{ij} are the coordinates of the proximal and distal end point of the i th segment;
 H_j is the coordinate of the hammer; q_i is the distance of the center of mass of the i th segment from its proximal end point in percentage of the total length of the segment;
 m_i is the mass of the i th segment in percentage of the total body mass of the athlete;
 M is the mass of the body of the athlete;
 7.257 kg. is the mass of the hammer. The mass of the cable and the grip of the hammer was assumed to be concentrated in the head of the hammer although it is in the neighbourhood of 100 gr.

The quantities q_i and m_i were taken from Dempster's cadaver data (Dempster, 1955) and are presented in Table 3. Although these anthropometric data are widely used in biomechanical research, they are a source of error, since it

is unlikely that the body composition of Dempster's cadavers is the same as that of athletes and especially of throwers. It was decided to accept this error as it would be constant in all the frames and will have no serious effect on the results.

TABLE 3
ANTHROPOMETRIC DATA OF THE SEGMENTS

From Dempster(1955)

Segment(i)	Length(q_i)	Mass (m_i)
Trunk	50.00	49.50
Head + Neck	56.70	7.90
Upper Arm	43.60	2.70
Lower Arm + Hand	67.70	2.26
Thigh	43.30	10.20
Lower Leg	43.30	4.65
Foot	42.90	1.46

(q_i % of segmental length from proximal point, m_i % of total body mass.)

Linear Kinematics.

The linear velocity and acceleration of the hammer, the CMb and the CMs were calculated numerically from the time displacement data. First central difference method was used for the above purpose, (Miller et al, 1973).

Instantaneous Radius and Center of Curvature.

The instantaneous radius(ρ) of curvature and the coordinates of the center of curvature (C_x , C_y , C_z) of the orbit of the hammer, the CMb and the CMs were calculated by using the following equations:

$$\rho = \frac{v^2}{[(x''v - x'u)^2 + (y''v - y'u)^2 + (z''v - z'u)^2]^{1/2}} \quad (12)$$

$$C_x = x + \frac{x''v - x'u}{(\kappa v)^2} \quad (13)$$

$$C_y = y + \frac{y''v - y'u}{(\kappa v)^2} \quad (14)$$

$$C_z = z + \frac{z''v - z'u}{(\kappa v)^2} \quad (15)$$

$$\begin{aligned} \text{with : } v &= x'^2 + y'^2 + z'^2 \\ u &= x'x'' + y'y'' + z'z'' \end{aligned}$$

where : ρ is the radius of curvature of the orbit;
 C_x, C_y, C_z are the coordinates of the center of curvature;
 x, y, z are the coordinates of the point of interest;
 x', y', z' are the velocities of the point in the X, Y and Z axis;
 x'', y'', z'' are the accelerations of the point in the same axes;
 κ is the curvature of the orbit which is $\kappa = 1/\rho$

The derivation of the above equations is based on vector analysis and is presented in appendix C. The quantities $x', y', z', x'', y'', z''$ were calculated numerically from the time displacement data of the point.

Tension of the Cable

The radius of curvature, the linear velocity, the mass of the hammer and the angle of the cable with the radius of curvature were utilized for the calculation of the tension

in the cable of the hammer. Thus,

$$F_t = \frac{m \cdot u^2}{\rho \cdot \cos \theta} \quad (16)$$

where: m is the mass of the hammer;
 u is the resultant velocity of the hammer;
 ρ is the radius of curvature;
 θ the angle of the cable with the radius ρ .

Angular Kinematics

Absolute and relative angular measurements were achieved through vector identities. Segments were expressed in terms of vectors in the three dimensional space.

The angle formed by two segments was found by applying the dot product between the vectors representing the segments.

Direction cosines of the vector segment were used to calculate the angle of the segment with the inertial axes.

The following angles were calculated:

Left knee angle, formed by the left thigh and the left leg;

Hip - shoulder angle, formed by the line of the hips and the line of the shoulder;

Trunk - vertical which is the angle of the trunk with the vertical axis;

Radius - cable angle which is the angle between the radius of curvature and the cable of the hammer;

Trunk - arms angle which is the angle between the trunk and the arms (origin of the arms was taken the middle point of the shoulders).

Moments and Products of Inertia.

In each frame the moments of inertia of the system were calculated about an orthogonal system of axes C(X', Y', Z') with origin at the CMs. This system of axes was parallel to the space-fixed system of axes O(X, Y, Z). (See Appendix B)

First, the moments and products of inertia of each segment about their center of mass was calculated for each frame. The following are the equations used for this purpose:

$$I'_{xx} = I''_{xx} \cdot \alpha_{11}^2 + I''_{yy} \cdot \alpha_{21}^2 + I''_{zz} \cdot \alpha_{31}^2 \quad (17)$$

$$I'_{yy} = I''_{xx} \cdot \alpha_{12}^2 + I''_{yy} \cdot \alpha_{22}^2 + I''_{zz} \cdot \alpha_{32}^2 \quad (18)$$

$$I'_{zz} = I''_{xx} \cdot \alpha_{13}^2 + I''_{yy} \cdot \alpha_{23}^2 + I''_{zz} \cdot \alpha_{33}^2 \quad (19)$$

$$I'_{xy} = -(\alpha_{11} \cdot \alpha_{12} \cdot I''_{xx} + \alpha_{21} \cdot \alpha_{22} \cdot I''_{yy} + \alpha_{31} \cdot \alpha_{32} \cdot I''_{zz}) \quad (20)$$

$$I'_{xz} = -(\alpha_{11} \cdot \alpha_{13} \cdot I''_{xx} + \alpha_{21} \cdot \alpha_{23} \cdot I''_{yy} + \alpha_{31} \cdot \alpha_{33} \cdot I''_{zz}) \quad (21)$$

$$I'_{yz} = -(\alpha_{12} \cdot \alpha_{13} \cdot I''_{xx} + \alpha_{22} \cdot \alpha_{23} \cdot I''_{yy} + \alpha_{32} \cdot \alpha_{33} \cdot I''_{zz}) \quad (22)$$

where : I''_{xx} , I''_{yy} , I''_{zz} are the principal moments of inertia of the i th segment;
 α_{11} , α_{12} , α_{13} are the direction cosines of the principal axes, X ($i = 1$), Y ($i = 2$) and Z ($i = 3$) axis relative to the space fixed system of axes.

The principal moments were taken from Whitsett's anthropometric data (Whitsett, 1963) and are presented in

Table 4. These data were normalized according to the mass and height of each athlete. The equations for the above normalization were taken from Dapena (1978) and are the following:

For the transverse and frontal axis,

$$I = I \cdot M \cdot S^2 / M \cdot S^2 \quad (23)$$

and for the longitudinal axis,

$$I = I \cdot M^2 \cdot S / M^2 \cdot S \quad (24)$$

where: I , is the principal moments presented by Whitsett;
 M , S are the average mass and height of Whitsett's subjects $M = 74.2 \text{ kg.}$, $S = 1.755 \text{ m.}$);
 M and S are the mass and the height of the subject at the present study.

TABLE 4

PRINCIPAL MOMENTS OF INERTIA OF THE SEGMENTS

From Whitsett (1963)

Segment	I''_x	I''_y	I''_x
Trunk	1.2606	1.3555	0.3118
Head + Neck	0.0248	0.0248	0.0168
Upper Arm	0.0213	0.0213	0.0024
Lower Arm + Hand	0.0081	0.0081	0.0016
Thigh	0.1052	0.1052	0.0209
Lower Leg	0.0505	0.0505	0.0050
Foot	0.0038	0.0038	0.0008

(presented measurements in $\text{kg} \cdot \text{m}^2$)

(I''_x principal moment about frontal axis)
 (I''_y principal moment about transverse axis)

(I''_z principal moment about longitudinal axis)

The longitudinal axis of a segments was taken as the Z principal axis with origin at the center of mass of the segment and direction towards the proximal end point. The X principal axis of the trunk was taken as principal axis parallel to the axis of the hips and with direction towards the right hip. For the non-trunk segments an assumption was made, that is, the segment moves in a plane in two successive frames. The plane was defined by the proximal end point of the segment at the (j)th frame, the center of mass of the segment at the same frame and the center of mass of the segment at the ($j+1$)th frame. After the definition of the plane, the vector of the X principal axis was defined as a vector normal to the Z axis at its origin and having direction towards the direction of the motion. The vector of the Y principal axis was then defined by the cross product of the Z and X vectors. The method is presented in appendix B.

The total moments and products of inertia of the system about its center of mass and for each frame, were found with the following equations:

$$I_x = \sum_{i=1}^{13} [I'_{x_i} + m_i (C_{y_i}^2 + C_{z_i}^2)] \quad (25)$$

$$I_y = \sum_{i=1}^{13} [I'_{y_i} + m_i (C_{x_i}^2 + C_{z_i}^2)] \quad (26)$$

$$I_z = \sum_{i=1}^{13} [I'_{z i} + m_i (C_{x i}^2 + C_{y i}^2)] \quad (27)$$

$$I_{xy} = \sum_{i=1}^{13} [I'_{xy i} + m_i C_{x i} C_{y i}] \quad (28)$$

$$I_{xz} = \sum_{i=1}^{13} [I'_{xz i} + m_i C_{x i} C_{z i}] \quad (29)$$

$$I_{yz} = \sum_{i=1}^{13} [I'_{yz i} + m_i C_{y i} C_{z i}] \quad (30)$$

where: I_x, I_y, I_z are the total moments and products of inertia of the system about the axes X, Y, Z
 m_i is the mass of the i th segment.
 $C_{x i}, C_{y i}, C_{z i}$ are the coordinates of the center of mass of the i th segment relative to the center of mass of the system.
 $I'_{x i}, I'_{y i}, I'_{z i}, I'_{xy i}, I'_{xz i}, I'_{yz i}$ are the moments and products of inertia of the i th segment about the axes X', Y', Z' .

Angular momentum.

The angular momentum of the system, was calculated with respect to an orthogonal system of axes passing from the center of mass of the system and parallel to the space-fixed axes. The total angular momentum of the system was found by the following equations:

$$\underline{L}_x = \sum_{i=1}^{13} [\underline{L}'_{x i} + \underline{L}''_{x i}] \quad (31)$$

$$\underline{L}_y = \sum_{i=1}^{13} [\underline{L}'_{y i} + \underline{L}''_{y i}] \quad (32)$$

$$\underline{L}_z = \sum_{i=1}^{13} [\underline{L}'_{z i} + \underline{L}''_{z i}] \quad (33)$$

where: $\underline{L}_x, \underline{L}_y, \underline{L}_z$ are vectors representing the angular momentum of the system about its center of mass;
 $\underline{L}'_{xi}, \underline{L}'_{yi}, \underline{L}'_{zi}$ are vectors representing the angular momentum of the i th segment about the center of mass of the system, considering the segment as a point mass;
 $\underline{L}''_{xi}, \underline{L}''_{yi}, \underline{L}''_{zi}$ are the vectors representing the angular momentum of the i th segment about its center of mass.

For the $\underline{L}'_{xi}, \underline{L}'_{yi}, \underline{L}'_{zi}$ the following general equation was used:

$$\underline{L} = m * (\underline{r}_1 \times \underline{r}_2) / \Delta t \quad (34)$$

where: m is the mass of the segment;
 $\underline{r}_1, \underline{r}_2$ are position vectors of the segment in two successive frames;
 Δt is the time interval between the two frames.

$\underline{L}''_{xi}, \underline{L}''_{yi}$ and \underline{L}''_{zi} , were calculated by utilizing the moments and products of inertia of the segments about their center of mass and their angular velocity about their principal axes. This method is different from the one presented by Dapena (1978). Dapena calculated the local angular momentum of the non-trunk segment only about the transverse axis and assumed that the local angular momentum about the other axes was too small to be considered. The local angular momenta of the segments for this study were calculated by using the following equations:

$$\underline{L}''_{xi} = I'_{xi} \cdot \omega_{xi} - I'_{xyi} \cdot \omega_{yi} - I'_{xzi} \cdot \omega_{zi} \quad (35)$$

$$\underline{L}''_{yi} = - I'_{xyi} \cdot \omega_{xi} + I'_{yi} \cdot \omega_{yi} - I'_{yzi} \cdot \omega_{zi} \quad (36)$$

$$L''_{zi} = -I'_{xzi} \cdot \omega_{xi} - I'_{yzi} \cdot \omega_{yi} + I'_{z_i} \cdot \omega_{zi} \quad (37)$$

where: I'_{xi} , I'_{yi} , I'_{zi} and I'_{xyi} , I'_{xzi} , I'_{yzi} are the moments and products of inertia of the i th segment about its center of mass;
 ω_{xi} , ω_{yi} , ω_{zi} are the angular velocities of the segment about the space fixed axes.

(See appendix B for details of this technique).

After the angular momentum of the system about the X, Y and Z axis was found, the total angular momentum of the system was calculated from the equation:

$$L = (L_x^2 + L_y^2 + L_z^2)^{1/2} \quad (38)$$

Axis of Momentum.

Axis of momentum of the system for each frame was defined as the axis which passes through the center of mass of the system and is coincident with the angular momentum vector. The direction cosines of the angular momentum are:

$$\beta_1 = L_x / (L_x^2 + L_y^2 + L_z^2)^{1/2} \quad (39)$$

$$\beta_2 = L_y / (L_x^2 + L_y^2 + L_z^2)^{1/2} \quad (40)$$

$$\beta_3 = L_z / (L_x^2 + L_y^2 + L_z^2)^{1/2} \quad (41)$$

The coordinates of the point of intersection of this axis with the ground are:

$$X = (\beta_3 \cdot X_1 - Z_1 \cdot \beta_1) / \beta_3 \quad (42)$$

$$Y = (\beta_3 \cdot Y_1 - Z_1 \cdot \beta_2) / \beta_3 \quad (43)$$

$$Z = 0 \quad (44)$$

where: X_1, Y_1, Z_1 are the coordinates of the center of mass.

Instantaneous angular velocity.

The instantaneous angular velocity of the system was defined as the angular velocity of the system about the system of axes passing through center of mass and parallel to the space-fixed system of axes. The following matrix equation was used for this purpose:

$$\begin{vmatrix} L_x \\ L_y \\ L_z \end{vmatrix} = \begin{vmatrix} I_x & -I_{xy} & -I_{xz} \\ -I_{xy} & I_y & -I_{yz} \\ -I_{xz} & -I_{yz} & I_z \end{vmatrix} \begin{vmatrix} \Omega_x \\ \Omega_y \\ \Omega_z \end{vmatrix} \quad (45)$$

where: $\Omega_x, \Omega_y, \Omega_z$ are the angular velocities about the X, Y, Z axes;

$I_x, I_y, I_z, I_{xy}, I_{xz}, I_{yz}$ the moments and products of inertia calculated with equations (17) to (22);

L_x, L_y, L_z are the angular momenta of the system calculated with equations (31) to (33).

The column matrix of the angular velocity in the equation (45) was found by multiplying the inverse of the moments of inertia matrix by the column matrix of the angular momenta. The magnitude of the resultant instantaneous angular velocity of the system was found by the equation:

$$\Omega = (\Omega_x^2 + \Omega_y^2 + \Omega_z^2)^{1/2} \quad (46)$$

External Torques of rotation.

The external torque of the rotation was defined as the rate of change of the angular momentum. Thus,

$$\tau = \Delta L / \Delta t \quad (47)$$

Forces of Translation.

The external forces of translation applied to the system were found by using the general formula:

$$\underline{F} = m\underline{a} \quad (48)$$

where: m is the mass of the system;

a is the acceleration of the CMs.

Kinetic Energy.

The kinetic energy of the system was found from the sum of the kinetic energy of rotation plus the kinetic energy of translation. Thus,

$$T = T_t + T_r \quad (49)$$

where: T_t is the kinetic energy of translation and T_r is the kinetic energy of rotation given as follows:

$$T_t = \frac{1}{2} M \cdot u^2 \quad (50)$$

$$T_r = \frac{1}{2} (I_x \omega_x^2 + I_y \omega_y^2 + I_z \omega_z^2 - 2I_{xy} \omega_x \omega_y - 2I_{xz} \omega_x \omega_z - 2I_{yz} \omega_y \omega_z) \quad (51)$$

where: M is the mass of the system;
 u is the velocity of the center of mass;
 I_x, I_y, I_z and I_{xy}, I_{xz}, I_{yz} are moments and products of inertia of the system;
 $\omega_x, \omega_y, \omega_z$ are the angular velocities.

All the programs for the data reduction and data analysis were written in HPL computer language by the author and the HP 9825B desk-top computer was used. The motion was divided into turns and each turn into single and double support phase. The results of each phase, each turn, and, each subject were compared to one another.

IV. RESULTS AND DISCUSSION

The sequence of presentation of the results found in this study is as follows: Results of the DLT tests; Error analysis; Kinematics and kinetics of the hammer; Kinematics and kinetics of the body Center of Mass; Segmental kinematics; Kinematics and kinetics of the system.

A. Results of the DLT Tests.

The DLT method together with six mathematical models for image refinement (Karara and Abdel Aziz, 1974) and three different calibration trees were tested. Criterion for these tests were the Root Mean Square (RMS) differences of measured versus simulated coordinates of the control points, or of control points which were treated as unknowns.

The results of tests on the first tree which was a 2-D frame filmed in different angular positions were unsatisfactory in that there was considerable deformation of its shape in rotation caused by its weight.

The results of tests on the second tree which was a 3-D frame are presented in Table 5.

TABLE 5

RMS DIFFERENCES OF THE CP FOR THE SECOND TREE

<u>Model</u>	<u>X RMS</u>	<u>Y RMS</u>	<u>Z RMS</u>	<u>MEAN</u>
No Ref.	1.1815	1.0214	0.8458	1.0162
Model II	1.1231	1.0998	0.8212	1.0147
Model III	1.1199	1.0944	0.8129	1.0091
Model IV	1.1329	1.1797	0.7611	1.0245
Model V	1.1115	1.4940	0.7678	1.1244
Model VI	1.3235	1.9939	0.5915	1.3030

(presented measurements in centimeters)

The results of the third tree which was geometric in shape and was used for the data collection of hammer throwing, are presented in Table 6. In this Table the first column contains the RMS of all the control points, the second column contains the RMS of 27 control points from the test when 6 points were treated as unknowns and the third column contains the results of the 6 points treated as unknowns.

TABLE 6

RMS DIFFERENCES OF THE CP FOR THE DATA COLLECTION TREE

<u>Model</u>		<u>33 CP</u>	<u>27 CP</u>	<u>6 Unknowns</u>
No Ref.	X	0.22	0.29	0.84
	Y	0.20	0.14	0.39
	Z	0.24	0.19	0.85
Model II	X	0.36	0.42	0.42
	Y	0.33	0.38	0.55
	Z	0.25	0.18	0.61
Model III	X	0.24	0.30	0.46
	Y	0.19	0.16	0.59
	Z	0.25	0.19	0.65
Model IV	X	0.24	0.28	0.27
	Y	0.19	0.14	0.60
	Z	0.25	0.19	0.72
Model V	X	0.29	0.29	0.38
	Y	0.20	0.14	0.74
	Z	0.25	0.20	0.86
Model VI	X	0.48	0.25	1.46
	Y	0.36	0.14	0.76
	Z	0.36	0.19	1.21

(presented measurements in centimeters)

The digitized, measured and simulated coordinates of the CP of the last tree, as well as the calibration coefficients of the DLT with model IV, are presented in Appendix D. The RMS error presented in Table 6, was the error of the DLT method in the present study. In a similar study of the DLT method, Shapiro (1978) found an error of ± 0.40 cm. in the X-axis, ± 0.40 cm. in the Y-axis and ± 0.50 cm. in the Z-axis. Dapena et al (1981), found a $RMS(X) = 1.50$ cm., $RMS(Y) = 1.32$ cm. and $RMS(Z) = 0.60$ cm.. With the second tree, Model III gave slightly better results than the other models, while with the data collection tree, Model IV gave the best results.

Another test on the data collection tree was the simulation of the coordinates of the location of the cameras with respect to the origin of the tree. These coordinates and the simulated distance of the cameras (ℓ_1 and ℓ_2) from the origin are presented in Table 7.

TABLE 7

SIMULATED COORDINATES AND DISTANCE OF CAMERAS

FROM ORIGIN WITH DIFFERENT MODELS

<u>Model</u>	<u>Camera #1</u>				<u>Camera #2</u>			
	X	Y	Z	ℓ_1	X	Y	Z	ℓ_2
No Ref.	35.75	-5.21	0.70	36.13	37.61	24.98	0.92	45.16
Model II	35.86	-5.22	0.70	36.24	37.72	25.04	0.92	45.28
Model III	35.95	-5.23	0.70	36.33	37.68	25.01	0.92	45.23
Model IV	35.91	-5.22	0.70	36.29	37.68	25.02	0.92	45.23
Model V	35.87	-5.18	0.70	36.25	37.65	25.00	0.92	45.20
Model VI	36.40	-5.26	0.71	36.78	38.22	25.36	0.92	45.88

(presented measurements in meters)

The X, Y, Z coordinates of the location of the two cameras with respect to the origin were not measured directly in the filming process. Only the distances of the cameras to the center of the throwing circle were measured, and they were found to be $\ell_1 \approx 36.20$ m. for camera #1 and $\ell_2 \approx 45.10$ m. for camera #2.

The results from the third tree were superior to the ones of the preliminary tests because in the preliminary tests the CP were randomly distributed in space and it is possible that they included higher measuring error.

In order to test the stability of the DLT for outside areas of the calibration tree, 6 CP located in this area were treated as unknowns (points 28 to 33 in Figure 3). The RMS error of the measured versus the simulated coordinates of these points are presented in Table 6, 3rd column. These results indicated that, use of a well constructed tree and Karara's models for image refinement enabled reliable data to be collected using a calibration tree smaller than the area of action. These results were expected, since the control points were used for the estimation of coefficients that indicate the orientation and location of the cameras in the filming process and the orientation of the secondary image in the digitizing process, rather than for the estimation of ratio parameters of control and unknown points. After these coefficients were computed, the spatial coordinates of a point under consideration were calculated based on the digitized coordinates of the point and the

calibration coefficients. Utilization of the mathematical models for image refinement corrected the transformed coordinates of a point if they were affected by film deformation and/or lens distortion error. These models were of significant value when a point under observation was located in the outer area of the image in film from at least one camera. Points near the outer area of the images in films from both cameras were expected to include larger error than other points. These areas however, were not used for analysis because a larger area than that taken up by the subject was filmed.

B. Error Analysis

The error involved in the analysed data of hammer throwing was classified as systematic error or random error.

Systematic error was the error inherent in the use of the DLT method. The main sources of this error were: a) the least square method used to derive the calibration coefficients; b) the limited precision of measurement of the CP's spatial coordinates and c) the digitizing error of these points. Another source of systematic error was the anthropometric data used for the length, mass and moments of inertia of the segments. The criterion for the estimation of the systematic error was the RMS difference of the measured versus simulated coordinates of the CP. This error was found to be $RMS(X) = 0.24$ cm., $RMS(Y) = 0.19$ cm. and $RMS(Z) = 0.25$ cm..

Random error was defined as the error mainly created by the researcher's inability to detect the exact location of points in the digitizing process. Other sources of this error were vibration of the cameras in the filming process and vibration of the projector and digitizer in the digitizing process. This error was estimated by redigitizing seven randomly selected frames. The RMS differences of all the points from the two digitizings were found to be $RMS(X) = 1.73 \text{ cm.}$, $RMS(Y) = 0.64 \text{ cm.}$, $RMS(Z) = 0.62 \text{ cm.}$. The differences were higher for poorly detected points and smaller for well detected points. The absolute differences of the two digitizings for the right hip (poorly detected point) and the hammer (well detected point) for the seven frames are presented in Table 8.

TABLE 8

ABSOLUTE DIFFERENCES OF TWO DIGITIZINGS

FOR THE RIGHT HIP AND THE HAMMER

	RIGHT HIP			HAMMER		
	X	Y	Z	X	Y	Z
FRAME #1	3.41	1.91	0.97	1.57	0.06	0.30
FRAME #2	3.34	0.16	0.68	0.28	0.17	0.28
FRAME #3	0.66	0.47	1.81	0.55	0.08	0.10
FRAME #4	1.04	0.46	1.86	0.01	0.00	0.10
FRAME #5	2.52	2.05	0.48	0.20	0.15	0.81
FRAME #6	2.56	1.05	0.17	0.76	0.95	0.22
FRAME #7	0.48	1.69	0.48	1.84	0.67	0.23

(presented measurements in centimeters)

It should be noted here that the X, Y, Z-axes presented in the above tests were the axes before the rotation, therefore the X-axis of the tests is the axis of the direction of the throw in the analyzed data.

Digital filters were used for the reduction of error in the data. The cut off frequency used was $F_c = 9$ Hz. for the hammer kinematics and $F_c = 6$ Hz. for all other parameters. This decision was based on study of the power spectra plots of the signal. Figures 5 and 6, are two examples of these plots for the X-axis of the hammer and the right hip points. An example of raw versus filtered data can be seen in Figure 7 which shows the acceleration of the hammer. This acceleration was calculated with first central differences from raw data and data filtered with cut off frequency $F_c = 9$ Hz.

C. Kinematics and Kinetics of the Hammer.

The analyzed throws were (a) a three turn throw of 81.66 m. (Subject 1); (b) a four turn throw of 79.44 m. (Subject 2); and (c) a four turn throw of 78.66 m. (Subject 3). Each turn was divided into single support phase and double support phase. The beginning of the single support phase (BSS) and the beginning of the double support phase (BDS) for each turn were used as reference instances for the analysis and presentation of data. Other reference instances for each turn were the times when the hammer reached the highest (MAX-Z) and the lowest (MIN-Z) points of its orbit.

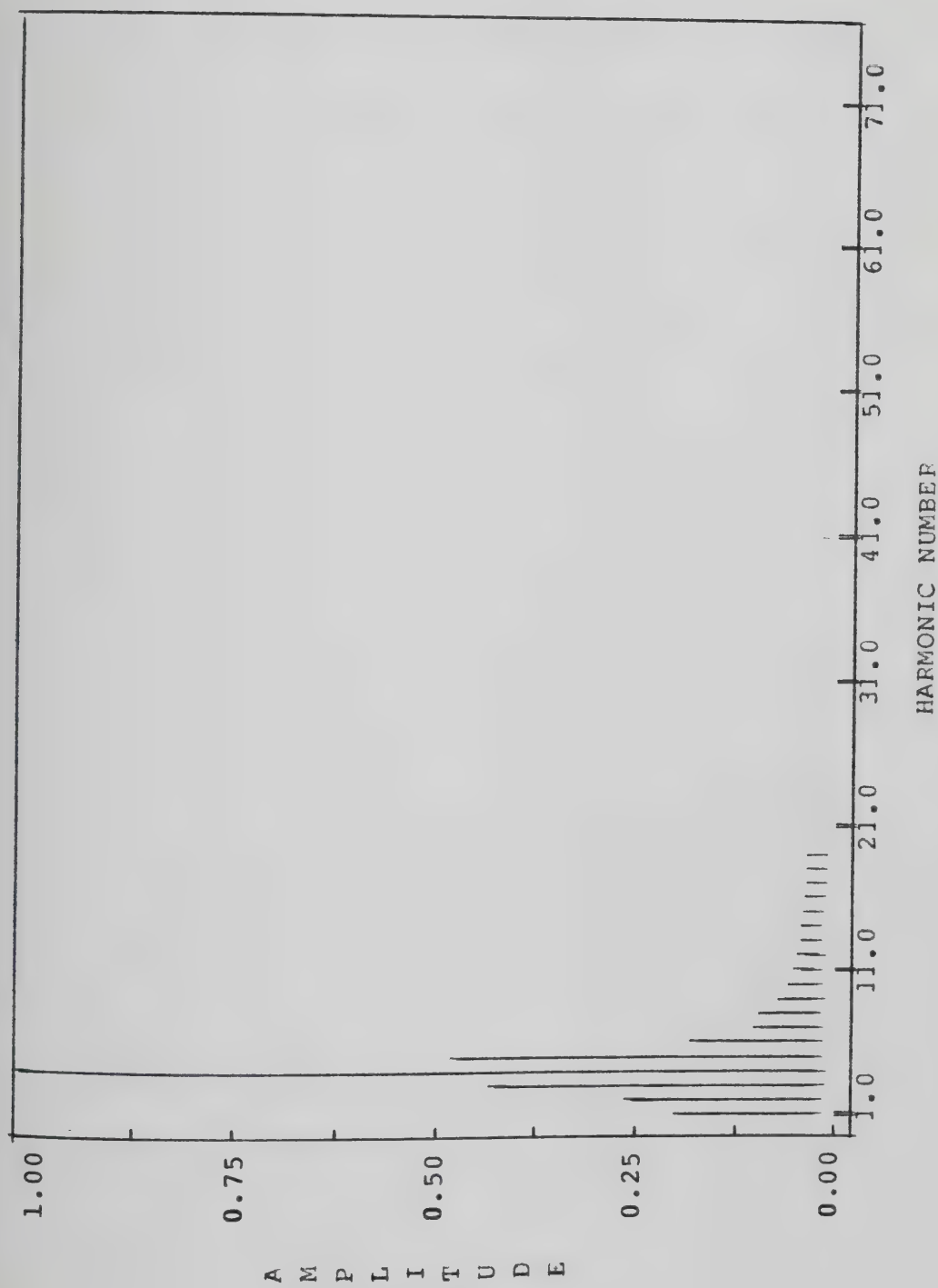


Figure 5: Power Spectra of the Hammer (X-Axis), Subject 1

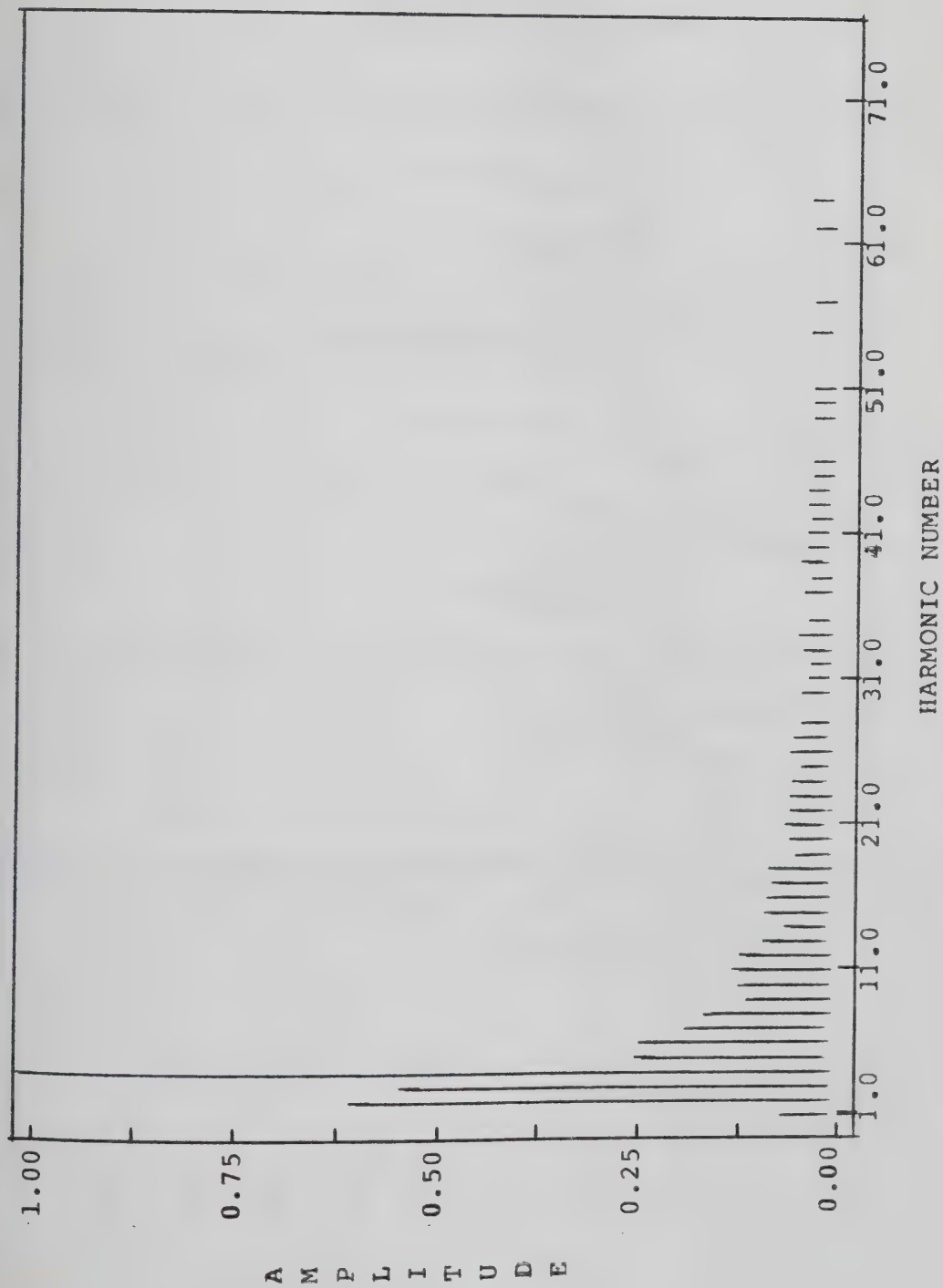


Figure 6: Power Spectra of the Right Hip (X-Axis), Subject 1

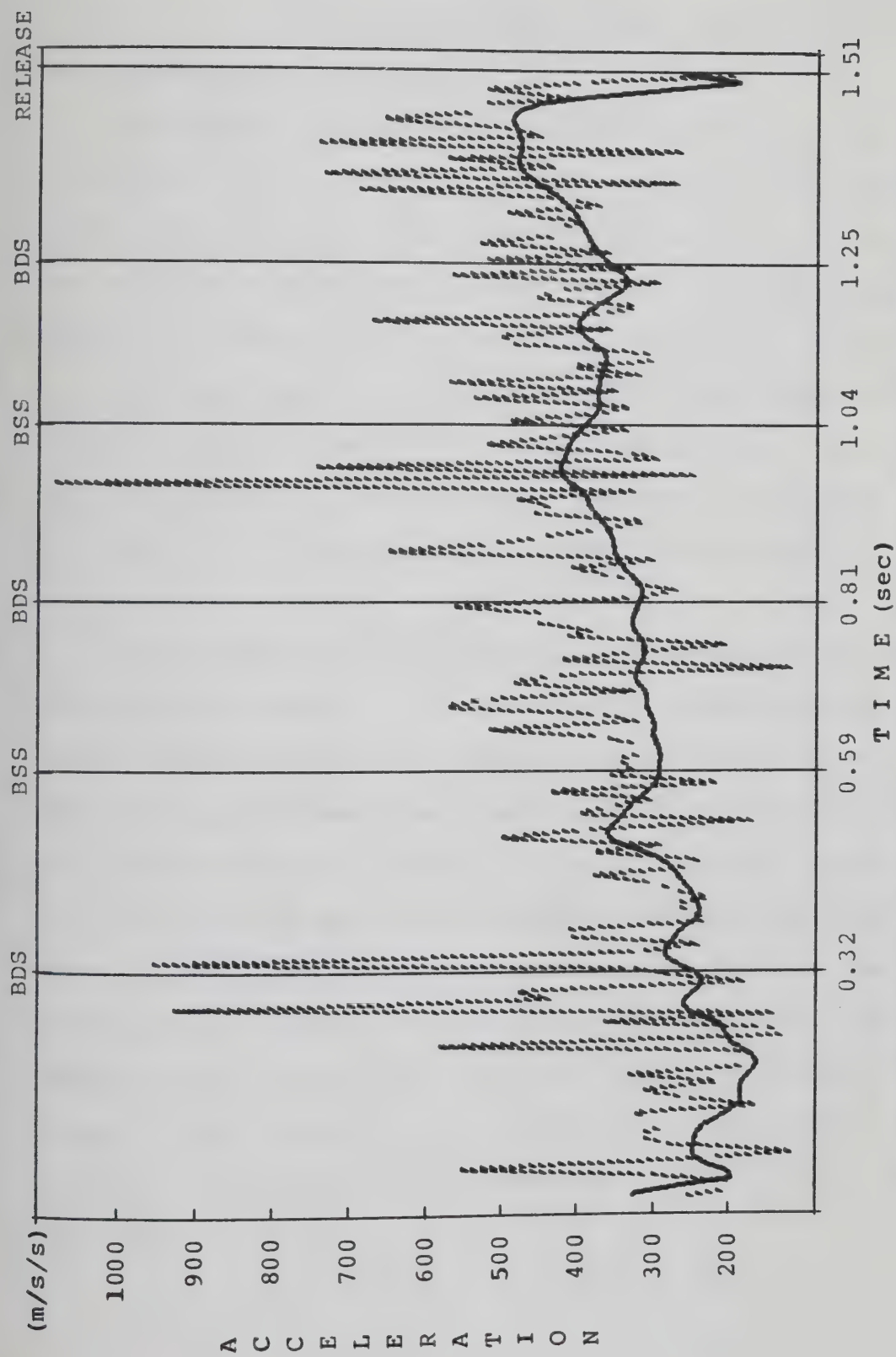


Figure 7: Acceleration of the Hammer, Raw and Filtered Data, Subject 1

The analysis of each throw started at the beginning of the first turn. No analysis was made of the preliminary swings of the hammer.

The height and angle of release were found to be 1.27 m. and 40.7° for Subject 1, 1.26 m. and 37.3° for Subject 2 and 1.28 m. and 37.6° for Subject 3. The angles of release for all the subjects were less than the calculated optimal angle of release which for an 80 m. throw was $\theta \cong 44.3^\circ$.

The maximum velocity of the hammer was found to be 30.99 m/s for Subject 1, 30.72 m/s for Subject 2 and 31.02 m/s for Subject 3. The maximum velocity of the hammer occurred 10 to 20 milliseconds before release for all subjects.

The timing of each throw and reference instance are presented in Table 9. In each turn the hammer reached the MAX-Z point in the single support phase and the MIN-Z in the double support phase. The time of the single support phase was shorter than the time of the double support phase for all the subjects and all the phases. Subject 3 had the fastest turn time for each turn. The same subject spent less time than the others in driving the hammer upward during the double support phase 22%, 27%, 24%, 38% of the double support time for each turn. The equivalent percentages for Subject 1 were 29%, 30%, 46% and for Subject 2, 31%, 32%, 29%, 39%.

TABLE 9TIMING OF EACH REFERENCE INSTANCE

Point	Subject 1	Subject 2	Subject 3
MAX-Z	----	0.29	0.18
BDS	----	0.41	0.24
MIN-Z	----	0.68	0.49
BSS	----	0.80	0.56
MAX-Z	0.23	0.98	0.75
BDS	0.32	1.07	0.79
MIN-Z	0.51	1.22	0.98
BSS	0.59	1.29	1.05
MAX-Z	0.75	1.45	1.20
BDS	0.81	1.52	1.25
MIN-Z	0.97	1.67	1.41
BSS	1.04	1.73	1.46
MAX-Z	1.18	1.88	1.63
BDS	1.25	1.95	1.67
MIN-Z	1.39	2.09	1.83
RELEASE	1.51	2.18	1.91

(presented measurements in seconds)

The spatial coordinates of the hammer for the different subjects showed that the hammer traveled in a spiral mode starting at an acute angle to the horizontal and finishing with the release angle. In the first turn Subject 2 rotated the hammer in a plane closer to the horizontal i.e. at a more acute angle than the other subjects and gradually changed this angle to the release angle. Figures 8, 9 and 10 present the trajectory of the hammer in the different planes for Subject 3.

The radius of curvature of the hammer for each of the three subjects can be seen in Figures 11, 12 and 13. The length of the radii oscillated from phase to phase and

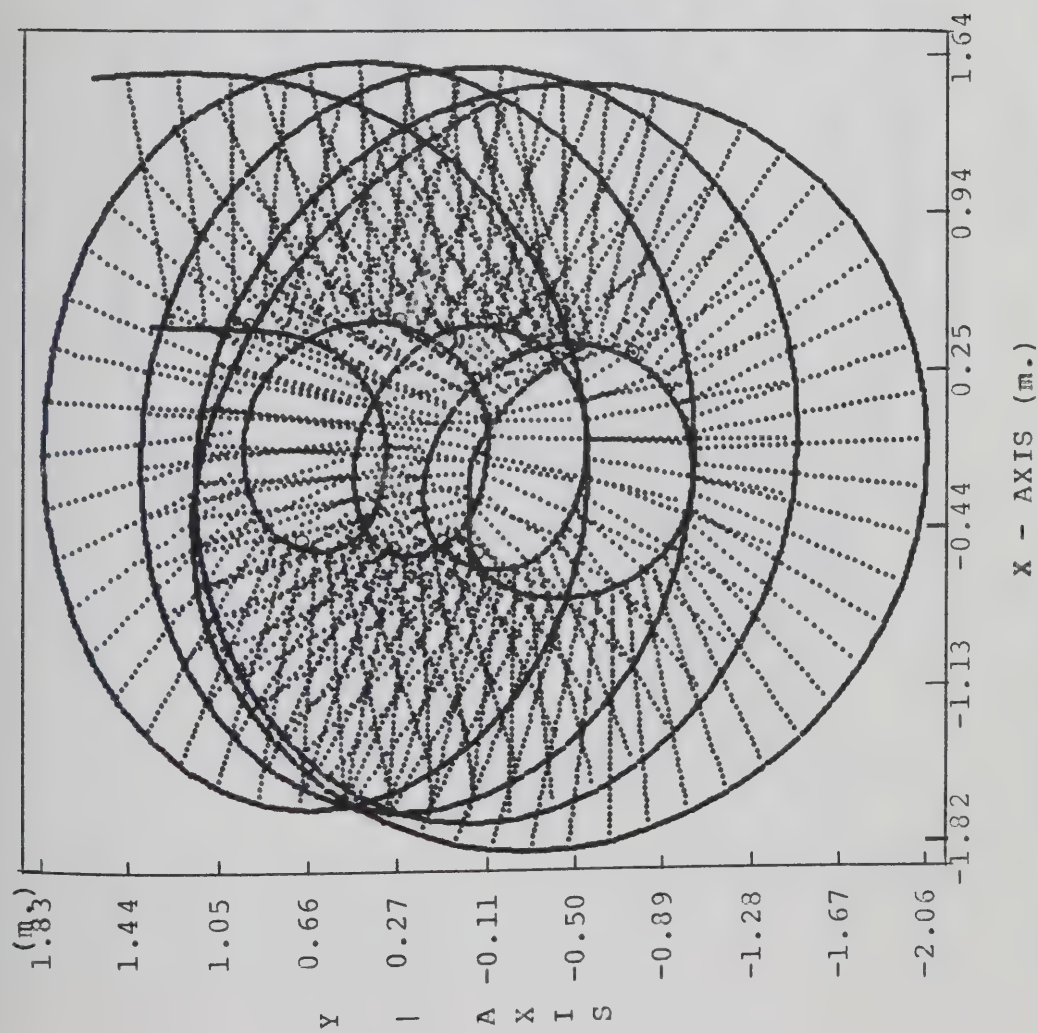


Figure 8: Trajectory of the Hammer in the X-Y Plane, Subject 3

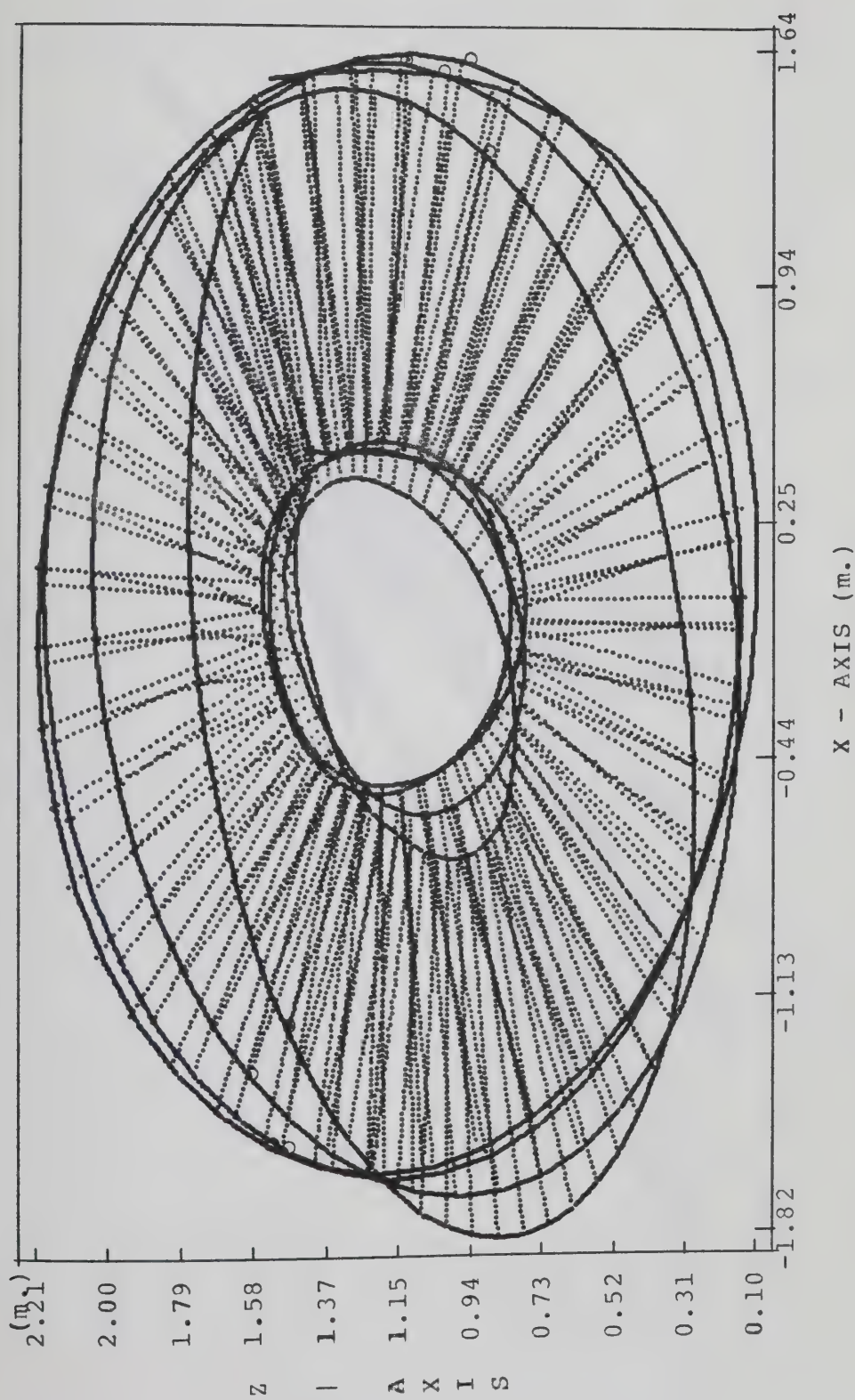


Figure 9: Trajectory of the Hammer in the X-Z Plane, Subject 3

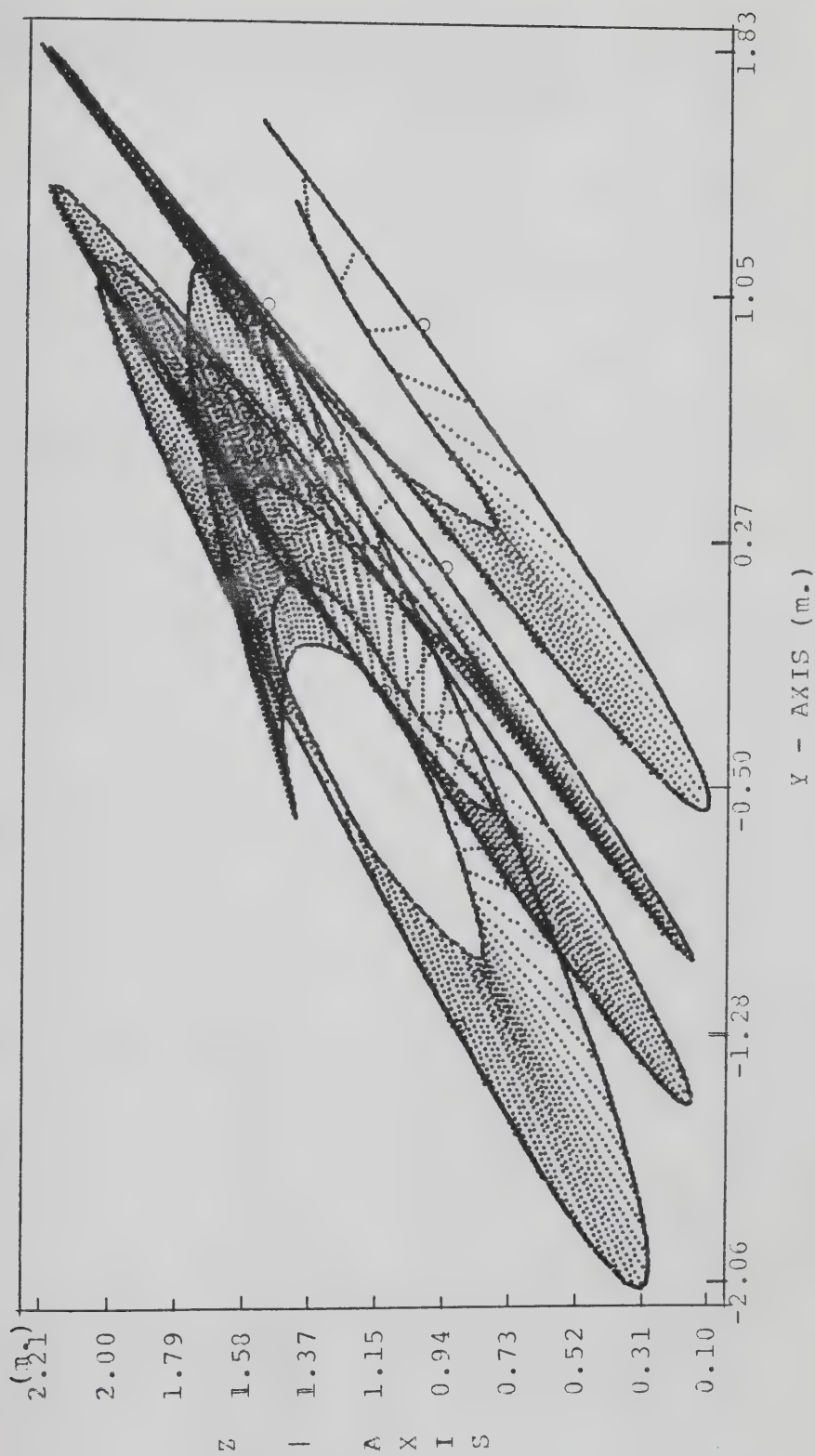
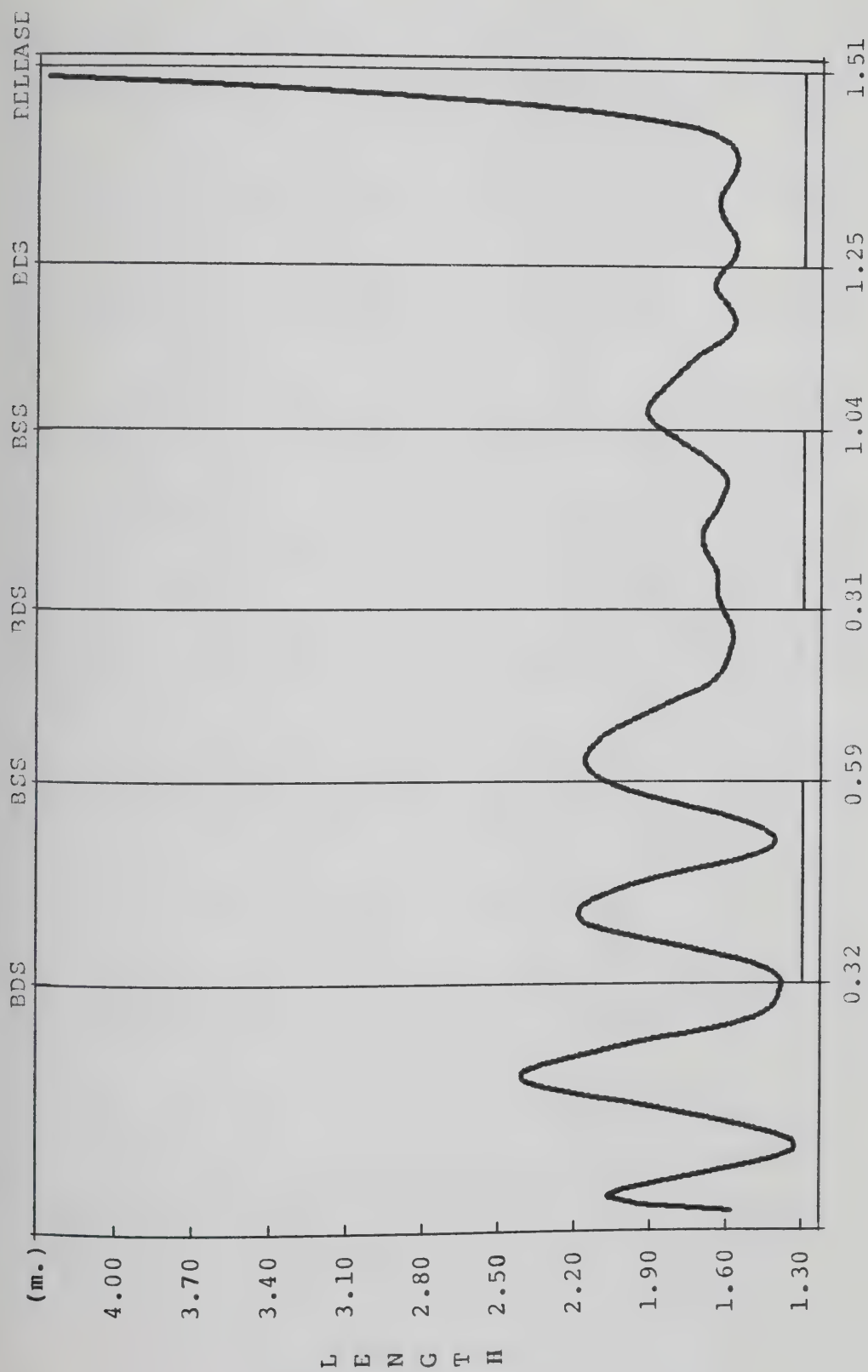
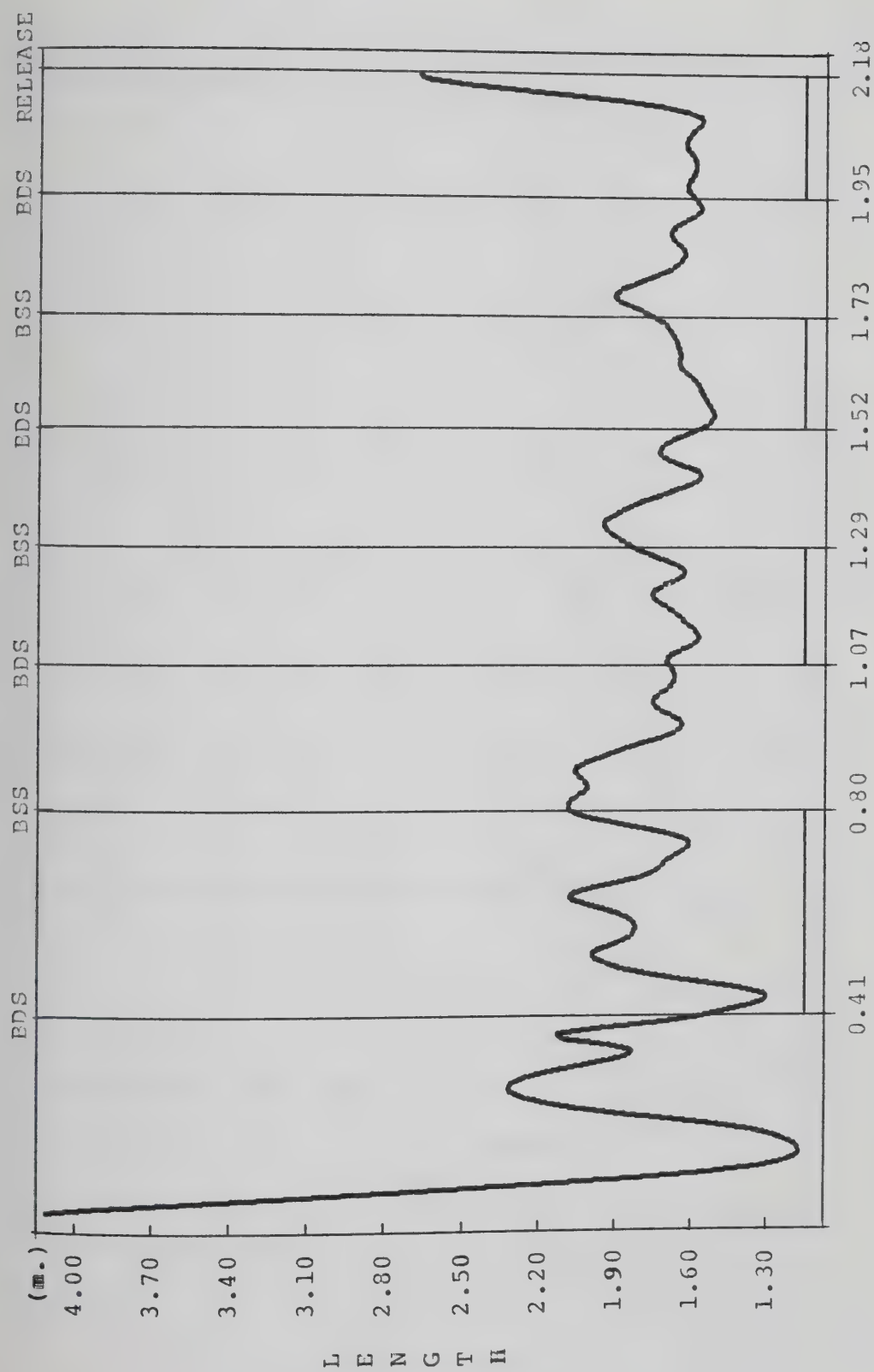


Figure 10: Trajectory of the Hammer in the Y-Z Plane, Subject 3



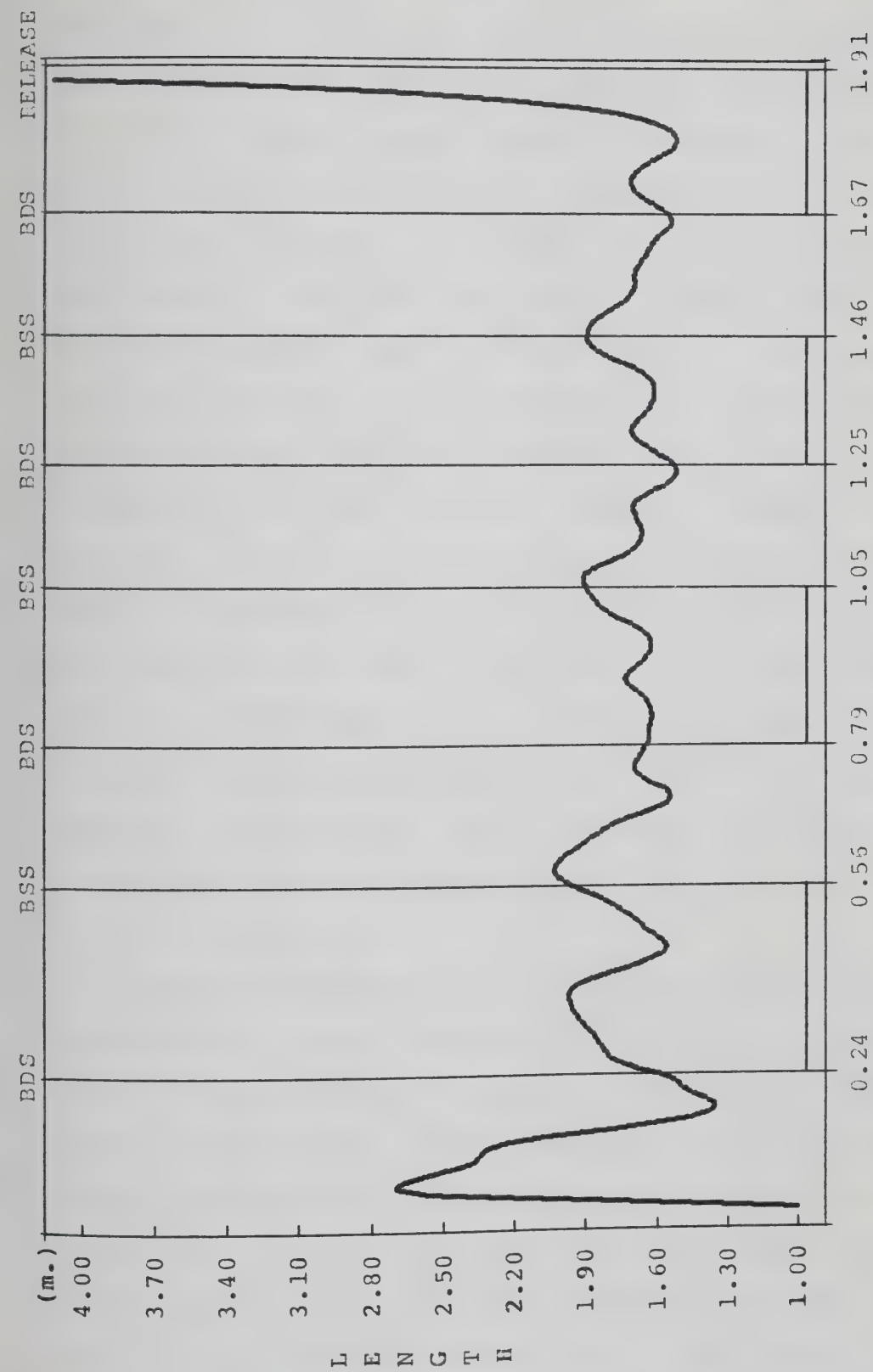
BDS=BEGINNING OF DOUBLE SUPPORT, BSS=BEGINNING OF SINGLE SUPPORT

Figure 11: Radius of Curvature of the Hammer, Subject 1



BDS=BEGINNING OF DOUBLE SUPPORT, BSS=BEGINNING OF SINGLE SUPPORT

Figure 12: Radius of Curvature of the Hammer, Subject 2

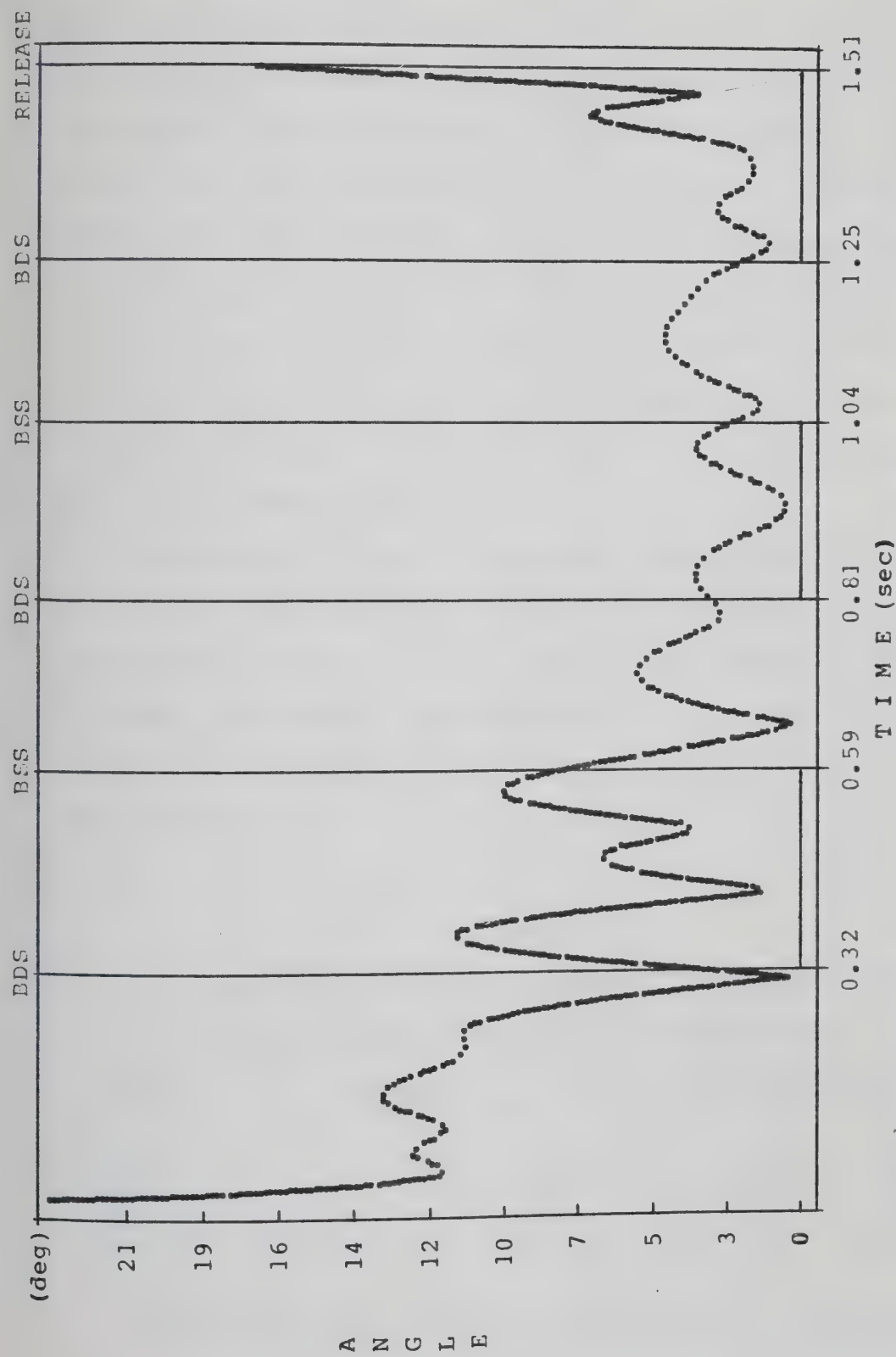


BDS=BEGINNING OF DOUBLE SUPPORT, BSS=BEGINNING OF SINGLE SUPPORT

Figure 13: Radius of Curvature of the Hammer, Subject 3

within the same phase. There was a gradual decrease of the amplitude of oscillation from turn to turn. For each turn the length of the radii became maximum at the beginning of the single support phase, gradually decreased during the single support phase and began increasing again in the double support phase. In the last turn, and after the radii had fallen to their minimum length, the amplitude of oscillation became very small for Subject 1 and 2. Subject 3 increased the radius after the BDS point and decreased it to a minimum length when the hammer was at the MIN-Z point. In comparison with other subjects, Subject 1 presented the smoothest oscillations with the highest amplitude, while Subject 2 presented the noisiest oscillations and Subject 3 the smallest amplitude. In the last double support phase, after the hammer passed from the MIN-Z, the radii's length increased and approached infinity at the release point for Subjects 1 and 3, while Subject 2 released the hammer before it started traveling in a straight line (i.e. with low length of radius).

The angle between the radius of curvature of the hammer and the cable for all the subjects ranged from 0° to 13° . Figure 14 represents the change of this angle for Subject 1, while Subjects 2 and 3 showed similar curves. This angle was greater in the first turn and decreased gradually until the second from the last turn, then increased again. During the single support phases the angle started with a small value and increased until the middle point of the phase. Before



BDS=BEGINNING OF DOUBLE SUPPORT, BSS=BEGINNING OF SINGLE SUPPORT

Figure 14: Angle of Radius of Curvature with Cable of Hammer, Subject 1

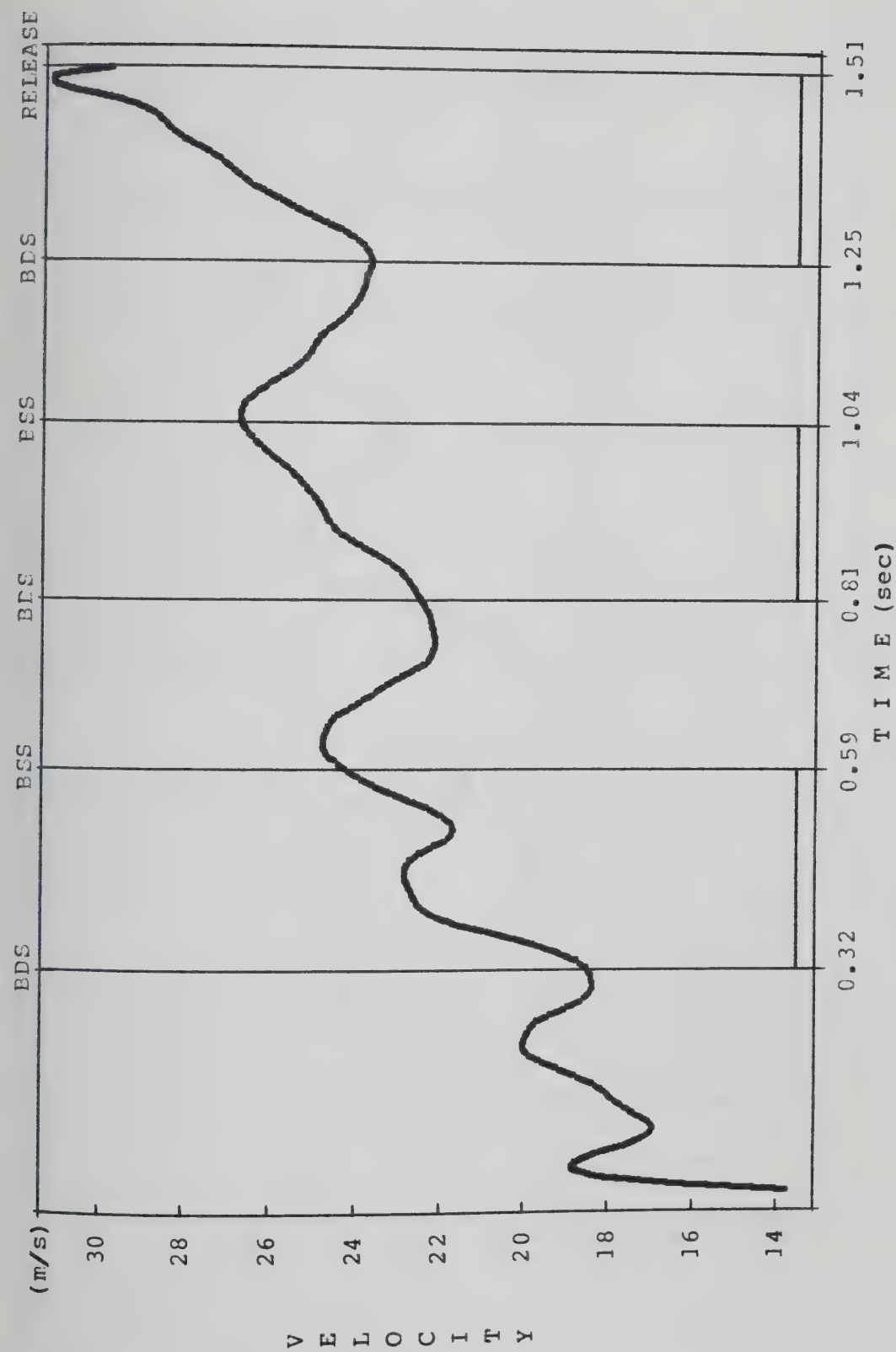
the hammer arrived at its MAX-Z point the angle started decreasing again arriving at a minimum at the end of the single support phase. In the double support phases the angle decreased from the beginning to the middle point of the phase and then increased again. In the last two turns and during the transition from double to single support and from single to double support the angle decreased. In the last turn the angle started increasing after the MIN-Z point arrived to a maximum angle then decreased until ≈ 40 milliseconds before the release and started increasing again until the release point.

Figures 15, 16 and 17 represent the velocity curves of the hammer. The velocity increased in the double support phases and decreased in the single support phases. There was a gradual increase of velocity from turn to turn. The contribution of each turn to the maximum velocity can be seen in Table 10.

TABLE 10
CONTRIBUTION OF EACH TURN TO THE MAXIMUM
VELOCITY AND ACCELERATION OF THE HAMMER

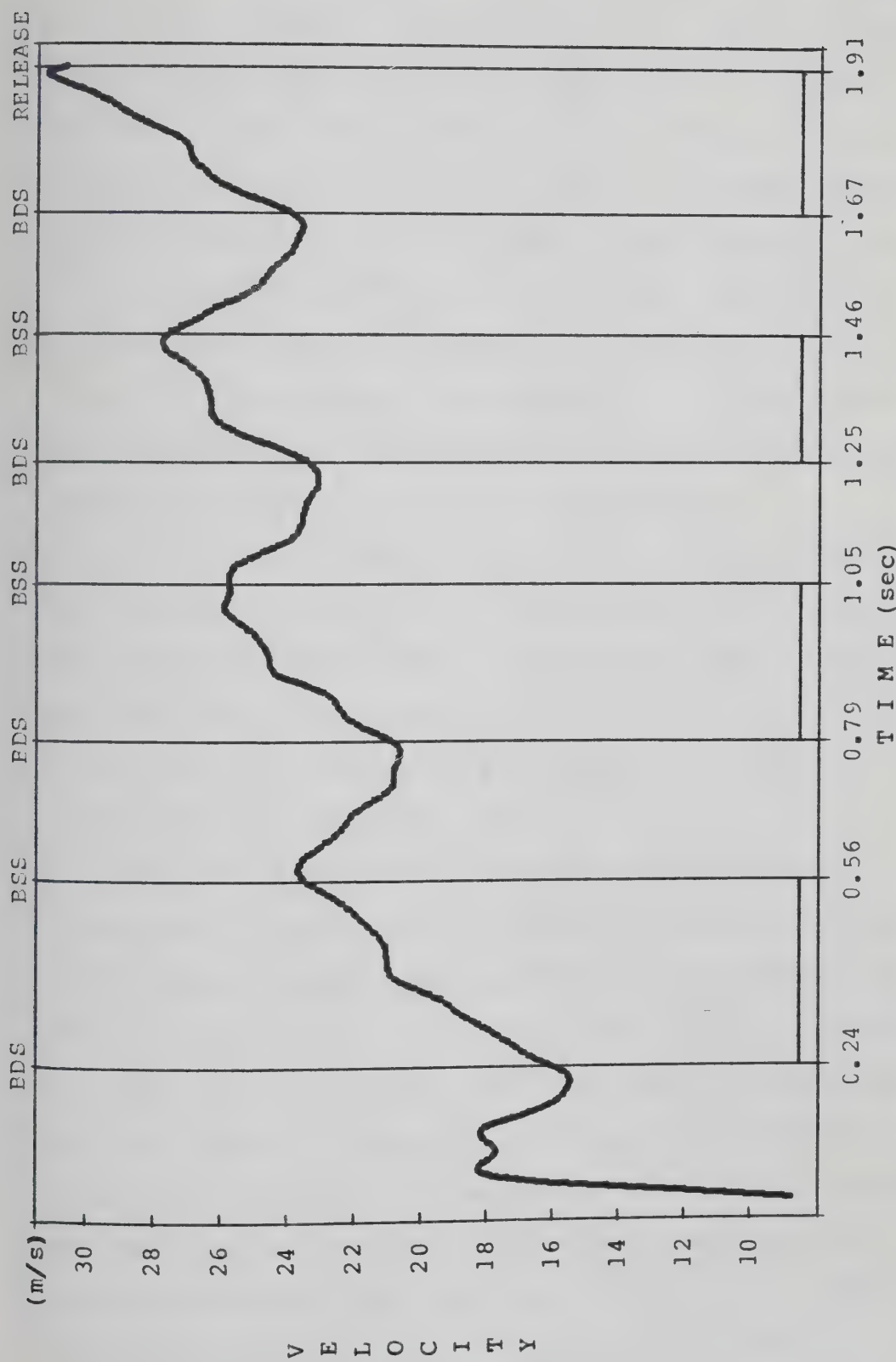
<u>TURN</u>	<u>VELOCITY</u>			<u>ACCELERATION</u>		
	S.1	S.2	S.3	S.1	S.2	S.3
First	--	69	76	--	56	61
Second	79	80	83	73	77	80
Third	86	86	89	86	80	89
Fourth	100	100	100	100	100	100

(presented measurements in percentage of maximum)



BDS=BEGINNING OF DOUBLE SUPPORT, BSS=BEGINNING OF SINGLE SUPPORT

Figure 15: Linear Velocity of the Hammer, Subject 1



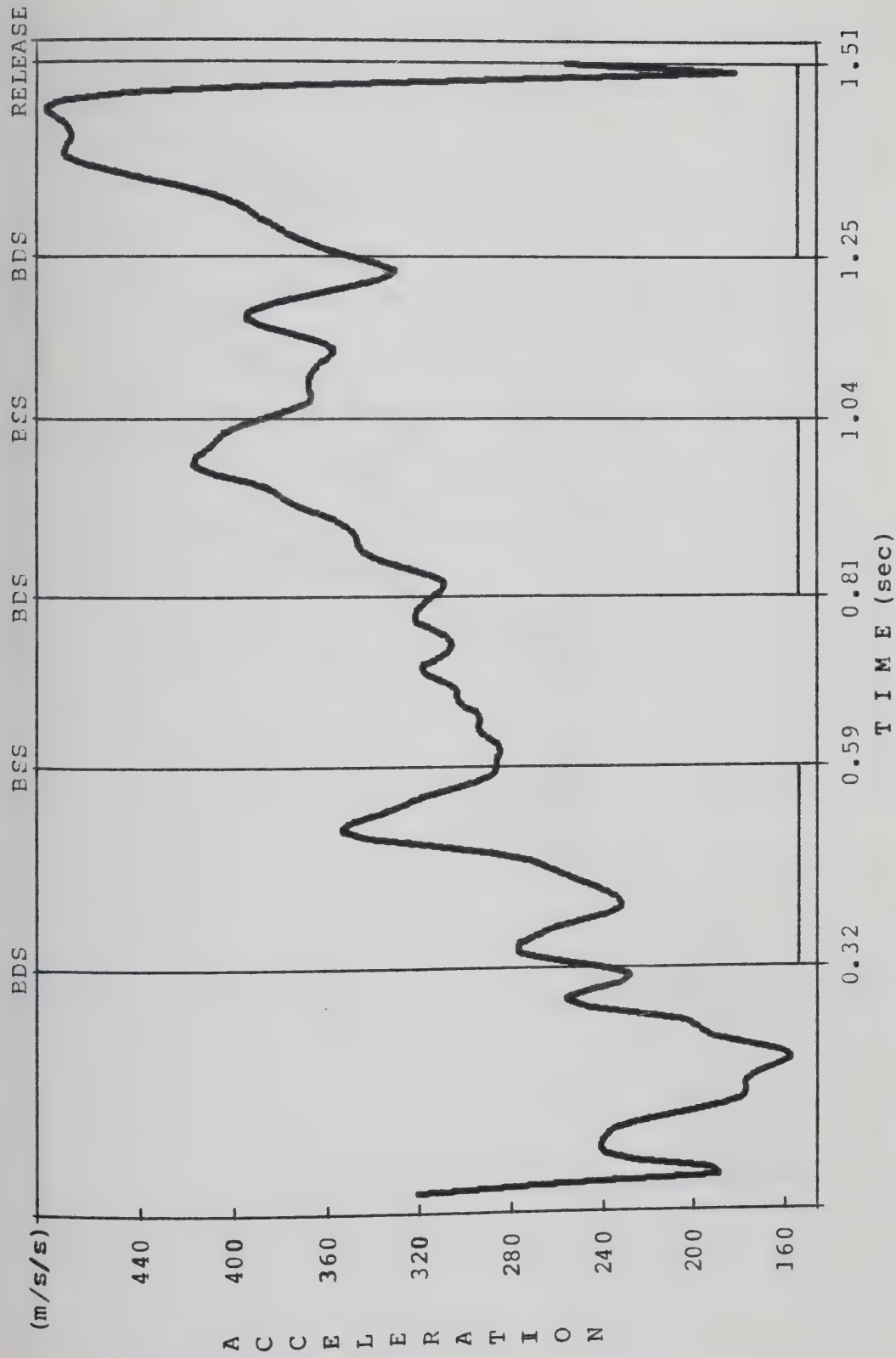
BDS=BEGINNING OF DOUBLE SUPPORT, BSS=BEGINNING OF SINGLE SUPPORT

Figure 17: Linear Velocity of the Hammer, Subject 3

There was a local minimum velocity at the BDS point in each turn, except in the second turn of Subjects 1 and 2 who achieved the local minimum velocity before that point (Figures 15 and 16). In each turn the hammer reached its local maximum velocity at the end of the double support phase and beginning of the single support phase. In the first single support phase the velocity curves showed great oscillations, probably caused by the athletes' effort to achieve a high velocity immediately. It was the velocity in the Y and Z axes which primarily contributed to the local maximum velocity of the hammer in each turn.

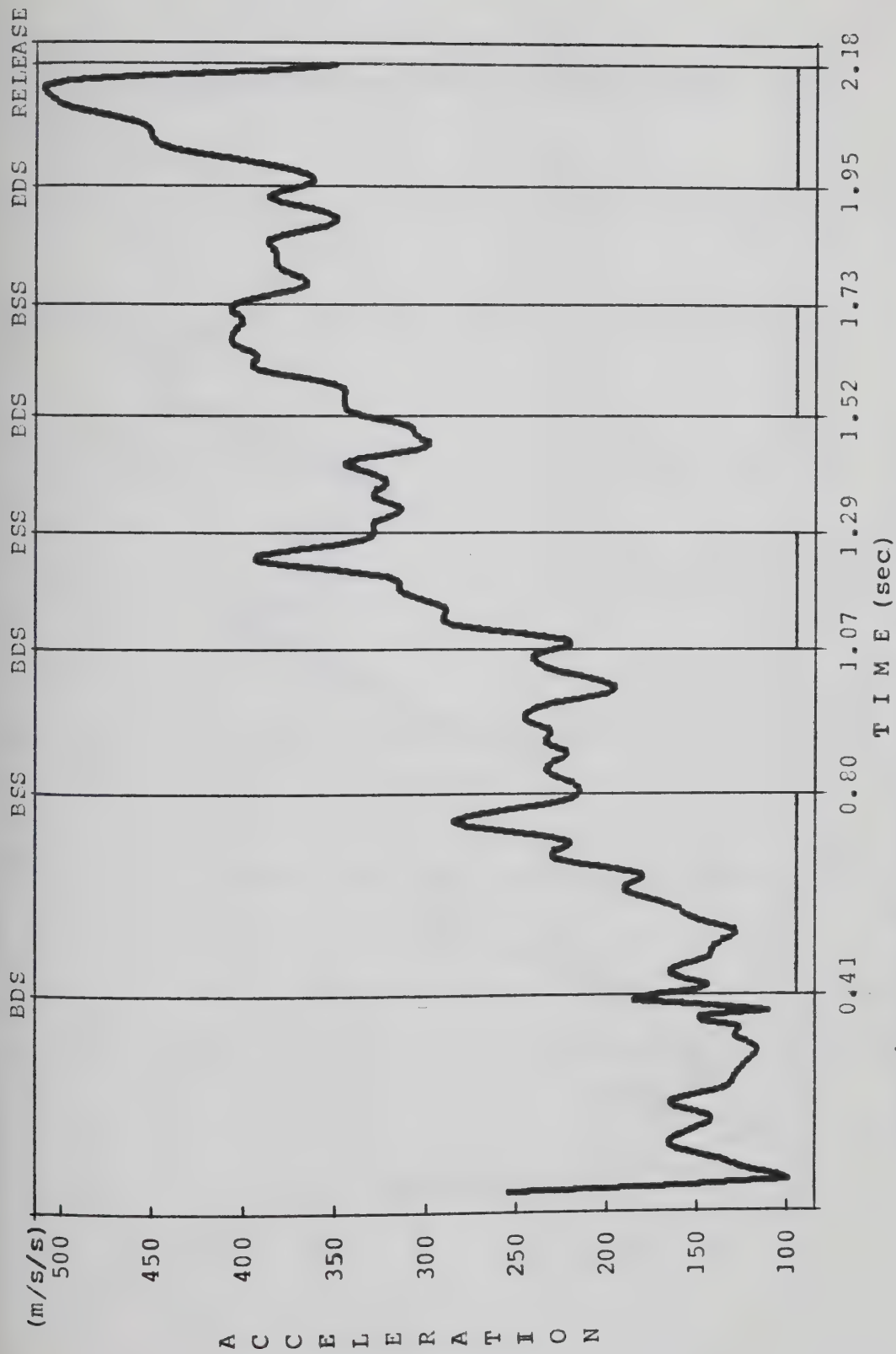
In the single support phases for all the subjects and for all but the first turn, the decrease in velocity was calculated in percentage of the maximum velocity. This decrease was found to be: 6%, 10% in each turn for Subject 1, 6%, 7%, 7% in each turn for Subject 2 and 8%, 7%, 12% in each turn for Subject 3.

The accelerations of the hammer for all subjects are presented in Figures 18, 19 and 20. The hammer accelerated in the double support phase and there was a gradual increase from turn to turn for each throw. The highest acceleration for each turn occurred at the time when the hammer reached the MIN-Z point of its orbit. The maximum acceleration was found to be 478 m/s^2 for Subject 1, 505 m/s^2 for Subject 2 and 492 m/s^2 for Subject 3. This global maximum occurred 60 milliseconds after the local MIN-Z point of the hammer and 60 milliseconds before the release point for Subject 1. The



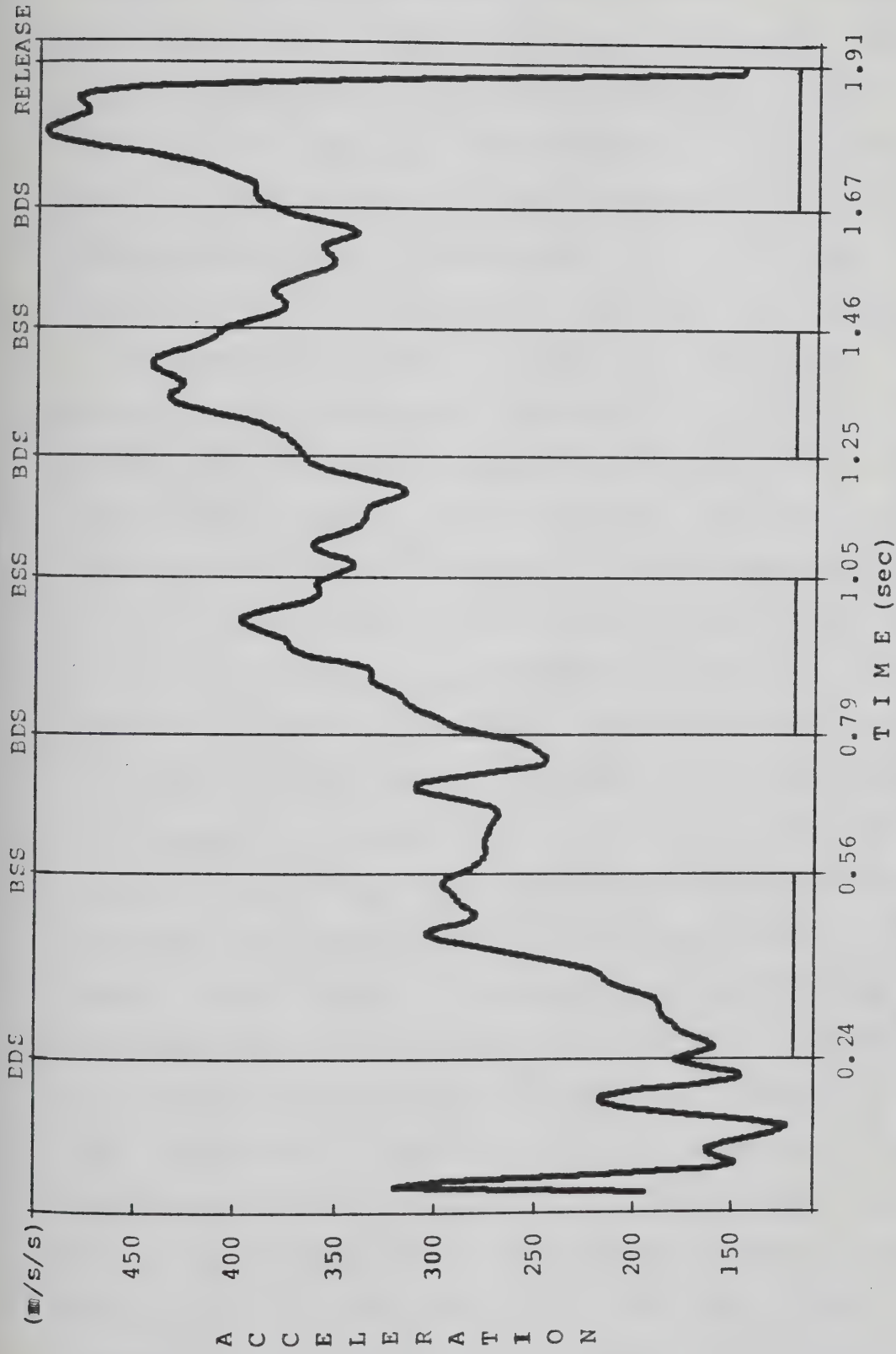
BDS=BEGINNING OF DOUBLE SUPPORT, BSS=BEGINNING OF SINGLE SUPPORT

Figure 18: Linear Acceleration of the Hammer, Subject 1



BDS=BEGINNING OF DOUBLE SUPPORT, BSS=BEGINNING OF SINGLE SUPPORT

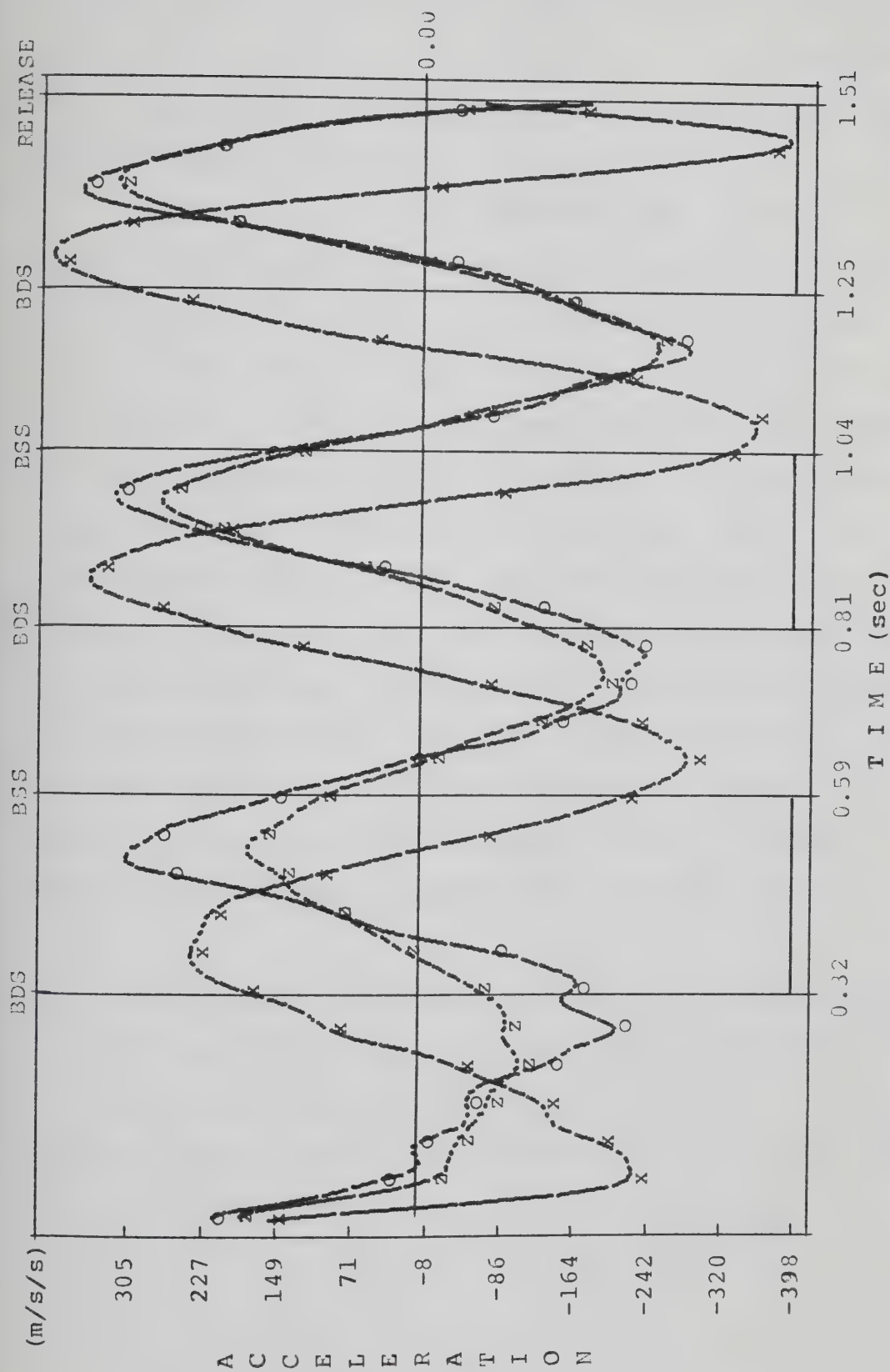
Figure 19: Linear Acceleration of the Hammer, Subject 2



BDS-BEGINNING OF DOUBLE SUPPORT, BSS-BEGINNING OF SINGLE SUPPORT

Figure 20: Linear Acceleration of the Hammer, Subject 3

equivalent times were 50 and 40 milliseconds for Subject 2 and 0 and 80 milliseconds for Subject 3. Subject 1 kept a high acceleration at the global maximum for a longer time than the other subjects, while Subject 3, after reaching the global maximum presented a second maximum of lower value approximately 50 milliseconds after the first peak. The contribution of each turn to the maximum acceleration for all subjects can be seen in Table 10. It was mainly the acceleration in the Y and Z-axes that contributed to the peaks of the resultant acceleration (Figure 21). In the single support phases the acceleration increased slightly, in the second turn for Subject 1, in the second and third turn for Subject 2 and in the third turn for Subject 3. In all the other single support phases the acceleration either remained the same or decreased. The accelerations presented different oscillations for the different subjects. Subject 1, increased the acceleration in the second single support phase, while, in the last single support the acceleration decreased until approximately 30 milliseconds before the hammer's MAX-Z. Then, it increased until the MAX-Z and when the hammer started traveling downwards to the BDS point the acceleration decreased again (Figure 18). Subject 2, in all the single support phases increased the acceleration from the BSS point until approximately 20 milliseconds before the MAX-Z. Then, he decreased the acceleration until the MAX-Z and increased it from there to the BDS point (Figure 19). Subject 3, in the second single support phase showed



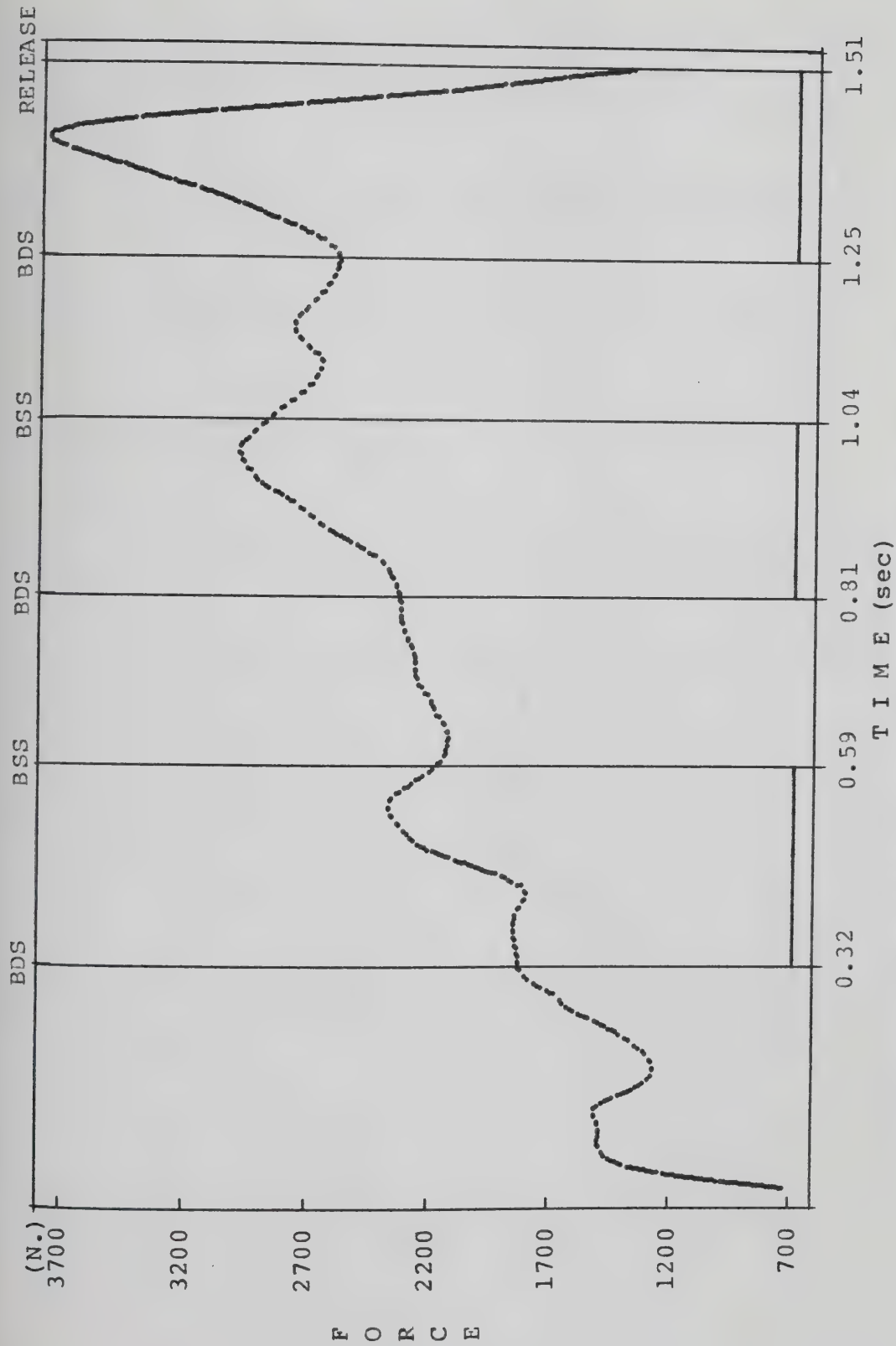
BDS=BEGINNING OF DOUBLE SUPPORT, BSS=BEGINNING OF SINGLE SUPPORT
X-AXIS(x), Y-AXIS(o), Z-AXIS(z)

Figure 21: Acceleration of the Hammer in the X, Y, Z Axes, Subject 1

opposite oscillations to the ones of Subject 2. In the last two turns he decreased the acceleration until approximately 10 milliseconds after the MAX-Z and increased from there to the BDS point (Figure 20).

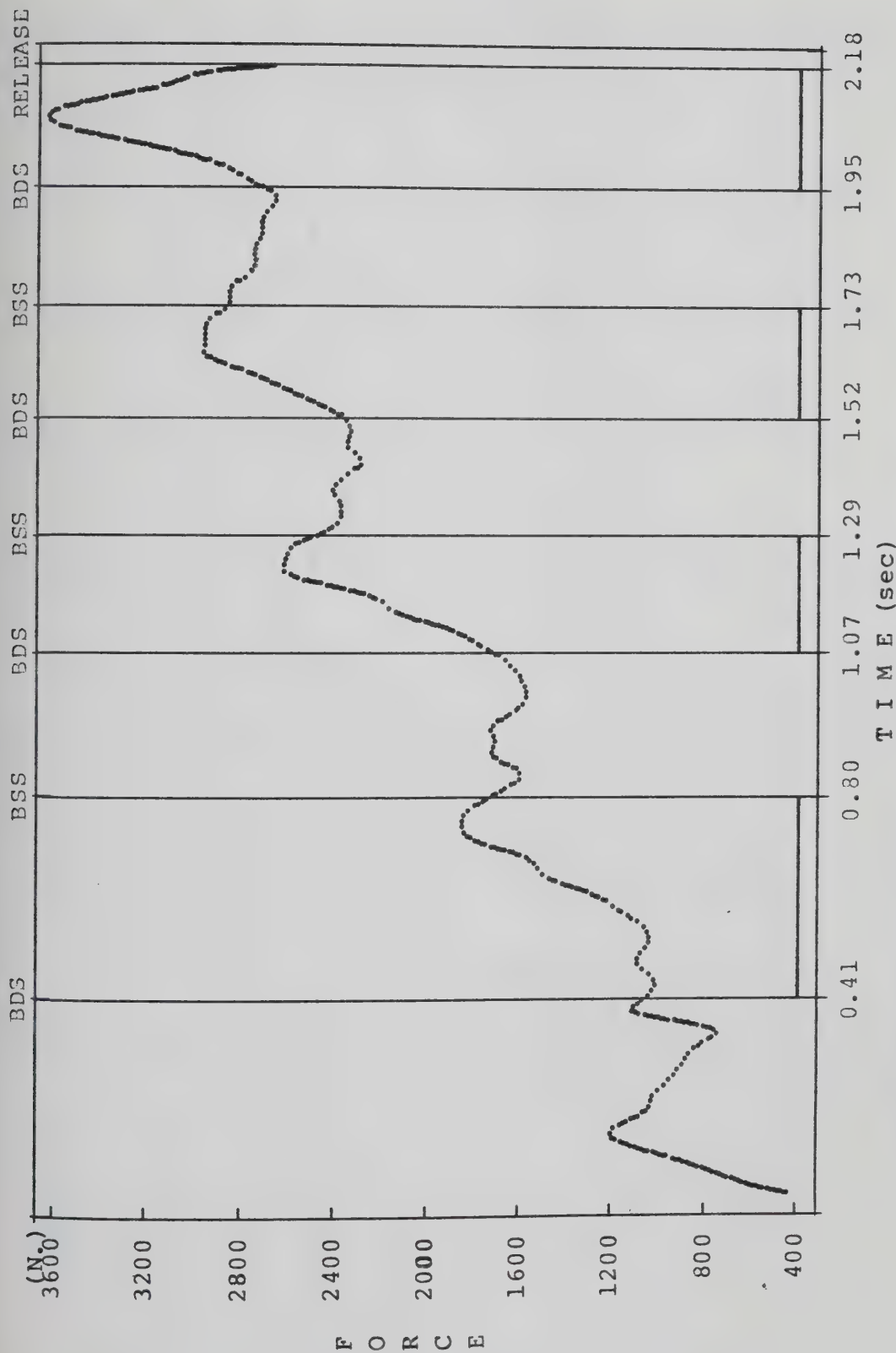
Figures 22, 23 and 24 represent the tension in the cable of the hammer calculated using equation (16). The tension was maximum when the hammer reached the lowest point of its orbit. This maximum tension was found to be 3730 N for Subject 1, 3602 N for Subject 2 and 3837 N for Subject 3. The contribution of each turn to the maximum tension was found to be 62%, 79% and 100% for Subject 1, 50%, 72%, 81% and 100% for Subject 2 and, 55%, 72%, 82% and 100% for Subject 3. For each turn the local maximum tension occurred in the double support phase. In the single support phase the tension decreased until the point where the hammer reached its MAX-Z and from that point the tension started increasing again. Only Subject 1 achieved an absolute increase of tension in the single support phase and only for the second turn.

The impulses applied to the hammer in different phases and for the different subjects are presented in Table 11. In the last double support phase Subject 1, applied a greater impulse than did the other subjects. This reflected the application of force over a longer period of time.



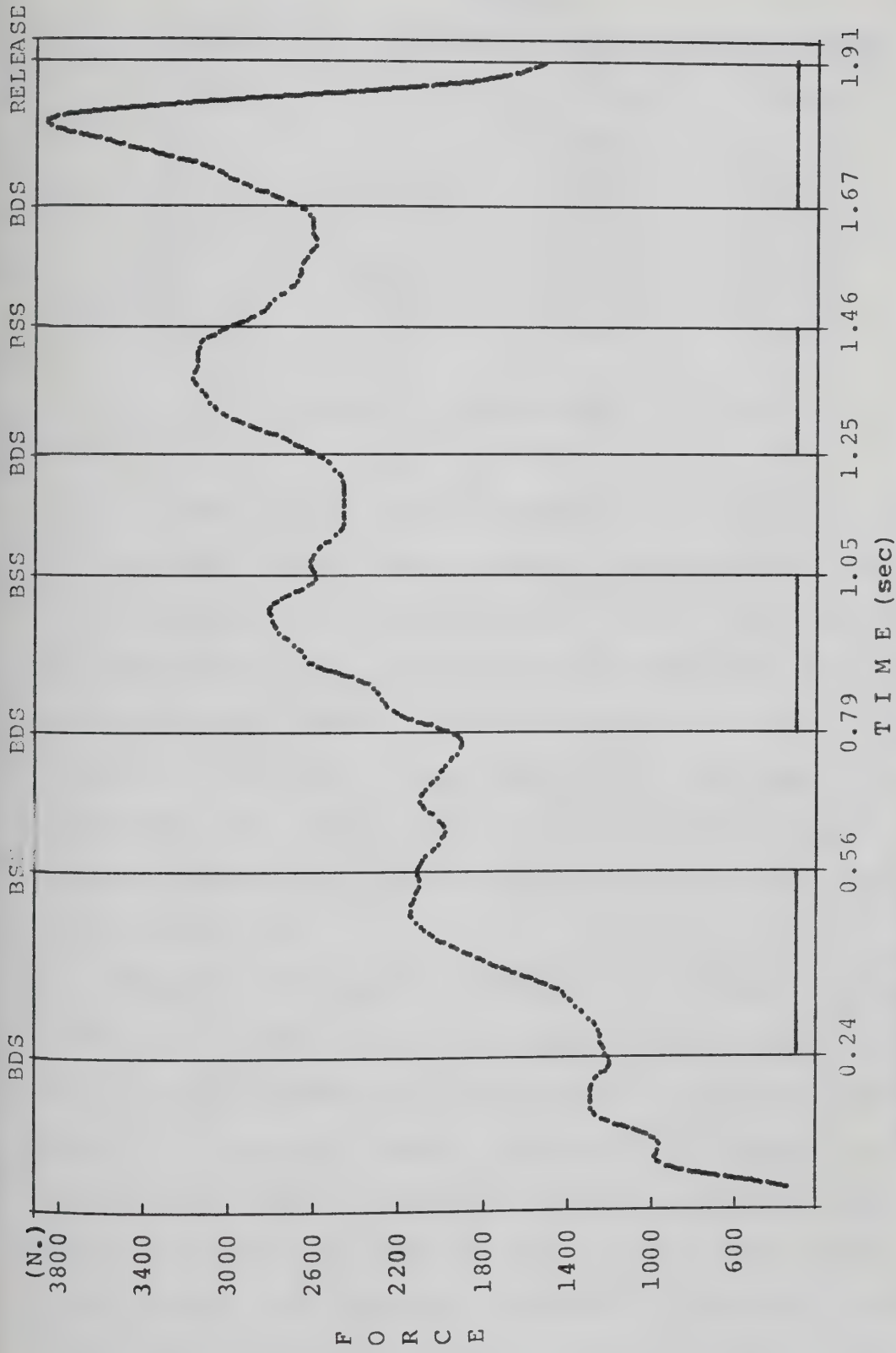
BDS=BEGINNING OF DOUBLE SUPPORT, BSS=BEGINNING OF SINGLE SUPPORT

Figure 22: Tension in the Cable of the Hammer, Subject 1



BDS=BEGINNING OF DOUBLE SUPPORT, BSS=BEGINNING OF SINGLE SUPPORT

Figure 23: Tension in the Cable of the Hammer, Subject 2



BDS=BEGINNING OF DOUBLE SUPPORT, BSS=BEGINNING OF SINGLE SUPPORT

Figure 24: Tension in the Cable of the Hammer, Subject 3

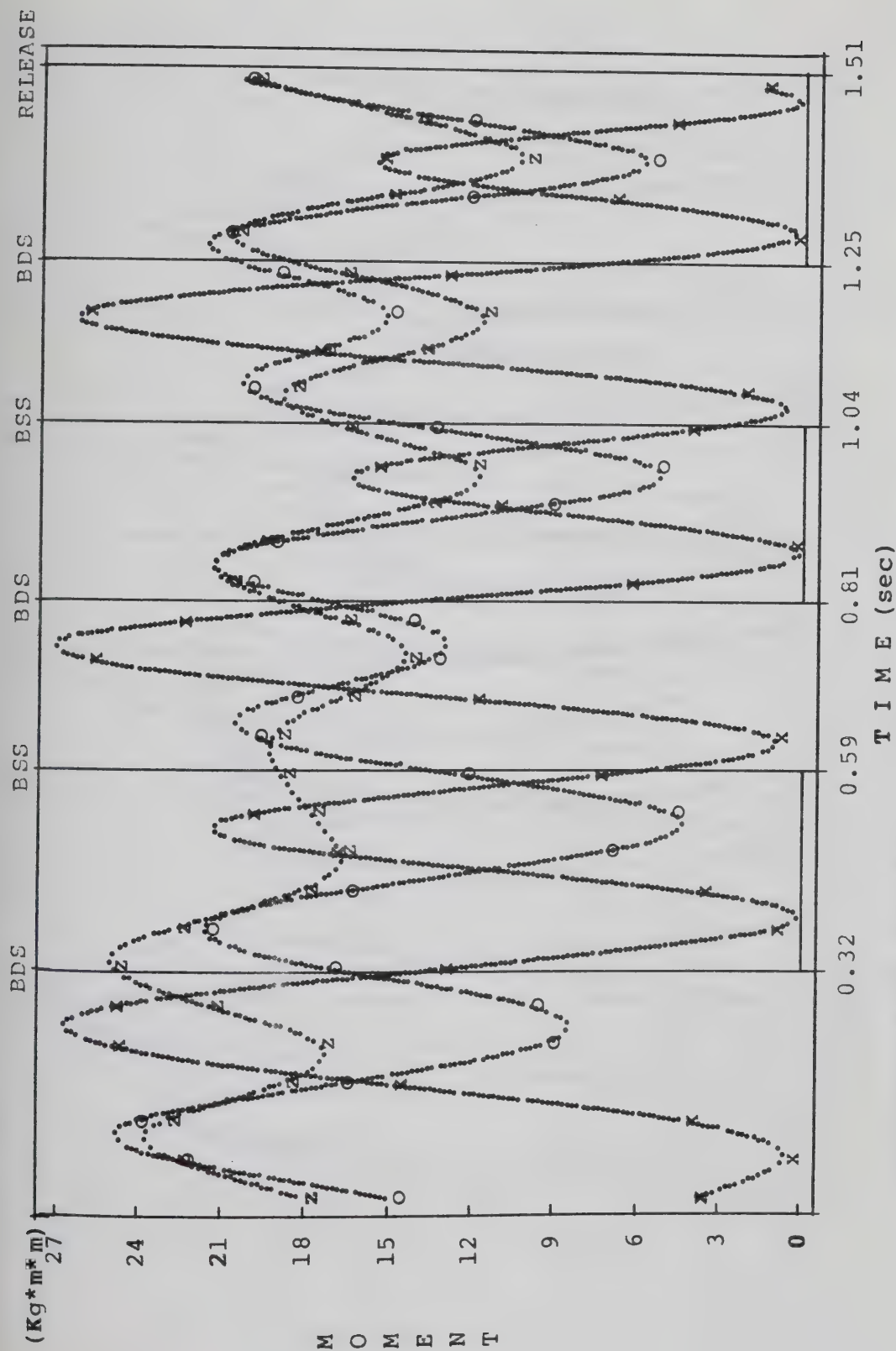
TABLE 11IMPULSE APPLIED UPON THE HAMMER FOR EACH PHASE

Phase	Subject 1	Subject 2	Subject 3
SS	-----	368.71	243.47
DS	-----	512.77	524.42
SS	419.01	439.07	454.73
DS	532.96	492.33	652.74
SS	484.44	510.67	497.06
DS	613.71	578.79	627.88
SS	556.73	598.18	433.49
DS	744.32	736.32	725.60

(presented measurements in N*s)

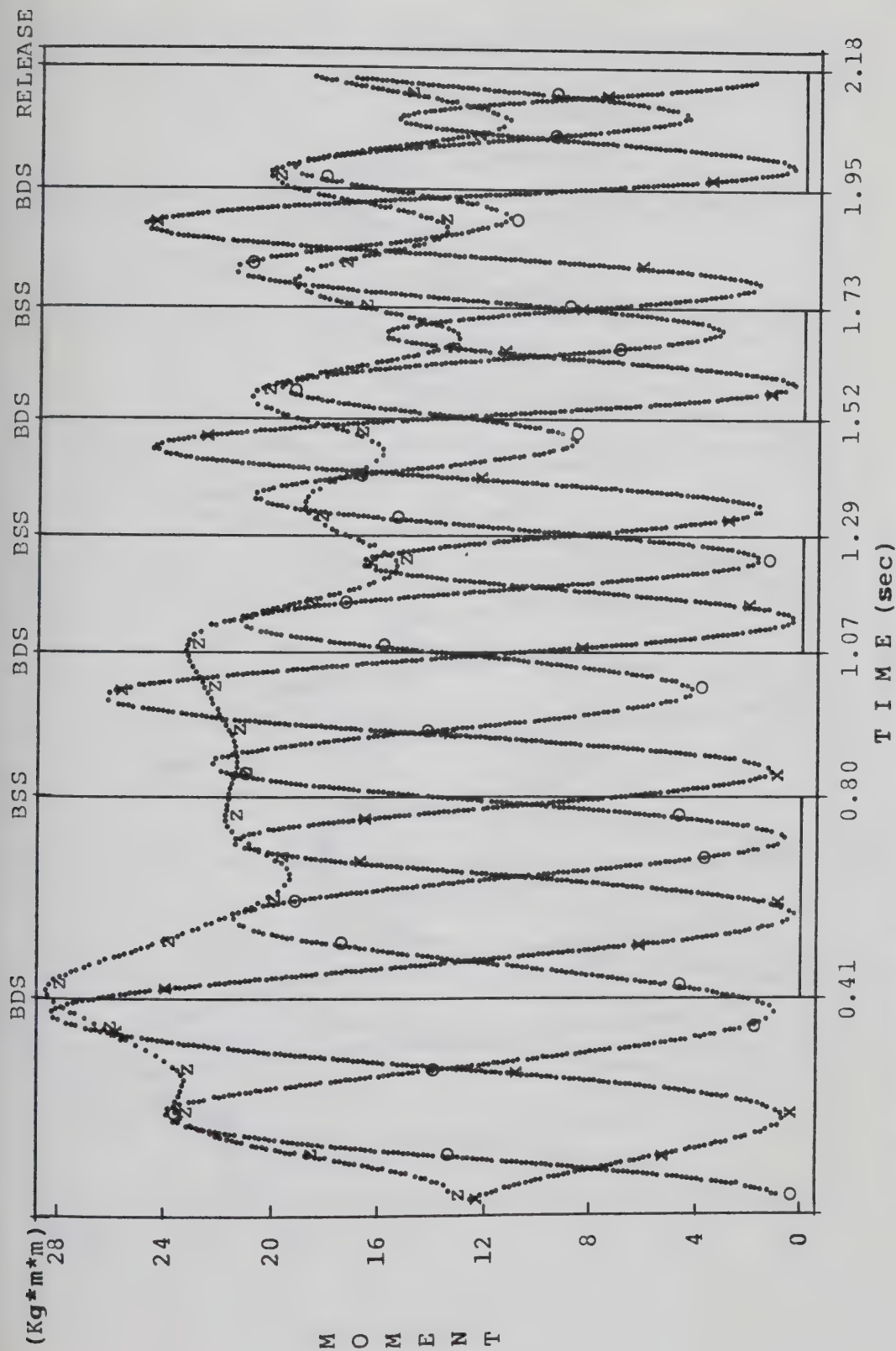
Figures 25, 26 and 27 represent the moments of inertia of the hammer about the orthogonal system of axes parallel to the inertial frame and passing through the center of mass of the system (CMs). In the first turn Subjects 2 and 3 achieved larger moment of inertia about the Z-axis than did Subject 1. This was because they rotated the hammer in a plane which was closer to the horizontal than to the vertical plane, with Subject 2 presenting an angle with the horizontal $\theta \cong 9^\circ$.

Figures 28, 29 and 30 represent the distance of the hammer to the CMs point. This distance increased in the single support phase and decreased in the double support phase. In the double support phase athletes pulled the hammer toward their CMs and in the single support phase the hammer traveled away from the CMs. In the first double support phase, the distance increased to the point where the hammer reached its MIN-Z, then it decreased again until the



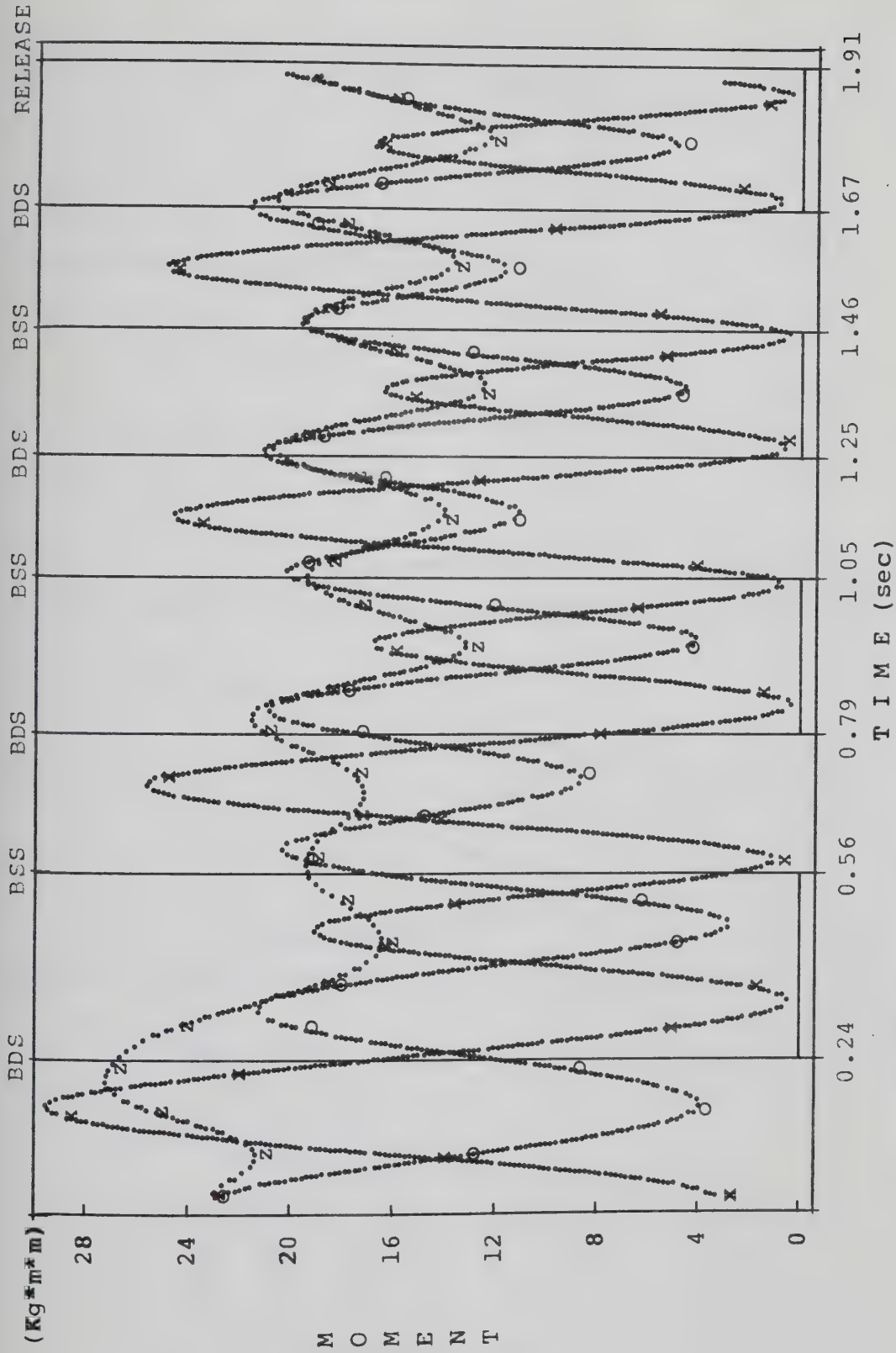
BDS-BEGINNING OF DOUBLE SUPPORT, BSS-BEGINNING OF SINGLE SUPPORT
X-AXIS(x), Y-AXIS(y), Z-AXIS(z)

Figure 25: Moments of Inertia of the Hammer, Subject 1



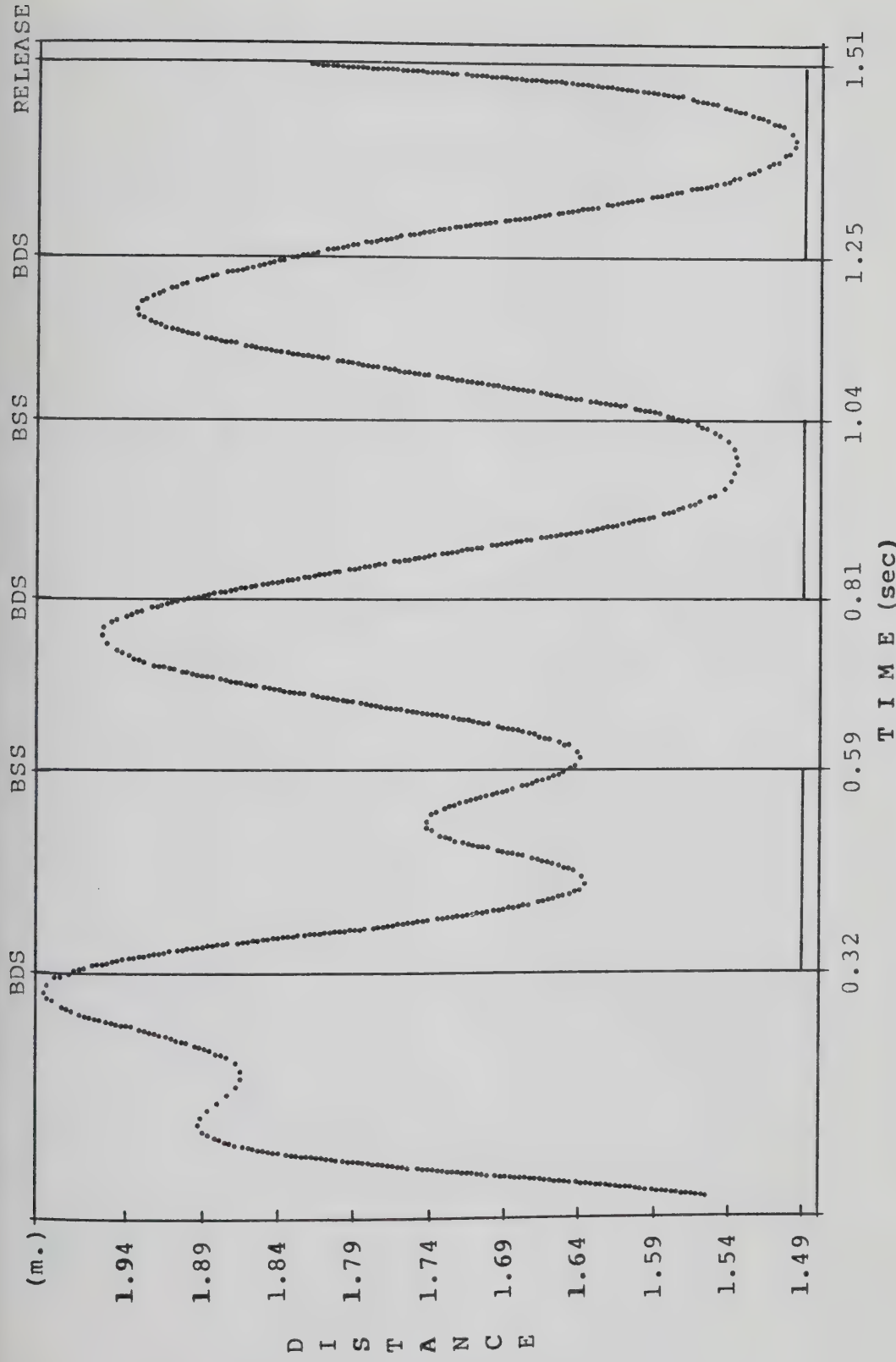
BDS=BEGINNING OF DOUBLE SUPPORT, BSS=BEGINNING OF SINGLE SUPPORT
X-AXIS(x), Y-AXIS(o), Z-AXIS(z)

Figure 26: Moments of Inertia of the Hammer, Subject 2



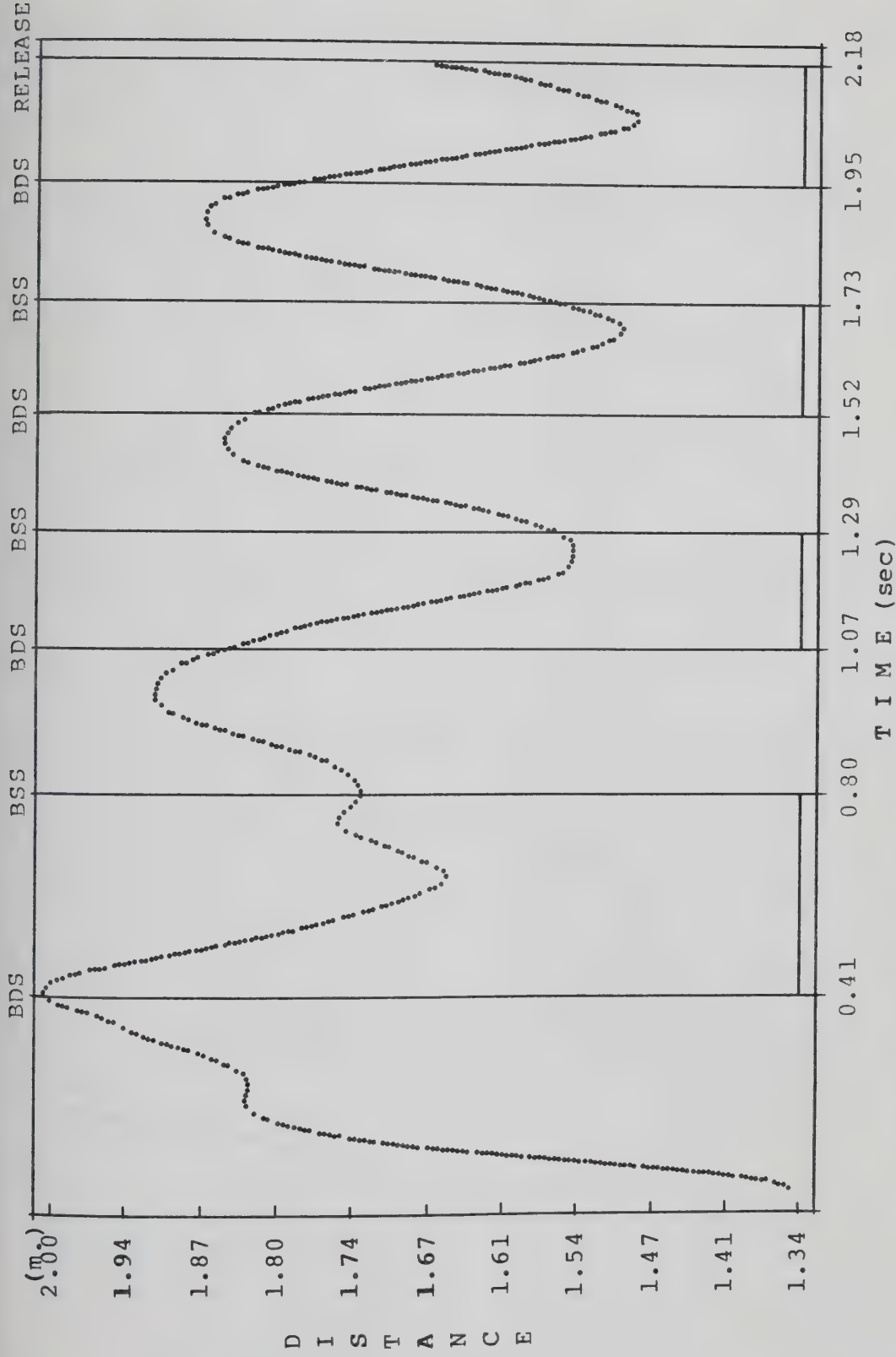
BDS=BEGINNING OF DOUBLE SUPPORT, BSS=BEGINNING OF SINGLE SUPPORT
X-AXIS(x), Y-AXIS(o), Z-AXIS(z)

Figure 27: Moments of Inertia of the Hammer, Subject 3



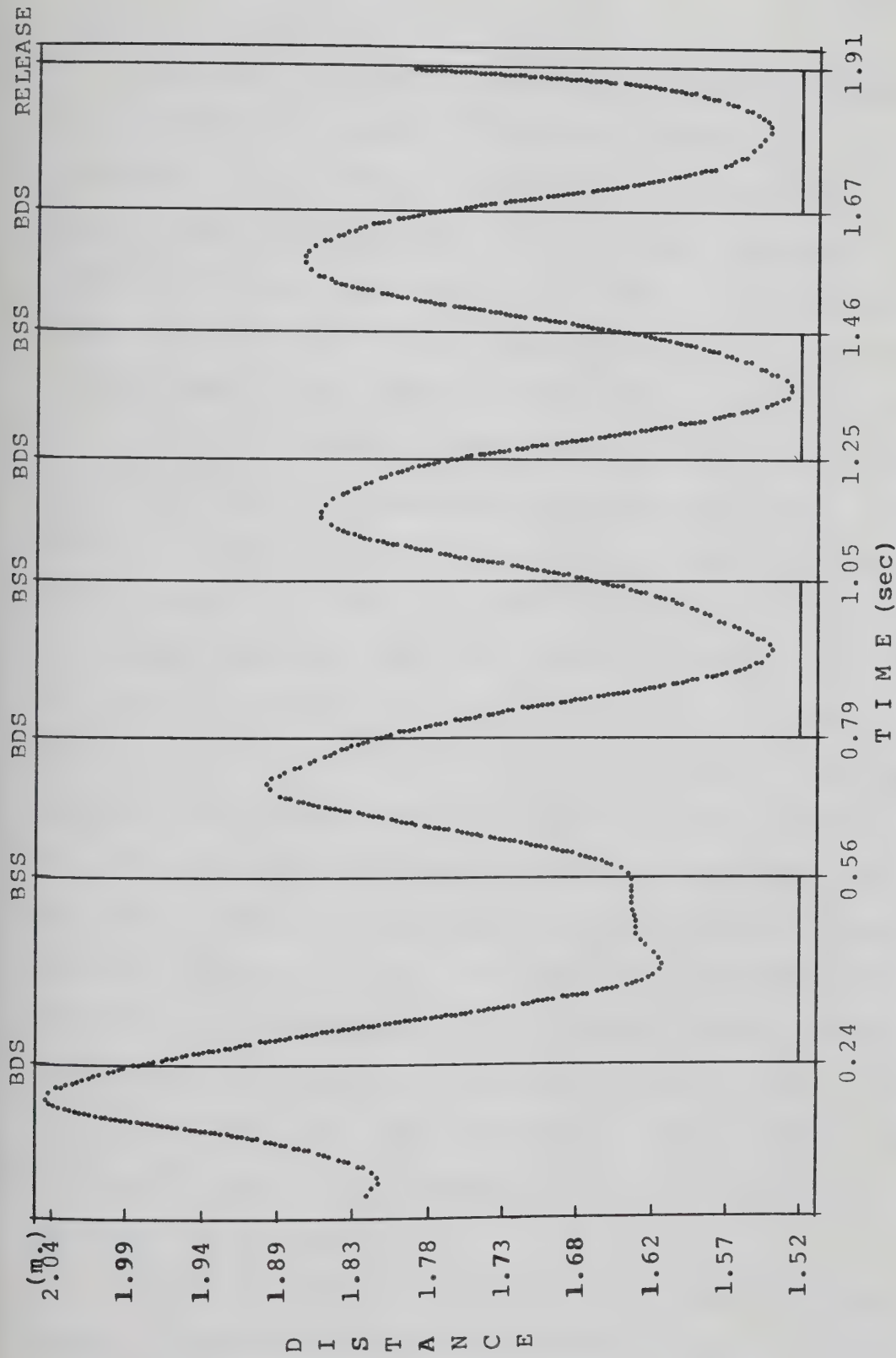
BDS=BEGINNING OF DOUBLE SUPPORT, BSS=BEGINNING OF SINGLE SUPPORT

Figure 28: Hammer - CMs Distance, Subject 1



BDS=BEGINNING OF DOUBLE SUPPORT, BSS=BEGINNING OF SINGLE SUPPORT

Figure 29: Hammer - CMs Distance, Subject 2



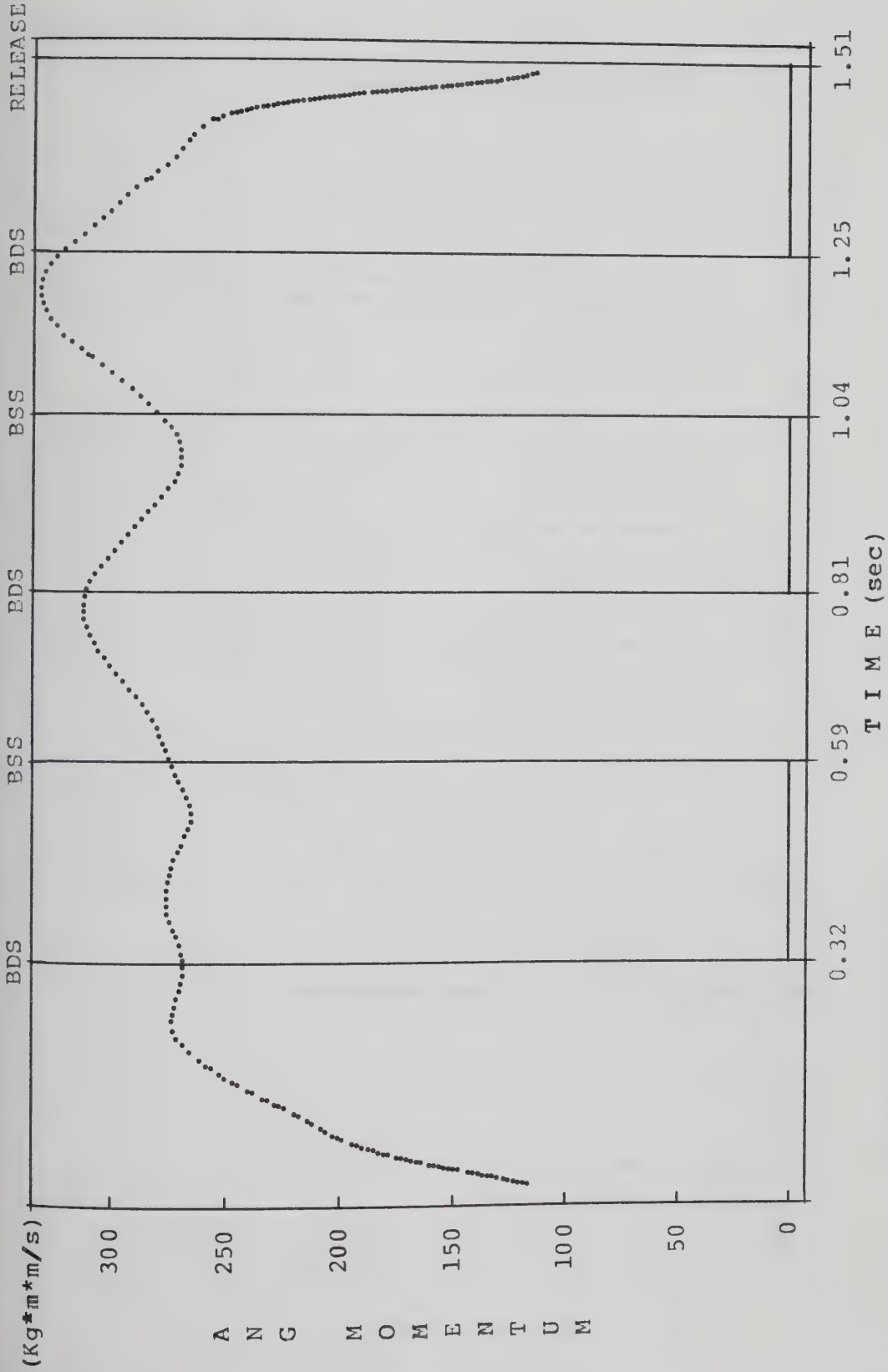
BDS=BEGINNING OF DOUBLE SUPPORT, BSS=BEGINNING OF SINGLE SUPPORT

Figure 30: Hammer - CMs Distance, Subject 3

BSS point. This happened with all the subjects, but was most evident in Subject 1.

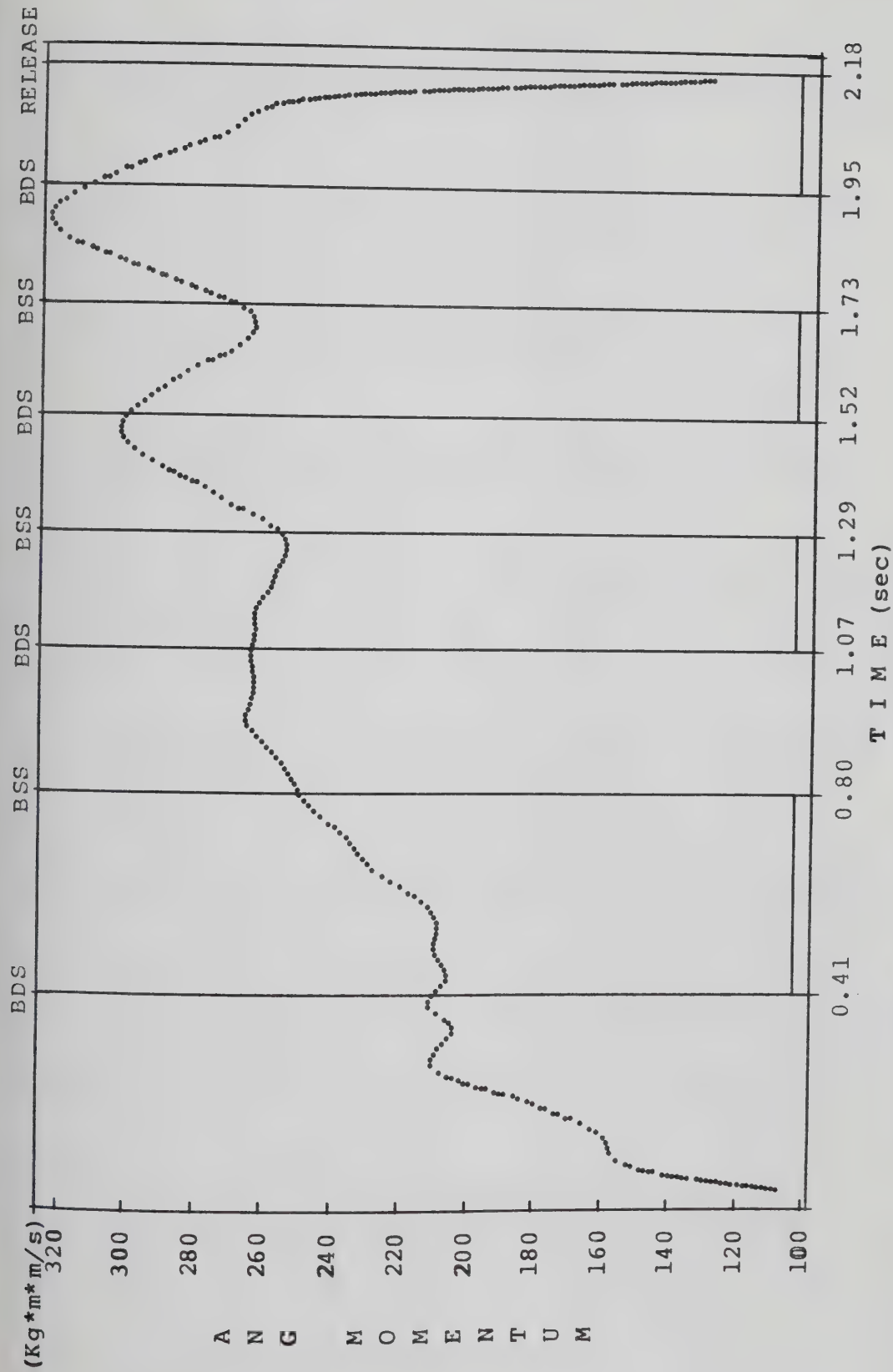
Figures 31, 32 and 33 represent the angular momentum of the hammer with respect to the CMs. The angular momentum increased in the single support phase and decreased in the double support phase. There was a gradual increase of the angular momentum from turn to turn. The maximum angular momentum was found to be: $327.95 \text{ Kg}\cdot\text{m}^2/\text{s}$ for Subject 1, $321.44 \text{ Kg}\cdot\text{m}^2/\text{s}$ for Subject 2 and, $319.81 \text{ Kg}\cdot\text{m}^2/\text{s}$ for Subject 3. In the first single support phase, Subject 1 reached and maintained until the beginning of the second single support phase, a local maximum angular momentum which was 83% of the global maximum. Subjects 2 and 3, reached 65% and 76% of the global maximum respectively and continued to increase the angular momentum until the end of the turn. The contribution of the last three turns to the maximum angular momentum was respectively: 83%, 94% and 100% for Subject 1, 82%, 93% and 100% for Subject 2 and, 88%, 96% and 100% for Subject 3. Subject 1, achieved in the end of the first turn what the others achieved in the end of the second turn in terms of angular momentum of the hammer. These results, compared with the radii of curvature of the hammer (Figures 11, 12, 13) indicate that the angular velocity of the hammer increased in the single support phase when its radius decreased in length.

Figures 34, 35 and 36 represent the angles between the angular momentum vector of the hammer and the X, Y and



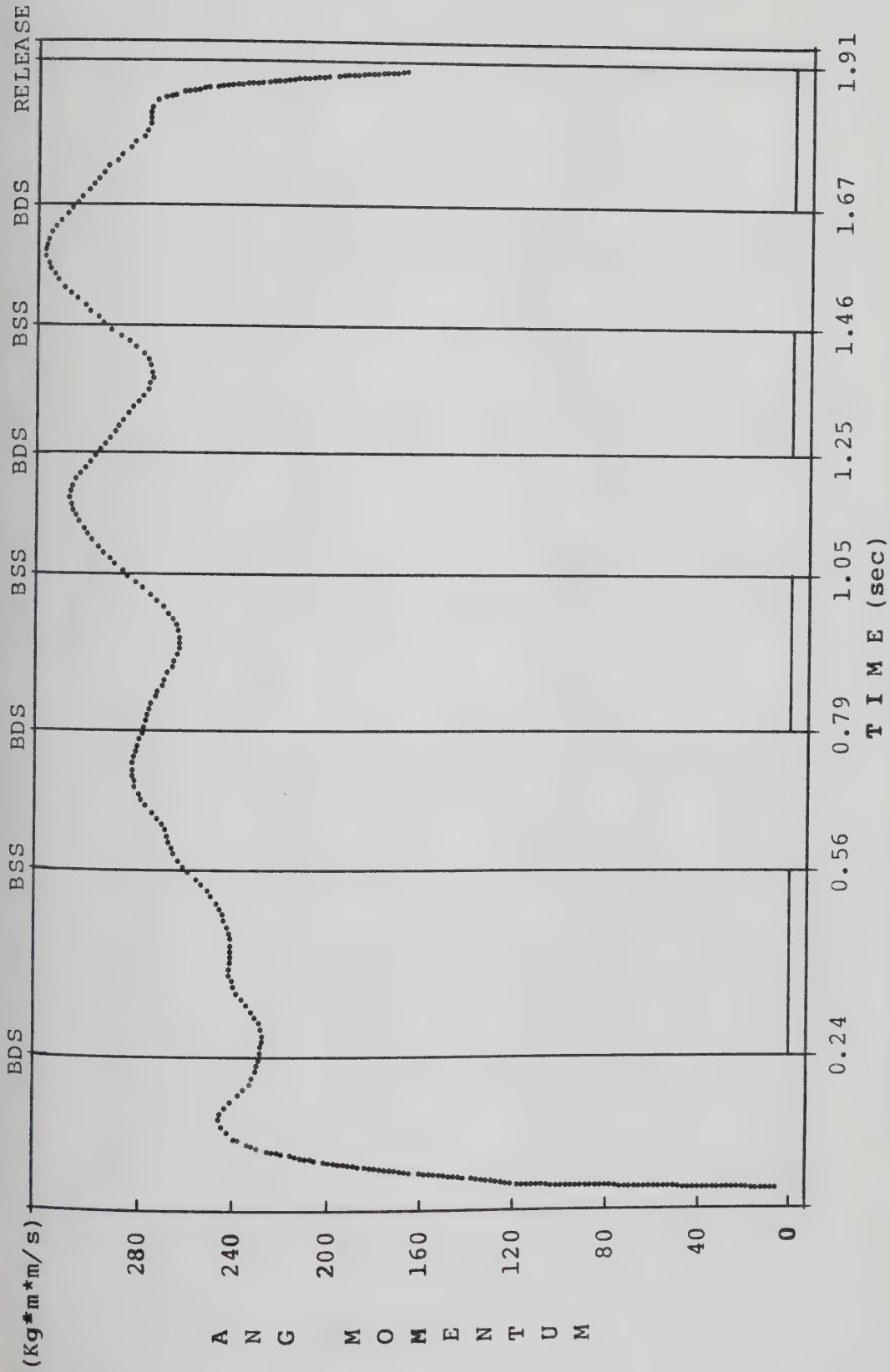
BDS=BEGINNING OF DOUBLE SUPPORT, BSS=BEGINNING OF SINGLE SUPPORT

Figure 31: Angular Momentum of the Hammer, Subject 1



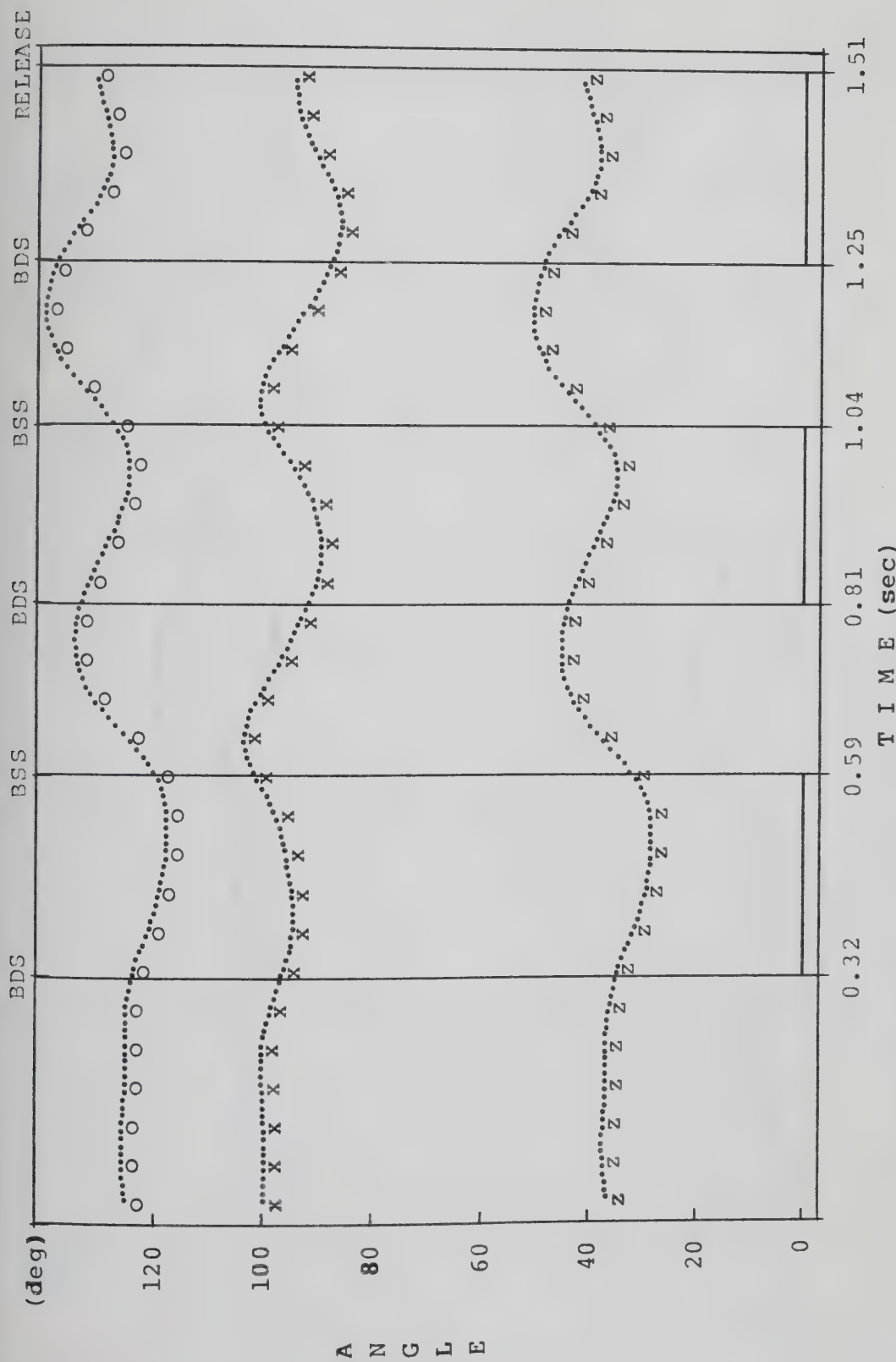
BDS=BEGINNING OF DOUBLE SUPPORT, BSS=BEGINNING OF SINGLE SUPPORT

Figure 32: Angular Momentum of the Hammer, Subject 2



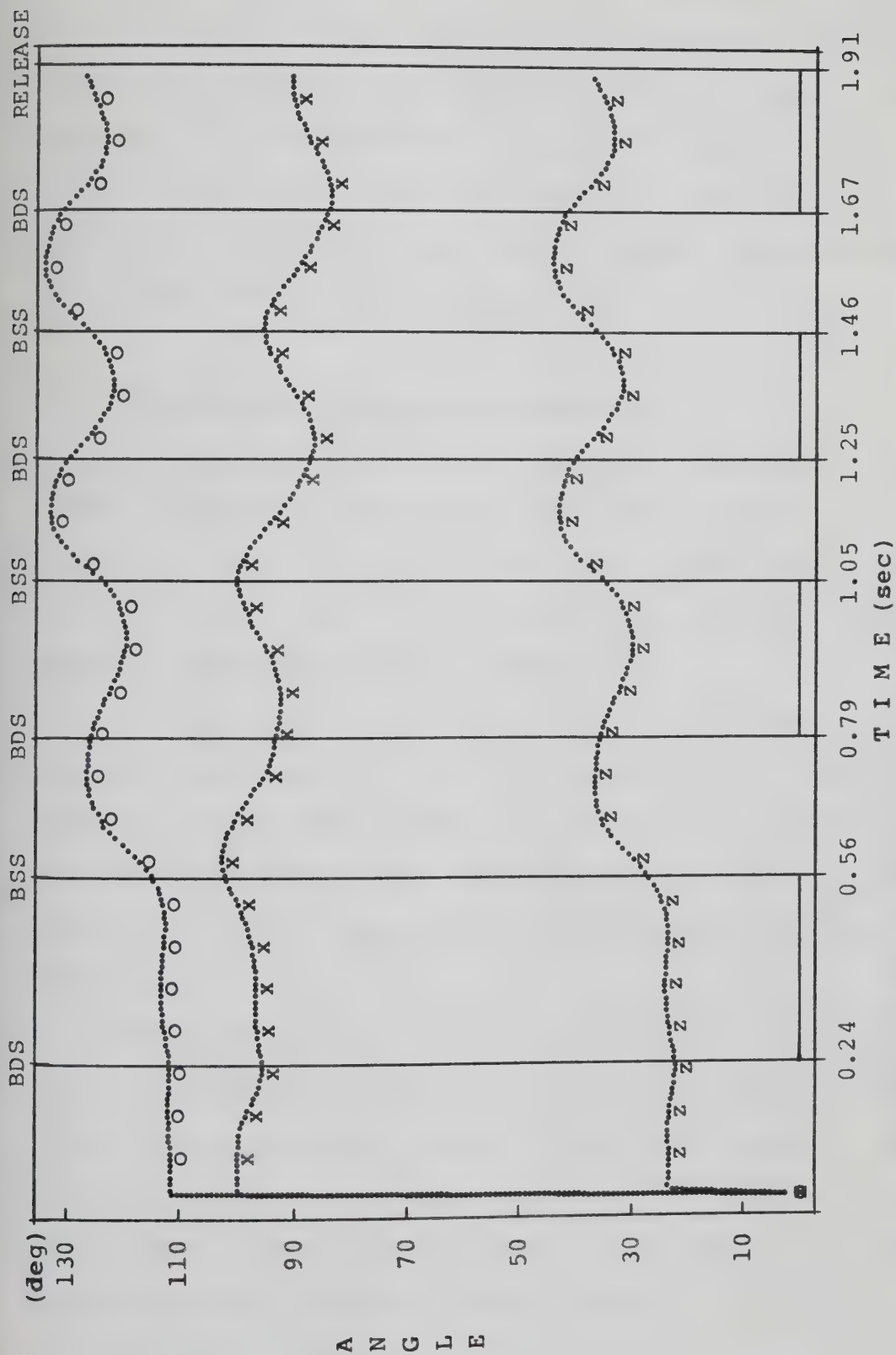
BDS=BEGINNING OF DOUBLE SUPPORT, BSS=BEGINNING OF SINGLE SUPPORT

Figure 33: Angular Momentum of the Hammer, Subject 3



BDS=BEGINNING OF DOUBLE SUPPORT, BSS=BEGINNING OF SINGLE SUPPORT
X-AXIS(x), Y-AXIS(o), Z-AXIS(z)

Figure 34: Direction Angles of the Hammer's Angular Momentum Vector, Subject 1



**BDS-BEGINNING OF DOUBLE SUPPORT, BSS-BEGINNING OF SINGLE SUPPORT
X-AXIS(x), Y-AXIS(y), Z-AXIS(z)**

Z-axis. These figures show the angular position of the plane of the hammer in space, which will be perpendicular to the vector. The angle of this plane with the vertical at the beginning of each throw was $\theta \approx 35^\circ$ for Subject 1, $\theta \approx 9^\circ$ for Subject 2 and $\theta \approx 25^\circ$ for Subject 3. This angle increased during the single support phases and decreased during the double support phases.

D. Kinematics and Kinetics of the Body.

Selected trajectories of the center of mass of the body (CMb) in different planes are presented in Figures 37, 38, 39 and 40. In the Y-Z plane, Subjects 2 and 3 had similar trajectories of CMb. In the X-Y and X-Z planes all three subjects presented similar trajectories.

The maximum vertical displacement of the CMb in each turn was less than 0.12 m. for all subjects. In the Z-axis the CMb moved in the opposite direction to the hammer except during the last turn when the maximum height of the CMb occurred at the release point same as the maximum height of hammer.

Figures 41, 42 and 43 represent the CMb radii of curvature. These figures indicate that the highest rotation of the CMb occurred at the end of the double support and beginning of the single support phase. The radii of the CMb became smallest at the same time as the radii of the hammer became greatest. Subjects 2 and 3 presented noisier oscillations of radius than Subject 1.

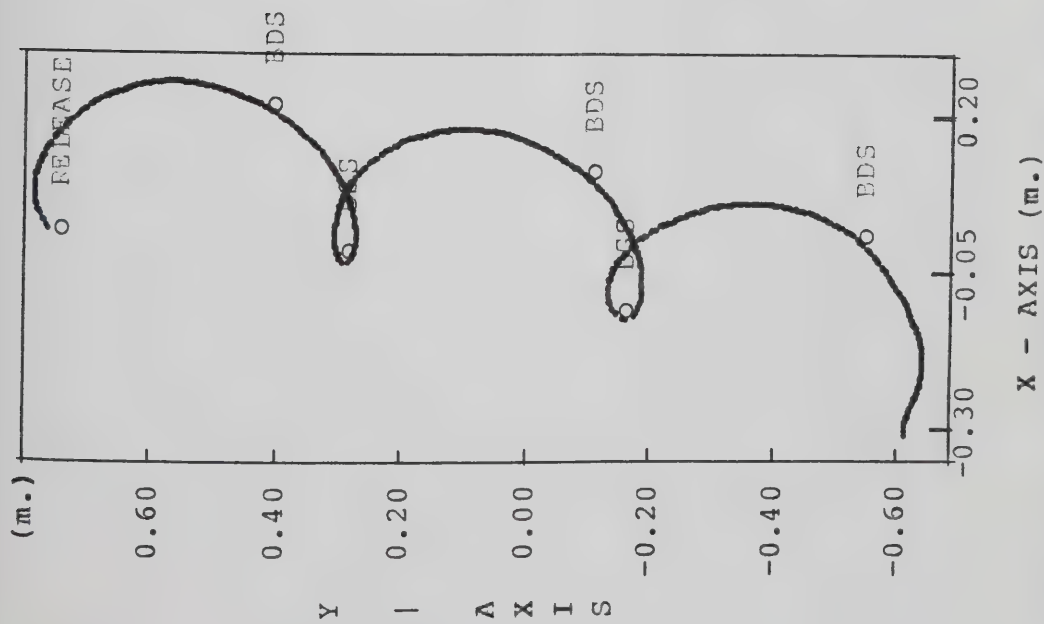


Figure 37: Trajectory of the CMB in the X-Y Plane, Subject 1

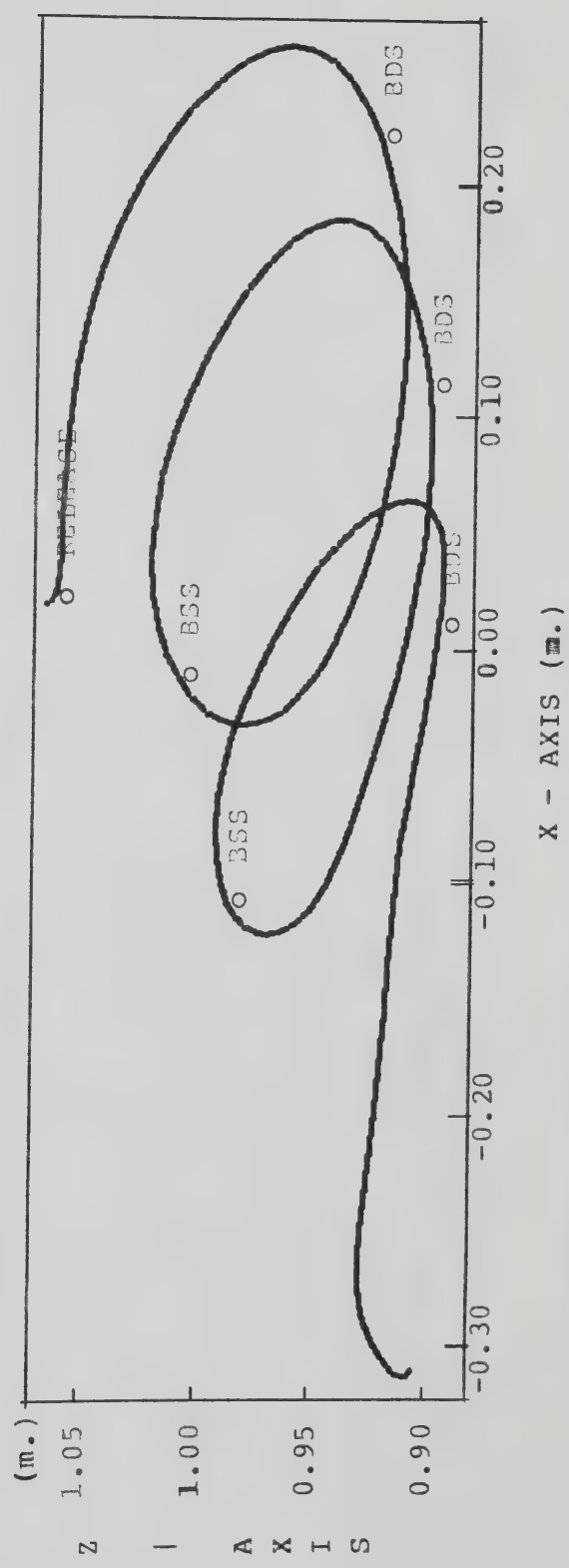


Figure 38: Trajectory of the CMB in the X-Z Plane, Subject 1

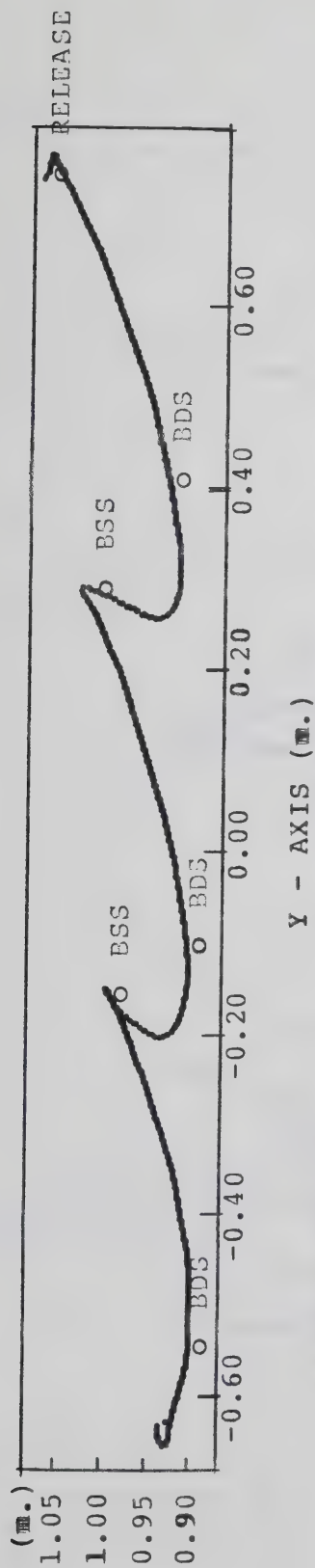


Figure 39: Trajectory of the CMb in the Y-Z Plane, Subject 1

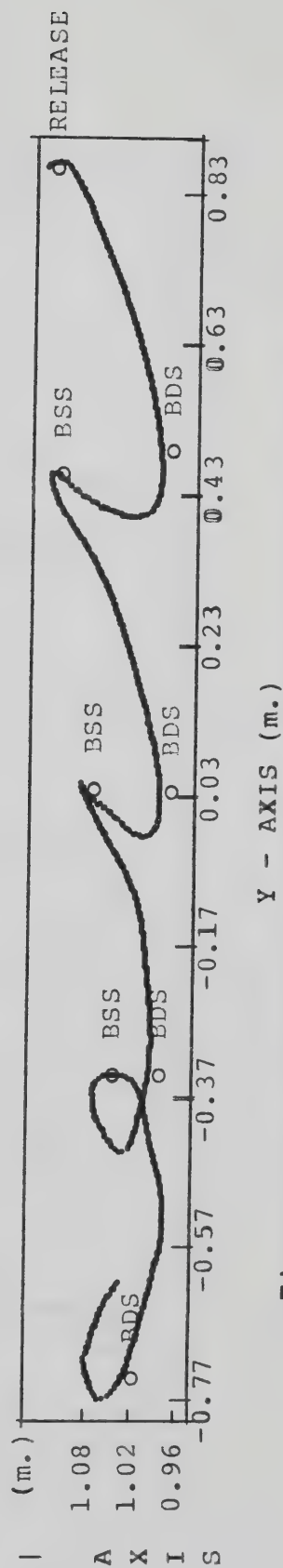
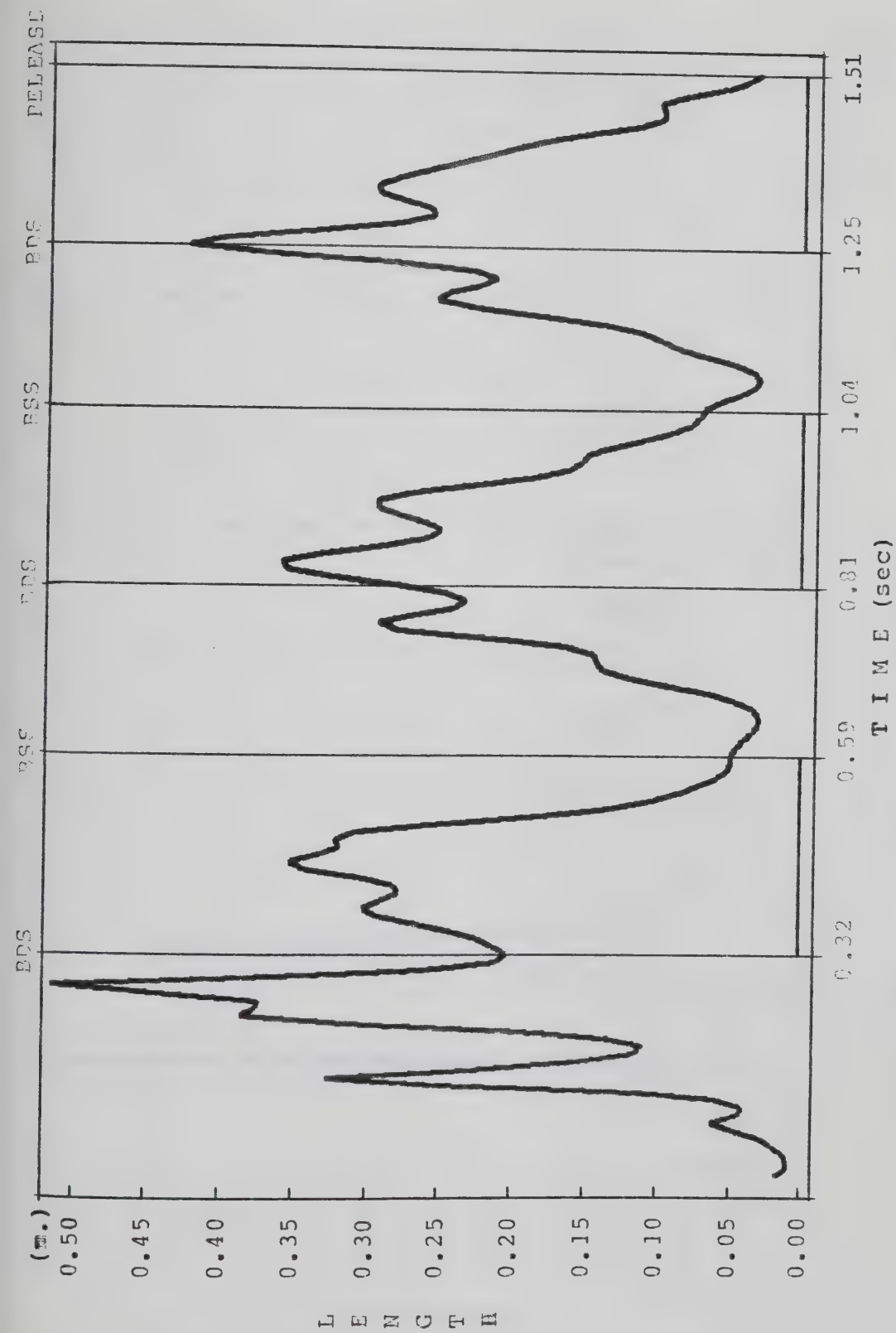
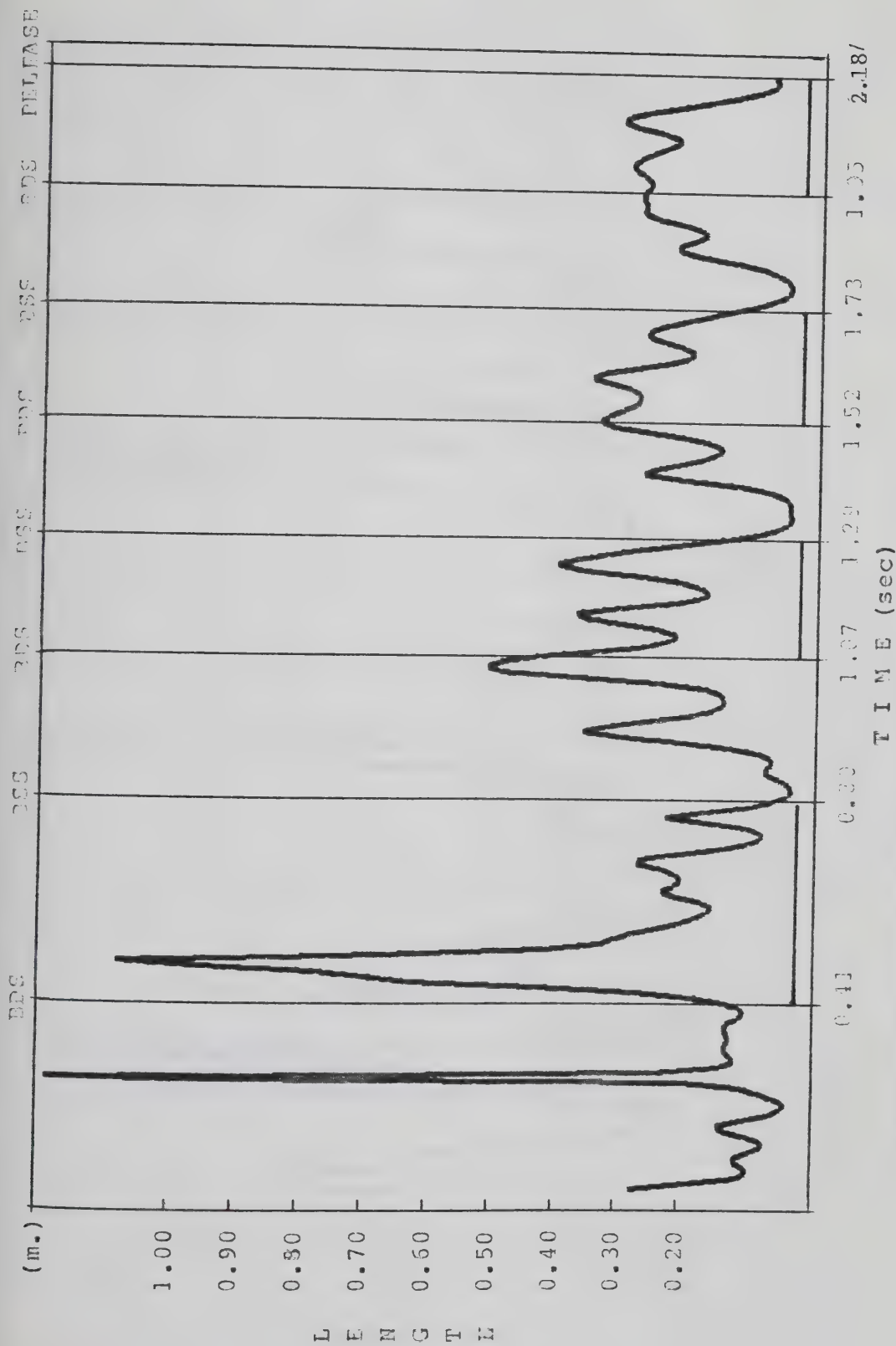


Figure 40: Trajectory of the CMB in the Y-Z plane, Subject 2



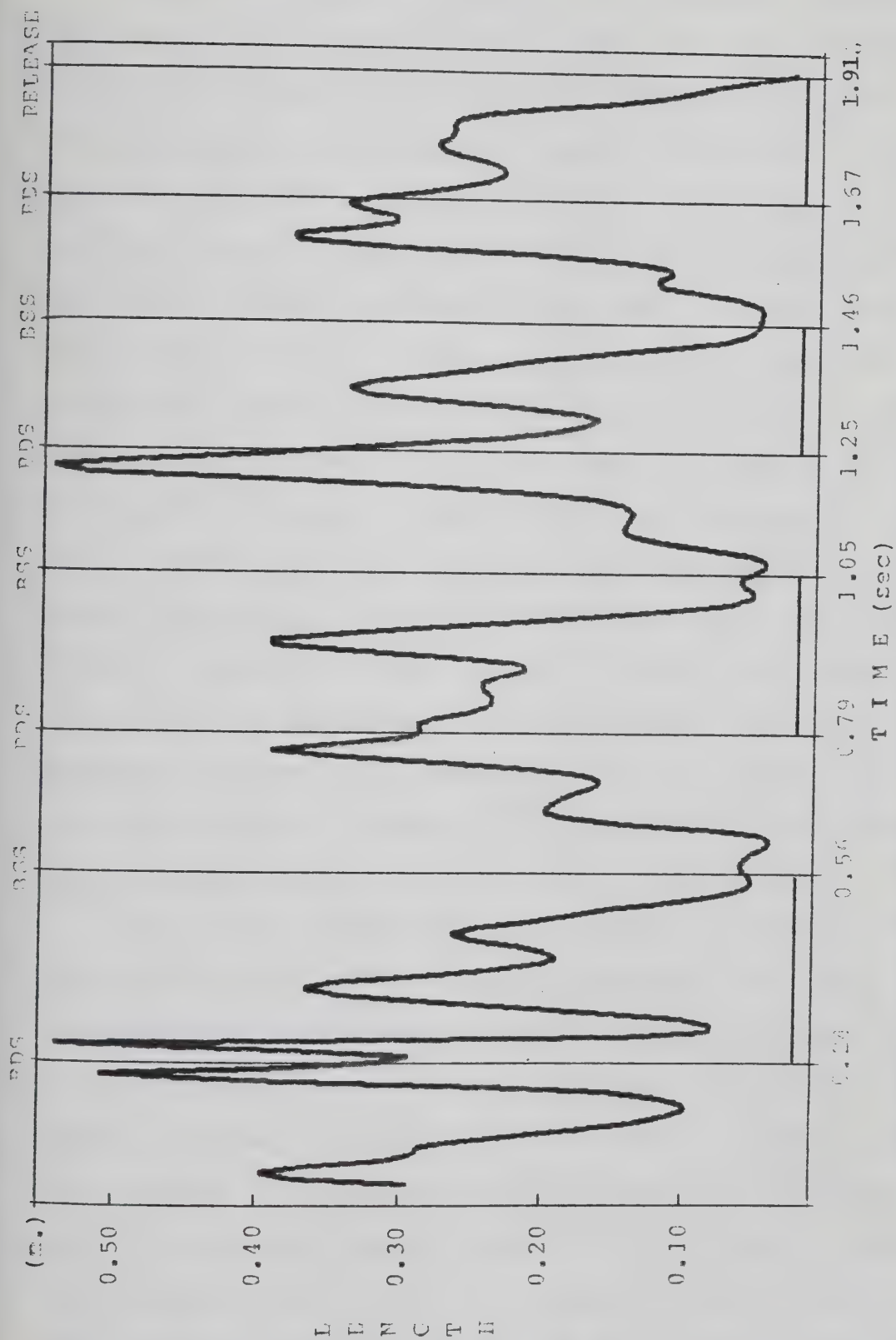
BDS=BEGINNING OF DOUBLE SUPPORT, BSS=BEGINNING OF SINGLE SUPPORT

Figure 41: Radius of Curvature of the CMB, Subject 1



BDS=BEGINNING OF DOUBLE SUPPORT, BSS=BEGINNING OF SINGLE SUPPORT

Figure 42: Radius of Curvature of the CMB, Subject 2

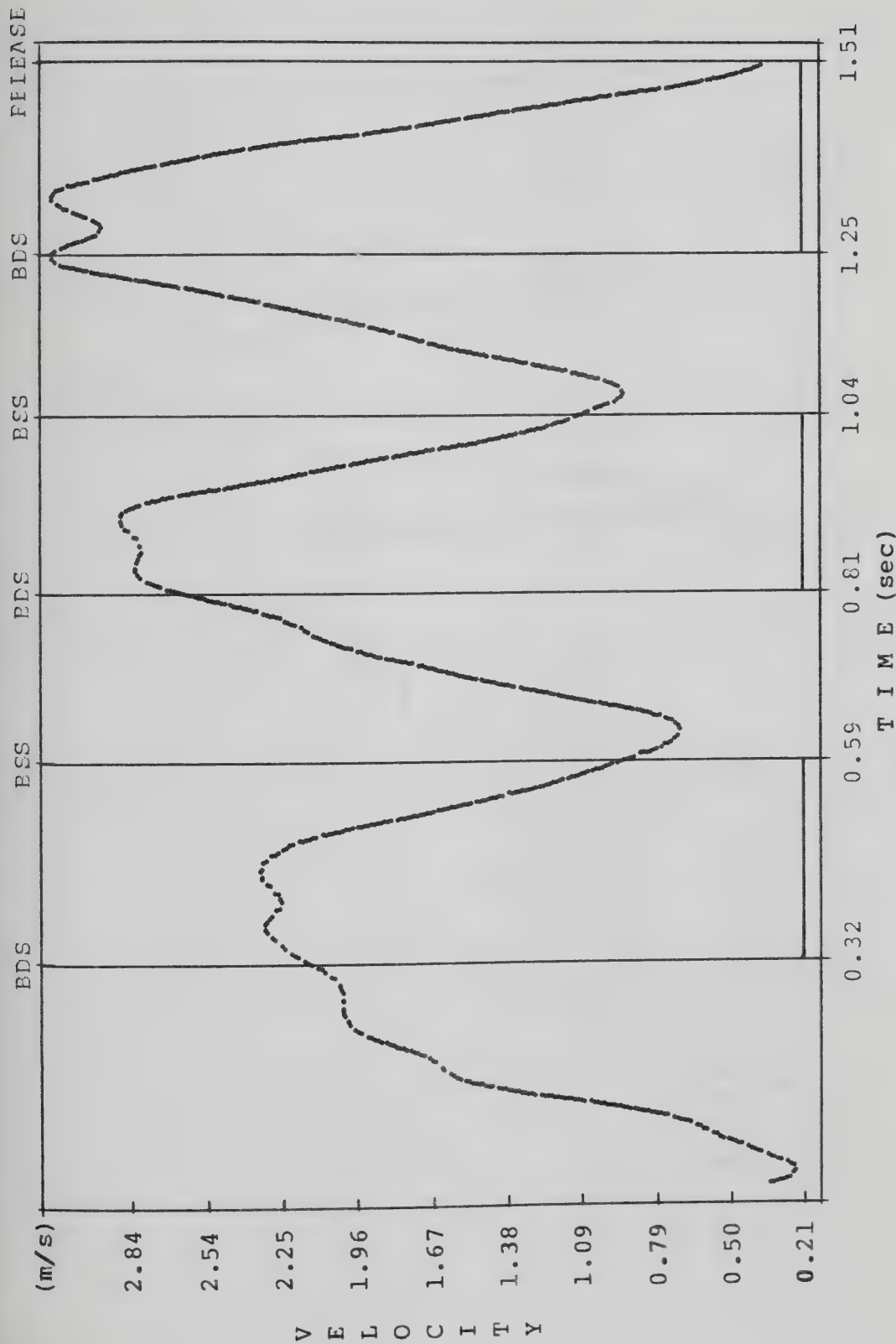


BDS=BEGINNING OF DOUBLE SUPPORT, BSS=BEGINNING OF SINGLE SUPPORT

Figure 43: Radius of Curvature of the CMB, Subject 3

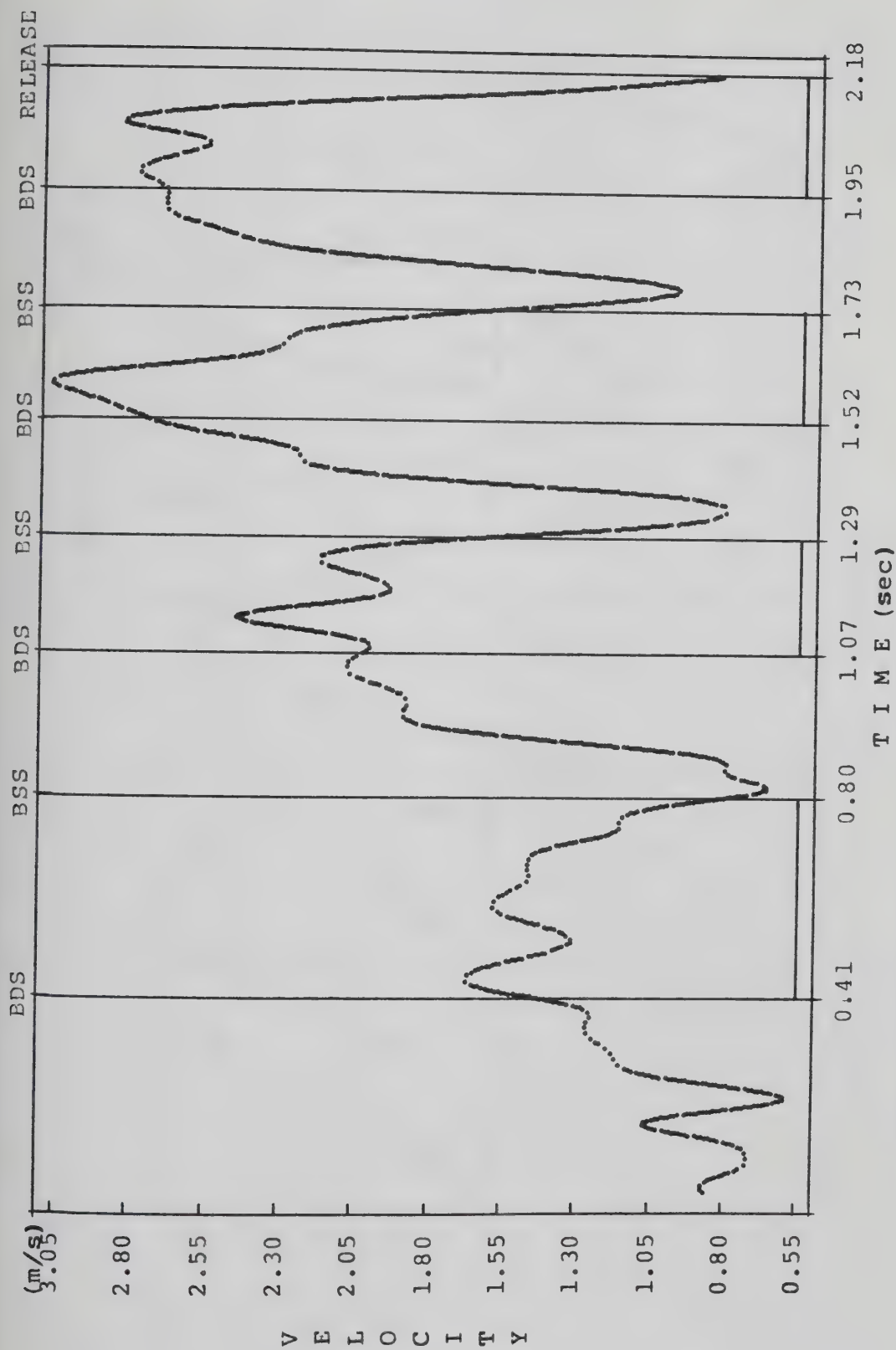
Figures 44 and 45 illustrate the resultant velocities of the CMb for Subjects 1 and 2. The velocity of CMb for Subject 3 was similar to the one of Subject 1. Subjects 1 and 3 presented a gradual increase of CMb velocity from turn to turn with the global maximum in the last turn. Subject 2 achieved the global maximum velocity in the second from the last turn. The maximum velocity for each turn occurred at the beginning of the double support phase and remained relatively constant until the middle of this phase. After this point there was a rapid decrease in the velocity and it was least during the transition from double support to single support phase. At the same time the velocity of the hammer reached its local maximum for each turn. It was the velocity component of CMb along the Y-axis which mainly contributed to the maximum. This, together with the Z component (Figure 46) indicated that in the first half of the double support phase the direction of the CMb's velocity was backwards and up (Y-Z plane, direction of throw).

The linear accelerations of the CMb for Subject 1 are presented in Figure 47. The accelerations of the other subjects were similar to the one presented in Figure 47 except about the Z-axis which are presented later in this chapter. The acceleration of the CMb became negative about all the axes in the double support phase. This indicated that in the double support phase the forces were transmitted to the hammer which obtained its maximum acceleration at the same time. The acceleration of the CMb in the Z-axis reached



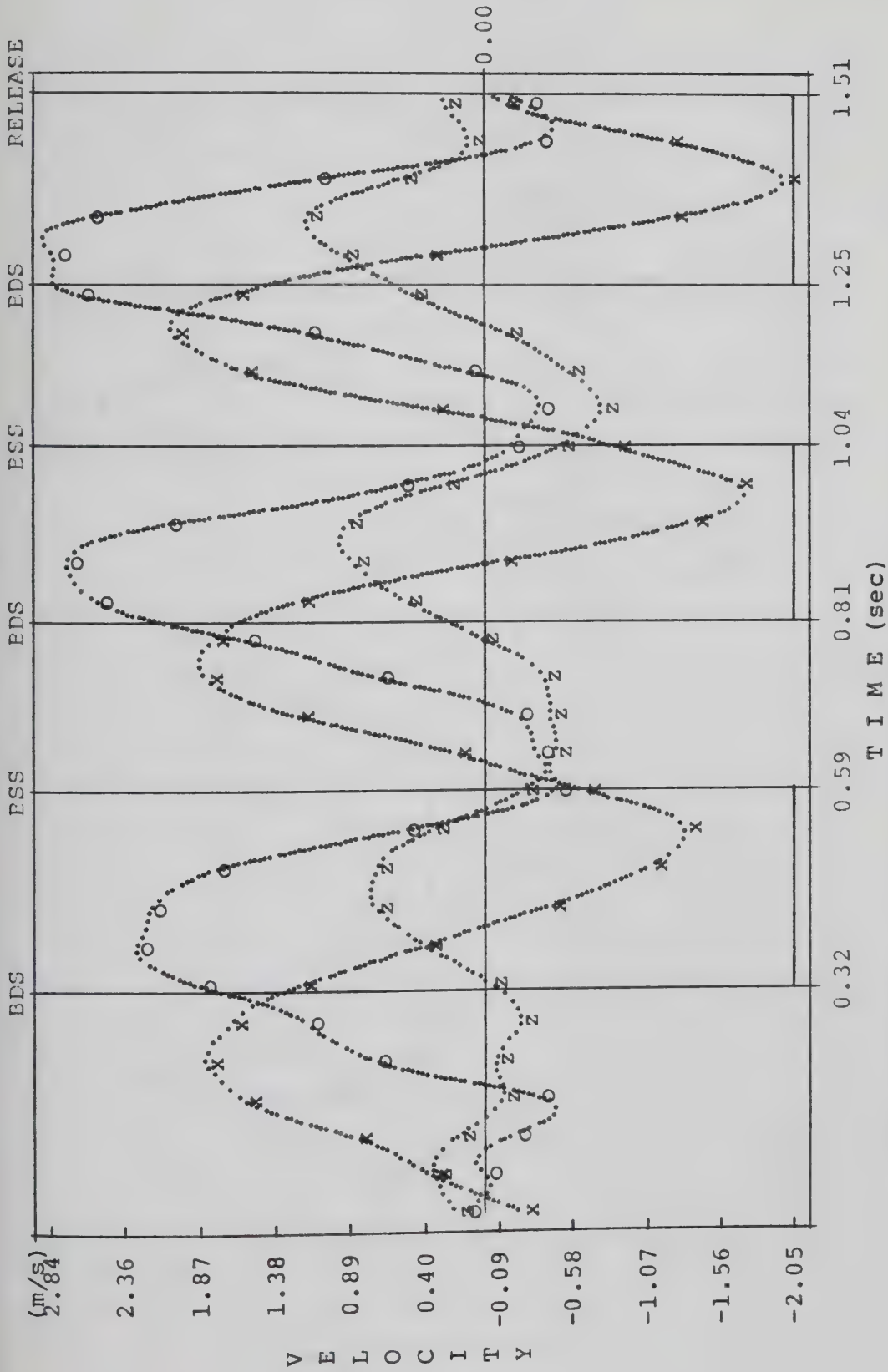
BDS=BEGINNING OF DOUBLE SUPPORT, BSS=BEGINNING OF SINGLE SUPPORT

Figure 44: Linear Velocity of the CMB, Subject 1



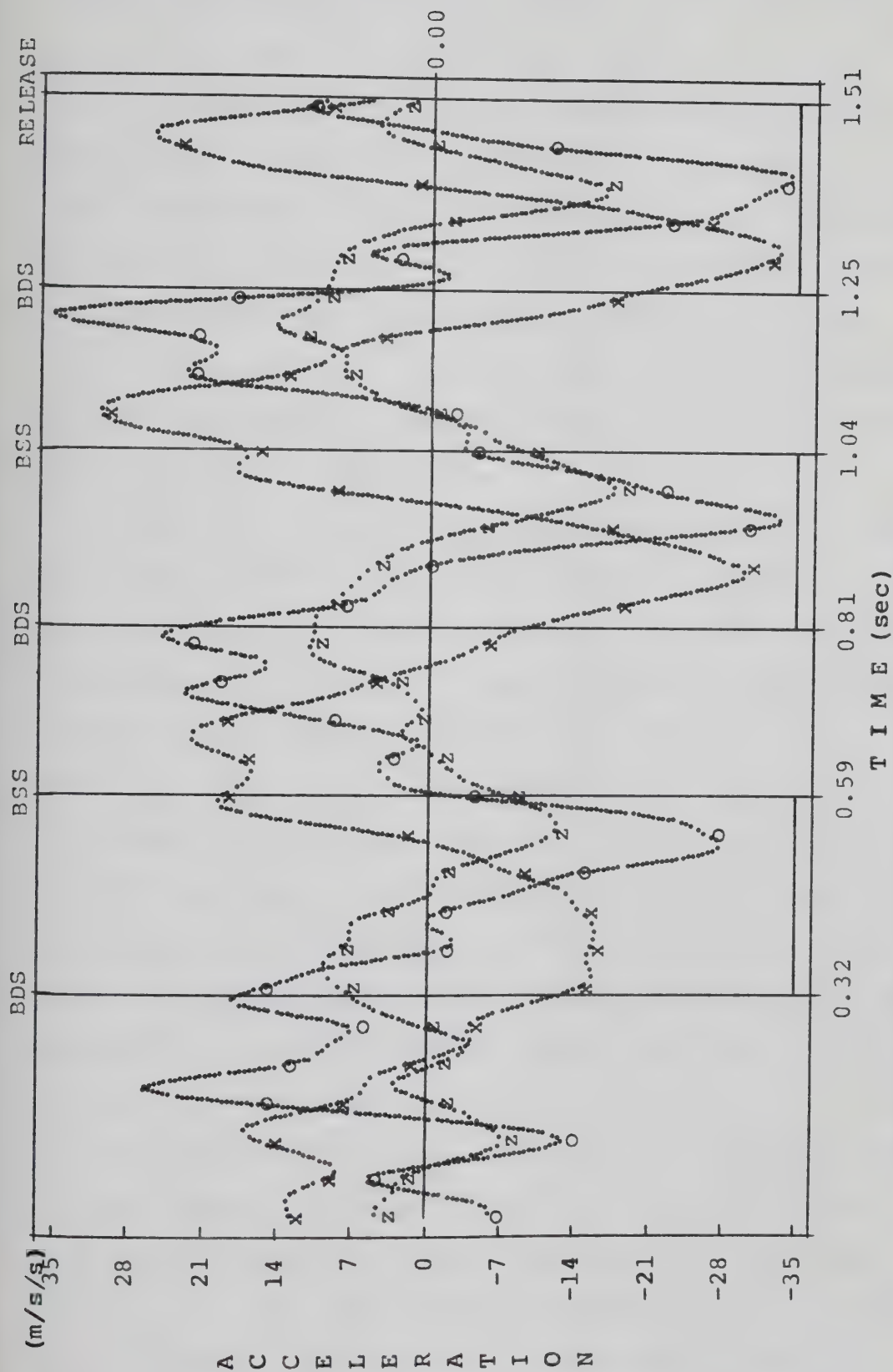
BDS=BEGINNING OF DOUBLE SUPPORT, BSS=BEGINNING OF SINGLE SUPPORT

Figure 45: Linear Velocity of the CMB, Subject 2



BDS-BEGINNING OF DOUBLE SUPPORT, BSS-BEGINNING OF SINGLE SUPPORT
X-AXIS(x), Y-AXIS(o), Z-AXIS(z)

Figure 45: Velocity of the CMb in the X, Y, Z Axes, Subject 1



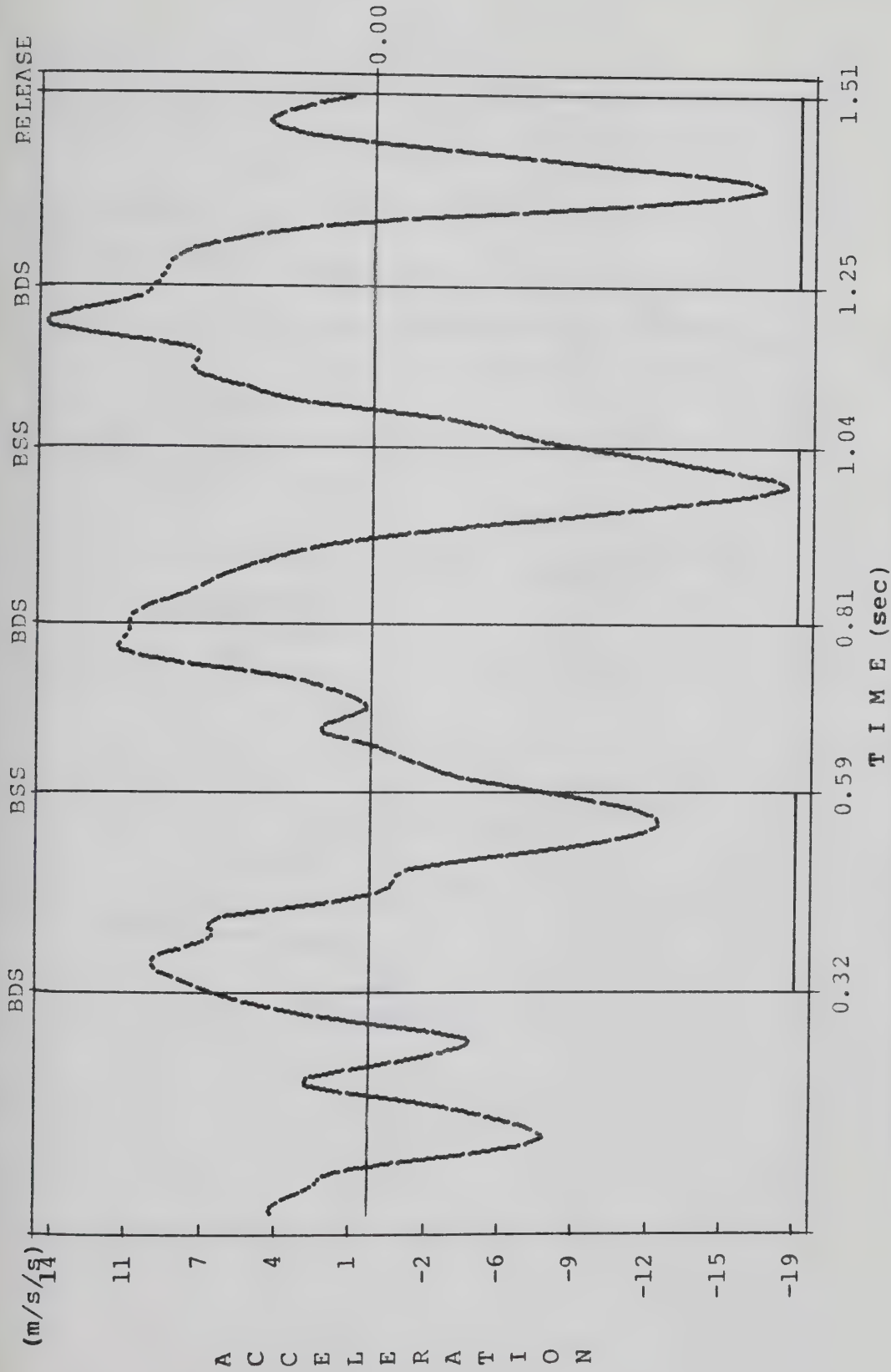
BDS=BEGINNING OF DOUBLE SUPPORT, BSS=BEGINNING OF SINGLE SUPPORT
X-AXIS(x), Y-AXIS(o), Z-AXIS(z)

Figure 47: Acceleration of the CMB in the X, Y, Z Axes, Subject 1

maximum and minimum values in different instances for different phases and for different subjects. In the first turn the maximum occurred after the BDS point while in the other turns this maximum occurred before that point. In the last double support phase Subject 2 had a continued decrease of acceleration until the release point. This did not occur with Subjects 1 and 3, who, after achieving a minimum acceleration when the hammer reached its MIN-Z, increased the CMb acceleration to a local peak just before the release point (Figures 48, 49 and 50).

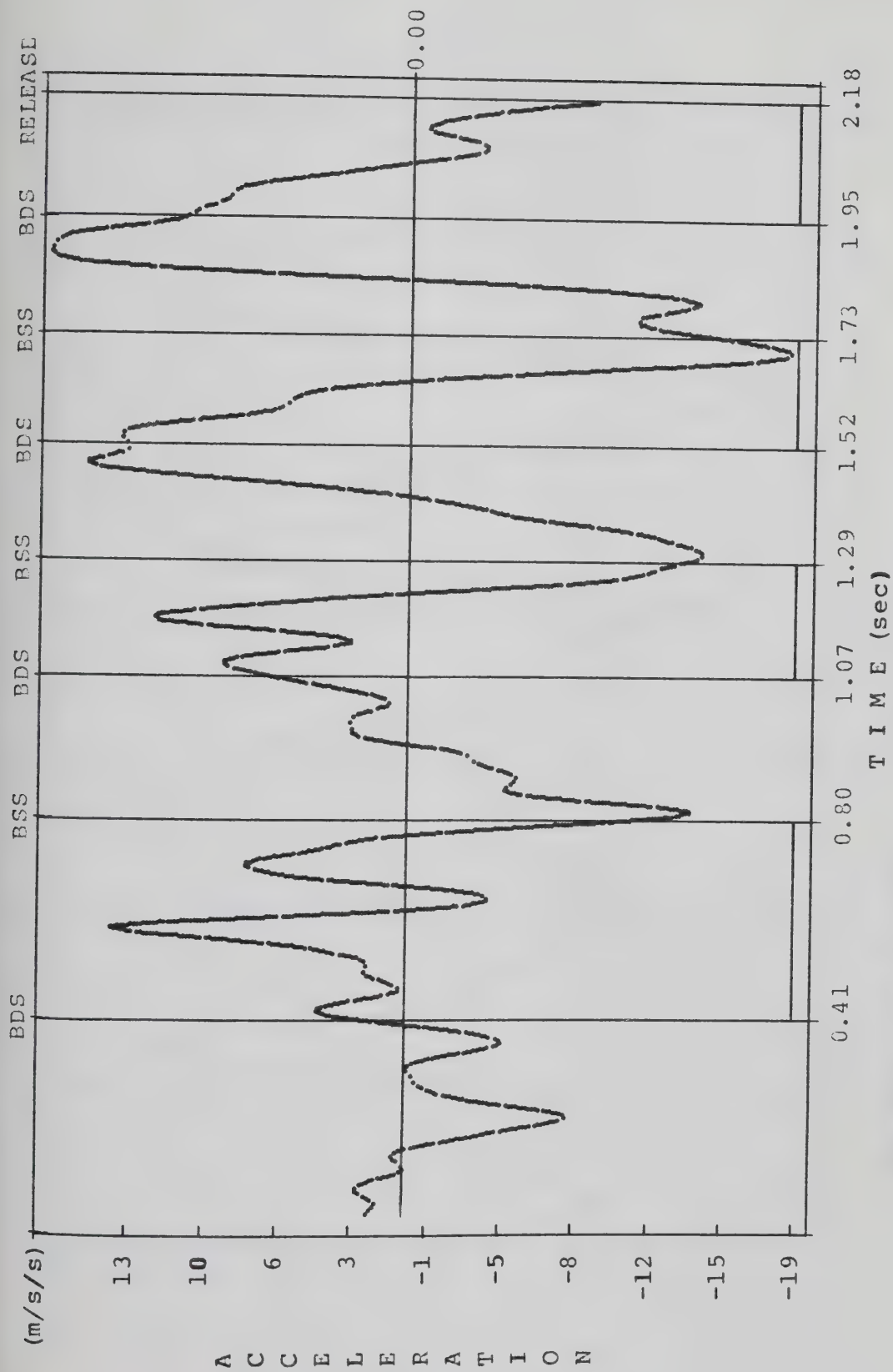
Figure 51 represents the moments of inertia of the body about the center of mass of the system for Subject 3. About the X and Y-axis the moments changed from minimum to maximum in every phase. About the Z-axis, Subjects 1 and 2 showed a generally lower moment in the first turn than in the other turns. In the last turn for Subject 1, in the last two turns for Subject 2 and in the last three turns for Subject 3, the moment became maximum at the beginning of the single support phase, then became minimum when the hammer reached the MIN-Z point. Increase of the moment of inertia about the Z-axis occurred in the double support during the time interval between the MIN-Z point and the BSS point.

Figures 52, 53 and 54 represent the angular momentum of the body about the center of mass of the system. There was a gradual increase of the angular momentum of the body from turn to turn. The global maximum occurred in the second from the last double support phase for Subjects 1 and 3, and in



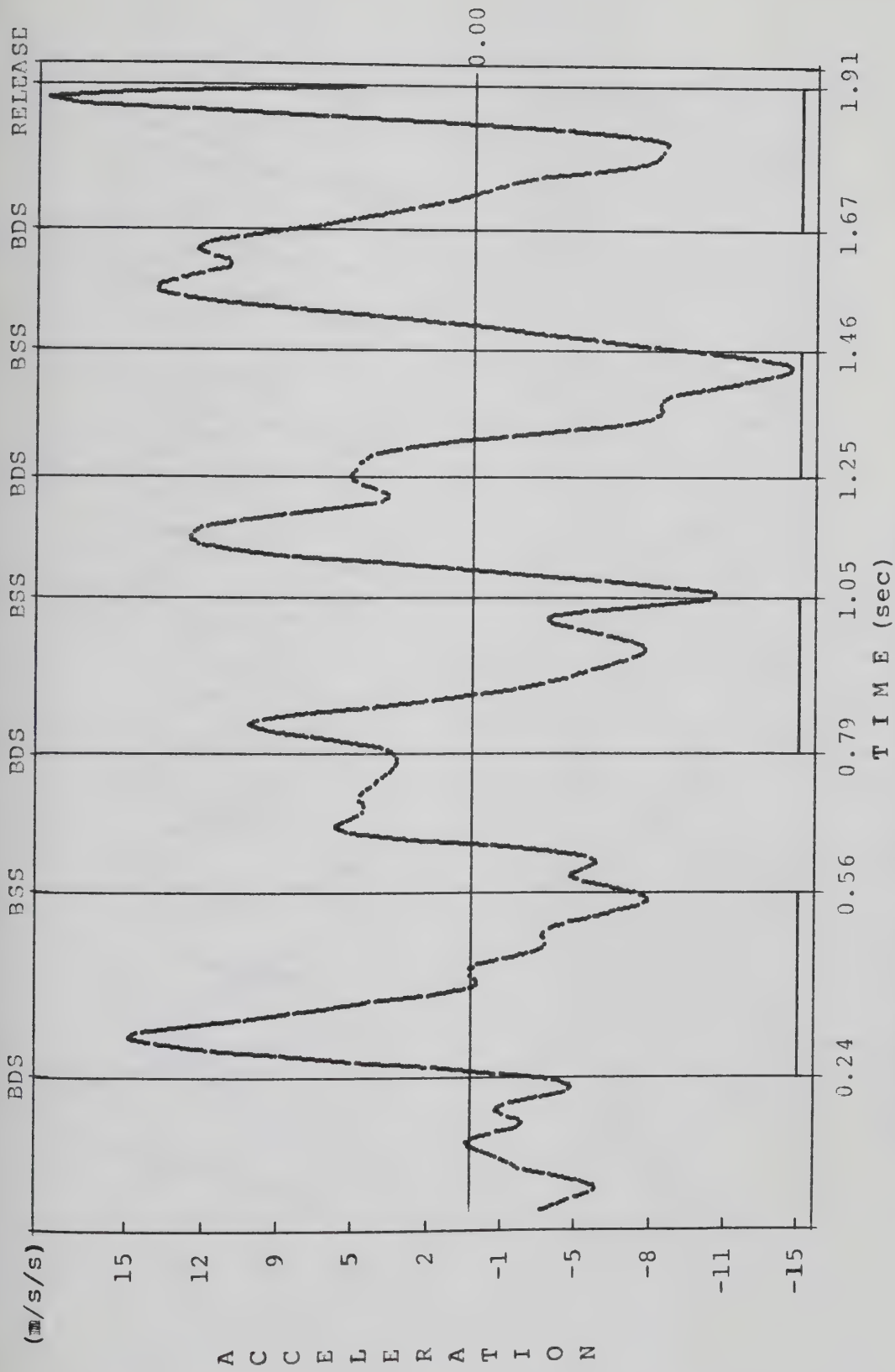
BDS-BEGINNING OF DOUBLE SUPPORT, BSS-BEGINNING OF SINGLE SUPPORT

Figure 48: Acceleration of the CMb in the Z Axis, Subject 1



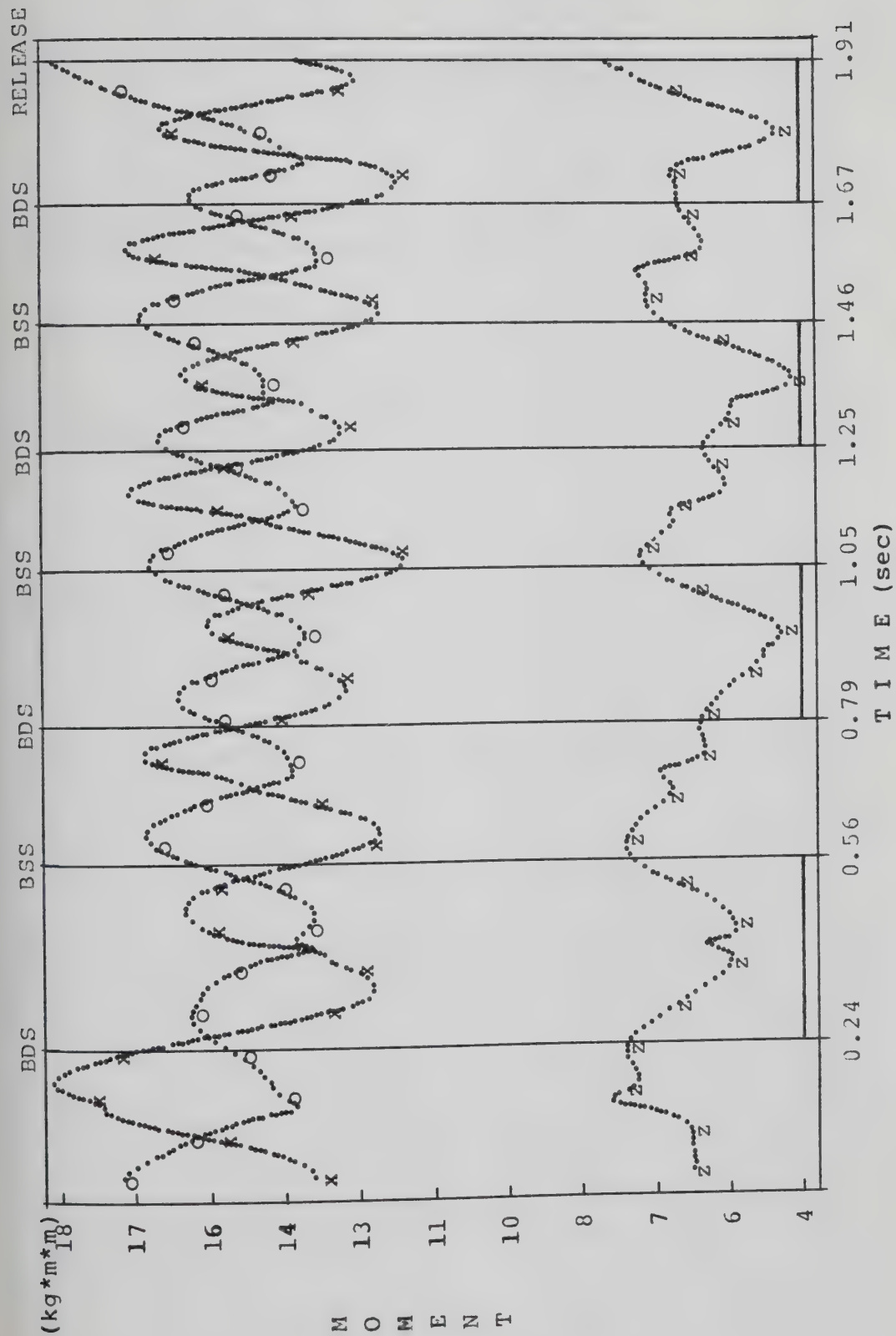
BDS-BEGINNING OF DOUBLE SUPPORT, BSS-BEGINNING OF SINGLE SUPPORT

Figure 49: Acceleration of the CMb in the Z Axis, Subject 2



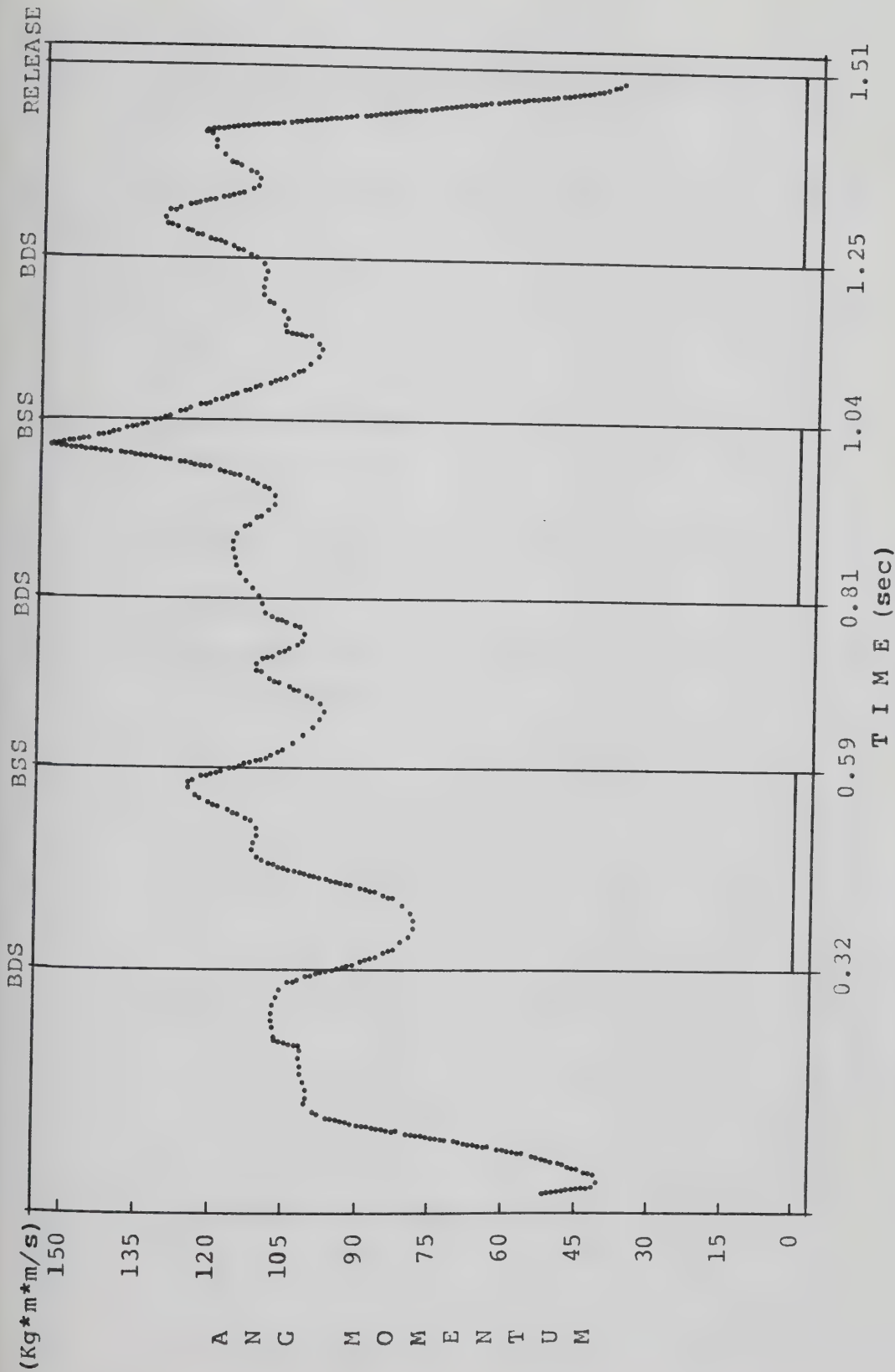
BDS=BEGINNING OF DOUBLE SUPPORT, BSS=BEGINNING OF SINGLE SUPPORT

Figure 50: Acceleration of the CMb in the Z Axis, Subject 3



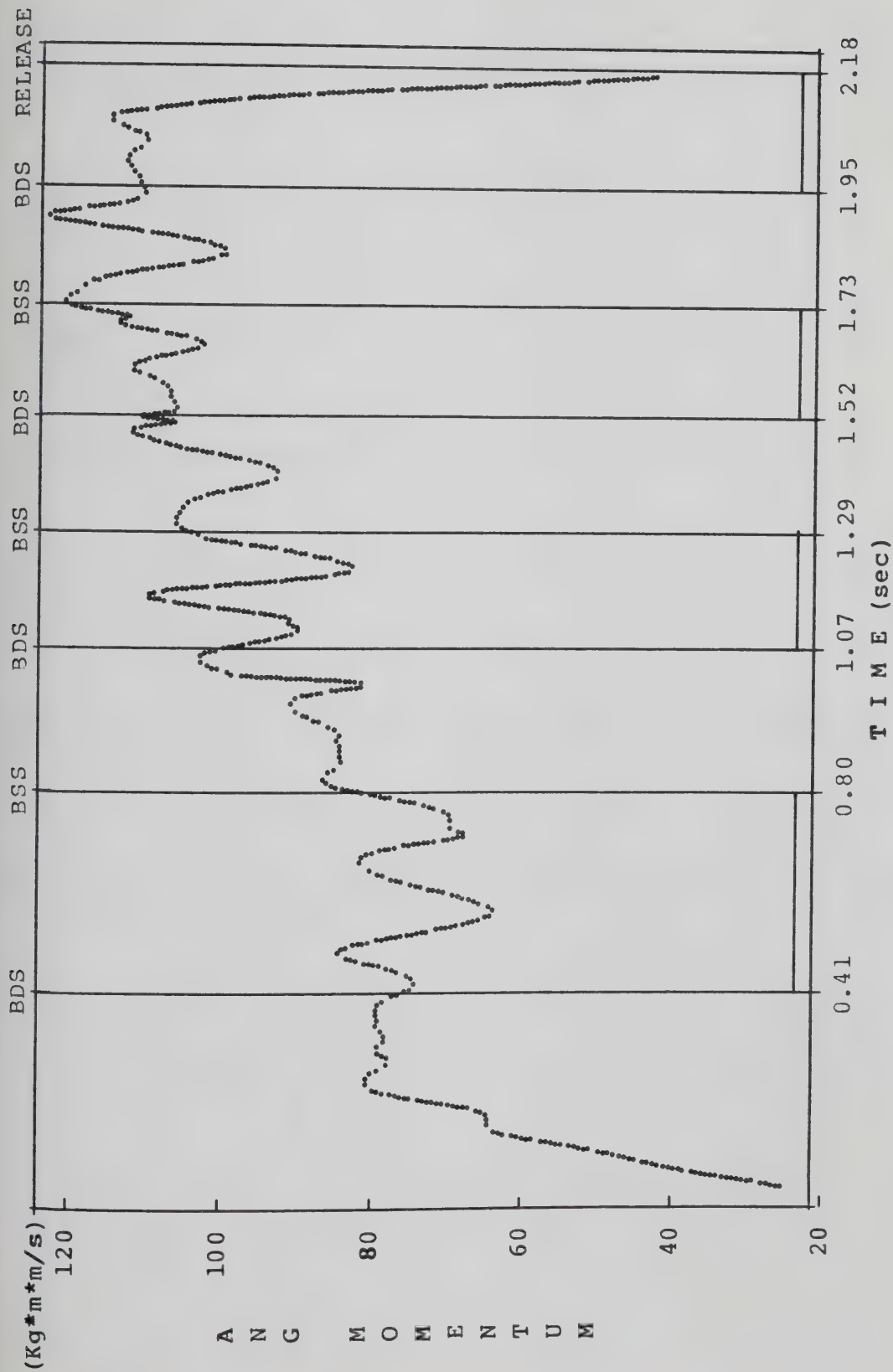
BDS=BEGINNING OF DOUBLE SUPPORT, BSS=BEGINNING OF SINGLE SUPPORT
X-AXIS(x), Y-AXIS(o), Z-AXIS(z)

Figure 51: Moments of Inertia of the Body about the CMs, Subject 3



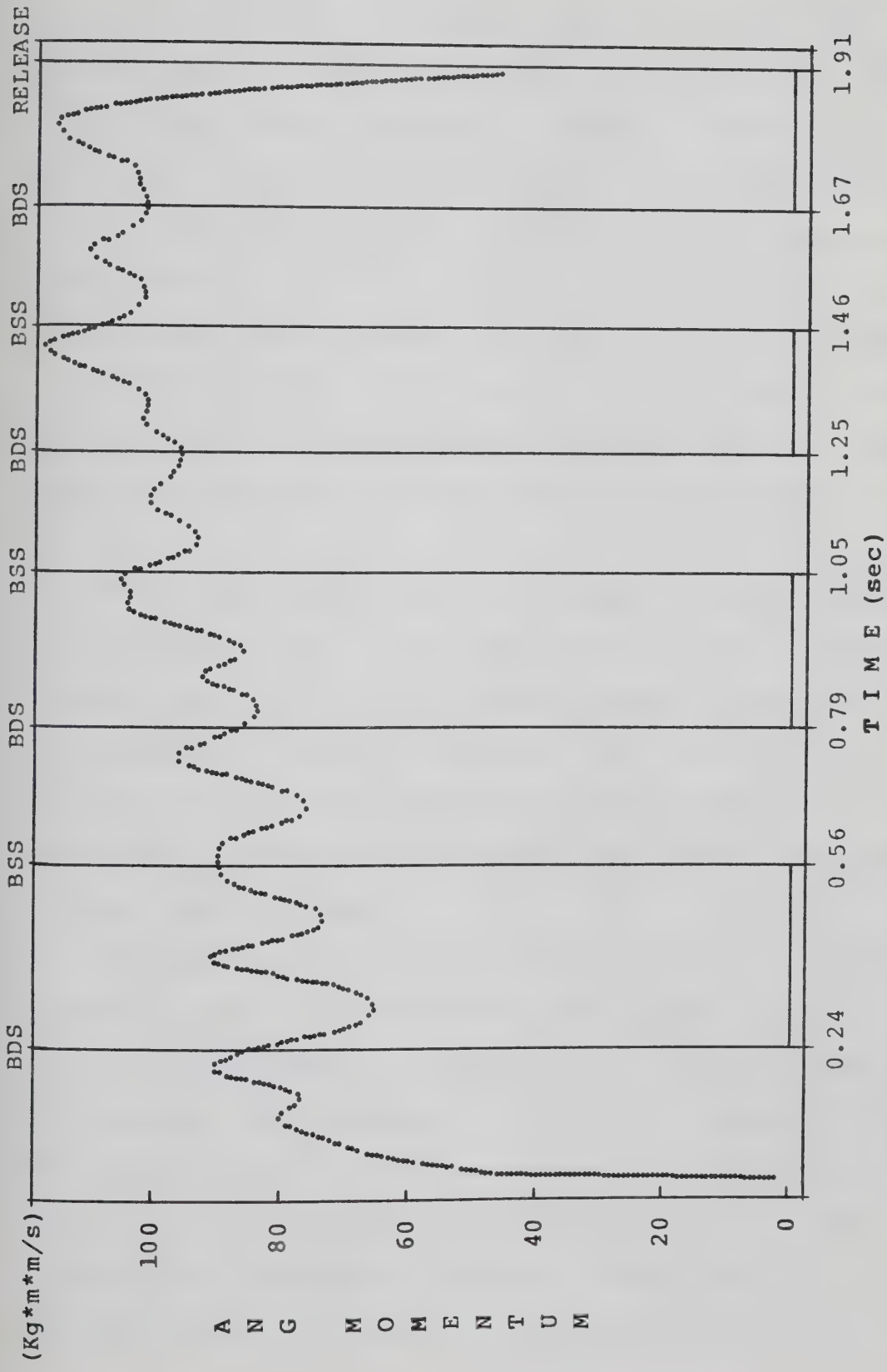
BDS=BEGINNING OF DOUBLE SUPPORT, BSS=BEGINNING OF SINGLE SUPPORT

Figure 52: Angular Momentum of the Body about the CMs, Subject 1



BDS=BEGINNING OF DOUBLE SUPPORT, BSS=BEGINNING OF SINGLE SUPPORT

Figure 53: Angular Momentum of the Body about the CMs, Subject 2



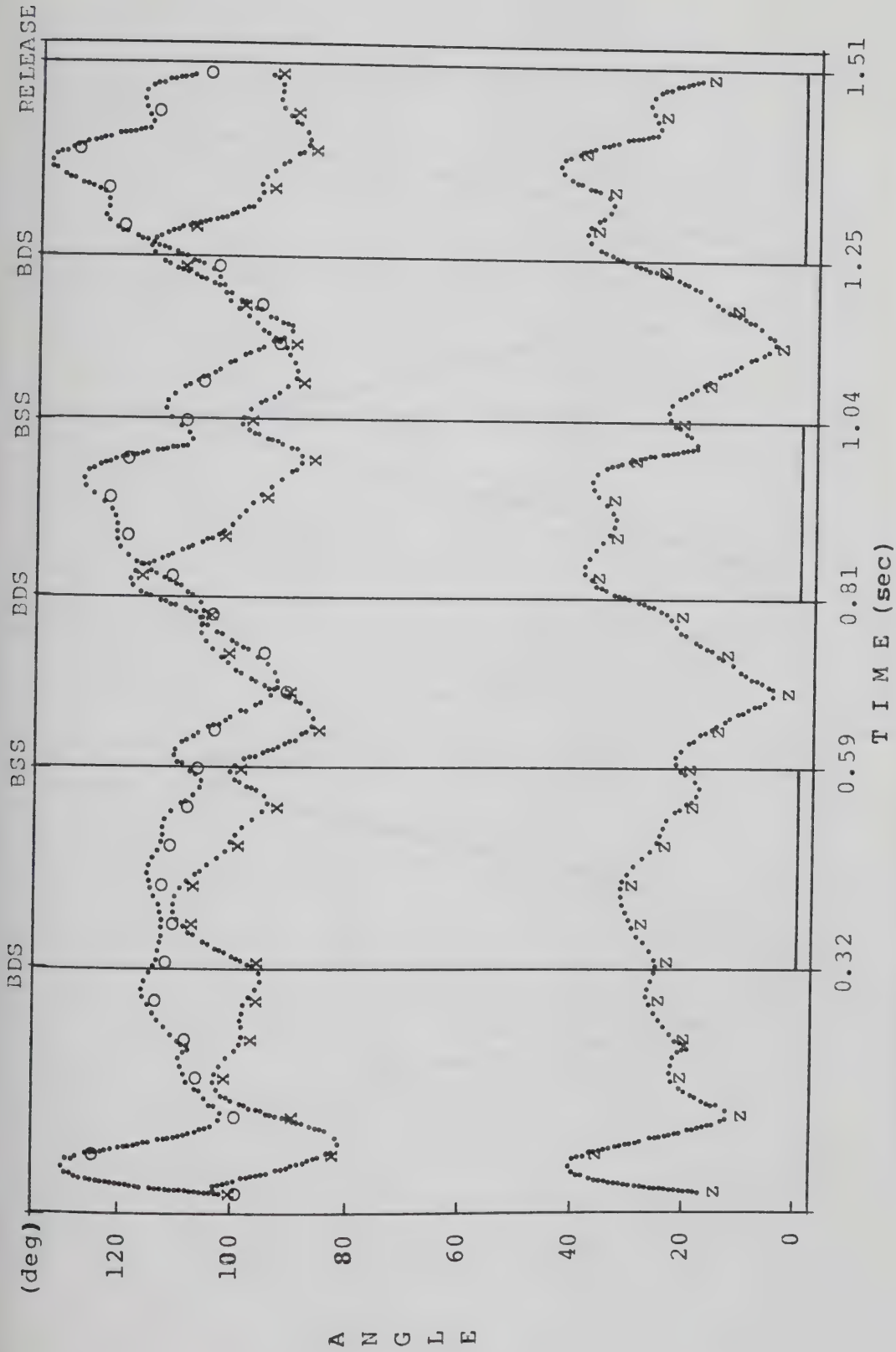
BDS=BEGINNING OF DOUBLE SUPPORT, BSS=BEGINNING OF SINGLE SUPPORT

Figure 54: Angular Momentum of the Body about the CMs, Subject 3

the last single support phase for Subject 2. Increase in the angular momentum of the body occurred during the first two double support phases for Subject 1, and during the first three double support phases for Subject 3. Subject 2 presented increases in this parameter during all but the last single support phases. Subject 2 also presented greater oscillations of the angular momentum during all the throw than did the other subjects. During the last double support phase, all subjects maintained a relatively constant angular momentum until the MIN-Z point. After the MIN-Z the angular momentum decreased rapidly until the release point was reached.

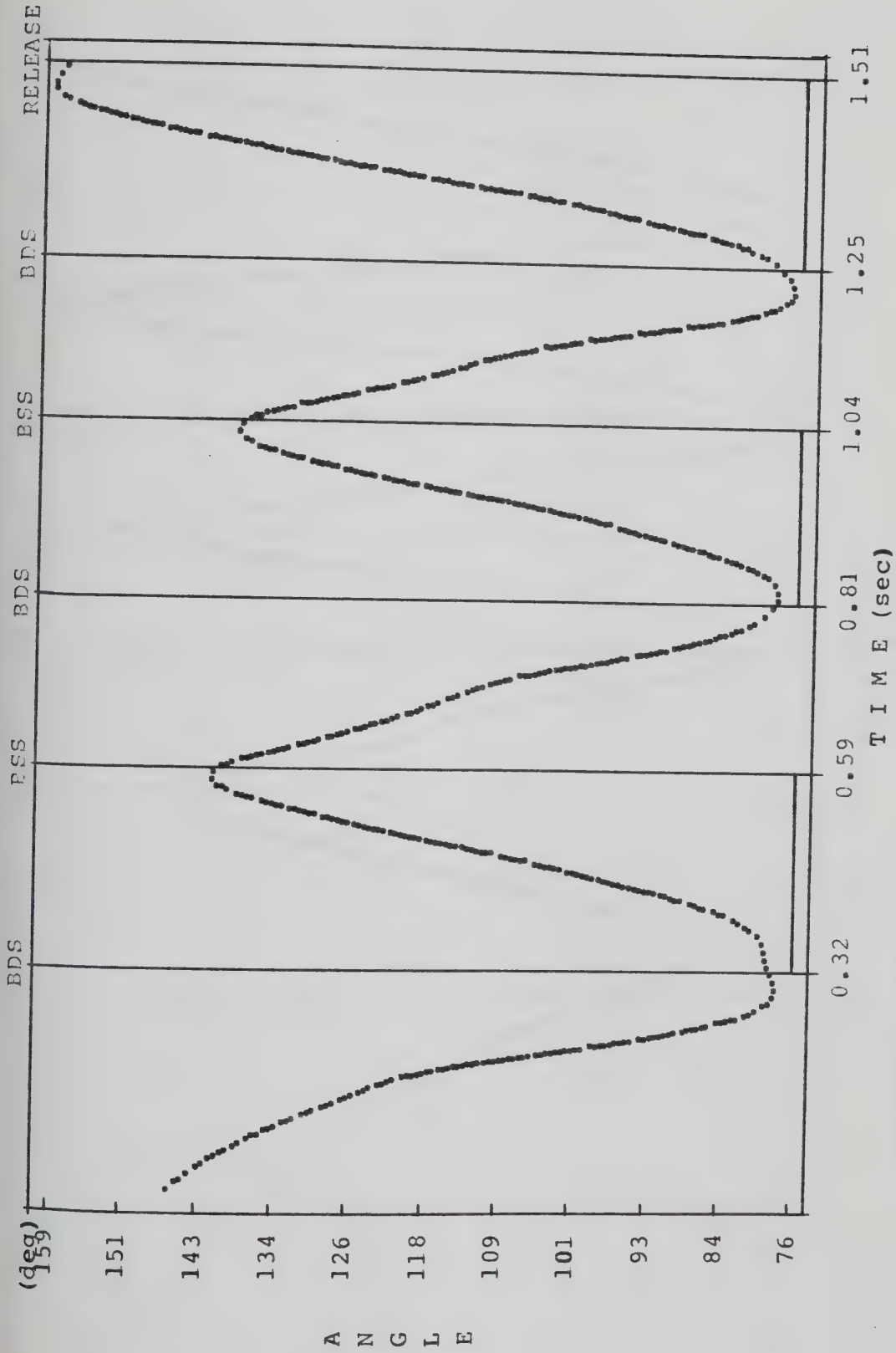
The direction angles of the angular momentum vector of the body for Subject 1 are presented in Figure 55. These angles together with the direction angles of the same vector of the hammer (Figure 34) indicate that the planes of movement of the hammer and body became parallel in the middle of the double support phase just before the hammer reached the MIN-Z point.

The angle of the knee joint of the supporting leg was analyzed. During the throw this angle ranged from 75° to 160° for all subjects. In each turn the angle was greater at the BSS point and least at the BDS point (Figures 56, 57 and 58). All subjects reached the greater angle of the knee in the last double support phase. During all but the last turn each subject presented a different pattern knee of flexion/extension. Subject 1 presented the same flexion and



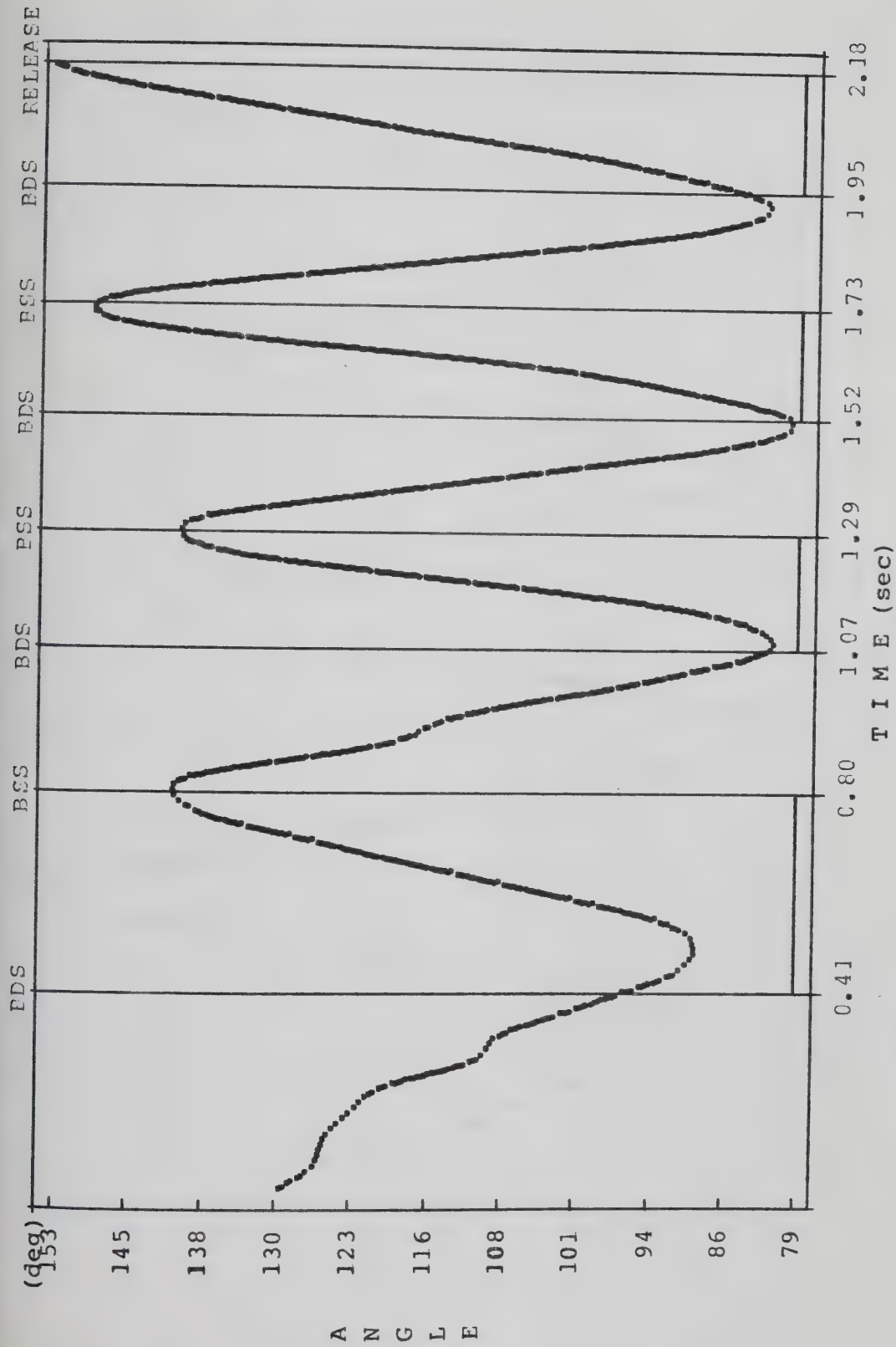
BDS=BEGINNING OF DOUBLE SUPPORT, BSS=BEGINNING OF SINGLE SUPPORT
 X-AXIS(x), Y-AXIS(o), Z-AXIS(z)

Figure 55: Direction Angles of the Angular Momentum Vector of the BODY, Subject 1



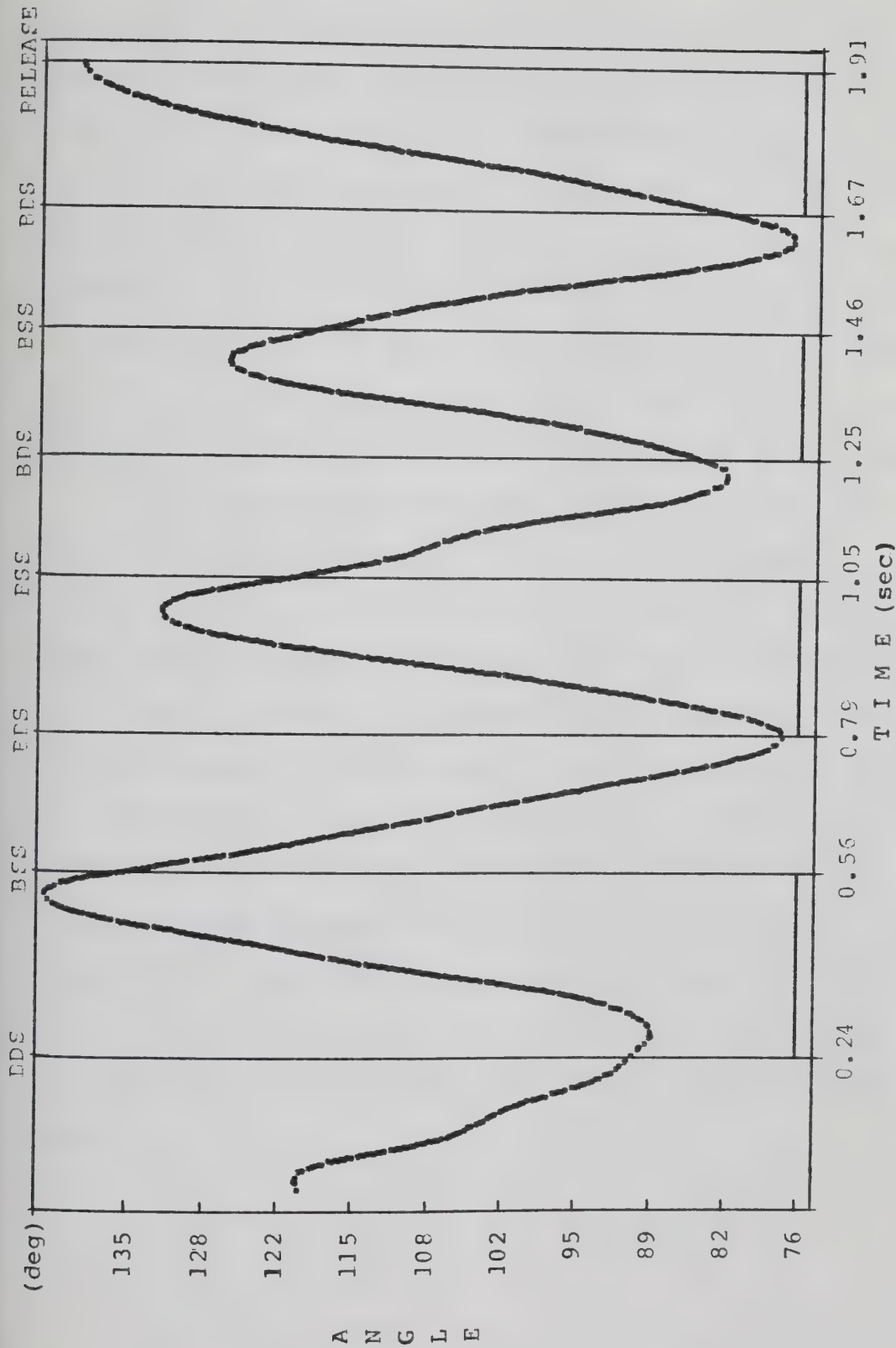
BDS=BEGINNING OF DOUBLE SUPPORT, BSS=BEGINNING OF SINGLE SUPPORT

Figure 56: Left Knee Angle, Subject 1



BDS=BEGINNING OF DOUBLE SUPPORT, BSS=BEGINNING OF SINGLE SUPPORT

Figure 57: Left Knee Angle, Subject 2



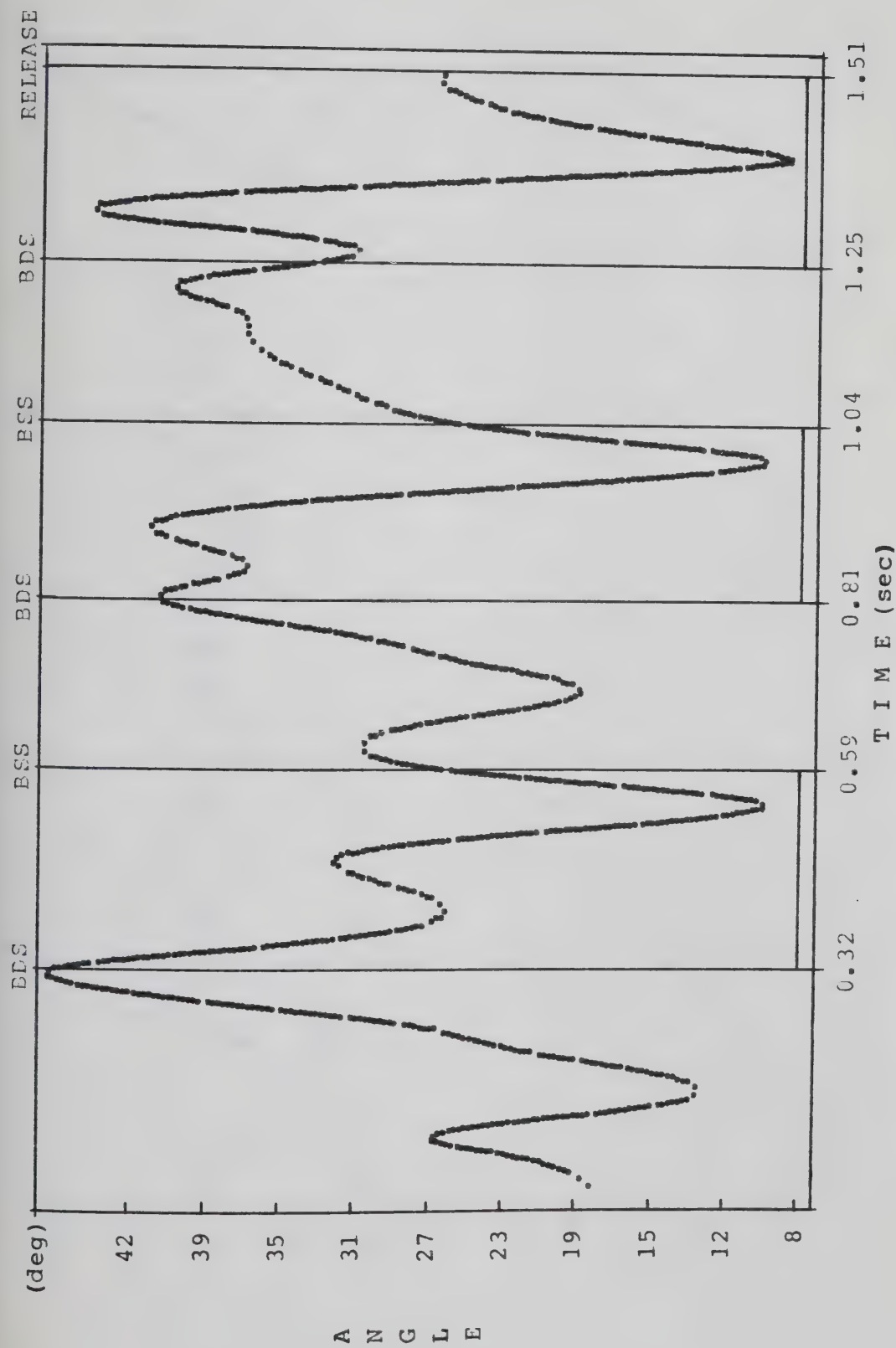
BDS=BEGINNING OF DOUBLE SUPPORT, BSS=BEGINNING OF SINGLE SUPPORT

Figure 58: Left Knee Angle, Subject 3

extension in the first and second turn. Subject 2, presented a gradual increase in extension after the first turn, while Subject 3 presented a gradual decrease of extension in the first three turns. Subject 3 started flexing his knee before the double support phase had terminated. This could indicate that he did not use all the double support time for force production. All the subjects started knee extension before the BDS point in the last turn. Subjects 1 and 3 reached maximum extension before the release point, while Subject 2, was still extending his knee at the time of release point.

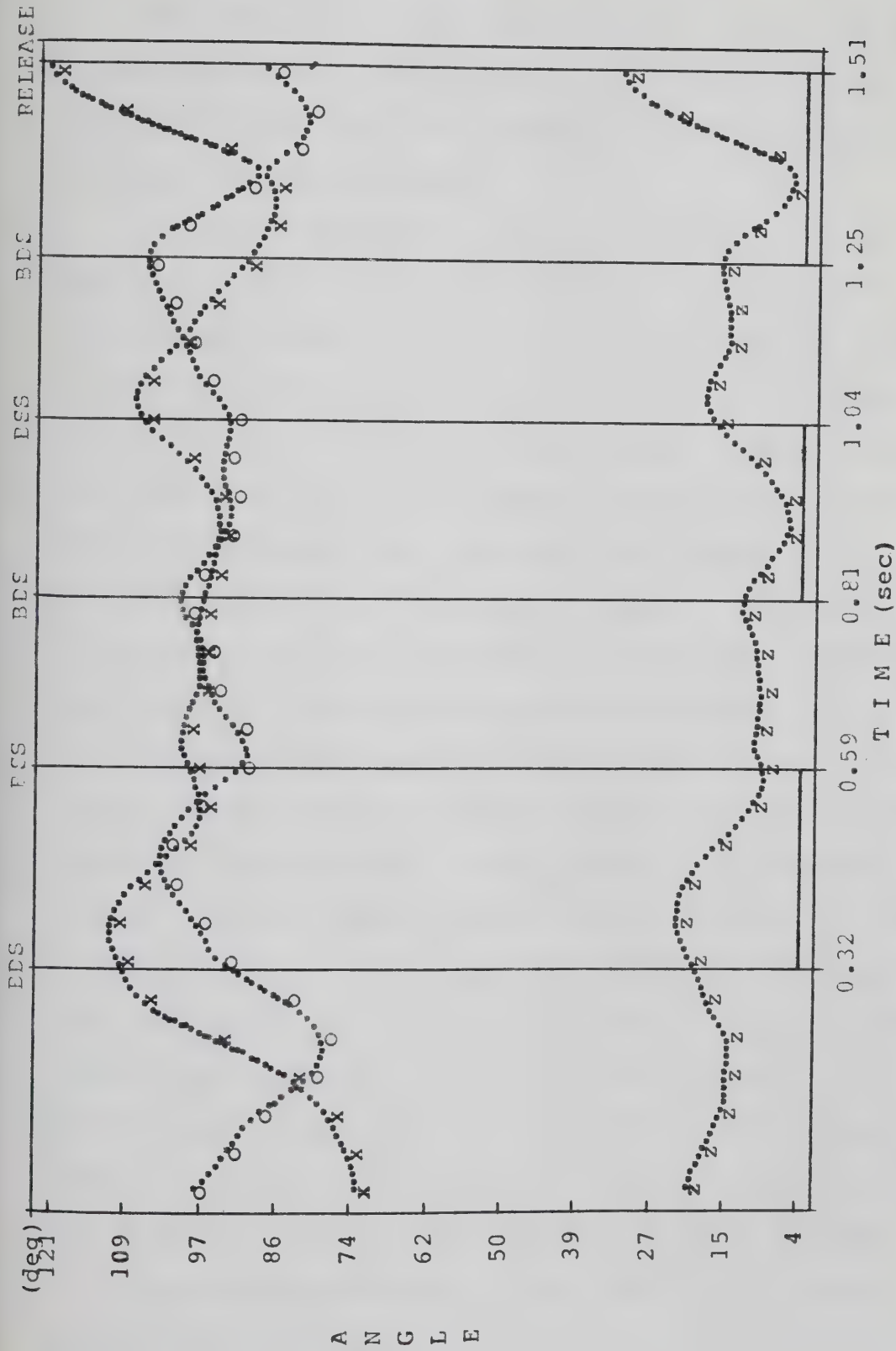
The angle of the hip line with the shoulder line ranged from 8° to 47° for Subject 1, 3° to 50° for Subject 2 and 6° to 59° for Subject 3 (Figure 59). In each turn the angle was greatest at the BDS point. The local minimum angle for each turn occurred before the double support phase was terminated and the angle started increasing again in the same phase.

The angles of the trunk with the X, Y and Z-axes changed as in Figure 60. Relative to the X and Z-axes the angles became maximum during the last double support phase, when the athletes applied a final force upon the hammer. In the same phase the angle of the trunk with the Y-axis became minimum before the release point and started increasing again.



BDS=BEGINNING OF DOUBLE SUPPORT, BSS=BEGINNING OF SINGLE SUPPORT

Figure 59: Hips - Shoulders Angle, Subject 1



BDS=BEGINNING OF DOUBLE SUPPORT, BSS=BEGINNING OF SINGLE SUPPORT
X-AXIS(x), Y-AXIS(o), Z-AXIS(z)

Figure 60: Angles of Trunk with the X, Y, Z Axes, Subject 1

E. Kinematics and Kinetics of the System

The analysis of the kinematics and kinetics of the system was based on the movement of the center of mass of the system (CMs) and the movement of the body segments plus the hammer about this point.

Figure 61 represents the spatial coordinates of the CMs, for Subject 1. The coordinates of the CMs point for the other subjects were similar to the ones presented in Figure 61. The maximum Z for each turn occurred in the middle of the single support phase, while the same maximum for the CMb occurred at the end of the double support phase. Figures 62, 63 and 64 represent the trajectory of the CMs in the different planes for Subject 3. Subjects 1 and 2 presented trajectories similar to Subject 3. In the horizontal plane the CMs moved in an parabolic epicycloid mode.

Figures 65, 66 and 67 represent the radii of curvature of the CMs for all the subjects. The CMs presented the greatest translation at the end of the single support and beginning of the double support phase. This translation was caused mainly by the movement of the CMb, which in this instance moved in the direction of the throw. The greatest translation among all the turns occurred at the beginning of the last double support phase. At this point, Subject 1 had greater translation than the other two subjects, achieving the highest velocity of his CMb at that point (Figure 44).

The resultant velocity of the CMs for each subject is presented in Figures 68, 69 and 70. The three turns allowed

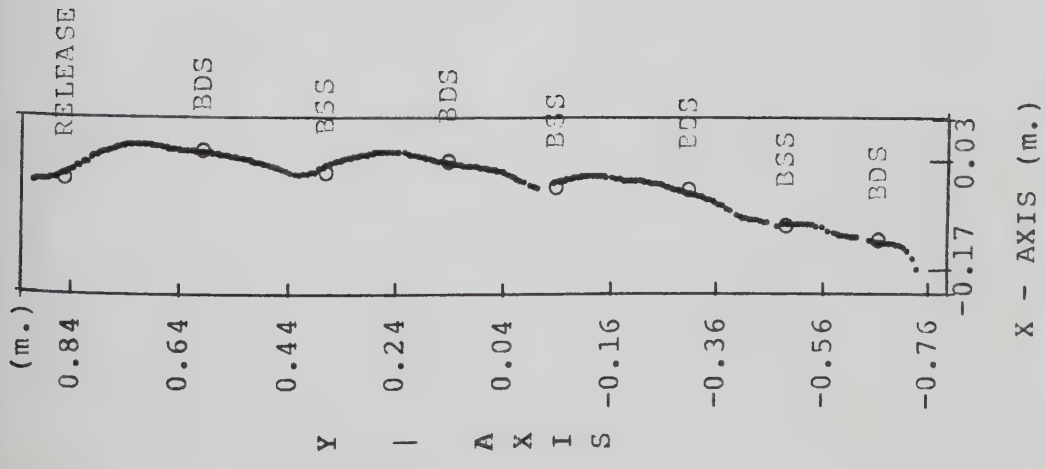


Figure 62: CMS Trajectory in the X-Y Plane, Subject 3

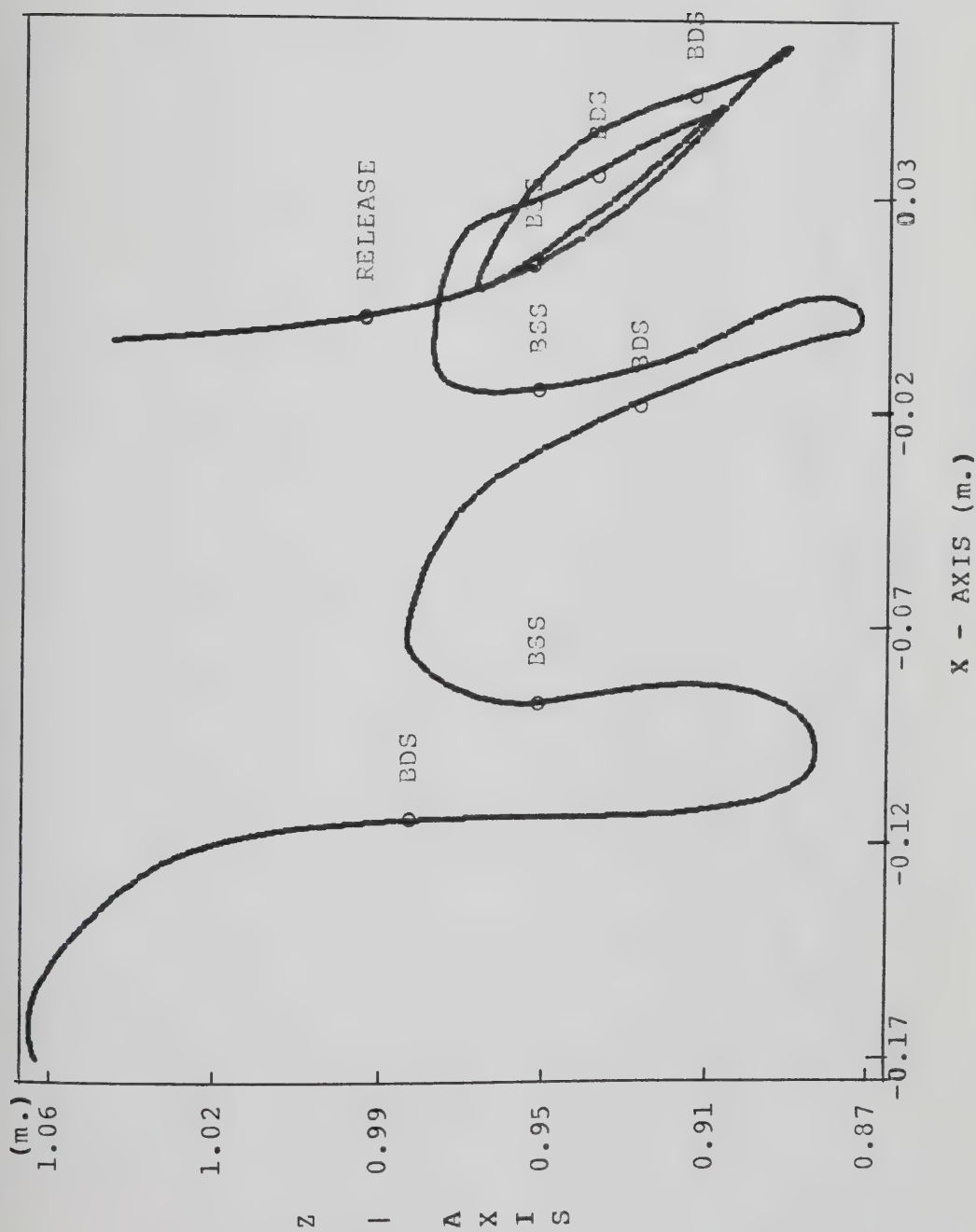


Figure 63: CMS Trajectory in the X-Z Plane, Subject 3

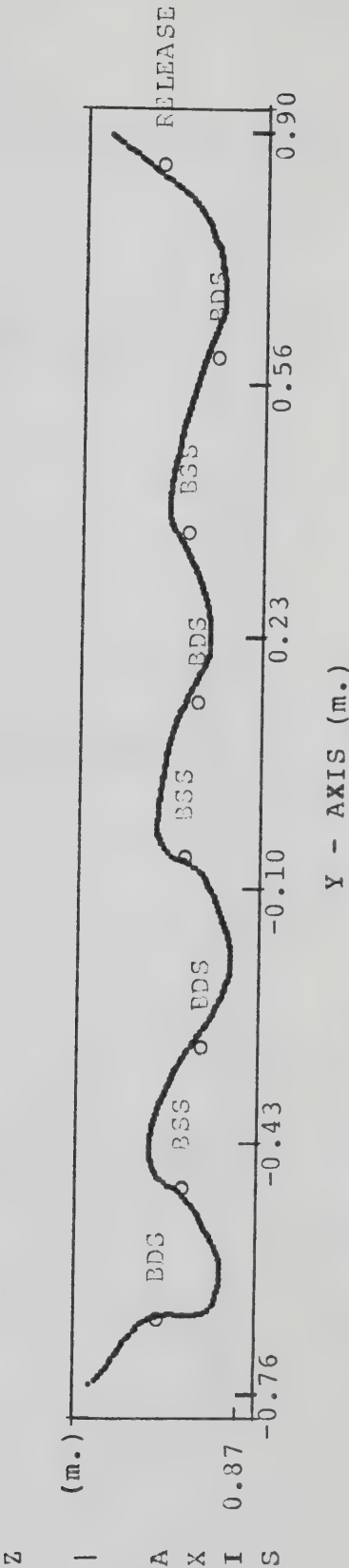
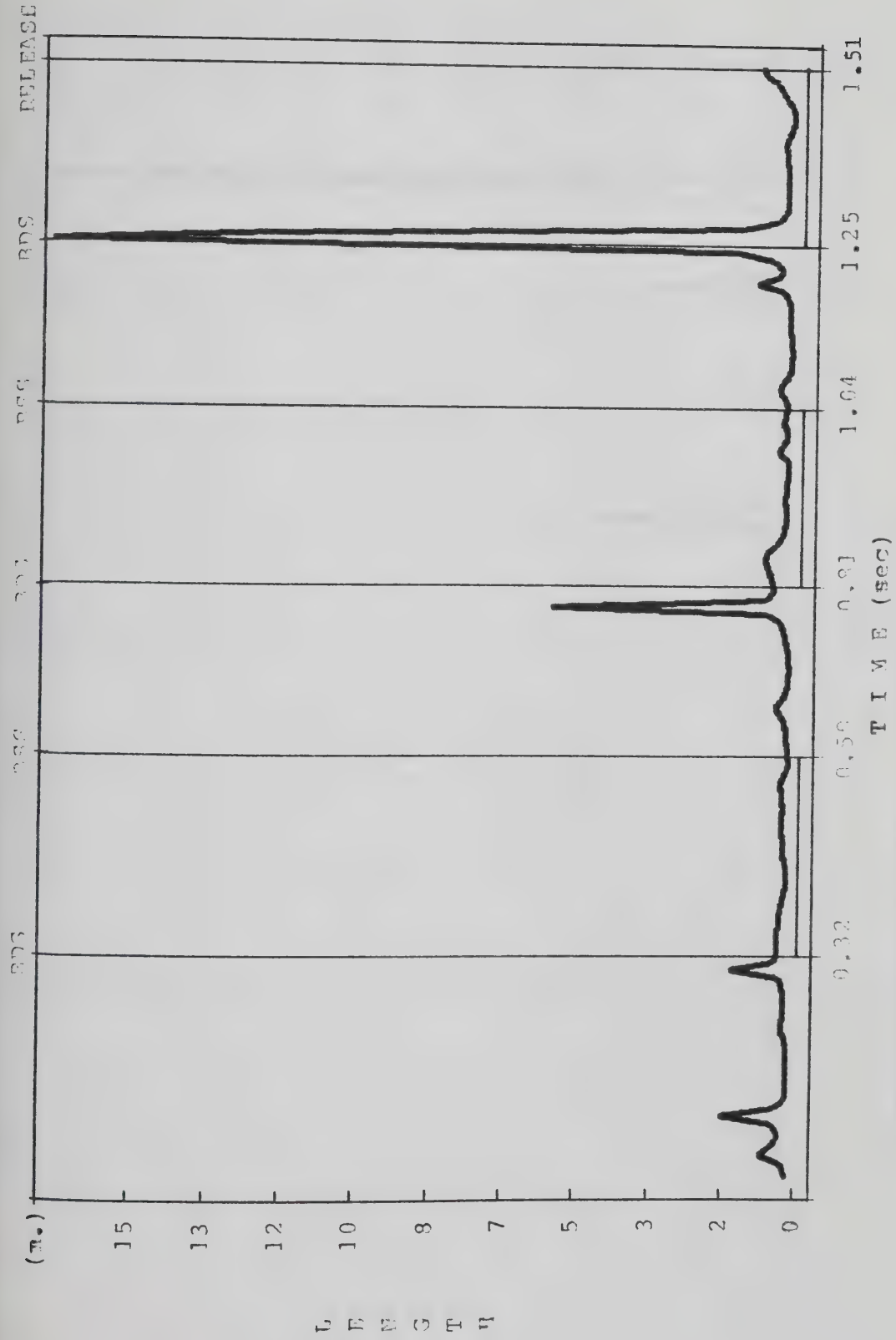
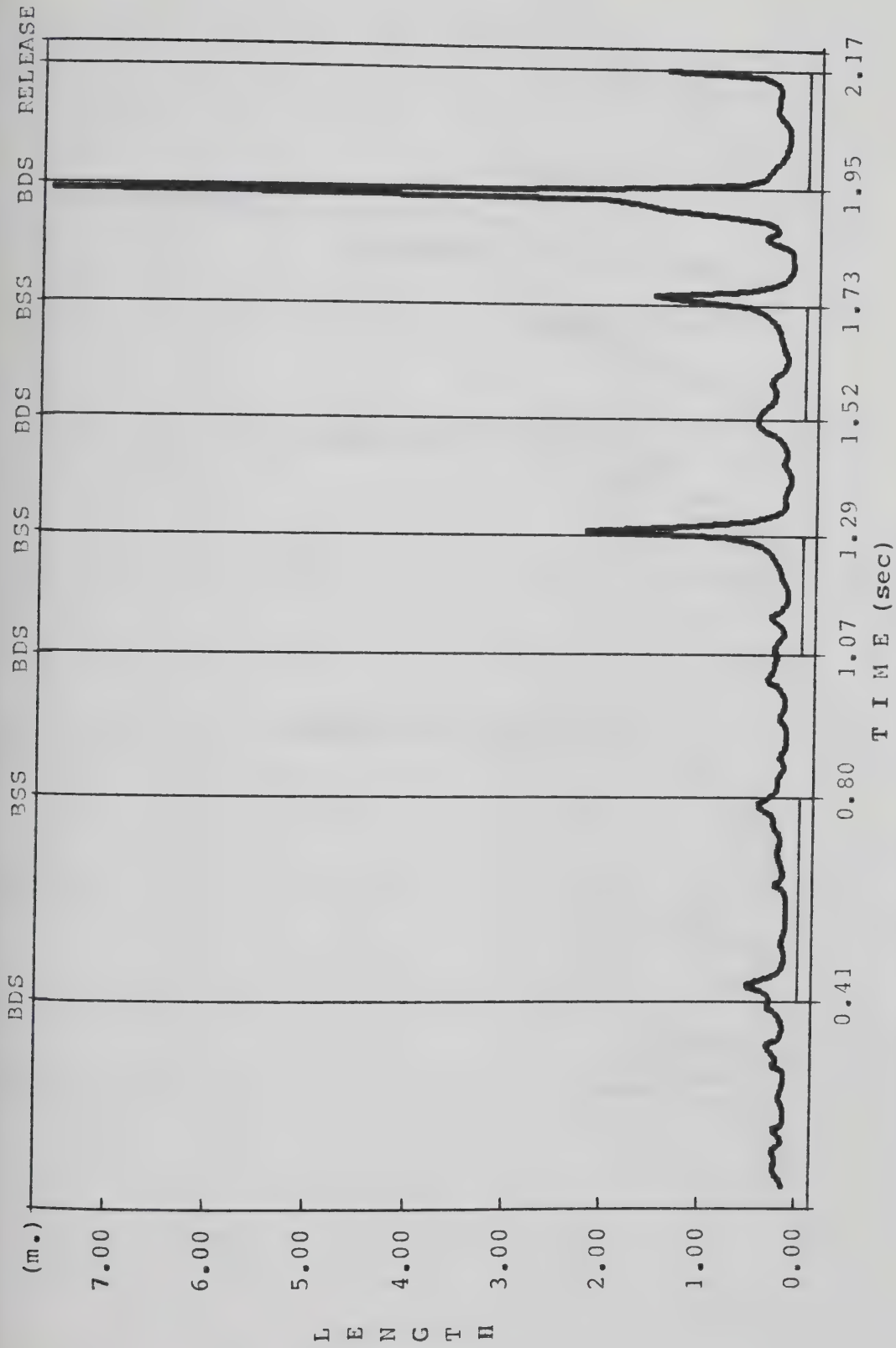


Figure 64: CMs Trajectory in the Y-Z Plane, Subject 3



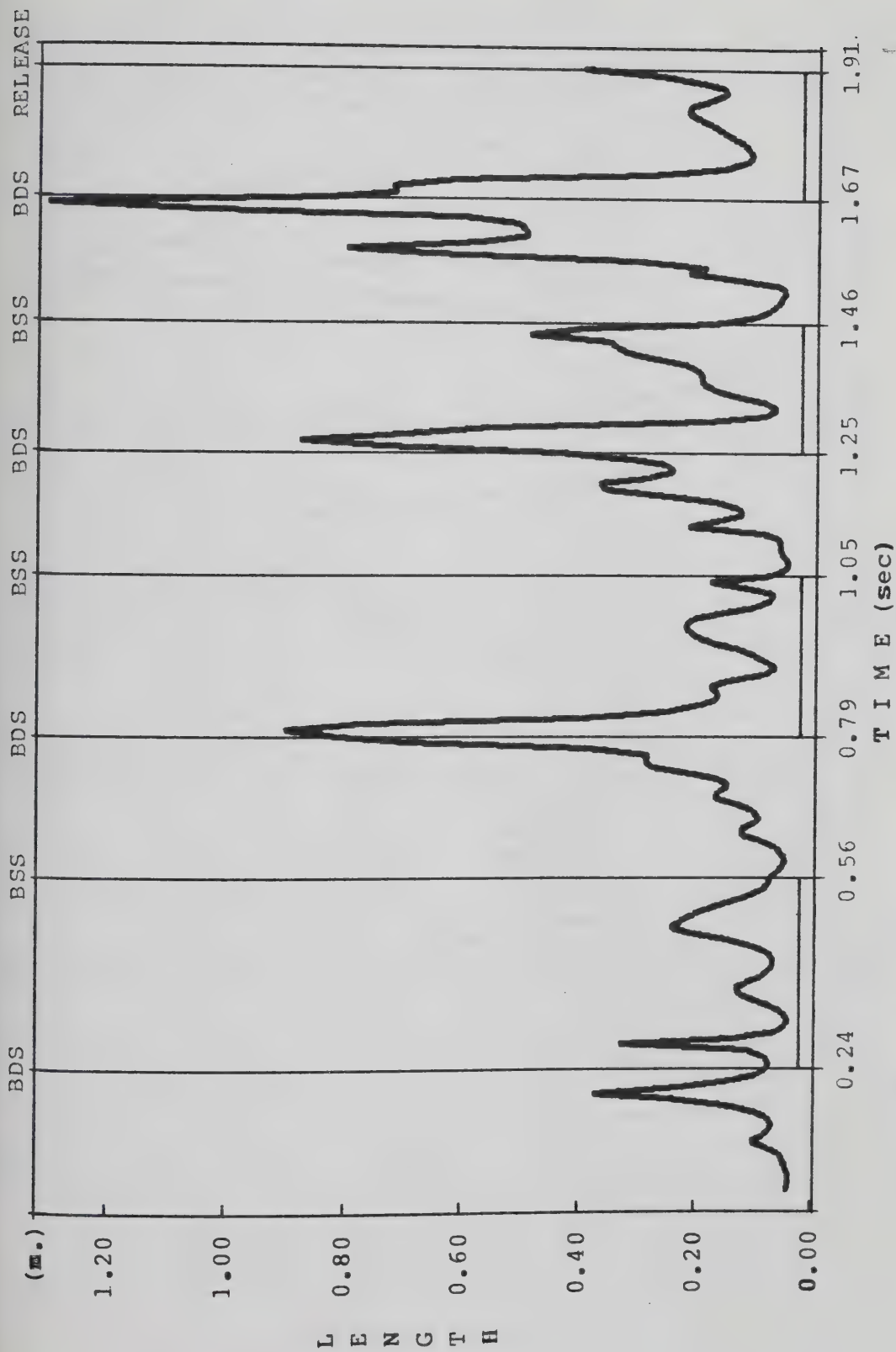
BDS=BEGINNING OF DOUBLE SUPPORT, BSS=BEGINNING OF SINGLE SUPPORT

Figure 65: Radius of Curvature of the CMs, Subject 1



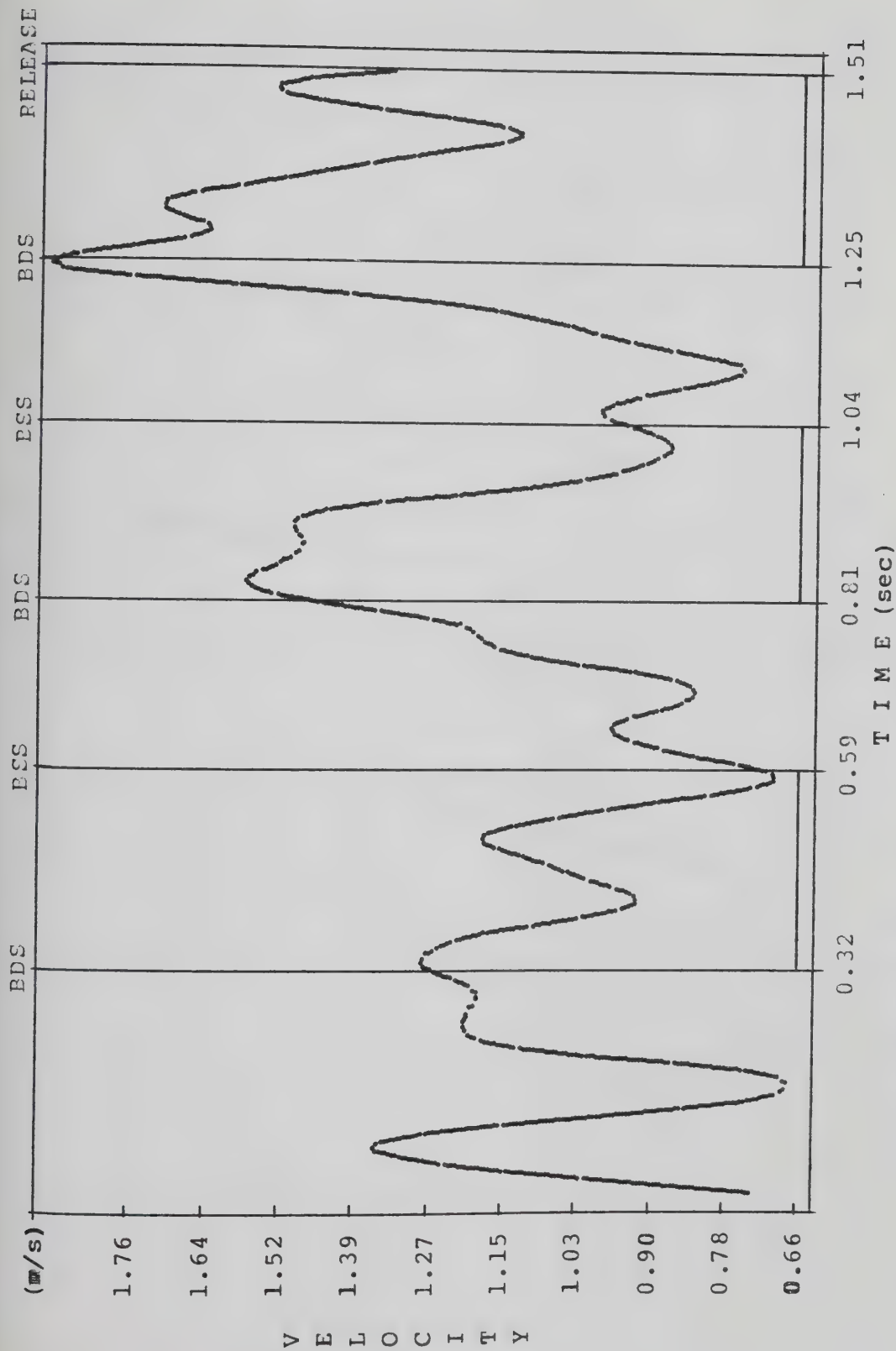
BDS-BEGINNING OF DOUBLE SUPPORT, BSS-BEGINNING OF SINGLE SUPPORT

Figure 66: Radius of Curvature of the CMS, Subject 2



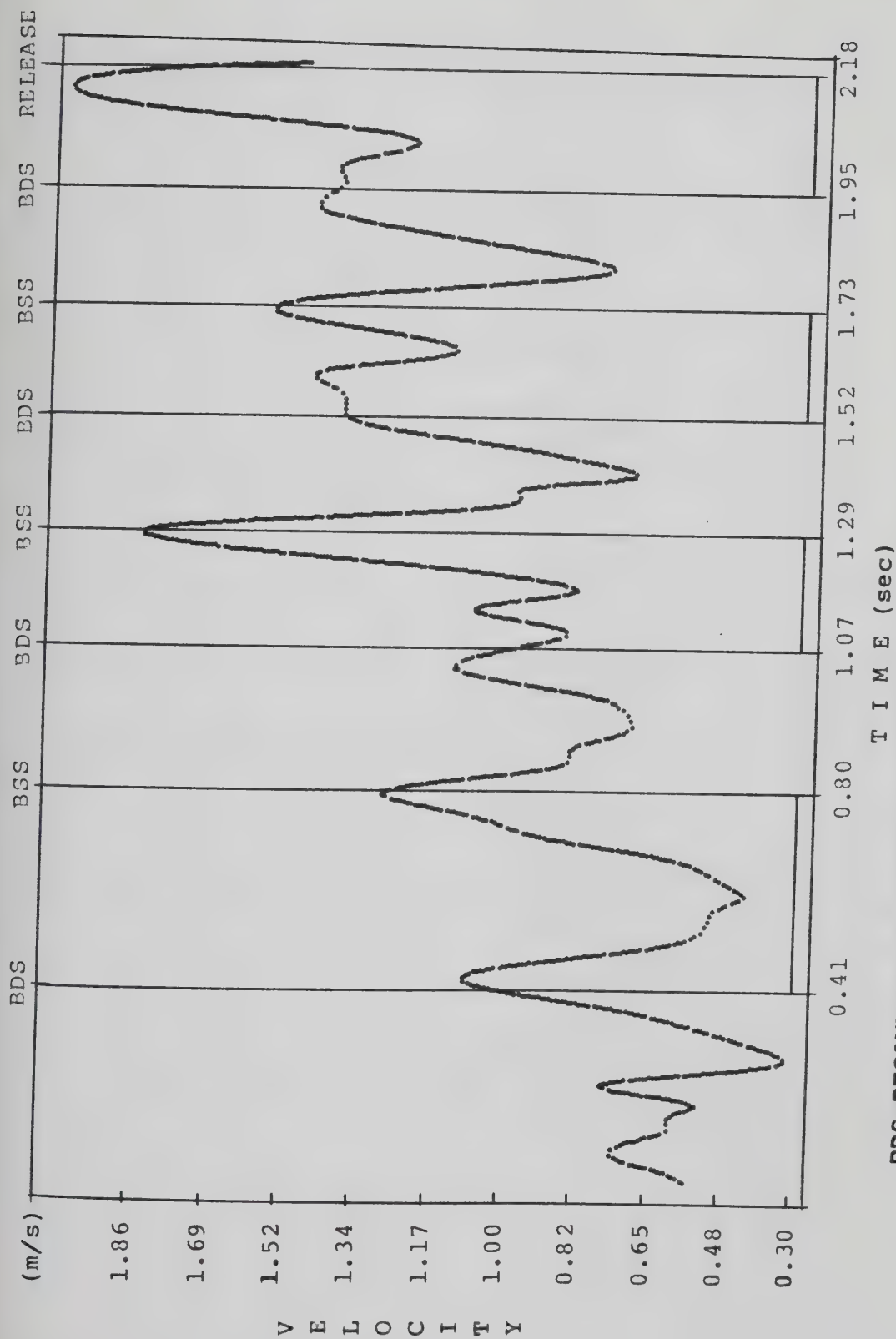
BDS=BEGINNING OF DOUBLE SUPPORT, BSS=BEGINNING OF SINGLE SUPPORT

Figure 67: Radius of Curvature of the CMs, Subject 3



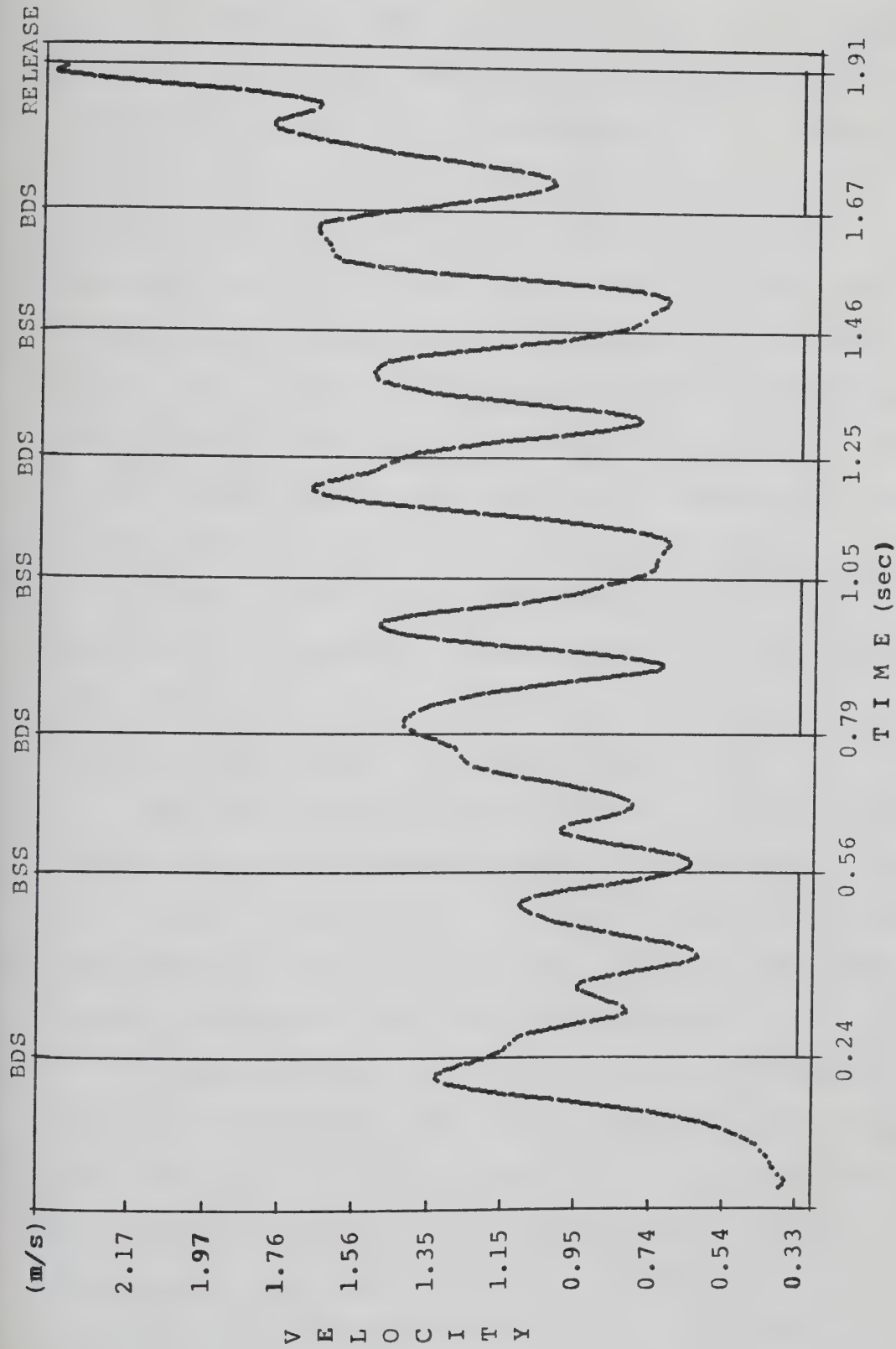
BDS=BEGINNING OF DOUBLE SUPPORT, BSS=BEGINNING OF SINGLE SUPPORT

Figure 68: Linear Velocity of the CMs, Subject 1



BDS=BEGINNING OF DOUBLE SUPPORT, BSS=BEGINNING OF SINGLE SUPPORT

Figure 69: Linear Velocity of the CMs, Subject 2



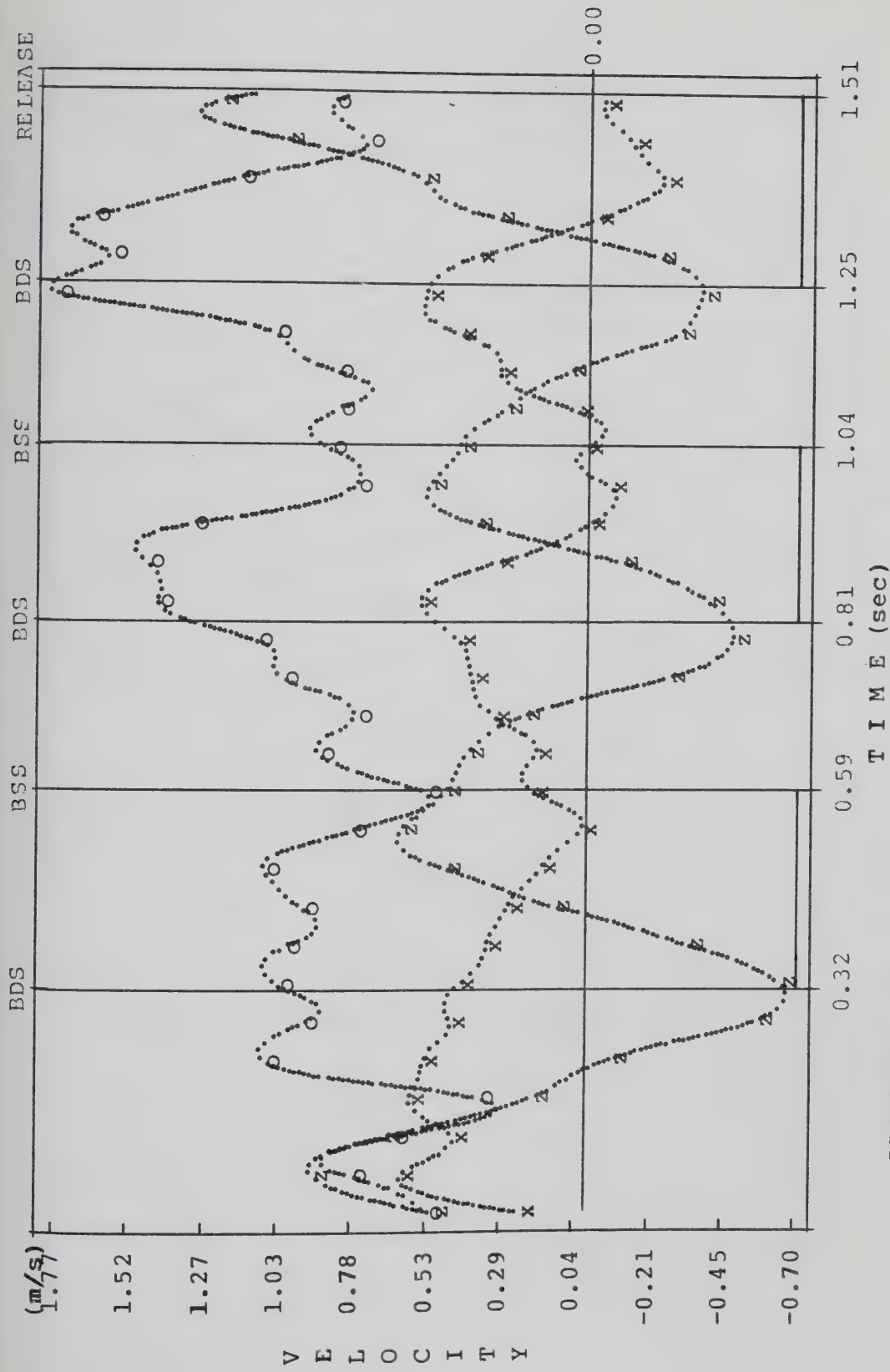
BDS=BEGINNING OF DOUBLE SUPPORT, BSS=BEGINNING OF SINGLE SUPPORT

Figure 70: Linear Velocity of the CMs, Subject 3

Subject 1 to have smoother velocity of CMs compared with the other subjects who used four turns. There was a gradual increase in velocity from turn to turn with the global maximum in the last turn. The maximum peak for Subject 1 occurred at the last BDS point. After this point the velocity decreased to a local minimum and increased again. Subjects 2 and 3, achieved their global maximum close to the release point. In the other turns, Subject 1 achieved his maximum and minimum velocities at the beginning of the double support phase and at the beginning of the single support phase respectively. Subject 2, achieved the maximum at the beginning of the single support phase and the minimum at the middle point of the same phase. Subject 3 who presented the greatest oscillations in velocity, achieved a first maximum at the end of the double support and a second maximum at the end of the single support phase.

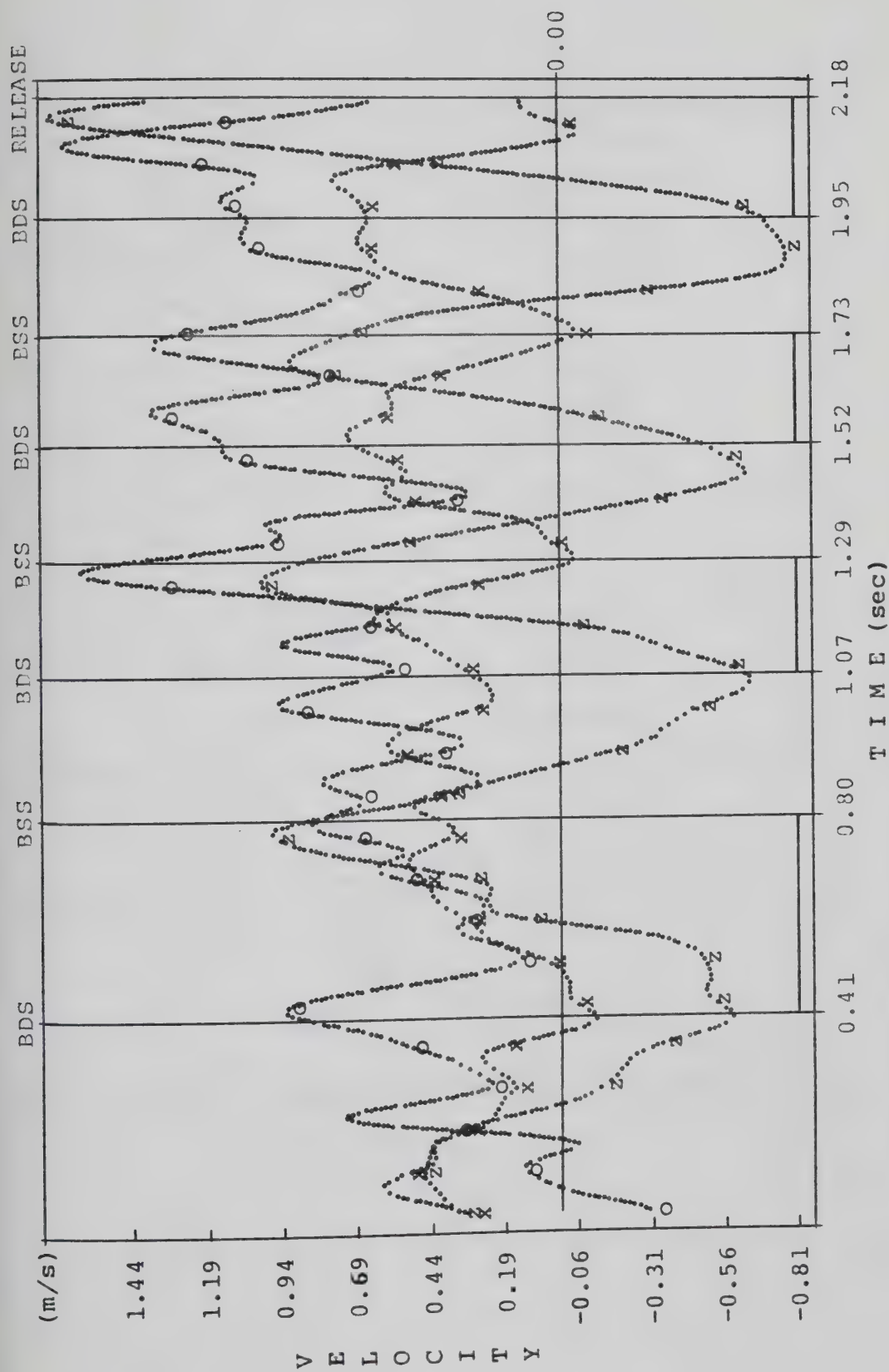
The linear velocities about the X, Y and Z-axes for all the subjects are presented in Figures 71, 72 and 73. It was the velocity in the Y direction which mainly contributed to the resultant velocity of the CMs. There was no common pattern of movement for the three subjects.

The acceleration curves of the CMs are presented in Figures 74, 75 and 76. The greater acceleration occurred in the direction of the throw (Y-axis) for all the subjects. In the last turn, Subject 1 achieved a great acceleration about the Z-axis, while in the direction of the Y-axis the acceleration was very small or negative. The same did not



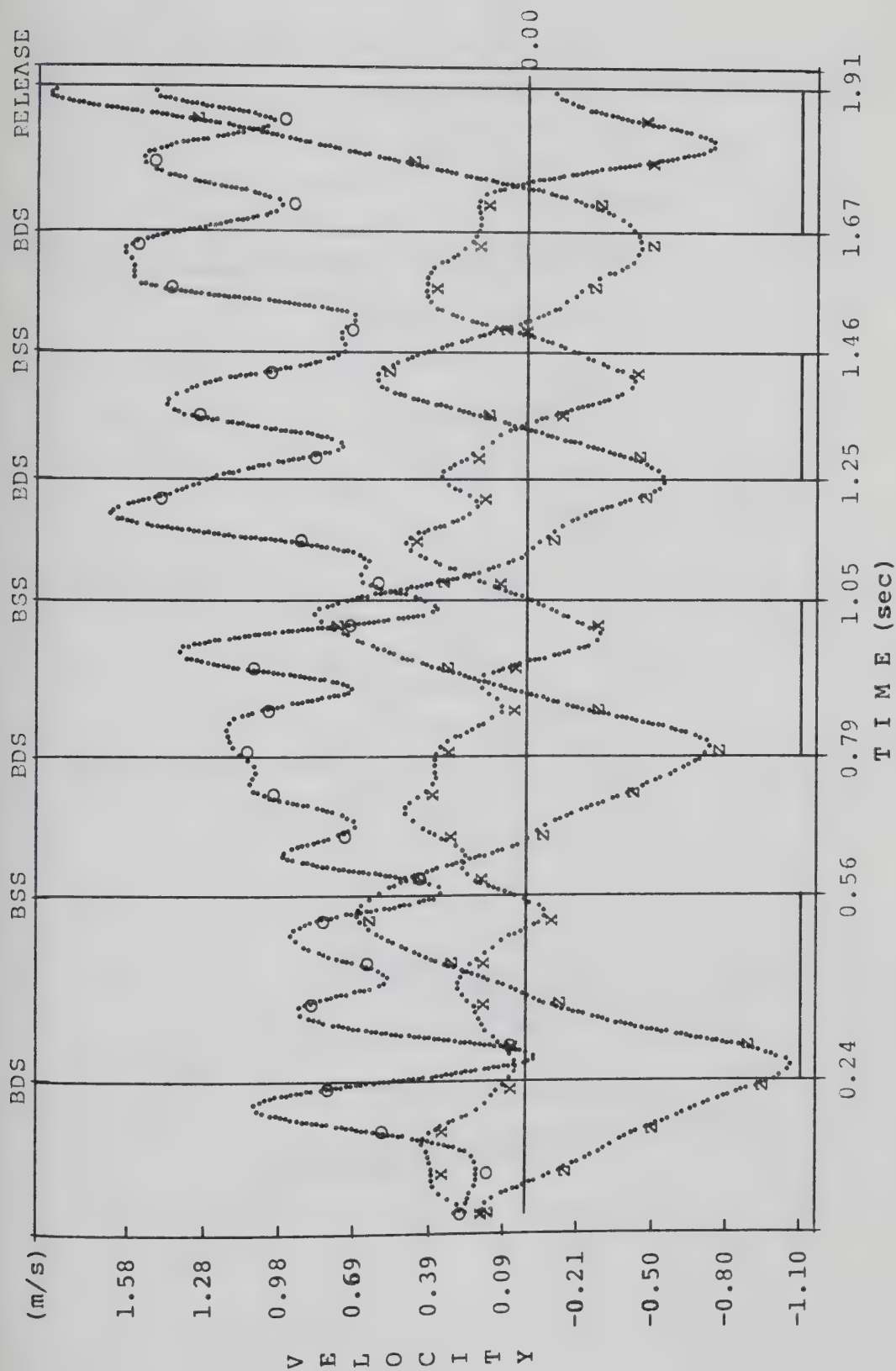
BDS=BEGINNING OF DOUBLE SUPPORT, BSS=BEGINNING OF SINGLE SUPPORT
X-AXIS(x), Y-AXIS(o), Z-AXIS(z)

Figure 71: Velocity of the CMs in the X, Y, Z Axes, Subject 1



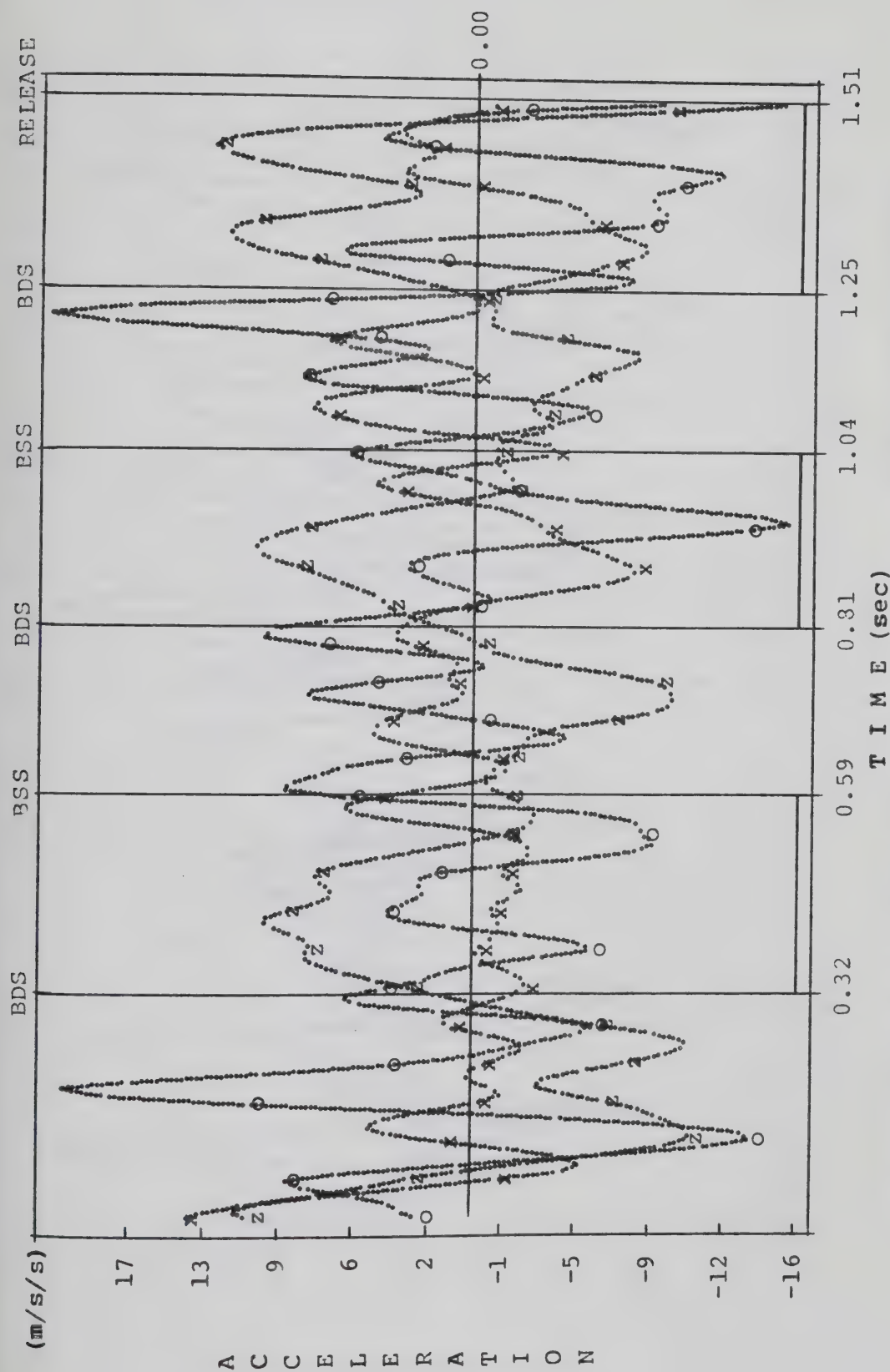
BDS=BEGINNING OF DOUBLE SUPPORT, BSS=BEGINNING OF SINGLE SUPPORT
X-AXIS(x), Y-AXIS(o), Z-AXIS(z)

Figure 72: Velocity of the CMs in the X, Y, Z Axes, Subject 2



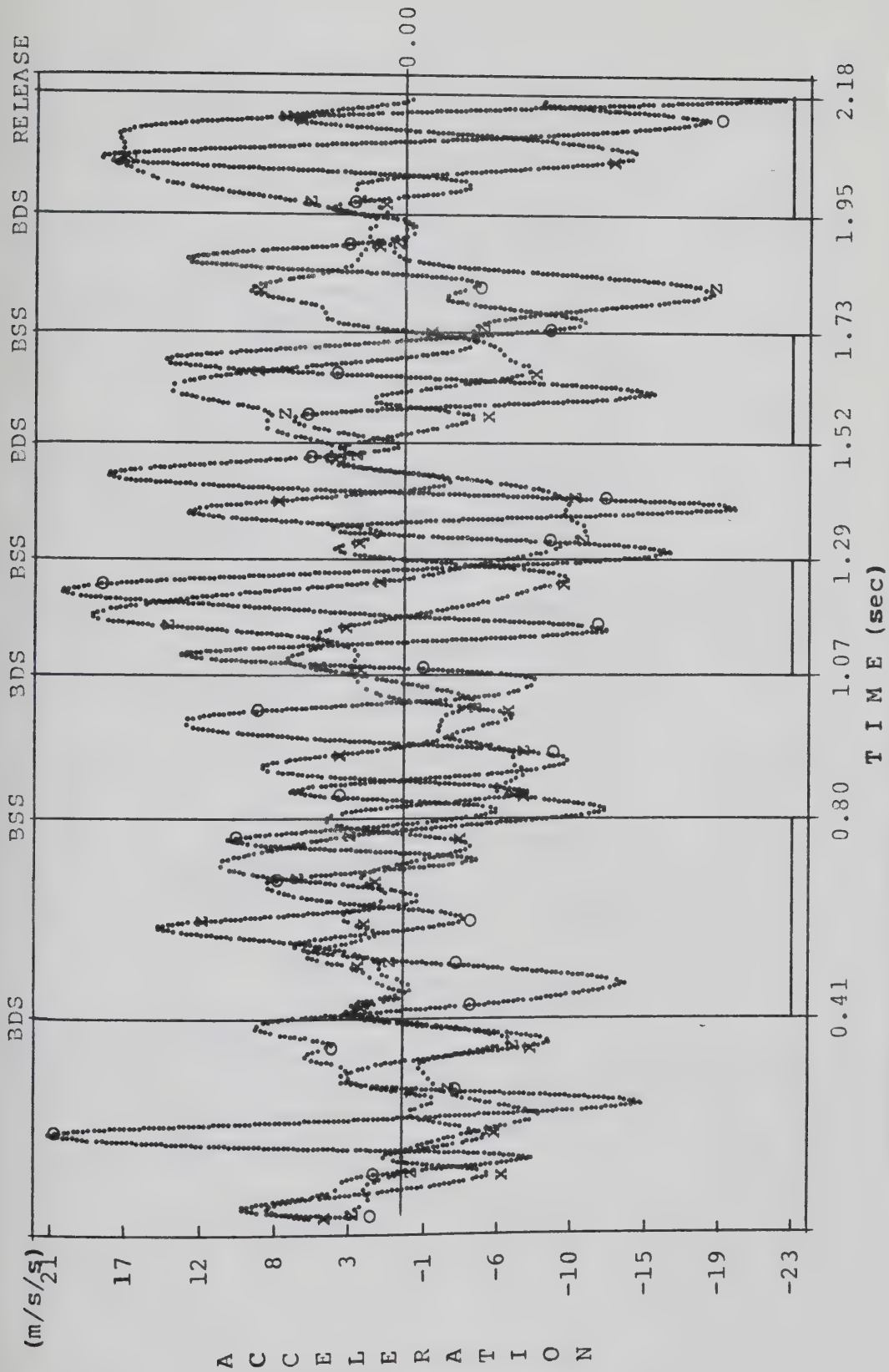
BDS-BEGINNING OF DOUBLE SUPPORT, BSS-BEGINNING OF SINGLE SUPPORT
X-AXIS(x), Y-AXIS(o), Z-AXIS(z)

Figure 73: Velocity of the CMs in the X, Y, Z Axes. Subject 3



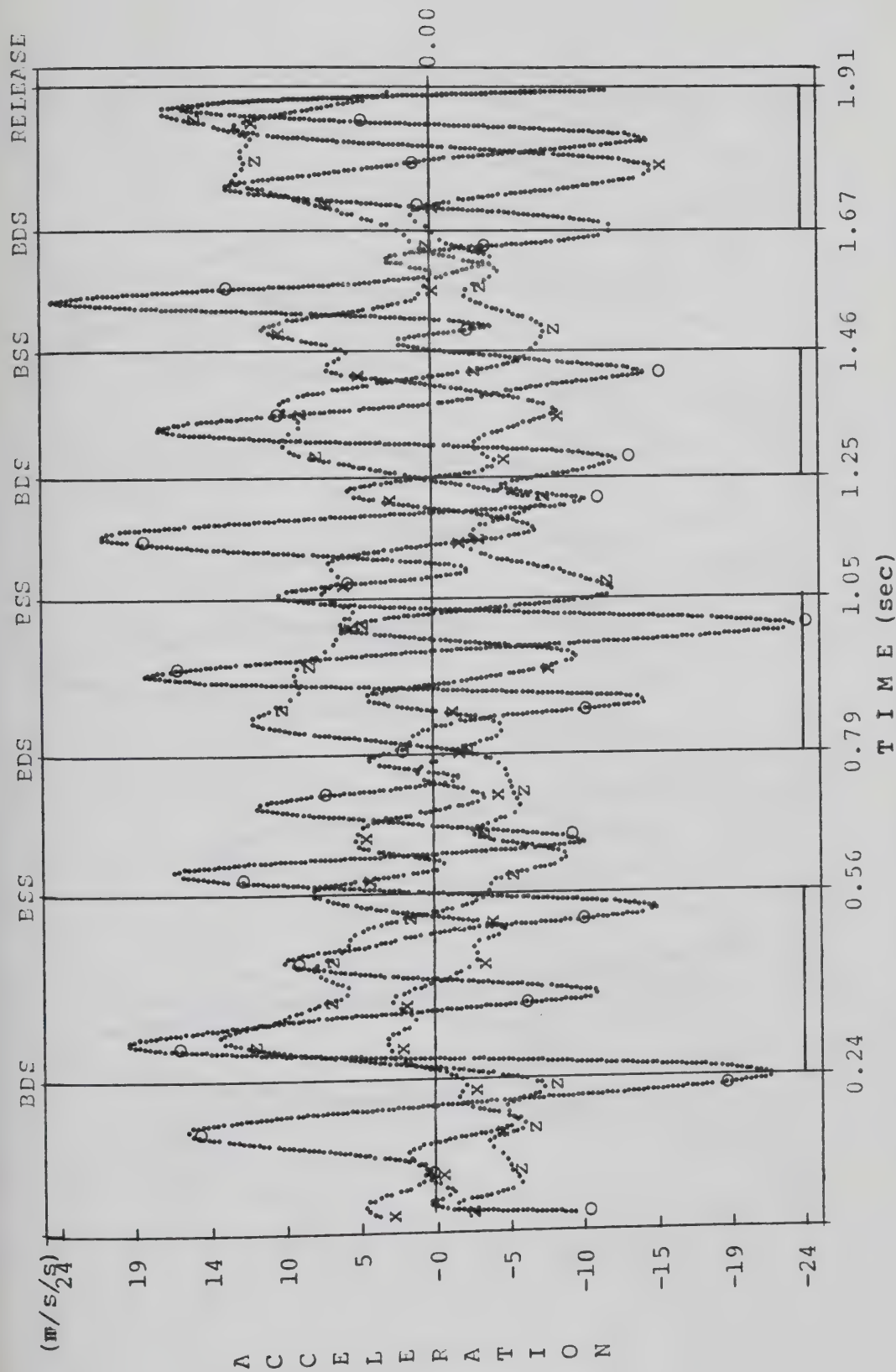
BDS=BEGINNING OF DOUBLE SUPPORT, BSS=BEGINNING OF SINGLE SUPPORT
X-Axis(x), Y-Axis(o), Z-Axis(z)

Figure 74: Acceleration of the CMs in the X, Y, Z Axes, Subject 1



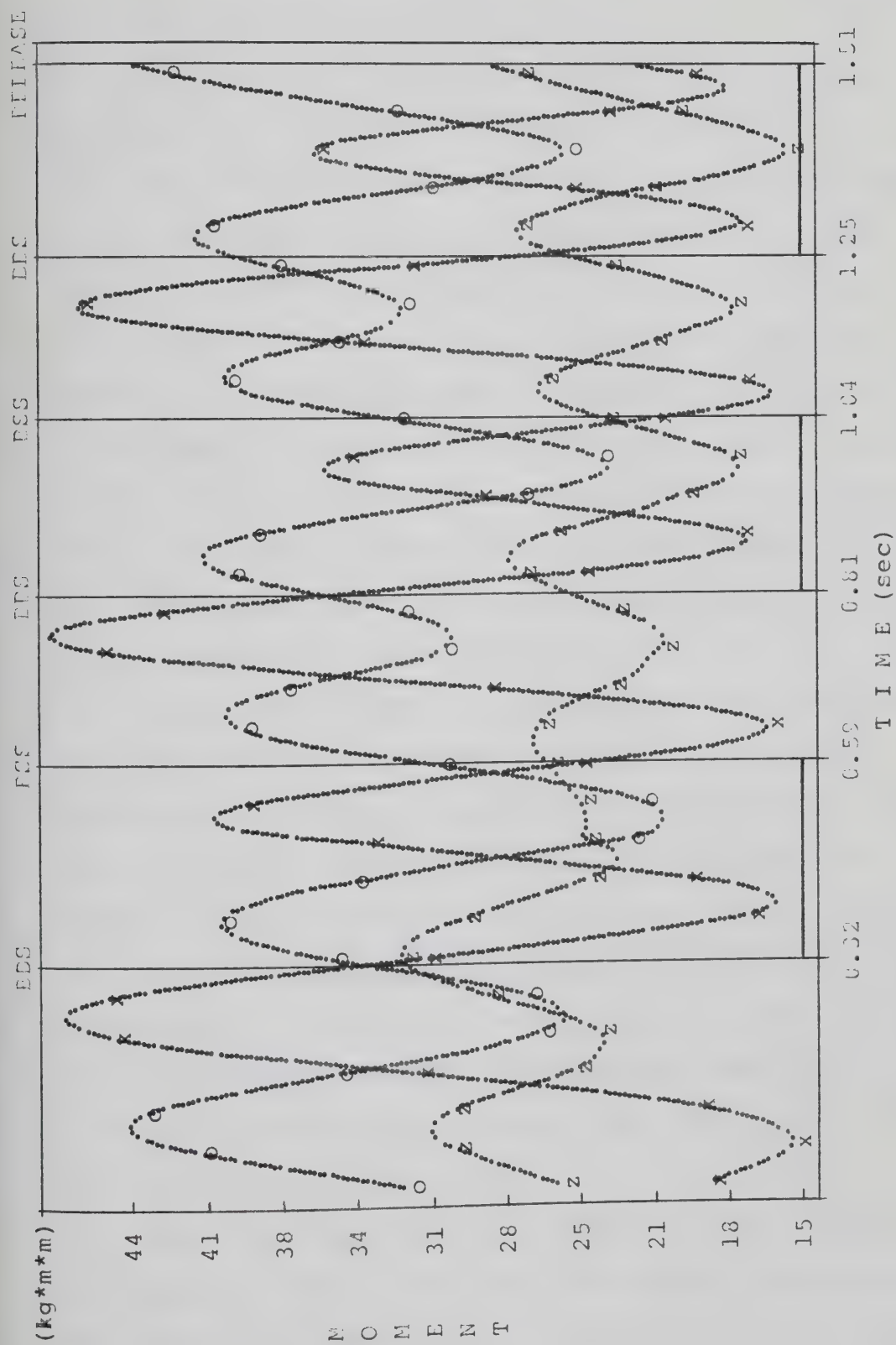
BDS=BEGINNING OF DOUBLE SUPPORT, BSS=BEGINNING OF SINGLE SUPPORT
X-AXIS(x), Y-AXIS(o), Z-AXIS(z)

Figure 75: Acceleration of the CMs in the X, Y, Z Axes, Subject 2



BDS=BEGINNING OF DOUBLE SUPPORT, BSS=BEGINNING OF SINGLE SUPPORT
X-AXIS(x), Y-AXIS(o), Z-AXIS(z)

Figure 76: Acceleration of the CMs in the X, Y, Z Axes, Subject 3



BDS=BEGINNING OF DOUBLE SUPPORT, BSS=BEGINNING OF SINGLE SUPPORT
X-AXIS(x), Y-AXIS(o), Z-AXIS(z)

Figure 77: Moments of Inertia of the System about its Center of Mass, Subject 1

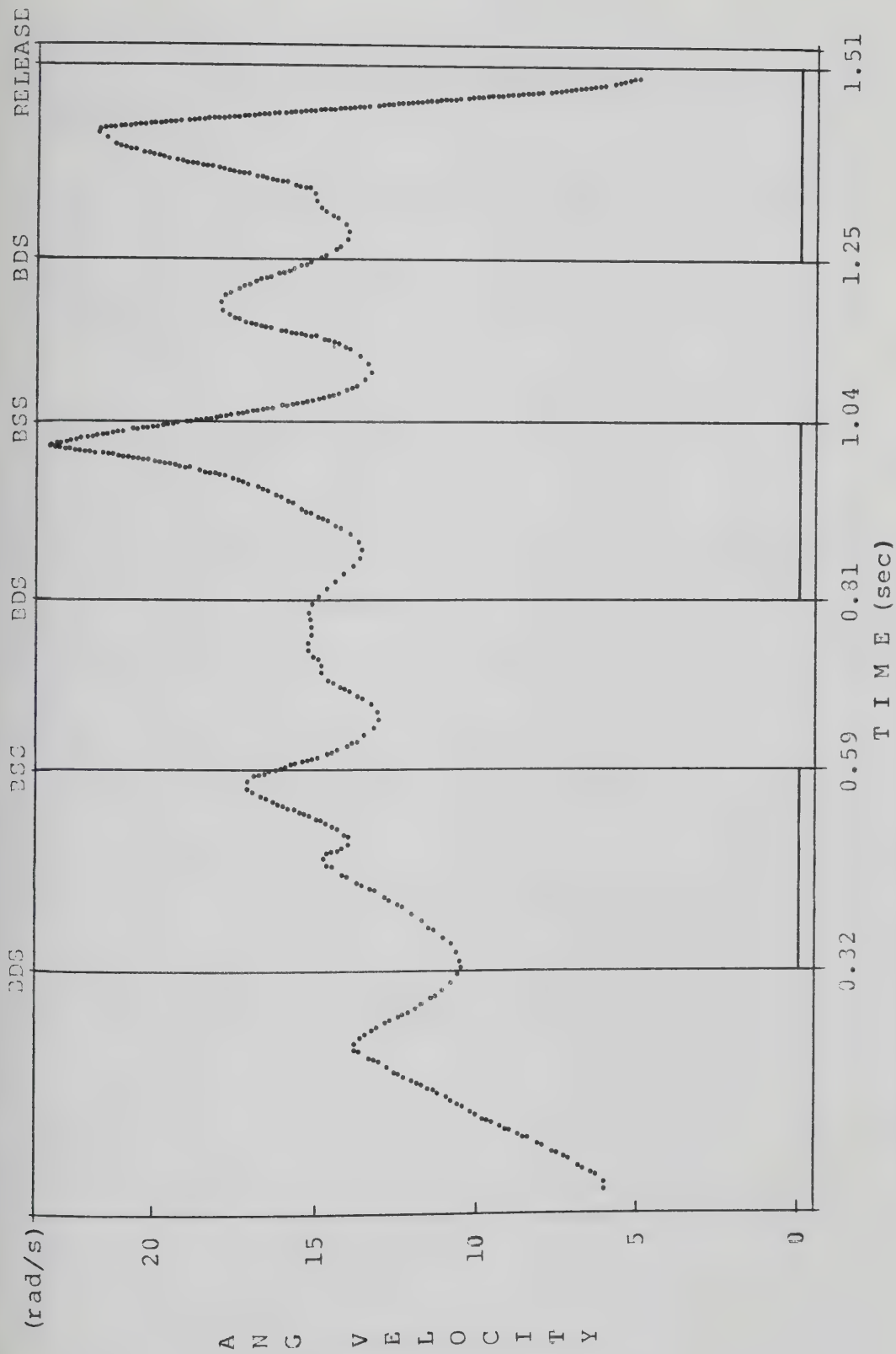
occur with Subjects 2 and 3 who had the same acceleration about the Y-axis as about the Z-axis.

The moments of inertia of the system for Subject 1, are presented in Figure 77. The moments of inertia of the system for the other subjects are similar to the ones of Subject 1. About the X-axis and when the hammer reached its MAX-Z the moment of inertia became greater than about the other axes in all the turns. After the first turn was completed, the moments of inertia about the Y and about the Z-axis changed in the same fashion. About the Z-axis the moment of inertia became minimum in the middle of the last double support phase. This was a result of the athletes' effort to apply all the forces in the vertical direction which drove the system necessarily closer to the vertical axis.

Figures 78, 79 and 80, represent the instantaneous angular velocity of the system. There was a gradual increase in the angular velocity of the system from turn to turn. It became maximum before the last BSS point for Subjects 1 and 3 and before the release point for Subject 2.

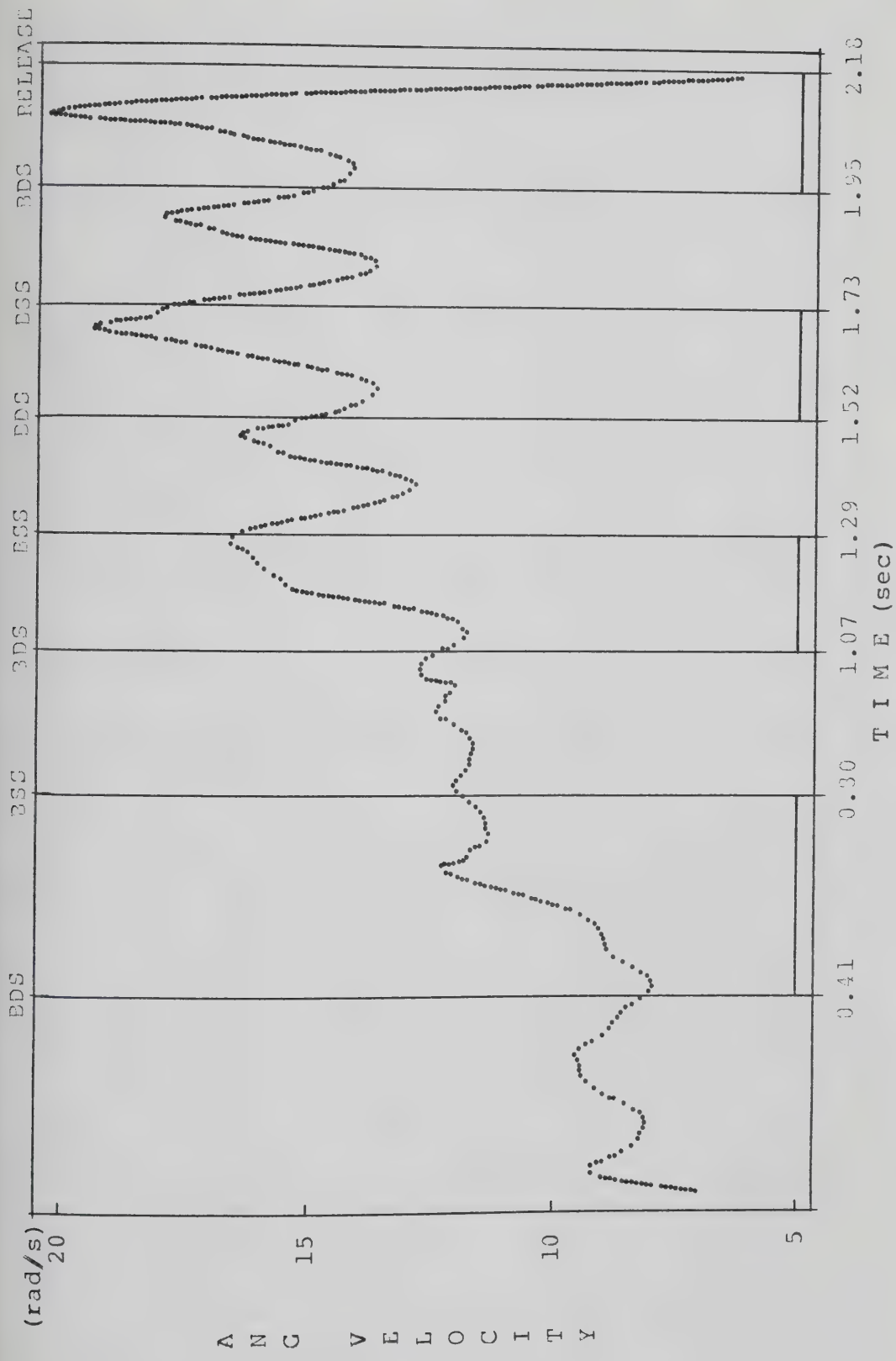
Figures 81, 82 and 83, represent the angular momentum of the system. The angular momentum of the system about the Z-axis was similar for all the subjects. About the Y-axis this momentum decreased gradually from turn to turn becoming minimum in the last BDS point.

Figure 84 represents the external torques of the system for Subject 1. About the Y and Z-axes these torques were maximum at the beginning of the throw and were minimum at



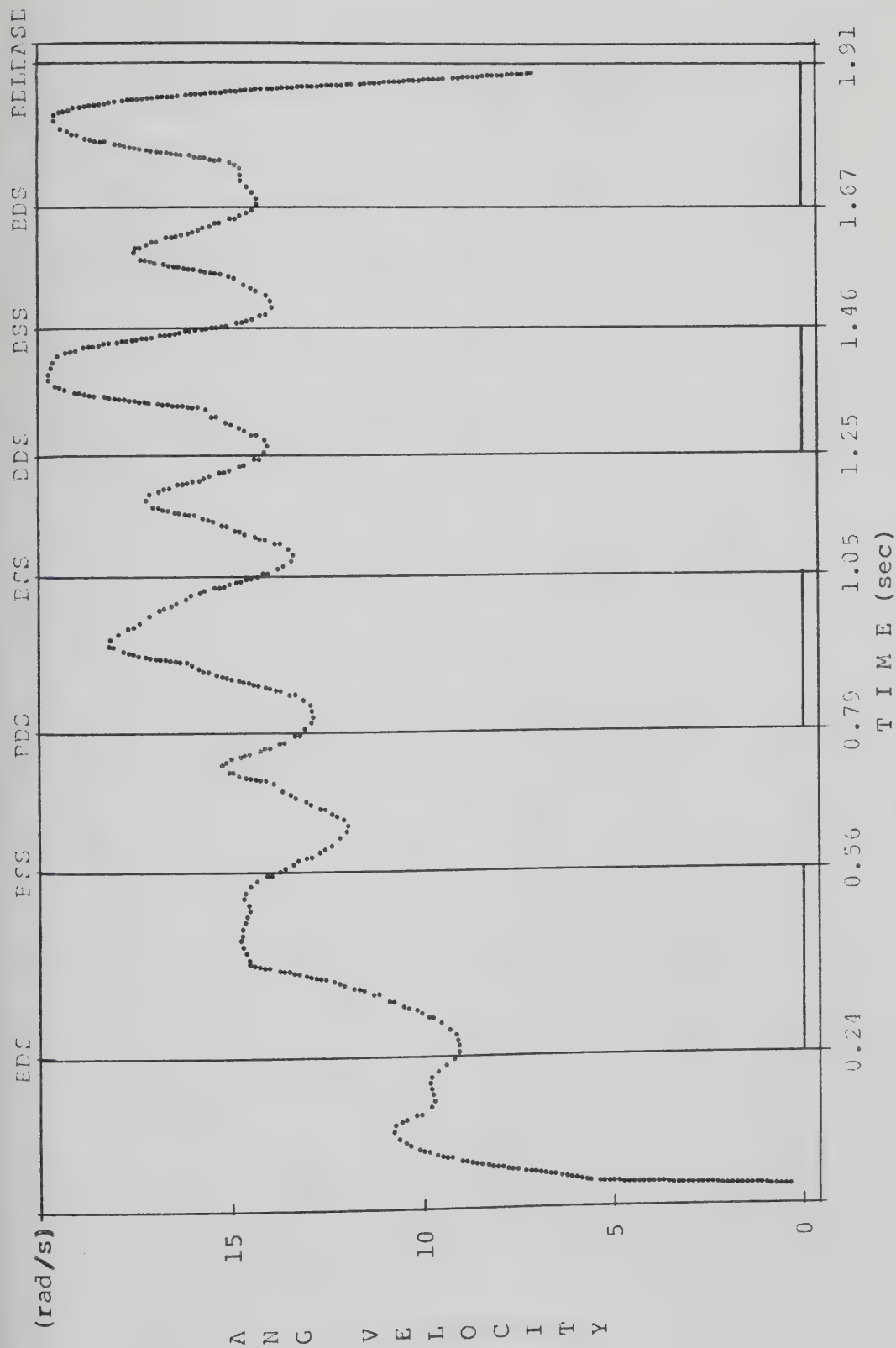
BDS=BEGINNING OF DOUBLE SUPPORT, BSS=BEGINNING OF SINGLE SUPPORT

Figure 78: Instantaneous Angular Velocity of the System, Subject 1



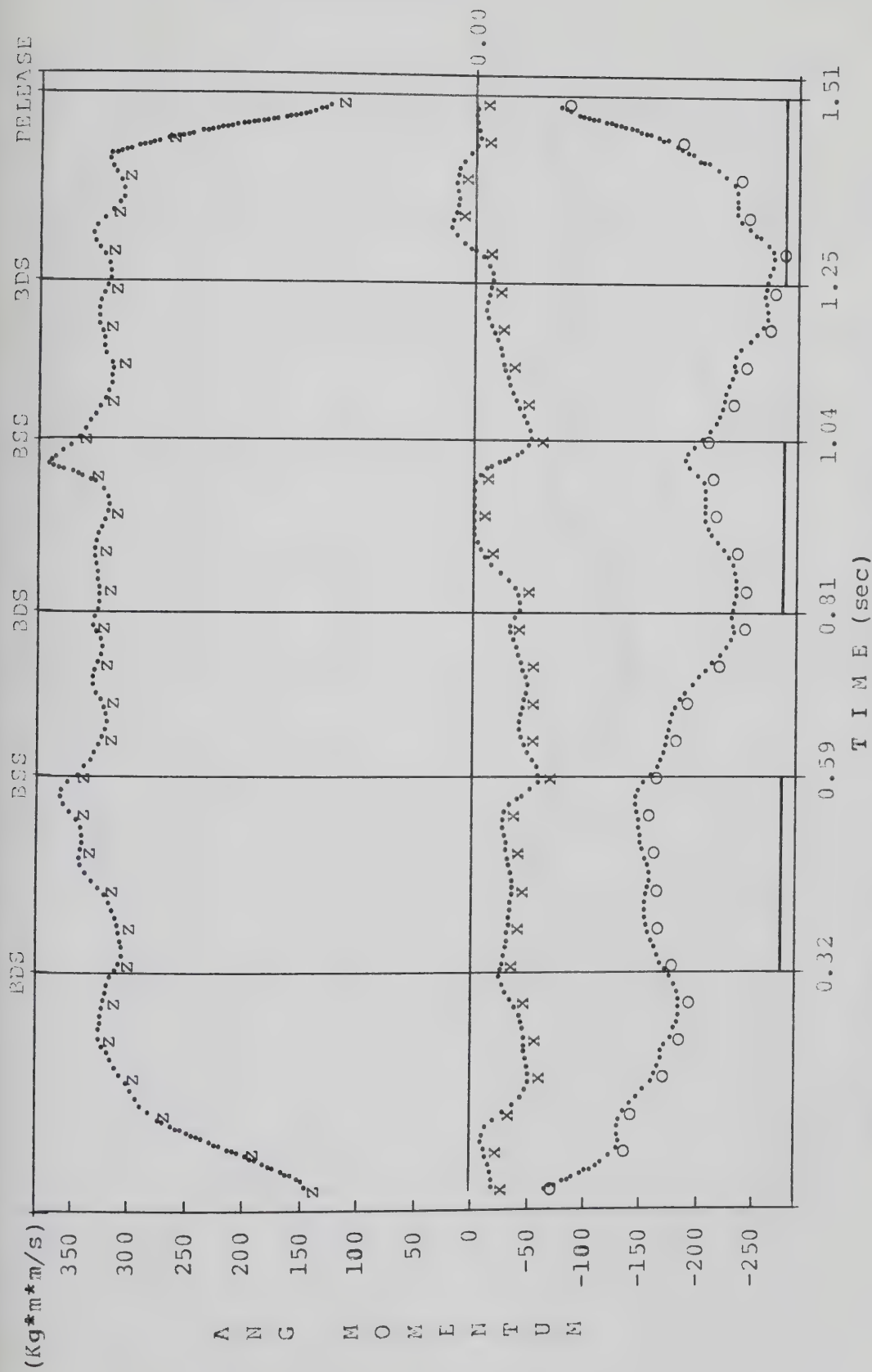
BDS=BEGINNING OF DOUBLE SUPPORT, BSS=BEGINNING OF SINGLE SUPPORT

Figure 79: Instantaneous Angular Velocity of the System, Subject 2



BDS=BEGINNING OF DOUBLE SUPPORT, BSS=BEGINNING OF SINGLE SUPPORT

Figure 80: Instantaneous Angular Velocity of the System, Subject 3



BDS=BEGINNING OF DOUBLE SUPPORT, BSS=BEGINNING OF SINGLE SUPPORT
X-AXIS(x), Y-AXIS(o), Z-AXIS(z)

Figure 81: Angular Momentum of the System in the X, Y, Z Axes, Subject 1



Figure 82: Angular Momentum of the System in the X, Y, Z Axes, Subject 2

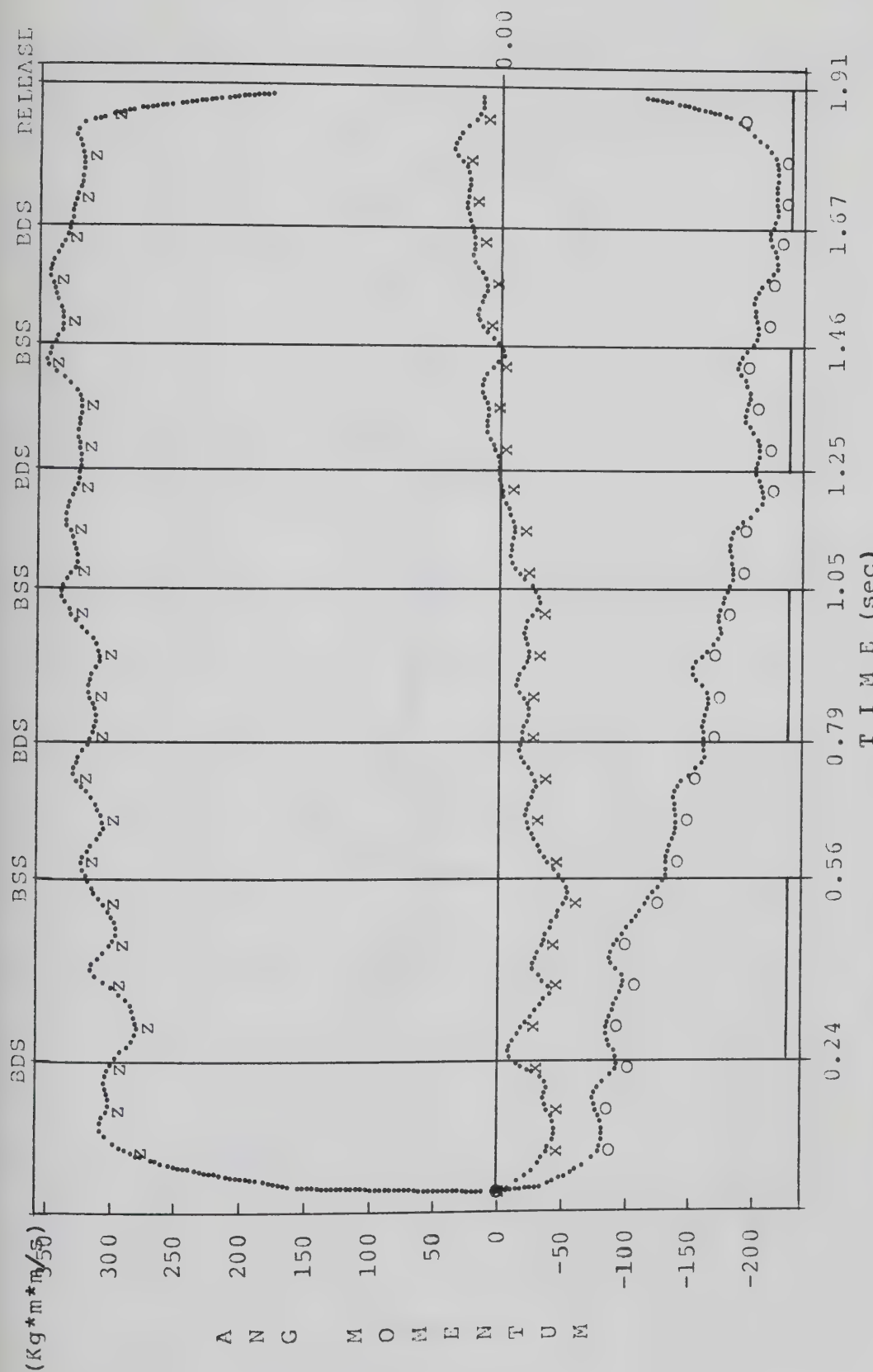
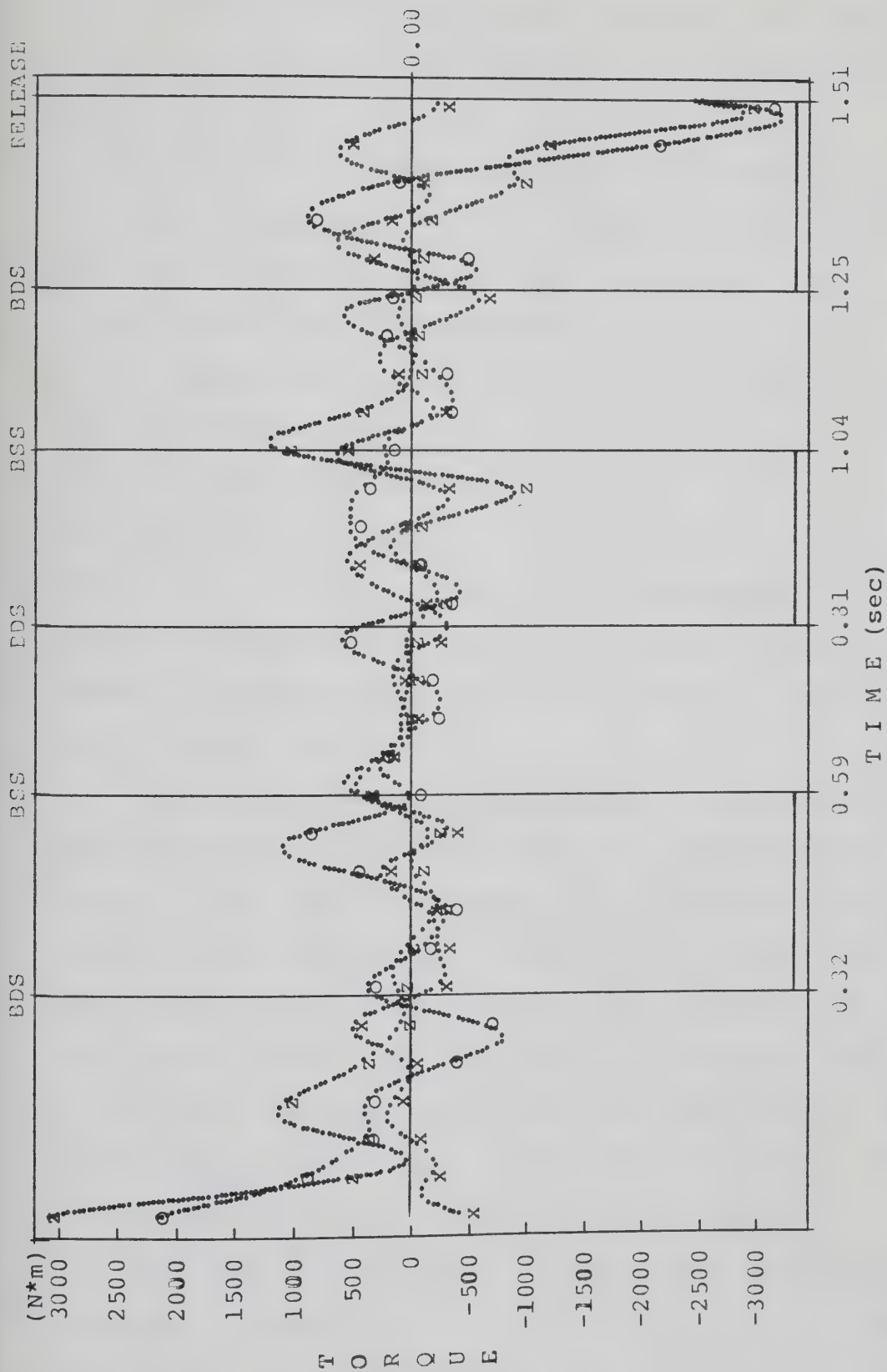


Figure 83: Angular Momentum of the System in the X, Y, Z Axes, Subject 3



BDS=BEGINNING OF DOUBLE SUPPORT, BSS=BEGINNING OF SINGLE SUPPORT
X-AXIS(x), Y-AXIS(y), Z-AXIS(z)

Figure 84: EXTERNAL TORQUES OF ROTATION of the System, Subject 1

the end of the throw. The torques remained very small in the single support phases and increased in the double support phases.

Figures 85, 86 and 87 represent the direction angles of the angular momentum vector of the system. The angle of this vector with the Y and Z-axes started increasing in the single support phase and became minimal at the end of the double support for all the subjects. The maximum angles of this vector were found to be: 130° with the Y-axis and 41° with the Z-axis for Subject 1, 123° with the Y-axis and 35° with the Z-axis for Subject 2 and, 125° with the Y-axis and 35° with the Z-axis for Subject 3. These angles occurred at the last BDS point for Subject 1 and Subject 2, while Subject 3 achieved this angle in the middle of the last double support phase.

Figure 88 represents the trajectories of the angular momentum vector for different subjects. These figures indicate that while the system rotated about an axis which was defined by the angular momentum vector, the angular momentum vector was also rotating about another axis. This axis passed through the CMs point and intersected the ground in the center of curvature of the orbit described by the ground intersection of the angular momentum vector. The second axis was the axis of precession of the system.

The total kinetic energy of the system for Subject 1 is presented in Figure 89. The energy was mainly rotational rather than translational (Figure 90) and increased gradually

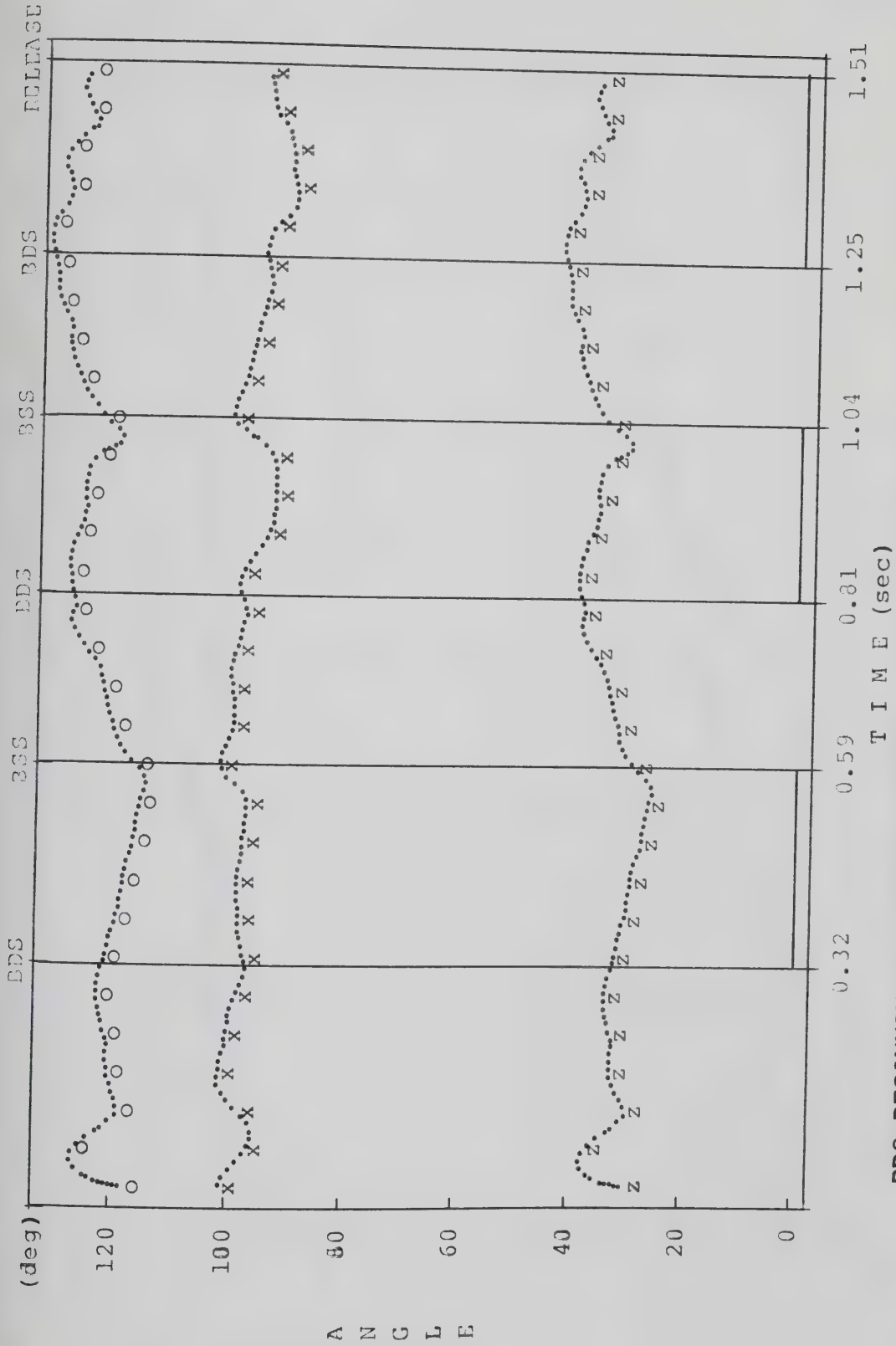


Figure 85: Direction Angles of the System's Angular Momentum Vector, Subject 1

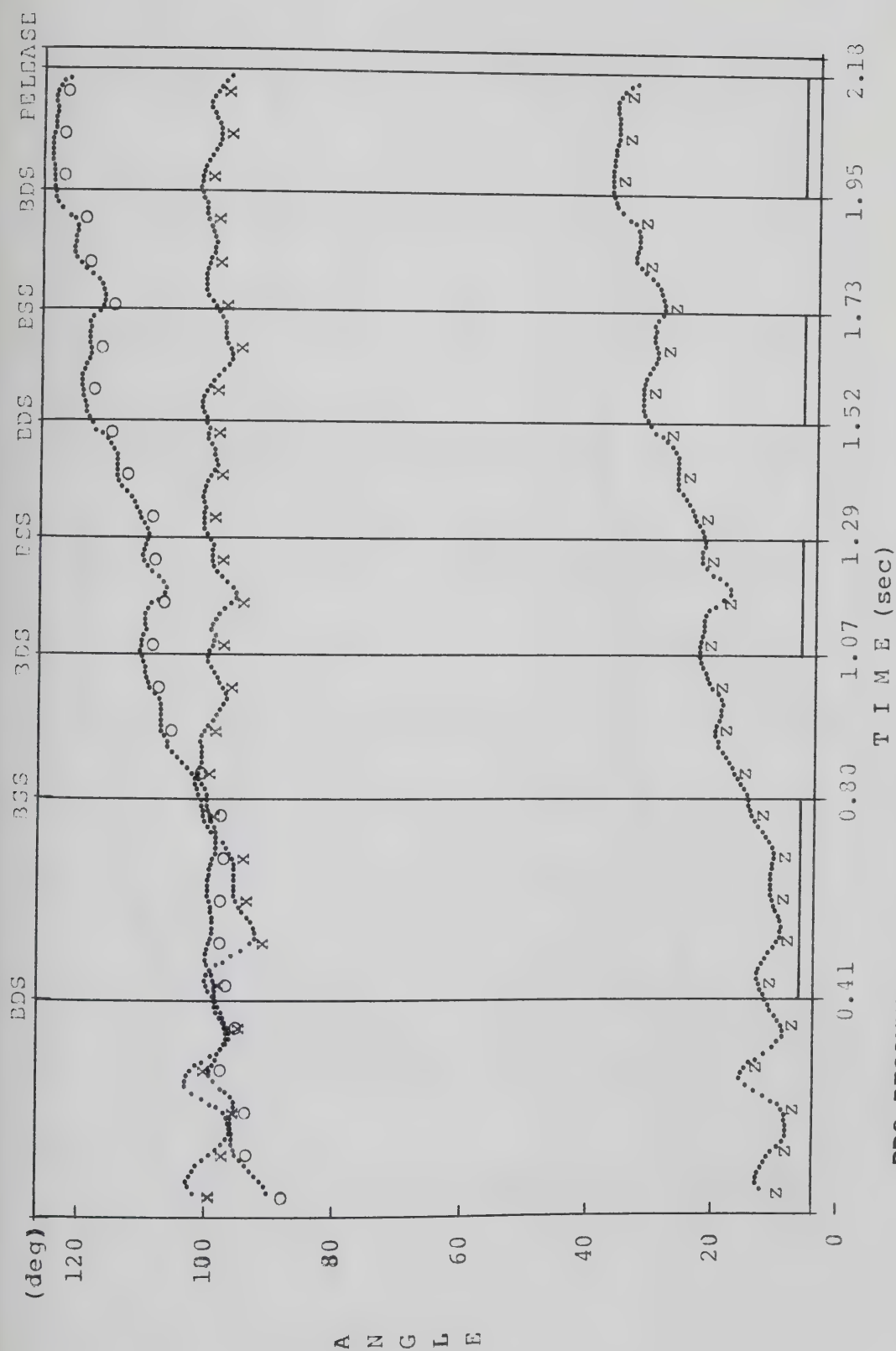


Figure 86: Direction Angles of the System's Angular Momentum Vector, Subject 2

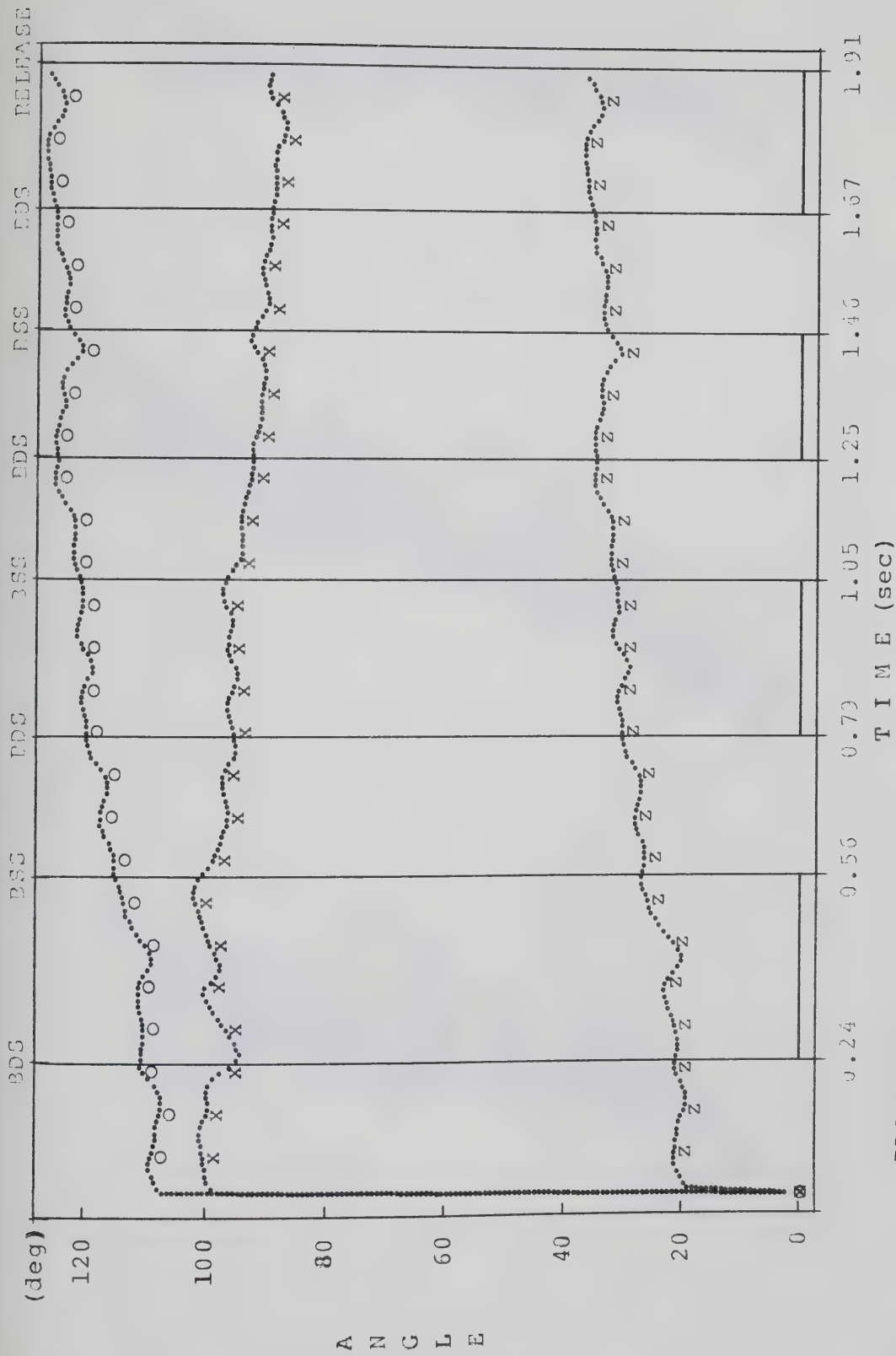


Figure 87: Direction Angles of the System's Angular Momentum Vector, Subject 3

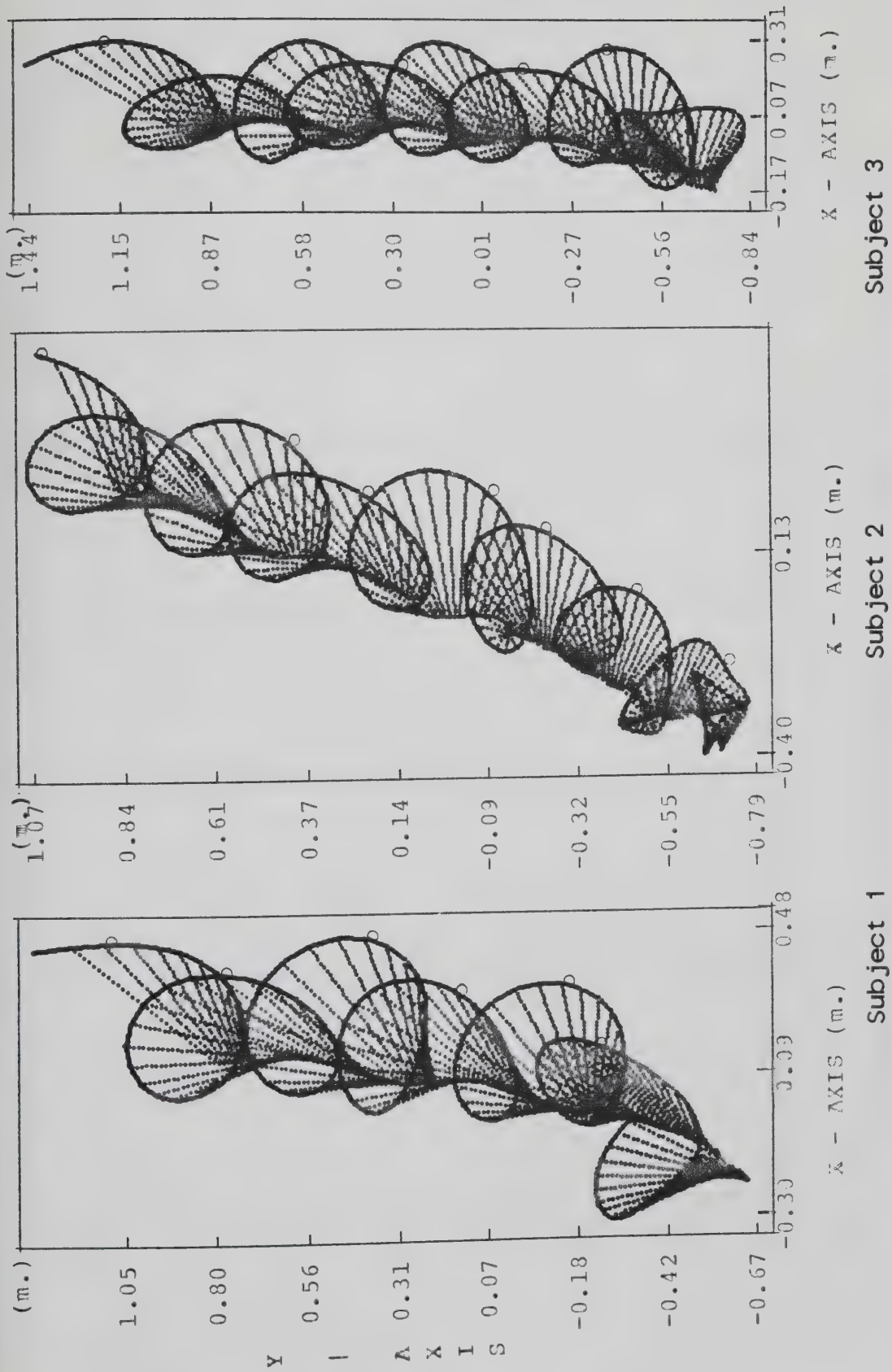
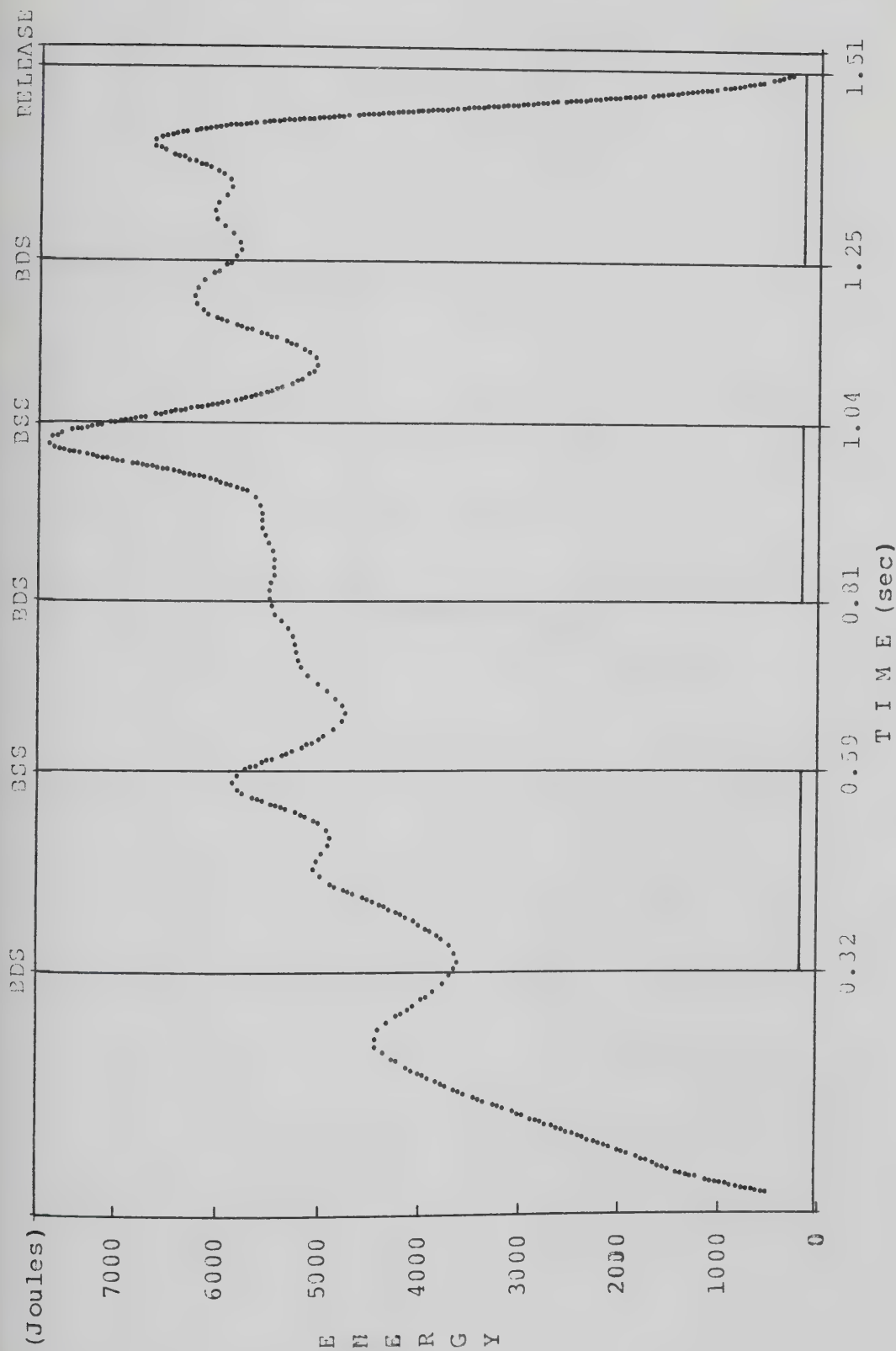
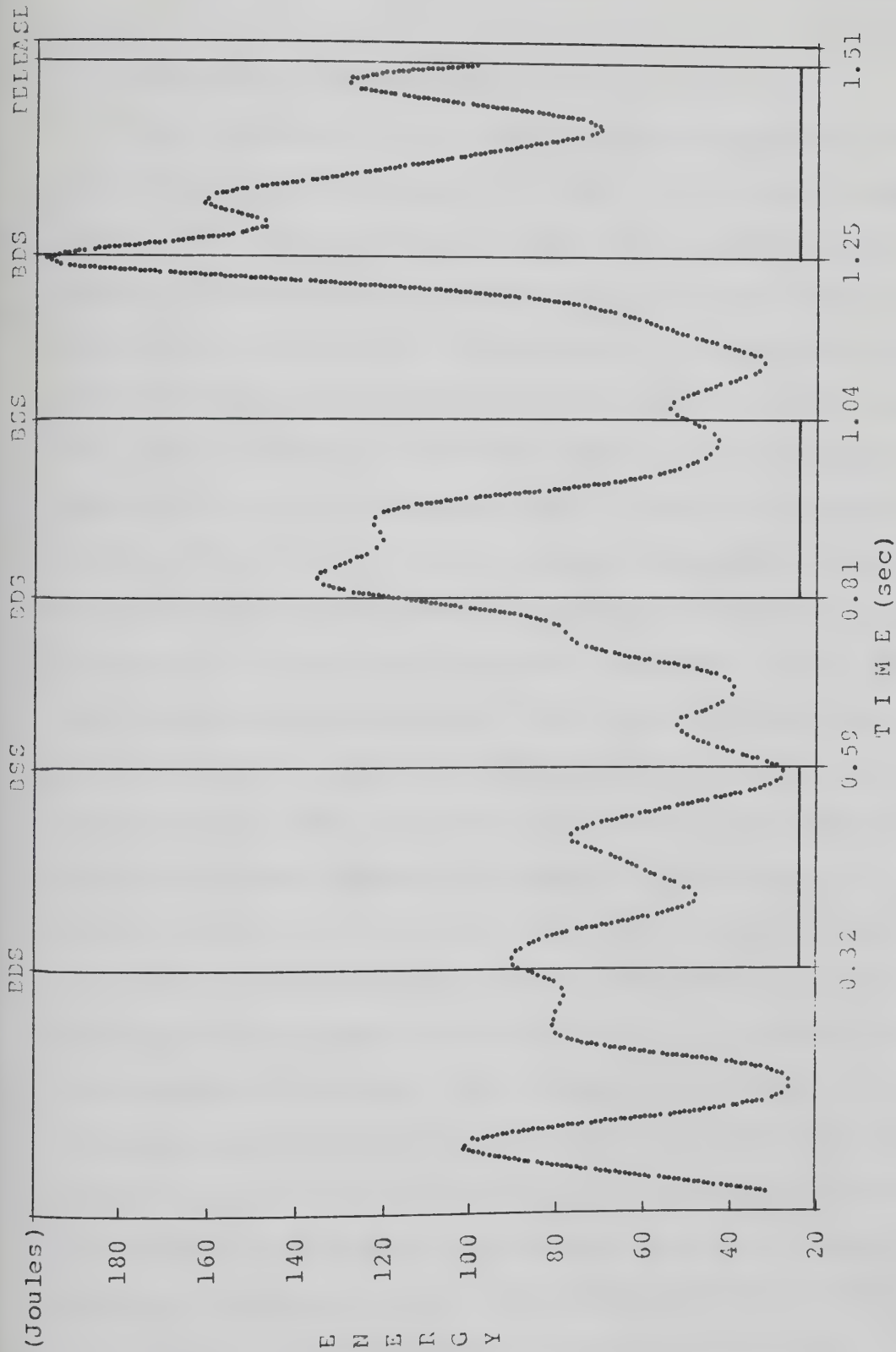


Figure 88: Trajectory of the Angular Momentum Vector in the X-Y Plane



BDS-BEGINNING OF DOUBLE SUPPORT, BSS-BEGINNING OF SINGLE SUPPORT

Figure 89: Total Kinetic Energy of the System, Subject 1



BDS=BEGINNING OF DOUBLE SUPPORT, BSS=BEGINNING OF SINGLE SUPPORT

Figure 90: Kinetic Energy of Translation of the System, Subject 1

in the same way as the angular momentum of the system.

F. Discussion of Hammer Throwing

The velocity of the hammer increased gradually from turn to turn, with a local increase in the double support phase and a local decrease in the single support phase. The global maximum velocity occurred 10 to 20 milliseconds before the release point. Theoretically, the hammer should have reached maximum velocity at the instant of release. The fact that it did not could be a result of data smoothing, of misdetection of the release frame or that the analyzed subjects did not utilize the maximum velocity of the hammer. To ensure that the timing of the maximum velocity was not affected by the smoothing of the data, the velocity was recalculated using raw data. This test confirmed the time of occurrence of the maximum velocity to be as presented above. By filming at 100f/s, at the release point the hammer moved ≈ 30 cm from one frame to the other. If there was a misdetection of the release frame then the hammer had been released in an interval of ≈ 60 cm. However, in such a case the height of release would have been ≈ 80 cm which seems unreasonable to believe. Also, assuming negligible air resistance during the flight of the hammer and by using equation (1), the calculated heights, angles and velocities of release could produce throws over 90 m. It is therefore reasonable to accept that the athletes did not utilize the maximum velocity of the hammer at the release point.

The height of release was lower than the standing height of the athletes' shoulders and it depended on the acceleration of the hammer in the vertical and in the throwing directions rather than on the height of the athletes.

The angle of release, although none of the athletes achieved the calculated optimal, was a critical factor for the final throwing distance. To improve the angle an athlete must learn how to break his horizontal motion and also how to achieve an angle of the plane of motion of the hammer which is closer to the optimal angle in the last turn. However, the length of the hammer might prevent this angle being achieved during the last turn since the ground would interfere.

A faster single support than double support phase for all the turns was a common characteristic of the three subjects. This was achieved by using the last part of the double support phase for initiating a fast turn. During the first half of the double support phases the CMb had achieved the greatest velocity in the direction of the throw. The torque of the CMb about the supporting foot created by the new position of the CMb with respect to the supporting foot obliged athletes to make a fast landing of the free foot. The free foot landed behind the supporting foot in the (Y, -X) section of the circle and in an angle of 70° measured from the Y-axis in the direction of rotation.

The acceleration of the hammer increased gradually from turn to turn with maximum local peaks in the double support phases. In the single support phases, athletes accelerated the hammer by rotating very fast and by reducing the moment of inertia of their body about the vertical axis. It was the duration of acceleration in the double support phase rather than the maximum acceleration that improved the final throwing distance.

The shoulders were continuously driven by the hips, while the hammer was continuously driven by the arms. This was accomplished by a very fast legs/hips rotation in the single support phase which allowed the athletes to have the greatest possible hip-shoulder angle at the beginning of the double support. It was only at the changing points from one support to the other that the hammer assisted the rotation of the system slightly.

The trunk was utilized by the athletes to transfer the angular momentum from legs/hips to the hammer. It received angular momentum from the legs/hips in the double support phase and transferred it to the hammer in the single support phase. Only in the last double support phase, after the force production from the lower limbs had been terminated, did athletes use the trunk as a force production system to improve the final velocity of the hammer. After this point, the shoulder musculature participated in increasing this parameter.

The knee joints achieved maximum extension at the release point, while in the other turns extension was less than maximum. This knee flexion/extension pattern helped athletes to rotate faster in the single support phases.

The moments of inertia of the body about the X and Y axes reached a local maximum and a local minimum in every phase of the throw. About the vertical axis and at the end of each double support phase the moments became maximum and decreased from there to the end of the double support phases. This helped athletes accelerate the hammer in the single support phase, even without utilizing any force initiated by the legs.

The hammer and the CMb rotated in parallel planes only at the point before the hammer reached its lowest point in the double support phase.

The system:athlete + hammer translated at the end of the single support and beginning of the double support phase. This translation was greater for the three turn throw, because the athlete had more freedom to move. Translation in the direction of the throw was least in the last turn for the three turn throw. The fourth turn did not allow athletes to break the translation of the system, resulting in a lower angle of release and probably a lower release velocity of the hammer.

The angular momentum of the system increased in the double support phase and decreased or remained relatively constant in the single support phase.

The direction of the angular momentum vector of the body came closer to the vertical at the middle point of the single support phase. At the same time the direction of the angular momentum vector of the hammer was at its greatest angular displacement from the vertical axis.

The torques for the rotation were mainly applied to the system during the double support phase.

The maximum angular velocity of the system for each turn occurred at the end of the double support phases. The time of occurrence of the global maximum angular velocity is important because it allows athletes to transfer the angular momentum of the system to linear momentum of the hammer. The result of bad timing was reflected in the radii of curvature of the hammer; Subjects 1 and 3 achieved a greater length of radii that did Subject 2.

A fourth turn served basically to smooth initiation of the throw rather than for increasing the dynamic parameters of the system. This turn could be detrimental in final distance since at the release point, athletes had the tendency not to break the horizontal movement. In the last turn, linear momentum of the system could not be transferred to the hammer. The cost could be a reduced angle of release of the hammer and possibly a reduced release velocity. A common mistake for Subjects 2 and 3 was that their CMs reached maximum velocity just before the release point, while Subject 1 achieved this maximum at the beginning of the last double support.

A heavy athlete will have some advantage over a lighter athlete although this does not seem to be a critical factor since a lighter athlete can balance the lack of great mass by rotating faster. The height of the athlete does not seem to be a critical factor either. Although a tall athlete could theoretically achieve a greater radius of rotation of the hammer and a better angle of release, the present analysis has demonstrated that this did not happen. An ideal hammer thrower would have very strong and fast legs, very good coordination, and a strong lower back. "A strong kid who is a very good dancer".

The system:athlete + hammer can be characterized as a heavy asymmetrical top which describes precessional motion. Since the angle of precession of the system varied, another characteristic of the top is nutation. The axis of precession of the system can be used in the coaches language as the axis of rotation.

V. SUMMARY AND CONCLUSIONS

The purpose of the present study was to develop a technique for analysis of the hammer throwing event and to analyze the technique of world caliber hammer throwers. To develop the technique for analysis, the DLT 3-D cinematographic method was tested. These tests included different mathematical models for image refinement, as well as the use of different calibration trees for the derivation of the calibration coefficients. It was found that a tree, geometrical in shape, together with mathematical model IV for image refinement (Karara and Abdel Aziz 1974), gave the most accurate results. The RMS error of measured versus simulated coordinates of the control points was: $\text{RMS}(X) = 0.24\text{cm}$, $\text{RMS}(Y) = 0.19\text{cm}$ and $\text{RMS}(Z) = 0.26\text{cm}$. Six points were chosen to be treated as unknowns in the outside area of the calibration tree. The error of these points was found to be: $\text{RMS}(X) = 0.27\text{cm}$, $\text{RMS}(Y) = 0.60\text{cm}$ and $\text{RMS}(Z) = 0.72\text{cm}$. The latter error indicates that a smaller calibration tree can be used to calibrate larger areas.

The calibration tree which gave the best results was used for the calibration of two cameras in the data collection of the hammer throwing study. The data were collected during the 1982 European Championship and the best throw of each of the three medalists was analysed. Two phase locked cameras were used for data collection. A Lagrangian polynomial was used for the time matching of frames, based on an external event which was a light of 10 Hz generated by

an external light generator and recorded on the sides of the films. The basic DLT equations together with model IV for image refinement (Karara and Abdel Aziz, 1974) were used for the transformation of the digitized to real life coordinates of selected body and object points. Digital filters were used to reduce the noise inherent to the data. The derived formulas for analysis of the data were based on rigid body dynamics and can be used for analysis of any rotational movement.

The results of the analysis of hammer throwing can be summerized as follows.

1. A faster single support phase than double support phase was a common characteristic for the three analyzed subjects. The torques of the CMs with respect to the supporting foot were the main reasons for the fast single support phase.
2. The height of release was lower than the height of the shoulders and it depended on the acceleration of the hammer in the vertical direction rather than on the height of the athletes.
3. The angle of release was a critical factor for the final throwing distance. However, the length of the hammer might prevent this angle being achieved during the last turn since the ground would interfere.
4. The angle of the plane of rotation of the hammer started from an acute angle with the horizontal plane and gradually changed from turn to turn to the release

angle.

5. The length of the radius of curvature of the hammer decreased from turn to turn until the instance when the hammer reached the minimum point in the Z-axis during the last turn. After that point the radius started increasing to become infinitive at the release point.
6. The hammer was continuously driven by the athletes and it was only at the changing points from one support to the other that the hammer slightly assisted the rotation of the system.
7. The velocity of the hammer increased gradually from turn to turn, with a local increase in the double support phase and a local decrease in the single support phase. The maximum velocity occurred 10 to 20 milliseconds before the release point.
8. The acceleration of the hammer increased gradually from turn to turn and in the double support phase. In the single support phase, the athletes improved the acceleration of the hammer by reducing the moment of inertia of their body about the vertical axis.
9. The hammer and the center of mass of the body rotated in parallel planes only at the point before the hammer reached its lowest point in the double support phase.
10. The maximum vertical displacement of the CMb in each turn was less than 0.12 cm.
11. The radius of curvature of the CMb had noisier oscillations in four turn throws than in a three turn

throw.

12. The linear velocity of the CMb increased during the single support phase in all the turns.
13. The moments of inertia of the body about the vertical axis increased during the second half of each double support phase. During the single support phase this parameter decreased continuously until approximately the middle point of the double support phase.
14. The angular momentum of the body increased from turn to turn reaching the maximum during the second from the last double support phase.
15. The knee joints achieved maximum extension at release point, while in the other turns extension was less. Only in the last double support phase, after the forces from the lower limbs had been transferred to the hammer, did athletes actively use the trunk as a force production system.
16. In the horizontal plane the CMs moved in a parabolic epicycloid mode.
17. The system: athlete+hammer translated at the end of the single support and beginning of double support phase. This translation was greater for the three turn throw, because the athlete had more freedom to move. Translation in the direction of the throw was least in the last turn for the three turn throw. A fourth turn did not allow athletes to break the translation of the system, resulting in a lower angle of release and

probably a lower release velocity of the hammer.

18. There was no common pattern of linear velocity of the system among the analysed subjects.
19. The vertical acceleration of the system during the last turn and the minimum horizontal acceleration in the direction of the throw in the same turn seem to be critical for a successful throw.
20. The maximum angular velocity of the system for each turn occurred at the end of the double support phase.
21. The angular momentum of the system increased at the end of the double support phases and decreased or remained relatively constant in the single support phases. It was the angular momentum of the body that directed the motion. The direction of the angular momentum vector of the body came close to the vertical at the middle point of the single support phase. At this time, the body rotated mainly about an almost vertical axis. During the same time the direction of the angular momentum vector of the hammer was at its furthest angular displacement from the vertical.
22. The torques for the rotation were mainly applied upon the system in the double support phase.
23. The kinetic energy of the system increased gradually from turn to turn and it was mainly caused by the rotation rather than the translation of the system.

On the basis of the results of the hammer throwing analysis the following conclusions seem justified.

1. An athlete should try to reduce the time of the single support as much as possible. This can be achieved by a) tilting backwards during the first half of the double support; b) by using the second half of the double support phase for a fast rotation; c) by rotating the free leg close to the supporting leg; d) by placing the free foot behind and on the right of the supporting foot and at a angle about 250° to the direction of the throwing axis (measuring the angle from the back of the circle and in the direction of the rotation).
2. A fourth turn is basically used for a smooth initiation of the throw rather than for increasing the dynamic parameters of the system. This turn might cost in final distance since at the release point, athletes have the tendency not to break the horizontal movement. The cost could be a reduced angle of release and possibly a reduced release velocity of the hammer.
3. It is the duration of acceleration in the double support phase rather than the maximum acceleration that improves the final throwing distance.
4. A heavy athlete will have some advantage over a lighter athlete, although this does not seem to be a critical factor, since a lighter athlete can offset the lack of great mass by rotating faster. The height of the athlete does not seem to be a critical factor either.

5. The length of the hammer might prevent athletes from achieving an optimal angle of release since the ground would interfere. Therefore, this length might have to be reduced in order for athletes to perform mechanically efficient throws.
6. The system: athlete+hammer can be characterized as a heavy assymetrical spinning top which describes precessional motion. The angle of precession of the system varied, therefore the system had another characteristic: nutation.
7. An ideal hammer thrower could be an athlete who has very strong and fast legs, who has very good coordination, who has a strong lower back muscle system and, who is not necessarily very tall. "A strong kid who is a very good dancer".

Recommendations

The following studies are recommendations on the basis of the present findings:

1. The DLT method should be tested on a statistical base to estimate the expected error in areas which are not covered by the calibration tree.
2. New methods should be found for the calculation of the anthropometric data of the body segments, based on individual characteristics of the analysed subjects.
3. A statistical study is recommended for comparison of the kinematic and kinetic parameters of different level

hammer throwers.

4. Direct force measurements should be used for the study of the forces involved in the different phases of the throw and their direction.
5. A study of hammer throwing in the last turn of the movement with a filming rate of at least 300 f/s is recommended to examine whether the highest velocity of the hammer does occur before the release point as it was found in the present study. If the results of such a study agree with those in the present study, then biomechanists, coaches and athletes should seek new throwing technique which will allow athletes to utilize this maximum velocity at the release point.

BIBLIOGRAPHY

- Abdel-Aziz, Y.I. and Karara, H.M. "Direct Linear Transformation from Comparator Coordinates into Object-Space Coordinates." Proceedings of the Symposium of Close-Range Photogrammetry Urbana, Illinois, Jan. 1971.
- Aleshinsky, S.Y. and Zatsiorsky, V.W. "Human Locomotion in Space Analyzed Biomechanically through a Multi-Link Chain Model." Journal of Biomechanics. 11:101-108, 1978.
- Alexander, M.J.L. and Colbourne, J. "A Method of Determination of the Angular Velocity Vector of a Limb Segment." Journal of Biomechanics. 13:1089-1093, 1980.
- Alexander, R. M. and Jayes, A.S. "Fourier Analysis of Force Exerted in Walking and Running." Journal of Biomechanics. 13:383-390, 1978.
- Anderson, C.C. "A Method of Data Collection and Processing for Cinematographic Analysis of Human Movement in Three Dimensions." Unpublished Master's Thesis, University of Wisconsin, 1970.
- Ariel, G.B., Walls, M.R., and Harman, E. "Biomechanical Analysis of Hammer Throwing." Conducted for U.S. Olympic Sport Medicine Committee, December, 1978.
- Ayoub, M.A., Ayoub, M.M. and Ramsey, J.D. "A Stereometric System for Measuring Human Motion." Human Factors. 12:523-535, 1970.
- Bergemann, B.W. "Three Dimensional Cinematography: a Flexible Approach. Research Quarterly. 45(3):302-309, 1974.
- Bernstein, N. The Coordination and Regulation of Movements. Pergamon Press, p:6, 1967.
- Canadian Track and Field Association, "Rules and By-Laws", 1981-1984 Edition.
- Curtis, A.B. and Powell, N.J.D. "Using Splines to Approximate Functions of one Variable to Prescribed Accuracy." A.E.R.E. Report 5602, 1967.

- Dainis, A. "Whole Body and Segment Center of Mass Determination from Kinematic Data." Journal of Biomechanics. 13:647-651, 1980.
- Dapena, J. "A Method to Determine the Angular Momentum of the Human Body about Three Orthogonal Axes Passing through its Center of Mass." Journal of Biomechanics. 11:251-256, 1978.
- Dapena, J. "Tangential and Perpendicular Forces in the Hammer Throw." Hammer Notes. 5:40-42, Edited by Kevin McGill, 1981.
- Dempster, W.T. "Space Requirements of the Seated Operator." DADC Technical Report 55-1159 Wright-Patterson Air Force Base, OH, 1955.
- Diffrient, N., Tilley, A.B. and Bardagjy, J.C. Humanscale 1/2/3. M.I.T., M.I.T. Press, Cambridge, Massachusetts, 1979.
- Doolittle, T.L. "Errors in Linear Measurements with Cinematographic Analysis." Kinesiology Review. 32-38, 1971.
- Dyson, G.H.G. The Mechanics of Athletics. Holms and Meier Publishers, New York, 7th Edition, 1977.
- Elmendorf, T.E. "The Relationship of Turn Time to Distance Thrown in Three and Four Turn Hammer Performances." Unpublished Master's Thesis, Indiana University, 1978.
- Felton, S. and Simonyi, G. "Modern European Hammer Technique I." Scholastic Coach. 38(7), 1969.
- Felton, S. and Simonyi, G. "Modern European Hammer Technique II." Scholastic Coach. 38(8). 1969.
- Hanavan, E.P. "A Mathematical Model of the Human Body, AMRL Technical Report 64-102 Wright-Patterson Air Force Base, OH, 1964.
- Hamming, R.W. Digital Filters. Prentice-Hall, Inc., New Jersey, 1977.
- Hatze, H. "A Mathematical Model for the Computational Determination of Parameter Values of Anthropomorphic Segments." Journal of Biomechanics. 13:833-843, 1980.
- Hatze, H. "A Method for Describing the Motion of Biological Systems." Journal of Biomechanics. 9:101-104, 1976.
- Hay, J.G. "Moment of Inertia of the Human Body. Kinesiology

IV. 43-52, 1974.

- Hay, J.G., Wilson, B.D. and Dapena, J. "A Computational Technique to Determine the Angular Momentum of a Human Body." Journal of Biomechanics 10:269-277, 1977.
- Jabs, R. "Velocity in Hammer Throwing." Track Technique. 77:2449-2450, 1979.
- Joshi, S.K. "Hammer Throwing Techniques Analyzed by High-Speed Photography." in Proceedings of the 9th International Congr High-Speed Photography. Edited by Hyser, W.G. and Chace, W.G., 1970.
- Karara, H.M. "Simple Cameras for Close-Range Applications." Photogrammetric Engineering. 28(5):447-451, 1972.
- Karara, H.M. and Abdel-Aziz, Y.I. "Accuracy Aspects of Non-Metric Imageries." Photogrammetric Engineering 1107-1117, 1974.
- Lapp, V.W. "A Study of Hammer Velocity and the Physical Factors Involved in Hammer Throwing." Research Quarterly. 6(3):134-144, 1935.
- Mc Kelvey, J.P. and Grotch, H. Physics for Science and Engineering. Happer & Row, Publishers, New-York, 1978.
- McLaughlin, T.M., Dillman, C.I. and Lardner T.J. "Biomechanical Analysis with Cubic Spline Functions." Research Quarterly. 48(3):569-582, 1977.
- Marzan, T. and Karara, H.M. "A Computer Program for Direct Linear Tranformation of the Colinearity Condition and some Applications of It." Proc. Symp. on Close-Range Photogrammetric Systems, Champaign(III), A.S.P., Fall Church, 420-476, 1975.
- Miller, A. and Harris, J.D. "Measurement of the Centre of Rotation of Human Joints from Multiple Exposure Photographs." Journal of Biomechanics. 10:383-384, 1977.
- Miller, D.I. "Three Dimensional Cinematography." in Proceedings of the Biomechanics Conference, Pennsylvania State University, August, 1971.
- Miller, D.I. and Nelson, R.C. Biomechanics of Sport. Lea and Febiger, New York, 1973.
- Miller, N.R., Shapiro, R. and McLaughlin, T.M. "A Technique for Obtaining Spatial Kinematic Parameters of

- Segments of Biomechanics Systems from Cinematographic Data." Journal of Biomechanics. 13:535-547, 1980.
- Noble, M.L. and Kelly, D.C. "Accuracy of Tri-axial cinematographic Analysis in determining Parameters of Curvilinear Motion." Research Quarterly. 40:643-645, 1969.
- Noss, J. "Control of Photographic Perspective in Motion Analysis." J.O.H.P.E.R. 7:81-84, Sept., 1967.
- Panjabi, M. "A Mathematical Approach for the Three-Dimensional Analysis of the mechanics of the Spine." Journal of Biomechanics. 4:203-211, 1971.
- Panjabi, M. "Centers and Angles of Rotation of Body Joints: A Study of Errors and Optimization." Journal of Biomechanics. 12:911-920, 1979.
- Payne, H.A. "Hammer Throwing." Amateur Athletic Association, London, 4th Edition, 1969.
- Payne, H.A. "Hammer Throwing - Bridging the Gap." in Sciences in Athletics, Edited by Terauds, J. and Dales, G., Academic Publishers, Del Mar, 1979.
- Pensose, T., Wood, G. and Blanksby, B. "The Accuracy of Position Data in Triaxial Cinematography." Australian Journal of Physical Education. 71:7-12, 1976.
- Pezzack, J.C., Norman, R.W. and Winter, D.A. "An Assessment of Derivative Determining Techniques for Motion Analysis." Journal of Biomechanics. 10:377-382, 1977.
- Plagenhoef, S. "Computer Program for obtaining Kinetic Data of Human Movement." Journal of Biomechanics. 1:221-234, 1968.
- Plagenhoef, S. Patterns of Human Motion. Prentice-Hall, Inc., New Jersey, 1971.
- Plagenhoef, S. "The Joint Force and Moment Analysis of all Body Segments when Performing a Non-Symmetric Three-Dimensional Motion." Medicine and Sport, Biomechanics III:8, 1973.
- Reinch, C.H. "Smoothing by Spline Functions." Numeriche Mathematic. 10:177-183, 1967.
- Riley, D.R., Garrett, R.E. and Garrett, G.E. "Three Dimensional Human Motion: Analysis and Simulation via Computer Graphics." Cinematography, Edited by Terauds, J., Academic Publishers, Del Mar, 1978.

- Samozwetov, A. "The Acceleration of the Hammer." The Throws. Edited by Wilt, F., Tafnews Press, U.S.A., 90, 1974.
- Shapiro, R. "Direct Linear Transformation Method for Three Dimensional Cinematography." Research Quarterly. 49(2):197-205, 1976.
- Soudan, K. and Deerckx, P. "Calculation of Derivatives and Fourier Coefficients of Human Motion Data, while using Spline Functions." Journal of Biomechanics. 12:21-26, 1979.
- Spiegel, M.R. "Fourier Series." SCHAUM'S OUTLINE SERIES. McGraw-Hill, New York, 1974.
- Van Gheluwe, B. "A New Three Dimentional Filming Technique Involving Simplified Alignment and Measurement Procedures." Biomechanics IV. pp. 476-481. Edited by Nelson, R. and Morehouse, C.A., University Park Press, Baltimore, 1974.
- Van Gheluwe, B. "Computerized Three Dimentional Cinematography for any Arbitrary Camera Setup." Biomechanics VI-A. 343-348. Edited by Nelson, R. and Morehouse, C.A., University Park Press, Baltimore, 1978.
- Walton, J.S. "Close-Range Cine-Photogrammetry: A Generalized Technique for Quantifying Gross Human Motion." Ph.D. Thesis, Pennsylvania State University, 1981.
- Whitsett, C.E. "Some Dynamic Response Characteristics of Weightless Man." AMRL Technical Report 63-18 Wright-Patterson Air Force Base, OH, 1963.
- Wilson, B.D. and Hay, J.G. "A Comparison of Three Methods for Determining the Angular Momentum of the Human Body." Biomechanics V-B. 467-475, Edited by Komi, P.V., University Park Press, Baltimore, 1976.
- Winter, D.A. Biomechanics of Human Movement. John Wiley and Sons, New York, 1979.
- Winter, D.A., Sidwall, H.G. and Hobson, D.A. "Measurement and Reduction of Noise in Kinematics of Locomotion." Journal of Biomechanics. 7:157-159, 1974.
- Wold, S. "Analysis of Kinetic Data by Means of Spline Functions." Chimica Scripta. 1:97-102, 1971.
- Wold, S. "Spline Functions in Data Analysis." Technometrics. 16(1):1-11, 1974.
- Wolfe, I., Bergen, N. and Narcessian, B. "Force and Momentum

in the Hammer Throw." Track Technique. 76:2409-2410, 1979.

Woltring, H.J., "Planar Control in Multi-Camera Calibration for 3-D Gait Studies." Journal of Biomechanics. 13:39-48, 1980.

Wood, G.A. and Jennings, L. "On the use of Spline Functions for Data Smoothing." Journal of Biomechanics. 12:477-479, 1979.

Zernicke, R.F., Caldwell, G. and Roberts, E.M. "Fitting Biomechanics Data with Cubic Spline Functions." Research Quarterly. 47(1):9-19, 1976.

APPENDIX A

DLT and Image Refinement Mathematical Models

Description of the DLT Technique.

This description is based on the technique invented by Abdel Aziz Karara in 1971 and presented by other investigators (Marzan et al, 1975; Walton, 1981; Miller et al, 1980). The technique is based on the basic theoretical concept of photogrammetry, that is: the photograph, being a perfect plane, is a central projection of the object space.

Figure A.1, is a geometric representation of the transformation of the 3-D object space onto the 2-D secondary image. The following manipulations are based on vector analysis.

Let:

$$\underline{P} = x\underline{n}_x + y\underline{n}_y + z\underline{n}_z \quad (\text{A.1})$$

$$\underline{Q} = a\underline{n}_k + b\underline{n}_m + c\underline{n}_n \quad (\text{A.2})$$

$$\underline{R} = x_0\underline{n}_x + y_0\underline{n}_y + z_0\underline{n}_z \quad (\text{A.3})$$

where: $x, y, z, a, b, c, x_0, y_0, z_0$, are scalars

and \underline{n}_i ($i=x, y, z, k, m, n$) unit vectors.

If s = the magnified principal distance then:

$$\underline{S} = -s\underline{n}_n \quad (\text{A.4})$$

Let:

$$\underline{p} = u\underline{n}_s + v\underline{n}_t \quad (\text{A.5})$$

$$\underline{q} = u_0\underline{n}_s + v_0\underline{n}_t \quad (\text{A.6})$$

where: u, v, u_0, v_0 are scalars

From figure 1 we have:

$$\underline{r} = \underline{p} - \underline{q} \quad (\text{A.7})$$

From (A.5), (A.6), (A.7)

$$\underline{r} = (u - u_0)\underline{n}_s + (v - v_0)\underline{n}_t \quad (\text{A.8})$$

Further observe that:

$$\underline{T} = \underline{r} + \underline{s} \quad (\text{A.9})$$

From (A.4), (A.8), (A.9)

$$\underline{T} = (u - u_0)\underline{n}_s + (v - v_0)\underline{n}_t - s\underline{n}_n \quad (\text{A.10})$$

Assume that \underline{n}_s and \underline{n}_t are orthogonal; then equation (A.10) can be written as follows:

$$T = (u - u_0)\underline{n}_k + (v - v_0)\underline{n}_m - s\underline{n}_n \quad (\text{A.11})$$

Using equations (A.11) and (A.2), and the colinearity conditions, we obtain:

$$\frac{a}{u - u_0} = - \frac{c}{s} \quad (\text{A.12})$$

$$\frac{b}{v - v_0} = - \frac{c}{s} \quad (\text{A.13})$$

From equations (A.12) and (A.13), we have:

$$u = u_0 - \frac{as}{c} \quad (\text{A.14})$$

$$v = v_0 - \frac{bs}{c} \quad (\text{A.15})$$

u and v are the scalar components of the vector \underline{p} which locates the image point I , with respect to the image reference frame. In digitizing, we have digitizer units not necessarily the same as those used to establish the object reference frame.

Introduce scale factors C_1, C_2 for \underline{n}_s and \underline{n}_t directions, respectively, and let;

$$U = C_1 u \quad (\text{A.16})$$

$$V = C_2 v \quad (\text{A.17})$$

From equations (A.14), (A.15), (A.16), (A.17),

$$U = C_1 \left(u_0 - \frac{as}{c} \right) \quad (\text{A.18})$$

$$V = C_2 \left(v_0 - \frac{bs}{c} \right) \quad (\text{A.19})$$

Equations (A.18) and (A.19) express the digitizer coordinates U, V in terms of a, b, c .

From Figure 1,

$$\underline{Q} = \underline{P} - \underline{R} \quad (\text{A.20})$$

From equations (A.1), (A.2), (A.20):

$$\underline{Q} = (x - x_0)\underline{n}_x + (y - y_0)\underline{n}_y + (z - z_0)\underline{n}_z \quad (\text{A.21})$$

Let $\theta_{11}, \theta_{12}, \theta_{13}$, be the direction cosines of \underline{n}_x with respect to the object space frame $(\underline{n}_k, \underline{n}_m, \underline{n}_n)$; $\theta_{21}, \theta_{22}, \theta_{23}$ be the direction cosines of \underline{n}_y with respect to the same frame; and $\theta_{31}, \theta_{32}, \theta_{33}$, be the direction cosines of \underline{n}_z with respect to the same frame. Then:

$$\underline{n}_x = \theta_{11}\underline{n}_k + \theta_{12}\underline{n}_m + \theta_{13}\underline{n}_n \quad (\text{A.22})$$

$$\underline{n}_y = \theta_{21}\underline{n}_k + \theta_{22}\underline{n}_m + \theta_{23}\underline{n}_n \quad (\text{A.23})$$

$$\underline{n}_z = \theta_{31}\underline{n}_k + \theta_{32}\underline{n}_m + \theta_{33}\underline{n}_n \quad (\text{A.24})$$

The θ_{ij} ($i=1,2,3, j=1,2,3$) form a 3-dimensional rotation matrix.

From equations (A.21), (A.22), (A.23) and (A.24), we obtain:

$$\begin{aligned} \underline{Q} = & [(x - x_0)\theta_{11} + (y - y_0)\theta_{21} + (z - z_0)\theta_{31}]\underline{n}_k \\ & + [(x - x_0)\theta_{12} + (y - y_0)\theta_{22} + (z - z_0)\theta_{32}]\underline{n}_m \\ & + [(x - x_0)\theta_{13} + (y - y_0)\theta_{23} + (z - z_0)\theta_{33}]\underline{n}_n \end{aligned} \quad (\text{A.25})$$

Equate the coefficients of equations (A.2) and (A.25):

$$a = (x - x_0)\theta_{11} + (y - y_0)\theta_{21} + (z - z_0)\theta_{31} \quad (\text{A.26})$$

$$b = (x - x_0)\theta_{12} + (y - y_0)\theta_{22} + (z - z_0)\theta_{32} \quad (\text{A.27})$$

$$c = (x - x_0)\theta_{13} + (y - y_0)\theta_{23} + (z - z_0)\theta_{33} \quad (\text{A.28})$$

From equations (A.14), (A.15), (A.26), (A.27) and (A.28):

$$U = \frac{L_1x + L_2y + L_3z + L_4}{L_9x + L_{10}y + L_{11}z + 1} \quad (\text{A.29})$$

$$V = \frac{L_5x + L_6y + L_7z + L_8}{L_9x + L_{10}y + L_{11}z + 1} \quad (\text{A.30})$$

where:

$$L_1 = C_1(u_0\theta_{13} - s\theta_{11})/d \quad (\text{A.31})$$

$$L_2 = C_1(u_0\theta_{23} - s\theta_{21})/d \quad (\text{A.32})$$

$$L_3 = C_1(u_0\theta_{33} - s\theta_{31})/d \quad (\text{A.33})$$

$$L_4 = -C_1[(u_0\theta_{13} - s\theta_{11})x_0 + (u_0\theta_{23} - s\theta_{21})y_0 + (u_0\theta_{33} - s\theta_{31})z_0]/d \quad (\text{A.34})$$

$$L_5 = C_2(v_0\theta_{13} - s\theta_{12})/d \quad (\text{A.35})$$

$$L_6 = C_2(v_0\theta_{23} - s\theta_{22})/d \quad (\text{A.36})$$

$$L_7 = C_2(v_0\theta_{33} - s\theta_{32})/d \quad (\text{A.37})$$

$$L_8 = -C_2[(v_0\theta_{13} - s\theta_{12})x_0 + (v_0\theta_{23} - s\theta_{22})y_0 + (v_0\theta_{33} - s\theta_{32})z_0]/d \quad (\text{A.38})$$

$$L_9 = \theta_{13}/d \quad (\text{A.39})$$

$$L_{10} = \theta_{23}/d \quad (\text{A.40})$$

$$L_{11} = \theta_{33}/d \quad (\text{A.41})$$

with:

$$d = -(x_0\theta_{13} + y_0\theta_{23} + z_0\theta_{33}) \quad (\text{A.42})$$

Equations (A.29) and (A.30) are the basic Direct Linear Transformations (DLT) equations.

L_i ($i=1,2,\dots,11$) are the transformation coefficients expressed in terms of seventeen separate elements.

(x_0, y_0, z_0) define the location of the camera with respect to

the object reference frame.

(u_0, v_0) define the location of the principal point in the secondary image.

(C_1, C_2) define the scale factors.

S defines the magnified principal distance.

θ_{ij} are the directional cosines defining the orientation of the camera, with respect to the object space. If the vectors \underline{n}_s and \underline{n}_t of the secondary image are not orthogonal, then the angle between the two vectors is the eighteenth element which express the eleven transformation coefficients. A minimum of six control points is required in order to solve a system of $2(K)$ [K = number of control points] linear equations and find the values of the eleven coefficients. This is an overdetermined system and to solve it a least squares method can be used. However, to reconstruct the three dimensional spatial coordinates, at least two observations from different points are required. Here two or more systems of $2(K)$ linear equations each have to be solved for the eleven coefficients of each camera. The DLT equations then are used to solve for the unknown (x, y, z) spatial coordinates of points in the space. In this case a system of $2(J)$ [J = number of observations] linear equations has to be solved for three unknowns. The same least squares method can be used.

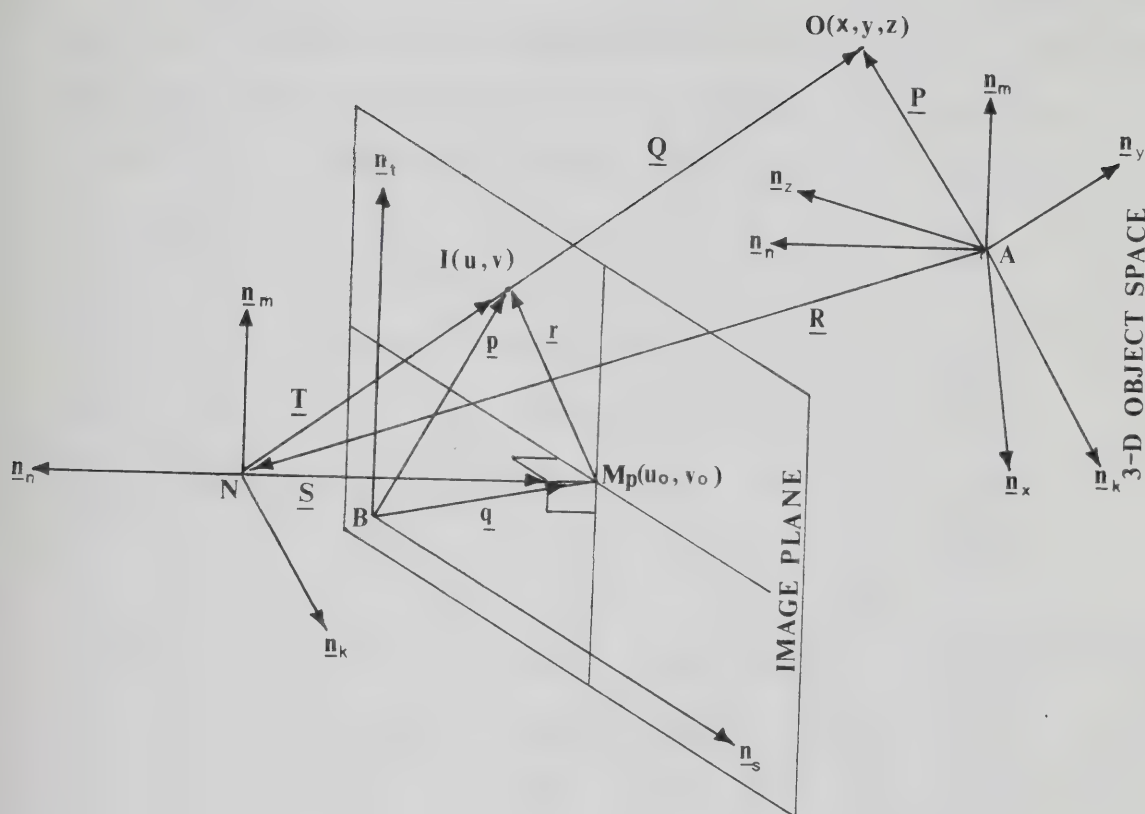


Figure A.1 Geometrical representation of the transformation of the 3-D object space onto the projected secondary image.

A = Origin in the object space;
 B = Origin in the image plane;
 N = Projection center;
 $M_p(u_o, v_o)$ = Principal point;
 $O(x, y, z)$ = A point in the object space;
 $I(u, v)$ = Photographic image of point O ;
 $\underline{n}_k, \underline{n}_m, \underline{n}_n$ = Right handed orthogonal triad;
 $\underline{n}_x, \underline{n}_y, \underline{n}_z$ = Right handed orthogonal triad of unit vectors;
 $\underline{n}_s, \underline{n}_t$ = Image plane orthogonal unit vectors;
 $\underline{P}, \underline{Q}, \underline{R}$ = Position vectors defining relative positions of A, N, O ;
 $\underline{p}, \underline{q}, \underline{r}$ = Position vectors defining relative positions of B, I, M_p ;
 \underline{S} = Position vector defining relative positions of M_p, N ;
 \underline{T} = Position vector defining relative positions of I, N ;

Solution of the Linear System

Let N be the number of the CP used then the system of equations takes the following matrix form: (X_i, Y_i, Z_i are the real life coordinates of the CP ($i=1$ to N number of C.P); U_i, V_i are the digitized coordinates of the same points.)

$$\begin{array}{cccccccccccc|l|l}
 X_1 & Y_1 & Z_1 & 1 & 0 & 0 & 0 & 0 & -X_1U_1 & -Y_1U_1 & -Z_1U_1 & L_1 & U_1 \\
 X_2 & Y_2 & Z_2 & 1 & 0 & 0 & 0 & 0 & -X_2U_2 & -Y_2U_1 & -Z_2U_2 & L_2 & U_2 \\
 X_3 & Y_3 & Z_3 & 1 & 0 & 0 & 0 & 0 & -X_3U_3 & -Y_3U_3 & -Z_3U_3 & L_3 & U_3 \\
 \dots & \dots & \dots & \dots & \dots & \dots & \dots & \dots & \dots & \dots & \dots & L_4 & \dots \\
 \dots & \dots & \dots & \dots & \dots & \dots & \dots & \dots & \dots & \dots & \dots & L_5 & \dots \\
 X_n & Y_n & Z_n & 1 & 0 & 0 & 0 & 0 & -X_nU_n & -Y_nU_n & -Z_nU_n & L_6 & U_n \\
 0 & 0 & 0 & 0 & X_1 & Y_1 & Z_1 & 1 & -X_1V_1 & -Y_1V_1 & -Z_1V_1 & L_7 & V_1 \\
 0 & 0 & 0 & 0 & X_2 & Y_2 & Z_2 & 1 & -X_2V_2 & -Y_2V_2 & -Z_2V_2 & L_8 & V_2 \\
 0 & 0 & 0 & 0 & X_3 & Y_3 & Z_3 & 1 & -X_3V_3 & -Y_3V_3 & -Z_3V_3 & L_9 & V_3 \\
 \dots & \dots & \dots & \dots & \dots & \dots & \dots & \dots & \dots & \dots & \dots & L_{10} & \dots \\
 0 & 0 & 0 & 0 & X_n & Y_n & Z_n & 1 & -X_nV_n & -Y_nV_n & -Z_nV_n & L_{11} & U_n
 \end{array} = \quad (A.43)$$

$[A] \qquad [B] [C]$

The solution of the above system is given by the following matrix equation:

$$B = (A^t \cdot A)^{-1} (A^t \cdot C) \quad (A.44)$$

where: A^t is the transpose of the Jacobian matrix $[A]$ and $(A^t \cdot A)^{-1}$ is the inverse of the $(A^t \cdot A)$ matrix.

The same equations are used for the second camera. After the

L_i ($i= 1$ to 11) and the L_i ($i= 1$ to 11) of the first and the second camera respectively have been calculated, the reconstruction of the 3-D real life coordinates of the CP is achieved by the following matrix equation.

$$\begin{bmatrix} (UL_9 - L_1) & (UL_{10} - L_2) & (UL_{11} - L_3) \\ (VL_9 - L_5) & (VL_{10} - L_6) & (VL_{11} - L_7) \\ (UL_9 - L_1) & (UL_{10} - L_2) & (UL_{11} - L_3) \\ (VL_9 - L_5) & (VL_{10} - L_6) & (VL_{11} - L_7) \end{bmatrix} \begin{bmatrix} X \\ Y \\ Z \end{bmatrix} = \begin{bmatrix} (L_4 - U) \\ (L_8 - V) \\ (L_4 - U) \\ (L_8 - V) \end{bmatrix} \quad (A.45)$$

$[E] \qquad [F] \quad [G]$

the solution then is given by the following matrix equation:

$$E^{-1} \cdot G = F \quad (A.46)$$

where: E^{-1} is the inverse of the E matrix.

In the equations of the system (A.45) the L_i ($i=1$ to 11) and U, V are the coefficients and the digitized coordinates of the CP from the first camera and L_i ($i=1$ to 11) U, V the same for the second camera.

Image Refinement

The coefficients of the equations (A.29) and (A.30) count for the transformation of the 3-D object space onto the 2-D secondary image and vice versa. However, in film analysis the above coefficients do not count for the distortions of the image due to the lens of the cameras and

the projector as well as to the film itself (We assumed that the film is a perfect plane which is not always the case.)

For the refinement of the image, Abdel Aziz and Karara (1974), have presented 6 mathematical models to be used together with the DLT equations. These models are:

MODEL I: Linear polynomial in U and V:

$$\Delta U = a_1 + a_2 U + a_3 V \quad (\text{A.47})$$

$$\Delta V = a_4 + a_5 U + a_6 V \quad (\text{A.48})$$

In this model, only the linear components of lens distortion and film deformation are taken into consideration.

Incorporating Model I into the basic DLT equations does not change their form. In other words, by using Model I in the DLT solution the number of unknowns remains 11.

MODEL II: One more unknown k_1 is added to Model I to account for symmetrical lens distortion:

$$\Delta U = a_1 + a_2 U + a_3 V + X k_1 r^2 \quad (\text{A.49})$$

$$\Delta V = a_4 + a_5 U + a_6 V + Y k_1 r^2 \quad (\text{A.50})$$

In this case, the DLT solution involves 12 unknowns.

MODEL III: An odd radial polynomial of the seventh degree is added to Model I to account for symmetrical lens distortion:

$$\Delta U = a_1 + a_2 U + a_3 V + X(k_1 r^2 + k_2 r^4 + k_3 r^6) \quad (\text{A.51})$$

$$\Delta V = a_4 + a_5 U + a_6 V + Y(k_1 r^2 + k_2 r^4 + k_3 r^6) \quad (\text{A.52})$$

The DLT solution in this instance involves 14 unknowns.

MODEL IV: Model III is combined with a model for asymmetrical lens distortion:

$$\begin{aligned}\Delta U = & a_1 + a_2U + a_3V + X(k_1r^2 + k_2r^4 + k_3r^6) \\ & + P_1(r^2 + 2X^2) + 2P_2XY\end{aligned}\quad (\text{A.53})$$

$$\begin{aligned}\Delta V = & a_4 + a_5U + a_6V + Y(k_1r^2 + k_2r^4 + k_3r^6) \\ & + P_2(r^2 + 2Y^2) + 2P_1XY\end{aligned}\quad (\text{A.54})$$

The DLT solution here involves 16 unknowns.

MODEL V: The same as Model IV, except that the radial polynomial accounting for lens distortion is a full polynomial of the seventh degree:

$$\begin{aligned}\Delta U = & a_1 + a_2U + a_3V \\ & + X(k_1r^2 + k_2r^3 + k_3r^4 + k_4r^5 + k_5r^6) \\ & + P_1(r^2 + 2X^2) + 2P_2XY\end{aligned}\quad (\text{A.55})$$

$$\begin{aligned}\Delta V = & a_4 + a_5U + a_6V \\ & + Y(k_1r^2 + k_2r^3 + k_3r^4 + k_4r^5 + k_5r^6) \\ & + P_2(r^2 + 2Y^2) + 2P_1XY\end{aligned}\quad (\text{A.56})$$

Here the DLT solution involves 18 unknowns.

MODEL VI: Same as Model V, except the polynomial in U and V is of the second degree, accounting for the nonlinear component of film deformation:

$$\begin{aligned}\Delta U = & a_1 + a_2U + a_3V + a_4U^2 + a_5V^2 \\ & + X(k_1r^2 + k_2r^3 + k_3r^4 + k_4r^5 + k_5r^6) \\ & + P_1(r^2 + 2X^2) + 2P_2XY\end{aligned}\quad (\text{A.57})$$

$$\begin{aligned}\Delta V = & a_6 + a_7U + a_8V + a_9U^2 + a_{12}V^2 \\ & + Y(k_1r^2 + k_2r^3 + k_3r^4 + k_4r^5 + k_5r^6)\end{aligned}$$

$$+ P_2(r^2 + 2Y^2) + 2P_1XY \quad (\text{A.58})$$

In this model, the DLT solution involves 22 unknowns.

In all the above models

U and V are the digitized coordinates of the point under consideration. If U_s & V_s are the image coordinates of the point of symmetry, then

$$X = U - U_s \text{ and } Y = V - V_s.$$

r = the length of the vector from the point of symmetry to the image point under consideration.

ΔU and ΔV are image refinement components.

a_i ($i=1, \dots, 10$) are coefficients of film deformation.

k_i ($i=1, \dots, 5$) are coefficients of symmetrical lens distortion.

P_1, P_2 are coefficients of asymmetrical lens distortion.

When one of the above models (except model I) has to be used with the DLT equations, then an over-determined systems of $2(K)$ non-linear equations have to be solved for the appropriate number of unknowns for each model. Introducing one of the models for image refinement, equations (A.29) and (A.30) take the following form:

$$U + \Delta U = \frac{L_1X + L_2Y + L_3Z + L_4}{L_9X + L_{10}Y + L_{11}Z + 1} \quad (\text{A.59})$$

$$V + \Delta V = \frac{L_5X + L_6Y + L_7Z + L_8}{L_9X + L_{10}Y + L_{11}Z + 1} \quad (\text{A.60})$$

where: X,Y,Z are the coordinates of the point in space.
 U,V are the digitized coordinates of the point.
 $L_i (i=1, \dots, 11)$ are coefficients named transformation coefficients.
 $\Delta U, \Delta V$ are image refinement components of lens distortion and film deformation.

Using one of the mathematical models for image refinement (except model I), the number of the coefficients increases and an increased number of CP is required. Table A.1 contains the number of coefficients and the minimum number of CP required for each model.

TABLE A.1
NUMBER OF UNKNOWNNS AND MINIMAL CONTROL POINTS
FOR EACH MATHEMATICAL MODEL

<u>Model</u>	<u>Unknowns</u>	<u>Control points</u>
No Ref.	11	6
Model II	12	6
Model III	14	7
Model IV	16	8
Model V	18	9
Model VI	22	11

For the optimal number of the object-space control points, a mathematical model is given by Karara and Abdel Aziz (1974):

$$S_s = \frac{S}{[2(n-u)]^{1/2}} \quad (\text{A.61})$$

where : S_s is the standard deviation of the standard deviations of the object-space coordinates
 S is the standard deviation of the object-space coordinates.
 n is the number of observations (in case of two cameras, it is twice the number of control points).
 u is the number of unknowns.

The same investigators have indicated that beyond 20 to 25 CP the improvements in the results are probably not worth the additional effort required to position the extra control points.

Solution of the Non-Linear System

Assume that model II is to be used. The equations (A.59) and (A.60) can be expressed in the following form:

$$F_1 = L_1X + L_2Y + L_3Z + L_4 \\ + (U + k_1Xr^2)(L_9X + L_{10}Y + L_{11}Z + 1) = 0 \quad (A.62)$$

$$F_2 = L_5X + L_6Y + L_7Z + L_8 \\ + (V + k_1Yr^2)(L_9X + L_{10}Y + L_{11}Z + 1) = 0 \quad (A.63)$$

Note: Model II doesn't include a_1, a_2, a_3, a_4, a_5 since these are components of the linear lens distortion and film deformation which are included in the basic 11 coefficients.

By expressing (A.62) and (A.63) in truncated Taylor series, we obtain:

$$\begin{aligned}
& F_1(L_1+\Delta L_1, L_2+\Delta L_2, L_3+\Delta L_3, L_4+\Delta L_4, L_5+\Delta L_5, L_6+\Delta L_6, L_7+\Delta L_7, \\
& L_8+\Delta L_8, L_9+\Delta L_9, L_{10}+\Delta L_{10}, L_{11}+\Delta L_{11}, k_1+\Delta k_1) \\
& = F_1(L_1, L_2, L_3, L_4, L_5, L_6, L_7, L_8, L_9, L_{10}, L_{11}, k_1) \\
& + (\Delta L_1 \cdot \Pi_{i1} + \Delta L_2 \cdot \Pi_{i2} + \Delta L_3 \cdot \Pi_{i3} + \Delta L_4 \cdot \Pi_{i4} + \Delta L_5 \cdot \Pi_{i5} + \Delta L_6 \cdot \Pi_{i6} \\
& + \Delta L_7 \cdot \Pi_{i7} + \Delta L_8 \cdot \Pi_{i8} + \Delta L_9 \cdot \Pi_{i9} + \Delta L_{10} \cdot \Pi_{i10} + \Delta L_{11} \cdot \Pi_{i11} + \\
& \Delta k_1 \cdot \Pi_{i1}) + \dots\dots\dots Q
\end{aligned} \tag{A.64}$$

where Q is components of the second or higher order and,

$$\Pi_{i1} = \frac{\partial F_i}{\partial L_1} \tag{A.65}$$

$$\Pi_{i2} = \frac{\partial F_i}{\partial L_2} \tag{A.66}$$

$$\Pi_{i3} = \frac{\partial F_i}{\partial L_3} \tag{A.67}$$

$$\Pi_{i4} = \frac{\partial F_i}{\partial L_4} \tag{A.68}$$

$$\Pi_{i5} = \frac{\partial F_i}{\partial L_5} \tag{A.69}$$

$$\Pi_{i6} = \frac{\partial F_i}{\partial L_6} \tag{A.70}$$

$$\Pi_{i7} = \frac{\partial F_i}{\partial L_7} \tag{A.71}$$

$$\Pi_{i8} = \frac{\partial F_i}{\partial L_8} \tag{A.72}$$

$$\Pi_{i9} = \frac{\partial F_i}{\partial L_9} \tag{A.73}$$

$$\Pi_{i10} = \frac{\partial F_i}{\partial L_{10}} \quad (\text{A.74})$$

$$\Pi_{i11} = \frac{\partial F_i}{\partial L_{11}} \quad (\text{A.75})$$

$$\Pi_{i12} = \frac{\partial F_i}{\partial k_1} \quad (\text{A.76})$$

For $i = 1, 2, 3, \dots, 2n$

The Jacobian of the system will be:

$$\begin{vmatrix} \Pi_{11} & \Pi_{12} & \Pi_{13} & \Pi_{14} & \dots & \Pi_{112} \\ \Pi_{21} & \Pi_{22} & \Pi_{23} & \Pi_{24} & \dots & \Pi_{212} \\ \Pi_{31} & \Pi_{32} & \Pi_{33} & \Pi_{34} & \dots & \Pi_{312} \\ \Pi_{41} & \Pi_{42} & \Pi_{43} & \Pi_{44} & \dots & \Pi_{412} \\ \Pi_{51} & \Pi_{52} & \Pi_{53} & \Pi_{54} & \dots & \Pi_{512} \\ \Pi_{61} & \Pi_{62} & \Pi_{63} & \Pi_{64} & \dots & \Pi_{612} \\ \dots & \dots & \dots & \dots & \dots & \dots \\ \Pi_{2n1} & \Pi_{2n2} & \Pi_{2n3} & \Pi_{2n4} & \dots & \Pi_{2n12} \end{vmatrix} = J \quad (\text{A.77})$$

Let J be the above matrix, then if G is the column matrix of the $\Delta L_1, \Delta L_2, \Delta L_3, \Delta L_4, \Delta L_5, \Delta L_6, \Delta L_6, \Delta L_7, \Delta L_8, \Delta L_9, \Delta L_{10}, \Delta L_{11}, \Delta k_1$, and C the column matrix of the $F_1, F_2, F_3, F_4, \dots, F_{2n}$, the solution is achieved by utilizing Newton's iterative method as following:

$$G = (J^t \cdot J)^{-1} (J^t \cdot C) \quad (\text{A.78})$$

where J' is the transpose of the Jacobian matrix.

The elements of the C matrix and in the first iteration are calculated from equations (A.62) and (A.63), by inserting the initial values of the 11 basic coefficients as have been calculated from the system of equations (A.44). Initial value for the k_1 element is used the zero value. The computer program is set to attenuate the iterations when the sum of the absolute values of the residuals is smaller or equal to the criteria value of 10^{-10} , $(\sum |R| \leq 10^{-10})$, or when the system stops converging.

Simulation of the Spatial Coordinates

After the choice of the appropriate model for the image refinement a number of 2J system of equations is solved for the reconstruction of the X, Y, Z coordinates of the points under consideration.

$$\begin{vmatrix} L_9(U+\Delta U)-L_1 & L_{10}(U+\Delta U)-L_2 & L_{11}(U+\Delta U)-L_3 \\ L_9(V+\Delta V)-L_5 & L_{10}(V+\Delta V)-L_6 & L_{11}(V+\Delta V)-L_7 \\ L_9(U+\Delta U)-L_1 & L_{10}(U+\Delta U)-L_2 & L_{11}(U+\Delta U)-L_3 \\ L_9(V+\Delta V)-L_5 & L_{10}(V+\Delta V)-L_6 & L_{11}(V+\Delta V)-L_7 \end{vmatrix} \begin{vmatrix} X \\ Y \\ Z \end{vmatrix} = \begin{vmatrix} L_4-(U+\Delta U) \\ L_8-(V+\Delta V) \\ L_4-(U+\Delta U) \\ L_8-(V+\Delta V) \end{vmatrix} \quad (A.79)$$

In order to use one of the mathematical models for image refinement, one must insert the coordinates of the center of symmetry of projection for each camera. These coordinates can be calculated by using the following two

equations:

$$U_s = \frac{L_1 L_9 + L_2 L_{10} + L_3 L_{11}}{L_9^2 + L_{10}^2 + L_{11}^2} \quad (\text{A.80})$$

$$V_s = \frac{L_5 L_9 + L_6 L_{10} + L_7 L_{11}}{L_9^2 + L_{10}^2 + L_{11}^2} \quad (\text{A.81})$$

The same way for U_s and V_s of the second camera. However, the above equations are not valid if the CP are not symmetrically distributed in space which is usually the case. Therefore, one must enter the coordinates of the center of symmetry manually.

After the calibration of the system and the digitizing of the coordinates of the points under observation is finished, the system of equations (A.79) is used to simulate the spatial coordinates of each point.

DLT Programs

The following programs and subroutines were written in HPL language for the H.P.9825B desk top microcomputer.

DATA ENTERING PROGRAM

Tape D.L.T.I.K.

track #0

file #0

DESCRIPTION

This program was designed to insert all the required information for the DLT calibration.

User enters:

1. The # of all CP;
2. The names of all CP;
3. The X, Y, Z measured coordinates of all CP;
4. User and project I.D. information.

User digitizes:

1. The U, V coordinates of all CP from both cameras;
2. The coordinates of the edges of each film for the Us and Vs.

The computer prints all information (except users and projects I.D. If you wish this information in print, it will be recorded in trk 1, file 0, string A\$[10, 60]).

After each entry the program is set to ask whether or not you have entered a parameter with error. If yes, then you should type in Yes or Y or y, and enter the correct parameter. This correction feature is not in use for names of the CP or I.D. information.


```

0: % "*****D.L.T.I.K., TRK 0, FILE 0*****"
1: "3-D CALIBRATION (DATA ENTERING)":
2: "Copyright@ 1984 by Iraklis Kollias":
3: ent "# OF ALL C.P.",N
4: dim B$(N,16),Q$(8),X(N),Y(N),Z(N),A(N,8),S(4),B(N,3),C(N,3),AS(10,60)
5: gsb "INSERT"
6: gsb "DIGI"
7: gsb "RECORD"
8: dsp "FIRST STEP DONE → USE FILE #1";end
9:
10: "INSERT":fxd 0
11: % "insert name of C.P."
12: for I=1 to N;pvt I;ent "NAME OF C.P.→ (max # of char=16)→ → →",B$(I)
13: next I
14: % "Insert the measured coordinates"
15: for I=1 to N;fmt 5,f2.0,".",c;wrt 16.5,I,B$(I)
16: ent "X→",X[I];ent "Y→",Y[I];ent "Z→",Z[I]
17: fmt 1,f2.0,x,c16,3f9.2,z;fmt 2,c;wrt 7.1,I,B$(I),X[I],Y[I],Z[I]
18: ent "ERROR ? (Yes or No)",Q$(1)
19: if cap(Q$(1,1))="Y";wrt 7.2," ERR";wtb 7,10,13;gto -3
20: wtb 7,10,13;next I
21: % "Output and corrections if any"
22: wtb 7,12;fmt 1,20x,52"="
23: fmt 2,20x," CONTROL POINTS MEASURED (X,Y,Z) COORDS"
24: fmt 3,45x,"Xcoord",4x,"Ycoord",4x,"Zcoord"
25: fmt 4,21x,f2.0,".",x,c16,3f10.2
26: wrt 7.1;wtb 7,10;wrt 7.2;wtb 7,10;wrt 7.1;wtb 7,10
27: wrt 7.3;wtb 7,10
28: for I=1 to N;wrt 7.4,I,B$(I),X[I],Y[I],Z[I];next I
29: wtb 7,10;wrt 7.1;wtb 7,12
30: ent "ANY CHANGE ? (Yes or No)",Q$;if cap(Q$(1,1))="Y";sfg 1;gsb "ERR"
31: if flgl;cflg 1;gto -5
32: ret
33:
34: "ERR":
35: enp "ROW #",r0;enp "COLUMN #",r1
36: if r1=1;enp X[r0]
37: if r1=2;enp Y[r0]
38: if r1=3;enp Z[r0]
39: ent "MORE CHANGES ? (Yes or No)",Q$;if cap(Q$(1,1))="Y";gto -4
40: ret
41:
*1894

```



```

41:
42: "DIGI":prt "USE THE 'tree' ORIGIN";spc 2
43: for I=1 to 2
44: if I=1;prt "FIRST FILM..."
45: if I=2;prt "SECOND FILM..."
46: dsp "digi TOP END OF FILM";red 4,r1,r2;beep
47: dsp "digi BOTTOM END OF FILM";red 4,r3,r4;beep
48: dsp "digi LEFT LEFT END OF FILM";red 4,r5,r6;beep
49: dsp "digi RIGHT END OF FILM";red 4,r7,r8;beep
50: if I=1;r2-(r2-r4)/2→S[1];r7-(r7-r5)/2→S[2]
51: if I=2;r2-(r2-r4)/2→S[3];r7-(r7-r5)/2→S[4]
52: prt "DIGIT 3 FRAMES OR 3 TIMES THE SAME FRAME";spc 2
53: for J=1 to 3
54: for K=1 to N
55: dsp " DIGITIZE ",B$(K);red 4,B[K,J],C[K,J];beep
56: next K
57: ent "E R R O R ? (Yes or No)",Q$;if cap(Q$[1,1])="Y";gto -3
58: next J
59: % "A[L,1]=Ucameral, A[L,3]=Vcameral"
60: % "A[L,5]=Ucamera2, A[L,7]=Vcamera2"
61: % "A[L,2],A[L,4],A[L,6],A[L,8] = S.D."
62: for L=1 to N
63: cll 'MEAN'(B[L,1],B[L,2],B[L,3],A[L,4I-3])
64: cll 'MEAN'(C[L,1],C[L,2],C[L,3],A[L,4I-1])
65: cll 'SD'(B[L,1],B[L,2],B[L,3],A[L,4I-3],A[L,4I-2])
66: cll 'SD'(C[L,1],C[L,2],C[L,3],A[L,4I-1],A[L,4I])
67: next L
68: fmt 2,c9," CONTROL POINTS DIGITIZED COORDS (in digi-units)"
69: fmt 5,x,f2.0,".",c17,f9.2,f9.4,f9.2,f9.4
70: gsb "PRINT"
71: for Y=1 to 100;dsp "second film now";beep;wait 10;next Y;next I
72: ret
73:
74: "MEAN":(p1+p2+p3)/3→p4;ret
75: "SD":√(((p4-p1)^2+(p4-p2)^2+(p4-p3)^2)/2)→p5;ret
76:
*12727

```



```

76:
77: "PRINT":
78: fmt 1,58"=";fmt 3,24x,"Xcoord",4x,"S.D.",5x,"Ycoord",4x,"S.D."
79: fmt 4,23x,"[J,",f3.0,"]",4x,"J,",f2.0,4x,"[J,",f3.0,"]",4x,"J,",f2.0
80: wtb 7,27,69;for A=1 to 20;wtb 7,32;next A;wtb 7,27,77
81: wrt 7.1;wtb 7,10
82: if I=1;wrt 7.2," FIRST-"
83: if I=2;wrt 7.2,"SECOND-"
84: wtb 7,10;wrt 7.1;wtb 7,10;wrt 7.3;wrt 7.4,4I-3,4I-2,4I-1,4I;wtb 7,10
85: for J=1 to N
86: wrt 7.5,J,B$(J),A[J,4I-3],A[J,4I-2],A[J,4I-1],A[J,4I]
87: next J
88: wtb 7,10;wrt 7.1;wtb 7,12;ret
89:
90: "RECORD":18N+6→r0;24N→r1;64N→r2
91: prt "STORAGE SPACE";prt "NAME OF C.P.",r0;prt "X, Y, Z coord",r1
92: prt "DIGIT. coord",r2;prt "-----"
93: prt "Mark files if you haven't done it yet!!!"
94: prt "-----"
95: prt "T#1-F#0 (I.D.info.)",650
96: prt "T#1-F#1 (C.P.names)",r0
97: prt "T#1-F#2 (X,Y,Z coords)",r1
98: prt "T#1-F#3 (U,Vcoords)",r2
99: prt "T#1-F#4 Us,Vscoords",208
100: for R=1 to 10;ent "I.D. INFORMATION(10*60char)",A$(R);next R
101: ent "ARE FILES MARKED ?? (Yes or No)",Q$
102: if cap(Q$[1,1])="Y";gto +2
103: rew;trk 1;mrk 1,650;mrk 1,r0;mrk 1,r1;mrk 1,r2;mrk 1,208
104: trk 1;fdf 0;rcf 0,A$[*]
105: trk 1;fdf 1;rcf 1,B$[*]
106: trk 1;fdf 2;rcf 2,X[*],Y[*],Z[*]
107: trk 1;fdf 3;rcf 3,A$[*]
108: trk 1;fdf 4;rcf 4,S$[*]
109: ret
*26247

```

CALIBRATION COEFFICIENTS (NO REFINEMENT) +TEST

Tape D.L.T.I.K.

track #0

file #1

DESCRIPTION

This program calculates the basic DLT coefficients. After the preliminary tests the basic DLT coefficients together with the coordinates of the point of symmetry are stored in file #4, track #1 of D.L.T.I.K. tape. It can also be used for testing the CP's coordinates to determine whether or not they are correct. After the calculation of the coefficients the X, Y, Z coordinates of the CP are simulated and printed.

Another test that this program is featured to run is the simulation of the X, Y, Z coordinates of the two cameras with respect to the tree origin.

Several runs with all the points and with less points are advisable to ensure that no errored CP participate in the calculation of the coefficients.


```

0: % "*****D.L.T.I.K., TRK 0, FILE 1*****"
1: "CALIBRATION COEFFICIENTS (NO REFINEMENT) +TEST":
2: "Copyright@ 1984 by Iraklis Kollias":
3: dim AS[50];" CALIBRATION WITH DLT (NO REFINEMENT)"→AS
4: ent "# OF ALL C.P.",r99;r99→A
5: dim X[A],Y[A],Z[A],A[A,8],H[4,3],I[3,4],N[3,3],J[4],K[3],O[3]
6: dim BS[A,16],QS[16]
7: ent "IS IT THE VERY FIRST RUN? (Y or N)",QS
8: ent "# OF CONTROL POINTS TO BE USED",C
9: dim B[2C,11],D[11,2C],C[2C],G[11],E[11,11],F[11],L[2,11],S[4],P[4]
10: trk 1;ldf 1,BS
11: trk 1;ldf 2,X[*],Y[*],Z[*]
12: trk 1;ldf 3,A[*]
13: if cap(QS[1,1])="Y";trk 1;ldf 4,S[*]
14: if cap(QS[1,1])#"Y";trk 1;ldf 4,L[*],S[*]
15: ara S→P;.01→W
16: "COEFF":0→r0
17: for L=1 to 3 by 2
18: 2(L-1)+1→A;A+2→B;1+r0→r0
19: for I=1 to C;I→C+J
20: WX[I]→B[I,1]→B[J,5];WY[I]→B[I,2]→B[J,6];WZ[I]→B[I,3]→B[J,7]
21: 0→B[I,5]→B[I,6]→B[I,7]→B[I,8]→B[J,1]→B[J,2]→B[J,3]→B[J,4]
22: -A[I,A]WX[I]→B[I,9];-A[I,A]WY[I]→B[I,10];-A[I,A]WZ[I]→B[I,11]
23: -A[I,B]WX[I]→B[J,9];-A[I,B]WY[I]→B[J,10];-A[I,B]WZ[I]→B[J,11]
24: 1→B[I,4]→B[J,8];A[I,A]→C[I];A[I,B]→C[J]
25: next I
26: trn B→D;mat DB→E;mat DC→F;inv E→E;mat EF→G
27: for J=1 to 11;G[J]→L[r0,J];next J
28: G[1]C[9]+G[2]G[10]+G[3]G[11]→r1
29: G[5]G[9]+G[6]G[10]+G[7]G[11]→r2
30: G[9]^2+G[10]^2+G[11]^2→r3
31: r1/r3→S[L];r2/r3→S[L+1]
32: next L
33: fmt ,26x,c
34: fmt 1,21x,"CALIBRATION COEFFICIENTS FOR TWO CAMERAS (",f2.0,"C.P.)"
35: fmt 2,20x,51"="
36: fmt 3,21x,"L[1,",f2.0,"] =",f14.10," L[2,",f2.0,"] =",f14.10
37: fmt 4,21x,"FIRST CAMERA",13x,"SECOND CAMERA"
38: fmt 5,22x,c
39: wrt 7.2;wtb 7,10;wrt 7.1,C;wrt 7,AS
40: wtb 7,10;wrt 7.2;wtb 7,10;wrt 7.4;wtb 7,10
41: for I=1 to 11;wrt 7.3,I,L[1,I],I,L[2,I];wtb 7,10;next I
42: wrt 7.2;wtb 7,12
43:
*7492

```



```

44: "C.P.RECOVERING":
45: for I=1 to 20;0→rI;wtb 7,32;next I;wtb 7,27,77
46: fmt 1,f2.0,z;fmt 2,f8.2,z;fmt 3,74"-";fmt 4,74"="
47: fmt 5,18x,c;fmt 6,9c8
48: wrt 7.4;wrt 7.5,A$;wrt 7.3
49: wrt 7.6,"Xm","Xs","dX","Ym","Ys","dY","Zm","Zs","dZ";wrt 7.3
50: wtb 7,27,86,int(12/64),int(12)
51: for I=1 to r99;wrt 7.1,I
52: for T=1 to 3
53: L[1,T+8]A[I,1]-L[1,T]→H[1,T]
54: L[1,T+8]A[I,3]-L[1,T+4]→H[2,T]
55: L[2,T+8]A[I,5]-L[2,T]→H[3,T]
56: L[2,T+8]A[I,7]-L[2,T+4]→H[4,T]
57: next T
58: L[1,4]-A[I,1]→J[1];L[1,8]-A[I,3]→J[2]
59: L[2,4]-A[I,5]→J[3];L[2,8]-A[I,7]→J[4]
60: trn H→I;mat IH→N;mat IJ→O;inv N→N;mat NO→K
61: X[I]→r1;K[1]/W→r2;r1-r2→r3
62: Y[I]→r4;K[2]/W→r5;r4-r5→r6
63: Z[I]→r7;K[3]/W→r8;r7-r8→r9
64: if I≤C;r3^2+r10→r10;r6^2+r11→r11;r9^2+r12→r12
65: if I>C;r3^2+r13→r13;r6^2+r14→r14;r9^2+r15→r15
66: for Y=1 to 9;wrt 7.2,rY;next Y
67: wtb 7,10,13;next I
68: wrt 7.3;fmt 1,c15,f11.2,2f24.2
69: r10+r13→r16;r11+r14→r17;r12+r15→r18
70: √(r10/C)→r10;√(r11/C)→r11;√(r12/C)→r12
71: if C<r99;√(r13/(r99-C))→r13;√(r14/(r99-C))→r14;√(r15/(r99-C))→r15
72: √(r16/r99)→r16;√(r17/r99)→r17;√(r18/r99)→r18
73: wtb 7,27,86,int(16/64),int(16)
74: if C<r99;wrt 7.1,"RMS OF C.P.",r10,r11,r12
75: if C<r99;wrt 7.1,"RMS OF UNKNOWNNS",r13,r14,r15
76: wrt 7.1,"TOTAL RMS",r16,r17,r18
77: fmt 1,c;wrt 7.1,"*** (Measurements in cm.)";wrt 7.4
78: wtb 7,12;wtb 7,27,69
79: ent "SHALL COEFF.. BE RECORDED? (Y,N)",Q$
80: if cap(Q$[1,1])#"Y";dsp "OH!! THANK'S";wait 2000;gto +4
81: prt "Us1,Vs1,Us2,Vs2"
82: for Y=1 to 4;prt P[Y],S[Y];spc ;P[Y]→S[Y];next Y
83: trk 1;rcf 4,L[*],S[*]
84: trk 0
85: % "CAMERAS COORDINATES"
86: for I=1 to 2;for J=1 to 3
87: L[I,J]→N[1,J];L[I,J+8]→N[2,J];L[I,J+4]→N[3,J]
88: next J
89: -L[I,4]→O[1];-1→O[2];-L[I,8]→O[3]
90: inv N→N;mat NO→K
91: prt "COORDs of CAMERA #",I
92: prt K[1]/W,K[2]/W,K[3]/W
93: next I
94: trk 0;dsp "E N D";end
*21401

```

REFINEMENT WITH Karara's MODELS (main program)

Tape D.L.T.I.K.

track #0

file #2

DESCRIPTION

This program was designed for the calculation of the DLT coefficients whenever one of the mathematical models for image refinement is used.

User enters

The # of all the CP in the data file

The Model # (2,3,4,5,6) to be used

The # of CP to be used for the calculation of the coefficients

The computer

loads the CP's data

loads the appropriate model to be used

calculates the coefficients

simulates the X,Y,Z coordinates of all the CP

prints in the small printer the sum of the residuals after each iteration

prints the measured, simulated and their differences

prints the RMS error of the CP

prints the RMS error of the unknowns if any

records the calibration coefficients in track #1, file 5(II), 6(III), 7(IV), 8(V), 9(VI)

After the tests of the points are finished it is advisable to run the program with all the correct points in order to calculate the coefficients that will be used in the recovery of the coordinates of points of interest.


```

0: % "*****D.L.T.I.K., TRK 0, FILE 2*****"
1: "REFINEMENT WITH Karara's MODELS":
2: "Copyright© 1984 by Iraklis Kollias":
3: ent "# of all the C.Points",P;P→r99
4: ent "MODEL TO BE USED",M;M→r98
5: ent "# OF CONTROL POINTS TO BE USED",C
6: if M=2;l2→Q
7: if M=3;l4→Q
8: if M=4;l6→Q
9: if M=5;l8→Q
10: if M=6;22→Q
11: Q→r97
12: dim L[2,11],S[4],H[4,3],I[3,4],N[3,3],J[4],K[3],O[3],A$[50]
13: dim X[P],Y[P],Z[P],A[P,8],M[P,2,5],B$[P,3]
14: dim Q[2,Q],E[Q,Q],B[2C,Q],D[Q,2C],C[2C],G[Q],F[Q],P[2,Q]
15: trk 1;ldf 1,B$
16: ldf 2,X[*],Y[*],Z[*]
17: ldf 3,A[*]
18: ldf 4,L[*],S[*]
19: for I=1 to 2
20: for J=1 to 11;L[I,J]→Q[I,J];next J
21: for K=12 to r97;O→Q[I,K];next K
22: next I
23: for I=1 to r99
24: A[I,1]→M[I,1,1];A[I,3]→M[I,1,2];A[I,5]→M[I,2,1];A[I,7]→M[I,2,2]
25: A[I,1]-S[1]→M[I,1,3];A[I,3]-S[2]→M[I,1,4]
26: A[I,5]-S[3]→M[I,2,3];A[I,7]-S[4]→M[I,2,4]
27: for J=1 to 2;√(M[I,J,3]^2+M[I,J,4]^2)→M[I,J,5];next J
28: next I
29: trk 0;ldf r98+1,57
30: "S":.01→w
31: gsb "MODEL"
32: wrt 7.3;fmt 1,cl5,fl1.2,2f24.2
33: r26+r29→r32;r27+r30→r33;r28+r31→r34
34: √(r26/C)→r26;√(r27/C)→r27;√(r28/C)→r28
35: if C<r99;√(r29/(r99-C))→r29;√(r30/(r99-C))→r30;√(r31/(r99-C))→r31
36: √(r32/r99)→r32;√(r33/r99)→r33;√(r34/r99)→r34
37: wtb 7,27,86,int(16/64),int(16)
38: if C<r99;wrt 7.1,"RMS OF C.P.",r26,r27,r28
39: if C<r99;wrt 7.1,"RMS OF UNKNOWN",r29,r30,r31
40: wrt 7.1,"TOTAL RMS",r32,r33,r34
41: fmt ,c;wrt 7,"*** (Measurements in cm.)";wrt 7.4
42: wtb 7,12
43: trk 1;rcf r98+3,P[*]
44: wtb 7,27,69;dsp "D O N E !!!";end
45: "COUT":fmt ,26x,c
46: fmt 1,2lx,"CALIBRATION COEFFICIENTS FOR TWO CAMERAS (",f2.0,"C.P.)"
47: fmt 3,2lx,"P[1",f2.0,"] =",f14.9," P[2",f2.0,"] =",f14.9
48: fmt 2,20x,51="";fmt 4,2lx,"FIRST CAMERA",13x,"SECOND CAMERA";fmt 5,2lx,
49: wrt 7.2;wtb 7,10;wrt 7.1,C;wrt 7,A$;wtb 7,10;wrt 7.2;wrt 7.4;wtb 7,10
50: for I=1 to r97;wrt 7.3,I,P[1,I],I,P[2,I];wtb 7,10;next I
51: wrt 7.2;wtb 7,12
52: for I=1 to 20;O→rI;wtb 7,32;next I;wtb 7,27,77
53: fmt 1,f2.0,z;fmt 2,f8.2,z;fmt 3,74="-";fmt 4,74="=";fmt 6,2x,9c8
54: fmt 5,18x,c;wrt 7.4;wrt 7.5,A$;wrt 7.3
55: wrt 7.6,"Xm","Xs","dX","Ym","Ys","dY","Zm","Zs","dZ";wrt 7.3
56: wtb 7,27,86,int(12/64),int(12);ret
*6080

```

SUBROUTINE MODEL II

Tape D.L.T.I.K.

track #0

file #3

DESCRIPTION

This subroutine is loaded at the end of the program in file #2. The basic DLT equations are used together with equations (A.49) and (A.50) for the calculation of the calibration coefficients.

```

0: gto "S"
1: "MODEL": "REFINEMENT WITH MODEL #2 (KARARA)" → AS
2: "Copyright© 1984 by Iraklis Kollias":
3: for I=1 to 2; 0 → r24 → r25; 106 → r90
4: "r1": beep; fxd 0; 1 → r24 → r24; dsp " PLEASE DON'T TOUCH → ", r24
5: if r24 > 8 and r25 > r90; gto "OK"
6: for J=1 to 12; Q[I, J] + G[J] → rJ → Q[I, J]; next J
7: for J=1 to C; J + C → L
8: W(r9X[J] + r10Y[J] + r11Z[J]) + 1 → r17
9: W(r1X[J] + r2Y[J] + r3Z[J]) + r4 → r18
10: W(r5X[J] + r6Y[J] + r7Z[J]) + r8 → r19
11: M[J, I, 1] → O; M[J, I, 2] → P; M[J, I, 3] → Q; M[J, I, 4] → R; M[J, I, 5] → S
12: O + r12RS2 → r20; P + r12RS2 → r21
13: r17r20 - r18 → C[J]; r17r21 - r19 → C[L]
14: wX[J] → B[J, 1] → B[L, 5]; wY[J] → B[J, 2] → B[L, 6]; wZ[J] → B[J, 3] → B[L, 7]
15: 1 → B[J, 4] → B[L, 8]
16: 0 → B[J, 5] → B[J, 6] → B[J, 7] → B[J, 8] → B[L, 1] → B[L, 2] → B[L, 3] → B[L, 4]
17: -wX[J]r20 → B[J, 9]; -wX[J]r21 → B[L, 9]
18: -wY[J]r20 → B[J, 10]; -wY[J]r21 → B[L, 10]
19: -wZ[J]r20 → B[J, 11]; -wZ[J]r21 → B[L, 11]
20: -Qr17S2 → B[J, 12]; -Rr17S2 → B[L, 12]
21: next J
22: if C > 6; trn B → D; mat DB → E; mat DC → F; inv E → E; mat EF → G
23: if C = 6; inv B → B; mat BC → G
24: r25 → r90; 0 → r22 → r25 → r26
25: for T=1 to 12; if abs(G[T]) ≤ 10-10; r22 + 1 → r22; next T
26: for J=1 to 12; abs(G[J]) + r25 → r25; next J
27: fxd 10; prt r25
28: for J=1 to 2C; abs(C[J]) + r26 → r26; next J
29: if r22 < 12; gto "r1"
30: "OK": for J=1 to 12; Q[I, J] → P[I, J]; next J
31: fxd 10; prt r26; fxd 0; prt r22, r24; next I
32: qsb "cOUT"
33: "C.P.RECOVERING": 0 → r26 → r27 → r28 → r29 → r30 → r31 → r32 → r33 → r34 → r35
34: for I=1 to 2; for J=1 to 12; P[I, J] → Q[I, J]; next J; next I
35: for I=1 to r99; wrt 7.1, I
36: for J=1 to 2; J + 2 → L
37: for K=1 to 12; Q[J, K] → rK; next K
38: M[I, J, 1] → O; M[I, J, 2] → P; M[I, J, 3] → Q; M[I, J, 4] → R; M[I, J, 5] → S
39: O + r12RS2 → r20; P + r12RS2 → r21
40: r1 - r9r20 → H[J, 1]; r5 - r9r21 → H[L, 1]
41: r2 - r10r20 → H[J, 2]; r6 - r10r21 → H[L, 2]
42: r3 - r11r20 → H[J, 3]; r7 - r11r21 → H[L, 3]
43: r20 - r4 → J[J]; r21 - r8 → J[L]
44: next J
45: trn H → I; mat IH → N; mat IJ → O; inv N → N; mat NO → K
46: X[I] → r1; K[1] / W → r2; r1 - r2 → r3
47: Y[I] → r4; K[2] / W → r5; r4 - r5 → r6
48: Z[I] → r7; K[3] / W → r8; r7 - r8 → r9
49: if I ≤ C; r32 + r26 → r26; r62 + r27 → r27; r92 + r23 → r23
50: if I > C; r32 + r29 → r29; r62 + r30 → r30; r92 + r31 → r31
51: for Y=1 to 9; wrt 7.2, rY; next Y
52: wtb 7, 10, 13; next I
53: ret
*9969

```

SUBROUTINE MODEL III

Tape D.L.T.I.K.

track #0

file #4

DESCRIPTION

This subroutine is loaded at the end of the program in file #2. The basic DLT equations are used together with equations (A.51) and (A.52) for the calculation of the calibration coefficients.

```

0: gto "S"
1: "MODEL": "REFINEMENT WITH MODEL #3 (KARARA)" → AS
2: "Copyright© 1984 by Iraklis Kollias":
3: for I=1 to 2; 0 → r24 → r25; 106 → r90
4: "rl": beep; fxd 0; 1 → r24 → r24; dso " PLEASE DON'T TOUCH → ", r24
5: if r24 > 8 and r25 > r90; gto "OK"
6: for J=1 to 14; Q[I, J] + G[J] → rJ → Q[I, J]; next J
7: for J=1 to C; J + C → L
8: W(r9X[J] + r10Y[J] + r11Z[J]) + 1 → r17
9: W(r1X[J] + r2Y[J] + r3Z[J]) + r4 → r18
10: W(r5X[J] + r6Y[J] + r7Z[J]) + r8 → r19
11: M[J, I, 1] → O; M[J, I, 2] → P; M[J, I, 3] → Q; M[J, I, 4] → R; M[J, I, 5] → S
12: O + Q(r12S2 + r13S4 + r14S6) → r20; P + R(r12S2 + r13S4 + r14S6) → r21
13: r17r20 - r18 → C[J]; r17r21 - r19 → C[L]
14: WX[J] → B[J, 1] → B[L, 5]; WY[J] → B[J, 2] → B[L, 6]; WZ[J] → B[J, 3] → B[L, 7]
15: 1 → B[J, 4] → B[L, 8]
16: 0 → B[J, 5] → B[J, 6] → B[J, 7] → B[J, 8] → B[L, 1] → B[L, 2] → B[L, 3] → B[L, 4]
17: -WX[J]r20 → B[J, 9]; -WX[J]r21 → B[L, 9]
18: -WY[J]r20 → B[J, 10]; -WY[J]r21 → B[L, 10]
19: -WZ[J]r20 → B[J, 11]; -WZ[J]r21 → B[L, 11]
20: -Qr17S2 → B[J, 12]; -Rr17S2 → B[L, 12]
21: -Qr17S4 → B[J, 13]; -Rr17S4 → B[L, 13]
22: -Qr17S6 → B[J, 14]; -Rr17S6 → B[L, 14]
23: next J
24: if C > 7; trn B → D; mat DB → E; mat DC → F; inv E → E; mat EF → G
25: if C = 7; inv B → B; mat BC → G
26: r25 → r90; 0 → r22 → r25 → r26
27: for T=1 to 14; if abs(G[T]) ≤ 10-10; r22 + 1 → r22; next T
28: for J=1 to 14; abs(G[J]) + r25 → r25; next J
29: fxd 10; prt r25
30: for J=1 to 2C; abs(C[J]) + r26 → r26; next J
31: if r22 < 14; gto "rl"
32: "OK": for J=1 to 14; Q[I, J] → P[I, J]; next J
33: fxd 10; prt r26; fxd 0; prt r22, r24; next I
34: qsb "cOUT"
35: "C.P.RECOVERING": 0 → r26 → r27 → r28 → r29 → r30 → r31 → r32 → r33 → r34 → r35
36: for I=1 to r99; wrt 7.1, I
37: for J=1 to 2; J + 2 → L
38: for K=1 to 14; P[J, K] → rK; next K
39: M[I, J, 1] → O; M[I, J, 2] → P; M[I, J, 3] → Q; M[I, J, 4] → R; M[I, J, 5] → S
40: O + Q(r12S2 + r13S4 + r14S6) → r20; P + R(r12S2 + r13S4 + r14S6) → r21
41: r1 - r9r20 → H[J, 1]; r5 - r9r21 → H[L, 1]
42: r2 - r10r20 → H[J, 2]; r6 - r10r21 → H[L, 2]
43: r3 - r11r20 → H[J, 3]; r7 - r11r21 → H[L, 3]
44: r20 - r4 → J[J]; r21 - r8 → J[L]
45: next J
46: trn H → I; mat IH → N; mat IJ → O; inv N → N; mat NO → K
47: X[I] → r1; K[1] / W → r2; r1 - r2 → r3
48: Y[I] → r4; K[2] / W → r5; r4 - r5 → r6
49: Z[I] → r7; K[3] / W → r8; r7 - r8 → r9
50: if I ≤ C; r32 + r26 → r26; r62 + r27 → r27; r92 + r28 → r28
51: if I > C; r32 + r29 → r29; r62 + r30 → r30; r92 + r31 → r31
52: for Y=1 to 9; wrt 7.2, rY; next Y
53: wtb 7, 10, 13; next I
54: ret
*14703

```

SUBROUTINE MODEL IV

Tape D.L.T.I.K.

track #0

file #5

DESCRIPTION

This subroutine is loaded at the end of the program in file #2. The basic DLT equations are used together with equations (A.53) and (A.54) for the calculation of the calibration coefficients.

```

0: gto "S"
1: "MODEL": "REFINEMENT WITH MODEL #4 (KARARA)" → A$
2: "Copyright© 1984 by Iraklis Kollias":
3: for I=1 to 2; 0 → r24 → r25; 106 → r90
4: "rl": beep; fxd 0; 1 → r24 → r24; dsp " PLEASE DON'T TOUCH → ", r24
5: if r24 > 8 and r25 > r90; gto "OK"
6: for J=1 to 16; Q[I, J] + G[J] → rJ → Q[I, J]; next J
7: for J=1 to C; J + C → L
8: W(r9X[J] + r10Y[J] + r11Z[J]) + 1 → r17
9: W(r1X[J] + r2Y[J] + r3Z[J]) + r4 → r18
10: W(r5X[J] + r6Y[J] + r7Z[J]) + r8 → r19
11: M[J, I, 1] → O; M[J, I, 2] → P; M[J, I, 3] → Q; M[J, I, 4] → R; M[J, I, 5] → S
12: O + Q(r12S2 + r13S4 + r14S6) + r15(S2 + 2Q2) + 2r16QR → r20
13: P + R(r12S2 + r13S4 + r14S6) + r16(S2 + 2R2) + 2r15QR → r21
14: r17r20 - r18 + C[J]; r17r21 - r19 + C[L]
15: WX[J] → B[J, 1] → B[L, 5]; WY[J] → B[J, 2] → B[L, 6]; WZ[J] → B[J, 3] → B[L, 7]
16: 1 → B[J, 4] → B[L, 8]
17: 0 → B[J, 5] → B[J, 6] → B[J, 7] → B[J, 8] → B[L, 1] → B[L, 2] → B[L, 3] → B[L, 4]
18: -WX[J]r20 → B[J, 9]; -WX[J]r21 → B[L, 9]
19: -WY[J]r20 → B[J, 10]; -WY[J]r21 → B[L, 10]
20: -WZ[J]r20 → B[J, 11]; -WZ[J]r21 → B[L, 11]
21: -Qr17S2 → B[J, 12]; -Rr17S2 → B[L, 12]
22: -Qr17S4 → B[J, 13]; -Rr17S4 → B[L, 13]
23: -Qr17S6 → B[J, 14]; -Rr17S6 → B[L, 14]
24: -r17(S2 + 2Q2) → B[J, 15]; -r17(S2 + 2R2) → B[L, 16]
25: -2r17QR → B[J, 16] → B[L, 15]
26: next J
27: if C > 8; trn B → D; mat DB → E; mat DC → F; inv E → E; mat EF → G
28: if C = 8; inv B → B; mat BC → G
29: r25 → r90; 0 → r22 → r25 → r26
30: for T=1 to 16; if abs(G[T]) ≤ 10-40; r22 + 1 → r22; next T
31: for J=1 to 16; abs(G[J]) + r25 → r25; next J
32: fxd 10; prt r25
33: for J=1 to 2C; abs(C[J]) + r26 → r26; next J
34: if r22 < 16; gto "rl"
35: "OK": for J=1 to 16; Q[I, J] → P[I, J]; next J
36: fxd 10; prt r26; fxd 0; prt r22, r24; next I
37: gsb "COUNT"
38: "C.P. RECOVERING": 0 → r26 → r27 → r28 → r29 → r30 → r31 → r32 → r33 → r34 → r35
39: for I=1 to r99; wrt 7.1, I
40: for J=1 to 2; J + 2 → L
41: for K=1 to 16; P[J, K] → rK; next K
42: M[I, J, 1] → O; M[I, J, 2] → P; M[I, J, 3] → Q; M[I, J, 4] → R; M[I, J, 5] → S
43: O + Q(r12S2 + r13S4 + r14S6) + r15(S2 + 2Q2) + 2r16QR → r20
44: P + R(r12S2 + r13S4 + r14S6) + r16(S2 + 2R2) + 2r15QR → r21
45: r1 - r9r20 → H[J, 1]; r5 - r9r21 → H[L, 1]
46: r2 - r10r20 → H[J, 2]; r6 - r10r21 → H[L, 2]
47: r3 - r11r20 → H[J, 3]; r7 - r11r21 → H[L, 3]
48: r20 - r4 → J[J]; r21 - r8 → J[L]
49: next J
50: trn H → I; mat IH → N; mat IJ → O; inv N → N; mat NO → K
51: X[I] → r1; K[1] / W → r2; r1 - r2 → r3
52: Y[I] → r4; K[2] / W → r5; r4 - r5 → r6
53: Z[I] → r7; K[3] / W → r8; r7 - r8 → r9
54: if I ≤ C; r32 + r26 → r26; r62 + r27 → r27; r92 + r28 → r28
55: if I > C; r32 + r29 → r29; r62 + r30 → r30; r92 + r31 → r31
56: for Y=1 to 9; wrt 7.2, rY; next Y
57: wtb 7, 10, 13; next I
58: ret
*27535

```

SUBROUTINE MODEL V

Tape D.L.T.I.K.

track #0

file #6

DESCRIPTION

This subroutine is loaded at the end of the program in file #2. The basic DLT equations are used together with equations (A.55) and (A.56) for the calculation of the calibration coefficients.

```

0: gto "S"
1: "MODEL": "REFINEMENT WITH MODEL #5 (KARARA)" → A$
2: "Copyright© 1984 by Iraklis Kollias":
3: for I=1 to 2; 0 → r24 → r25 → r26; 106 → r90
4: "rl": beep; fxd 0; 1 → r24 → r24; dsp " PLEASE DON'T TOUCH → ", r24
5: if r24 > 8 and r25 > r90; gto "OK"
6: for J=1 to 18; Q[I,J] + G[J] → rJ → Q[I,J]; next J
7: for J=1 to C; J + C → L
8: W(r9X[J] + r10Y[J] + r11Z[J]) + 1 → r36
9: W(r1X[J] + r2Y[J] + r3Z[J]) + r4 → r37
10: W(r5X[J] + r6Y[J] + r7Z[J]) + r8 → r38
11: M[J,I,1] → O; M[J,I,2] → P; M[J,I,3] → Q; M[J,I,4] → R; M[J,I,5] → S
12: O + Q(r12S2 + r13S3 + r14S4 + r15S5 + r16S6) + r17(S2 + 2Q2) + 2r18QR → r20
13: P + R(r12S2 + r13S3 + r14S4 + r15S5 + r16S6) + r18(S2 + 2R2) + 2r17QR → r21
14: r36r20 - r37 → C[J]; r36r21 - r38 → C[L]
15: WX[J] → B[J,1] → B[L,5]; WY[J] → B[J,2] → B[L,6]; WZ[J] → B[J,3] → B[L,7]
16: 1 → B[J,4] → B[L,8]
17: 0 → B[J,5] → B[J,6] → B[J,7] → B[J,3] → B[L,1] → B[L,2] → B[L,3] → B[L,4]
18: -WX[J]r20 → B[J,9]; -WX[J]r21 → B[L,9]
19: -WY[J]r20 → B[J,10]; -WY[J]r21 → B[L,10]
20: -WZ[J]r20 → B[J,11]; -WZ[J]r21 → B[L,11]
21: -Qr36S2 → B[J,12]; -Rr36S2 → B[L,12]
22: -Qr36S3 → B[J,13]; -Rr36S3 → B[L,13]
23: -Qr36S4 → B[J,14]; -Rr36S4 → B[L,14]
24: -Qr36S5 → B[J,15]; -Rr36S5 → B[L,15]
25: -Qr36S6 → B[J,16]; -Rr36S6 → B[L,16]
26: -r36(S2 + 2Q2) → E[J,17]; -r36(S2 + 2R2) → B[L,18]
27: -2r36QR → B[J,18] → B[L,17]
28: next J
29: if C > 9; trn B → D; mat DE → E; mat DC → F; inv E → E; mat EF → G
30: if C = 9; inv B → B; mat BC → G
31: r25 → r90; 0 → r22 → r25 → r26
32: for T=1 to 18; if abs(G[T]) ≤ (2)10(-10); r22 + 1 → r22; next T
33: for J=1 to 18; abs(G[J]) + r25 → r25; next J
34: fxd 10; prt r25
35: for J=1 to 2C; abs(C[J]) + r26 → r26; next J
36: if r22 < 18; gto "rl"
37: "OK": for J=1 to 18; Q[I,J] → P[I,J]; next J
38: fxd 10; prt r26; fxd 0; prt r22, r24; next I
39: gsb "COUT"
40: "C.P.RECOVERING": 0 → r26 → r27 → r23 → r29 → r30 → r31 → r32 → r33 → r34 → r35
41: for I=1 to r99; wrt 7.1, I
42: for J=1 to 2; J + 2 → L
43: for K=1 to 18; P[J,K] → rK; next K
44: A[I,J,1] → O; M[I,J,2] → P; M[I,J,3] → Q; M[I,J,4] → R; M[I,J,5] → S
45: O + Q(r12S2 + r13S3 + r14S4 + r15S5 + r16S6) + r17(S2 + 2Q2) + 2r18QR → r20
46: P + R(r12S2 + r13S3 + r14S4 + r15S5 + r16S6) + r18(S2 + 2R2) + 2r17QR → r21
47: r1 - r9r20 → H[J,1]; r5 - r9r21 → H[L,1]
48: r2 - r10r20 → H[J,2]; r6 - r10r21 → H[L,2]
49: r3 - r11r20 → H[J,3]; r7 - r11r21 → H[L,3]
50: r20 - r4 → J[J]; r21 - r8 → J[L]
51: next J
52: trn H → I; mat IH → N; mat IJ → O; inv N → N; mat NO → K
53: X[I] + r1; K[1] / W → r2; r1 - r2 → r3
54: Y[I] + r4; K[2] / W → r5; r4 - r5 → r6
55: Z[I] + r7; K[3] / W → r8; r7 - r8 → r9
56: if I ≤ C; r32 + r26 → r26; r62 + r27 → r27; r92 + r23 → r23
57: if I > C; r32 + r29 → r29; r62 + r30 → r30; r92 + r31 → r31
58: for Y=1 to 9; wrt 7.2, rY; next Y
59: wtb 7, 10, 13; next I
60: ret
*32508

```

SUBROUTINE MODEL VI

Tape D.L.T.I.K.

track #0

file #7

DESCRIPTION

This subroutine is loaded at the end of the program in file #2. The basic DLT equations are used together with equations (A.57) and (A.58) for the calculation of the calibration coefficients.

```

0: gto "S"
1: "MODEL": "REFINEMENT WITH MODEL #6 (KARARA)" -> AS
2: "Copyright@ 1984 by Iraklis Kollias":
3: for I=1 to 2; 0 -> r24 -> r43 -> r25 -> r26; 10^6 -> r90
4: "r1": beep; fxd 0; 1 -> r24 -> r24; dsp " PLEASE DON'T TOUCH -> ", r24
5: if r24 > 8 and r25 > r90; gto "OK"
6: for J=1 to 22; Q[I,J] + G[J] -> rJ -> Q[I,J]; next J
7: for J=1 to C; J + C -> L
8: W(r9X[J] + r10Y[J] + r11Z[J]) + 1 -> r36
9: W(r1X[J] + r2Y[J] + r3Z[J]) + r4 -> r37
10: W(r5X[J] + r6Y[J] + r7Z[J]) + r8 -> r38
11: M[J,I,1] -> O; M[J,I,2] -> P; M[J,I,3] -> Q; M[J,I,4] -> R; M[J,I,5] -> S
12: O + Q(r12S^2 + r13S^3 + r14S^4 + r15S^5 + r16S^6) + r17(S^2 + 2Q^2) + 2r18QR -> r41
13: P + R(r12S^2 + r13S^3 + r14S^4 + r15S^5 + r16S^6) + r18(S^2 + 2R^2) + 2r17QR -> r42
14: r19O^2 + r20P^2 + r41 -> r39; r21O^2 + r22P^2 + r42 -> r40
15: r36r39 - r37 -> C[L]; r36r40 - r38 -> C[L]
16: WX[J] -> B[J,1] -> B[L,5]; WY[J] -> B[J,2] -> B[L,6]; WZ[J] -> B[J,3] -> B[L,7]
17: 1 -> B[J,4] -> B[L,8]
18: 0 -> B[J,5] -> B[J,6] -> B[J,7] -> B[J,8] -> B[L,1] -> B[L,2] -> B[L,3] -> B[L,4]
19: -WX[J]r39 -> B[J,9]; -WX[J]r40 -> B[L,9]
20: -WY[J]r39 -> B[J,10]; -WY[J]r40 -> B[L,10]
21: -WZ[J]r39 -> B[J,11]; -WZ[J]r40 -> B[L,11]
22: -Qr36S^2 -> B[J,12]; -Rr36S^2 -> B[L,12]
23: -Qr36S^3 -> B[J,13]; -Rr36S^3 -> B[L,13]
24: -Qr36S^4 -> B[J,14]; -Rr36S^4 -> B[L,14]
25: -Qr36S^5 -> B[J,15]; -Rr36S^5 -> B[L,15]
26: -Qr36S^6 -> B[J,16]; -Rr36S^6 -> B[L,16]
27: -r36(S^2 + 2Q^2) -> B[J,17]; -r36(S^2 + 2R^2) -> B[L,18]
28: -2r36QR -> B[J,18] -> B[L,17]
29: -r36O^2 -> B[J,19] -> B[L,21]; -r36P^2 -> B[J,20] -> B[L,22]
30: 0 -> B[J,21] -> B[J,22] -> B[L,19] -> B[L,20]
31: next J
32: if C > 11; trn B -> D; mat DB -> E; mat DC -> F; inv E -> E; mat EF -> G
33: if C = 11; inv B -> B; mat BC -> G
34: r25 -> r90; 0 -> r43 -> r25 -> r26
35: for J=1 to 22; if abs(G[J]) <= (2)10^(-10); r43 + 1 -> r43; next J
36: for J=1 to 22; abs(G[J]) + r25 -> r25; next J
37: fxd 10; prt r25
38: for J=1 to 2C; abs(C[J]) + r26 -> r26; next J
39: if r43 < 22; gto "r1"
40: "OK": for J=1 to 22; Q[I,J] + P[I,J]; 0 -> G[J]; next J
41: fxd 10; prt r26; fxd 0; prt r43, r24; next I
42: qsb "COU"
43: "C.P.RECOVERING": 0 -> r26 -> r27 -> r28 -> r29 -> r30 -> r31 -> r32 -> r33 -> r34 -> r35
44: for I=1 to r99; wrt 7.1, I
45: for J=1 to 2; J + 2 -> L
46: for K=1 to 22; P[J,K] -> rK; next K
47: M[I,J,1] -> O; M[I,J,2] -> P; M[I,J,3] -> Q; M[I,J,4] -> R; M[I,J,5] -> S
48: O + Q(r12S^2 + r13S^3 + r14S^4 + r15S^5 + r16S^6) + r17(S^2 + 2Q^2) + 2r18QR -> r41
49: P + R(r12S^2 + r13S^3 + r14S^4 + r15S^5 + r16S^6) + r18(S^2 + 2R^2) + 2r17QR -> r42
50: r41 + r19O^2 + r20P^2 -> r39; r42 + r21O^2 + r22P^2 -> r40
51: r1 - r9r39 -> H[J,1]; r5 - r9r40 -> H[L,1]
52: r2 - r10r39 -> H[J,2]; r6 - r10r40 -> H[L,2]
53: r3 - r11r39 -> H[J,3]; r7 - r11r40 -> H[L,3]
54: r39 - r4 -> J[J]; r40 - r8 -> J[L]
55: next J
56: trn H -> I; mat IH -> N; mat IJ -> O; inv N -> N; mat NO -> K
57: X[I] -> r1; K[1] / W -> r2; r1 - r2 -> r3
58: Y[I] -> r4; K[2] / W -> r5; r4 - r5 -> r6
59: Z[I] -> r7; K[3] / W -> r8; r7 - r8 -> r9
60: if I <= C; r3^2 + r26 -> r26; r6^2 + r27 -> r27; r9^2 + r28 -> r28
61: if I > C; r3^2 + r29 -> r29; r6^2 + r30 -> r30; r9^2 + r31 -> r31
62: for Y=1 to 9; wrt 7.2, rY; next Y
63: wtb 7, 10, 13; next I
64: ret
*6279

```

DATA DIGI FOR DLT

Tape D.L.T.I.K.

track #0

file #8

DESCRIPTION

With this program, the user digitizes the points of interest from films from both cameras. The maximum # of frames for 20 points in each frame is $N = 87$ frames when the memory capacity of the computer is 64 Kbytes. If more frames are to be analysed the digitizing should be done in groups of points. The latest was the case for the hammer throwing analysis where 222 frames were analyzed for subject 2.

User enters

of analyzed points from each frame

of frames

5 lines of comments with 60 characters each

the names of the points for analysis

track and file to record the U,V coordinates of the points from the film of the first camera

track and file to record the U,V coordinates of the points from the film of the second camera

marks the files for the coordinates (the # of bites is printed)

The computer prints the comments, the names of the points and the files where the data are recorded.

The film from the first camera is to be digitized first. The film from the second camera is to be digitized second.

```

0: % "*****D.L.T.I.K., TRK 0, FILE 8*****"
1: % "DATA DIGI FOR DLT"
2: "Copyright© 1984 by Iraklis Kollias":
3: ent "# OF ANALYSED POINTS IN each FR.",G
4: ent "# OF FRAMES [20points max#=87]",N
5: G→r0;dim A[N,G,2],D[N,G,2],A$[G,30],Q$[20],D$[5,60]
6: for I=1 to 5;ent "I.D. and COMMENTS",B$[I];next I
7: fmt 2,20x,c;for I=1 to 5;wrt 7.2,B$[I];next I
8: for I=1 to G;prt I;ent "NAME OF POINT",A$[I];next I
9: fmt 2,20x,f3.0,2x,c;for I=1 to G;wrt 7.2,A$[I];next I
10: for I=1 to 2
11: for J=1 to N
12: for K=1 to G
13: dsp "DIGITIZE POINT",A$[K];red 4,U,V;beep
14: if I=1;U→A[J,K,1];V→A[J,K,2]
15: if I=2;U→D[J,K,1];V→D[J,K,2]
16: next K
17: ent "DIGI ERROR ?? [Yes or ...]",Q$
18: if cap(Q$[1,1])="Y";dsp "DO IT AGAIN";wait 1500;gto -6
19: dsp "NEXT FRAME IS ",J+1;wait 1500;next J
20: for K=1 to 100;dsp "LOAD THE SECOND FILM";wait 555;next K
21: next I
22: dsp "INSERT U,V TAPE; 'CONTINUE'";sto
23: prt "EACH FILE HAS",N*G*16,"BITES";spc 2
24: dsp "MARK THE FILES then 'CONTINUE'";stp
25: ent "trk FOR U,V from 1st CAMERA",r0;ent "FILE",r1
26: trk r0;rcf r1,A[*]
27: ent "trk for U,V form 2st CAMERA",r2;ent "FILE",r3
28: trk r2;rcf r3,D[*]
29: fmt 2,20x,"U,V FROM FIRST CAMERA IN TRACK #",f3.0,"FILE #",f3.0
30: wrt 7.2,r0,r1
31: fmt 2,20x,"U,V FROM SECOND CAMERA IN TRACK#",f3.0,"FILE #",f3.0
32: wrt 7.2,r2,r3
33: wtb 7,12;dsp "DONE";end
*29408

```

X,Y,Z,RECOVERY WITH DLT (KARARA's MODELS)

Tape D.L.T.I.K.

track #0

file #9

DESCRIPTION

This program is for the recovery of the coordinates of the points for analysis. The basic DLT equations with the appropriate model for image refinement are used for this purpose. User enters
model to be used (2,3,4,5,6) # of analyzed points in each frame

of frames

track and file where the U,V coordinates from the first camera

track and file where the U,V coordinates from the second camera

track and file where the X,Y,Z coordinates of each point to be stored. *Each point will be recorded in one file, that is in the first file will be point #1 (ie right eye) in the second file will be point #2 (ie left ear)..... in the last file will be point #last (i.e. coca cola label of the left shoe)*

The computer

loads the coefficients of the DLT

loads the subroutine with the appropriate model

loads the U,V from both cameras

calculates the X,Y,Z coordinates of each point

marks the files for storing the X,Y,Z coordinates

records the X,Y,Z coordinates in files

The X,Y,Z coordinates of each point are recorded in its file with an array of $G[3,N]$ where $N = \#$ of frames and $G[1,N] = X$, $G[2,N] = Y$ and $G[3,N] = Z$.

```

0: % "*****D.L.T.I.K., TRK 0, FILE 9*****"
1: % "X,Y,Z,RECOVERY WITH DLT (KARARA's MODELS)"
2: "Copyright@ 1984 by Iraklis Kollias":
3: ent "MODEL TO BE USED",M;12→C
4: % "Loads the coefficients"
5: if M=3;14→C
6: if M=4;16→C
7: if M=5;18→C
8: if M=6;22→C
9: dim P[2,C],L[2,11],S[4]
10: trk 1;fdf 4;ldf 4,L[*],S[*]
11: trk 1;fdf 3+M;ldf 3+M,P[*]
12: dim H[4,3],I[3,4],N[3,3],J[4],K[3],O[3],M[2,5]
13: % "Loads the MODEL"
14: trk 0;fdf M+7;ldf M+7,39
15: "PP":dsp "INSERT DATA TAPE; 'CONTINUE'";stp
16: % "Loads the data"
17: ent "# OF ANALYSED POINTS IN each FR.",G
18: ent "# OF FRAMES [20points max#=37F]",N
19: G→r0;dim G[3,N],A[N,G,2],D[N,G,2]
20: ent "trk with U,V from 1st CAMERA",r0;ent "FILE",r1;trk r0;ldf r1,A[*]
21: ent "trk with U,V from 2st CAMERA",r0;ent "FILE",r1;trk r0;ldf r1,D[*]
22: ent "TRK# TO RECORD Xi,Yi,Zi",r51
23: ent "FILE # TO BEGIN WITH",r52;r52-1→r52
24: prt "STARTING FILE=",r52+1;spc ;prt "# OF FILE=",G
25: prt "EACH FILE HAS",N*24,"BITES";spc 2
26: dsp "INSERT X,Y,Z, TAPE; 'CONTINUE'";stp
27: for A=1 to r0;for I=1 to N;dsp A,I
28: A[I,A,1]→M[1,1];A[I,A,2]→M[1,2]
29: D[I,A,1]→M[2,1];D[I,A,2]→M[2,2]
30: M[1,1]-S[1]→M[1,3];M[1,2]-S[2]→M[1,4]
31: M[2,1]-S[3]→M[2,3];M[2,2]-S[4]→M[2,4]
32: for K=1 to 2;√(M[K,3]^2+M[K,4]^2)→M[K,5];next K
33: gso "RCV"
34: next I
35: if A+r52=0;rew;trk r51;mrk 1,N*24;rcf A+r52,G[*]
36: if A+r52#0;trk r51;fdf A+r52;mrk 1,N*24;rcf A+r52,G[*]
37: next A
38: dsp "DONE";end
*27362

```

SUBROUTINE MODEL II

Tape D.L.T.I.K.

track #0

file #10

DESCRIPTION

This subroutine is loaded at the end of the program in file #9. The solution is based on equation (A.79). The basic DLT equations are used together with equations (A.49) and (A.50) for the calculation of the 3-D coordinates.

```

0: % "MODEL #2"
1: gto "PP"
2: "RCV":
3: for J=1 to 2;J+2→L
4: for K=1 to C;P[J,K]→rK;next K
5: M[J,1]→O;M[J,2]→P;M[J,3]→Q;M[J,4]→R;M[J,5]→S
6: O+r12RS^2→r20;P+r12RS^2→r21
7: r1-r9r20→H[J,1];r5-r9r21→H[L,1]
8: r2-r10r20→H[J,2];r6-r10r21→H[L,2]
9: r3-r11r20→H[J,3];r7-r11r21→H[L,3]
10: r20-r4→J[J];r21-r8→J[L]
11: next J
12: trn H→I;mat IH→N;mat IJ→O;inv N→N;mat NO→K
13: for T=1 to 3;K[T]→G[T,I];next T
14: ret
*26595

```

 SUBROUTINE MODEL III

Tape D.L.T.I.K.

track #0

file #11

DESCRIPTION

This subroutine is loaded at the end of the program in file #9. The solution is based on equation (A.79). The basic DLT equations are used together with equations (A.51) and (A.52) for the calculation of the 3-D coordinates.

```

0: % "MODEL #3"
1: gto "PP"
2: "RCV":
3: for J=1 to 2;J+2→L
4: for K=1 to C;P[J,K]→rK;next K
5: M[J,1]→O;M[J,2]→P;M[J,3]→Q;M[J,4]→R;M[J,5]→S
6: O+Q(r12S^2+r13S^4+r14S^6)→r20;P+R(r12S^2+r13S^4+r14S^6)→r21
7: r1-r9r20→H[J,1];r5-r9r21→H[L,1]
8: r2-r10r20→H[J,2];r6-r10r21→H[L,2]
9: r3-r11r20→H[J,3];r7-r11r21→H[L,3]
10: r20-r4→J[J];r21-r8→J[L]
11: next J
12: trn H→I;mat IH→N;mat IJ→O;inv N→N;mat NO→K
13: for T=1 to 3;K[T]→G[T,I];next T
14: ret
*15131
  
```

SUBROUTINE MODEL IV

Tape D.L.T.I.K.

track #0

file #12

DESCRIPTION

This subroutine is loaded at the end of the program in file #9. The solution is based on equation (A.79). The basic DLT equations are used together with equations (A.53) and (A.54) for the calculation of the 3-D coordinates.

```

0: % "MODEL #4"
1: gto "PP"
2: "RCV":
3: for J=1 to 2;J+2>L
4: for K=1 to C;P[J,K]>rK;next K
5: M[J,1]>O;M[J,2]>P;M[J,3]>Q;M[J,4]>R;M[J,5]>S
6: O+Q(r12S^2+r13S^4+r14S^6)+r15(S^2+2Q^2)+2r16QR>r20
7: P+R(r12S^2+r13S^4+r14S^6)+r16(S^2+2P^2)+2r15QR>r21
8: r1-r9r20>H[J,1];r5-r9r21>H[L,1]
9: r2-r10r20>H[J,2];r6-r10r21>H[L,2]
10: r3-r11r20>H[J,3];r7-r11r21>H[L,3]
11: r20-r4>J[J];r21-r8>J[L];next J
12: trn H>I;mat IH>N;mat IJ>O;inv N>N;mat NO>K
13: for T=1 to 3;K[T]>G[T,I];next T
14: ret
*782

```

SUBROUTINE MODEL V

Tape D.L.T.I.K.

track #0

file #13

DESCRIPTION

This subroutine is loaded at the end of the program in file #9. The solution is based on equation (A.79). The basic DLT equations are used together with equations (A.55) and (A.56) for the calculation of the 3-D coordinates.

```

0: % "MODEL #5"
1: gto "PP"
2: "RCV":
3: for J=1 to 2;J+2→L
4: for K=1 to C;P[J,K]→rK;next K
5: M[J,1]→O;M[J,2]→P;M[J,3]→Q;M[J,4]→R;M[J,5]→S
6: O+Q(r12S^2+r13S^3+r14S^4+r15S^5+r16S^6)+r17(S^2+2Q^2)+2r18QR→r20
7: P+R(r12S^2+r13S^3+r14S^4+r15S^5+r16S^6)+r18(S^2+2R^2)+2r17QR→r21
8: r1-r9r20→H[J,1];r5-r9r21→H[L,1]
9: r2-r10r20→H[J,2];r6-r10r21→H[L,2]
10: r3-r11r20→H[J,3];r7-r11r21→H[L,3]
11: r20-r4→J[J];r21-r8→J[L]
12: next J
13: trn H→I;mat IH→N;mat IJ→O;inv N→N;mat NO→K
14: for T=1 to 3;K[T]→G[T,I];next T
15: ret
*1931

```

 SUBROUTINE MODEL VI

Tape D.L.T.I.K.

track #0

file #14

DESCRIPTION

This subroutine is loaded at the end of the program in file #9. The solution is based on equation (A.79). The basic DLT equations are used together with equations (A.57) and (A.58) for the calculation of the 3-D coordinates.

```

0: % "MODEL #6"
1: gto "PP"
2: "RCV":
3: for J=1 to 2;J+2→L
4: for K=1 to C;P[J,K]→rK;next K
5: A[J,1]→O;M[J,2]→P;M[J,3]→Q;M[J,4]→R;M[J,5]→S
6: O+Q(r12S^2+r13S^3+r14S^4+r15S^5+r16S^6)+r17(S^2+2Q^2)+2r18QR→r41
7: P+R(r12S^2+r13S^3+r14S^4+r15S^5+r16S^6)+r18(S^2+2R^2)+2r17QR→r42
8: r41+r19O^2+r20P^2→r39;r42+r21O^2+r22P^2→r40
9: r1-r9r39→H[J,1];r5-r9r40→H[L,1]
10: r2-r10r39→H[J,2];r6-r10r40→H[L,2]
11: r3-r11r39→H[J,3];r7-r11r40→H[L,3]
12: r39-r4→J[J];r40-r8→J[L]
13: next J
14: trn H→I;mat IH→N;mat IJ→O;inv N→N;mat NO→K
15: for T=1 to 3;K[T]→S[T,I];next T
16: ret
*22729

```


APPENDIX B

Moments and Products of Inertia Angular momentum and Instantaneous Angular Velocity

This appendix deals with the calculation of the moments of inertia of the system athlete plus hammer about a space-fixed orthogonal system of axes with origin at the center of mass of the system.

Moments and Products of Inertia with respect to CMs

Figure B.1 is a representation of a i th body segment in space. Let O be the center of mass of the system (CMs) and let C be the center of mass of the i th segment. Let X, Y, Z be right handed orthogonal system of axes fixed in space and having origin at the point O . They are translating as the center of mass of the system translates. Axes X', Y', Z' are parallel axes to the X, Y, Z with origin at point C_i . Axes Xc_i, Yc_i, Zc_i , are the principal axes of the i th segment, having origin at the point C .

The sum of the moments of products of inertia of the 13 segments about the point O are given by the following equations:

$$I_x = \sum_{i=1}^{13} [I'_{x_i} + m_i (C_{y_i}^2 + C_{z_i}^2)] \quad (B.1)$$

$$I_y = \sum_{i=1}^{13} [I'_{y_i} + m_i (C_{x_i}^2 + C_{z_i}^2)] \quad (B.2)$$

$$I_z = \sum_{i=1}^{13} [I'_{z_i} + m_i (C_{x_i}^2 + C_{y_i}^2)] \quad (B.3)$$

$$I_{xy} = \sum_{i=1}^{13} [I'_{xy_i} + m_i \cdot C_{x_i} \cdot C_{y_i}] \quad (B.4)$$

$$I_{xz} = \sum_{i=1}^{13} [I'_{xzi} + m_i \cdot C_{xi} \cdot C_{zi}] \quad (B.5)$$

$$I_{yz} = \sum_{i=1}^{13} [I'_{yzi} + m_i \cdot C_{yi} \cdot C_{zi}] \quad (B.6)$$

where: I_x, I_y, I_z are the moments of inertia of the system about the axes X, Y, Z

m_i is the mass of the i th segment.

C_{xi}, C_{yi}, C_{zi} are the coordinates of the center of mass of the i th segment relative to the center of mass of the system.

$I'_{xi}, I'_{yi}, I'_{zi}, I'_{xyi}, I'_{xzi}, I'_{yzi}$ are the moments and products of inertia of the i th segment about the axes X', Y', Z' .

Moments and Products of Inertia of segments about their CM

The moments and the products of inertia of the i th segment with respect to the axes $X', Y',$ and Z' passing from its CM, are calculated using the following equations:

$$I'_x = I''_{xi} \cdot \alpha_{11}^2 + I''_{yi} \cdot \alpha_{21}^2 + I''_{zi} \cdot \alpha_{31}^2 \quad (B.7)$$

$$I'_y = I''_{xi} \cdot \alpha_{12}^2 + I''_{yi} \cdot \alpha_{22}^2 + I''_{zi} \cdot \alpha_{32}^2 \quad (B.8)$$

$$I'_z = I''_{xi} \cdot \alpha_{13}^2 + I''_{yi} \cdot \alpha_{23}^2 + I''_{zi} \cdot \alpha_{33}^2 \quad (B.9)$$

$$I'_{xy} = -(\alpha_{11} \cdot \alpha_{12} \cdot I''_{xi} + \alpha_{21} \cdot \alpha_{22} \cdot I''_{yi} + \alpha_{31} \cdot \alpha_{32} \cdot I''_{zi}) \quad (B.10)$$

$$I'_{xz} = -(\alpha_{11} \cdot \alpha_{13} \cdot I''_{xi} + \alpha_{21} \cdot \alpha_{23} \cdot I''_{yi} + \alpha_{31} \cdot \alpha_{33} \cdot I''_{zi}) \quad (B.11)$$

$$I'_{yz} = -(\alpha_{12} \cdot \alpha_{13} \cdot I''_{xi} + \alpha_{22} \cdot \alpha_{23} \cdot I''_{yi} + \alpha_{32} \cdot \alpha_{33} \cdot I''_{zi}) \quad (B.12)$$

where : $I''_{xi}, I''_{yi}, I''_{zi}$ are the principal moments of inertia of the i th segment. These data were taken from Whitsett's anthropometric data, (Whitsett, 1963), and are presented in table 8 in the methodology chapter. The principal moments were normalized according to the height and mass of each athlete.

$\alpha_{11}, \alpha_{12}, \alpha_{13}$ are the direction cosines of the Xc ($i = 1$), Yc ($i = 2$) and Zc ($i = 3$) axis relative

to the X', Y', Z' system of axes.

Calculation of Direction Cosines of the Principal Axes

The following is a description of the technique used to calculate the direction cosines of the X_c, Y_c and Z_c axis.

The vectors representing the axes X_c, Y_c, Z_c are:

$$\underline{X_c} = \alpha_{11}\underline{i} + \alpha_{12}\underline{j} + \alpha_{13}\underline{k} \quad (B.13)$$

$$\underline{Y_c} = \alpha_{21}\underline{i} + \alpha_{22}\underline{j} + \alpha_{23}\underline{k} \quad (B.14)$$

$$\underline{Z_c} = \alpha_{31}\underline{i} + \alpha_{32}\underline{j} + \alpha_{33}\underline{k} \quad (B.15)$$

where: $\underline{i}, \underline{j}, \underline{k}$ are the unit vectors of the axes X', Y', Z' .

Direction Cosines of Z_c

The direction cosines of $\underline{Z_c}$ are given by the following equations:

$$\alpha_{31} = \frac{p_1}{(p_1^2 + p_2^2 + p_3^2)^{1/2}} \quad (B.16)$$

$$\alpha_{32} = \frac{p_2}{(p_1^2 + p_2^2 + p_3^2)^{1/2}} \quad (B.17)$$

$$\alpha_{33} = \frac{p_3}{(p_1^2 + p_2^2 + p_3^2)^{1/2}} \quad (B.18)$$

where: p_1, p_2, p_3 are the coordinates of the proximal end point P of the segment measured with respect to the origin C.

Direction Cosines of X_c

Referring to figure B.1, line X_c is the intersection of the planes (G) and (E). Plane (E) is normal to the line segment Z_c at point C. At the j th frame, the equation of the plane (E) is:

$$\alpha_{31}X + \alpha_{32}Y + \alpha_{33}Z = 0 \quad (B.19)$$

where: α_{31} , α_{32} , α_{33} are the direction cosines of Z_c and have been calculated previously using Equations (B.16), (B.17) and (B.18).

Plane (G) is defined by the points $P(p_1, p_2, p_3)$, which is the proximal end point of the i th segment in the j th frame; the point $C(c_1, c_2, c_3)$, which is the center of mass of the segment in the j th frame, ($c_1 = c_2 = c_3 = 0$); and $Q(q_1, q_2, q_3)$ which was the center of mass of the segment in the $(j+1)$ th frame measured from the point C at the j th frame. For the trunk segment point Q is defined by the right hip point at the same frame and its coordinates are measured from the center of mass of the trunk at the same frame.

The equation of plane (G) is:

$$Ax + By + Cz = 0 \quad (B.20)$$

The coefficients of the equations of the plane (G) can be found from the following equations:

$$A p_1 + B p_2 + C p_3 = 0 \quad (B.21)$$

$$A q_1 + B q_2 + C q_3 = 0 \quad (\text{B.22})$$

By setting $A = 1$ and rewritting equations (B.21) and (B.22) in a matrix form, we obtain:

$$\begin{vmatrix} p_2 & p_3 \\ q_2 & q_3 \end{vmatrix} \begin{vmatrix} B \\ C \end{vmatrix} = \begin{vmatrix} -p_1 \\ -q_1 \end{vmatrix} \quad (\text{B.23})$$

This system can be solved numerically for B and C . Since line X_c is the intersection of planes (E) and (G), it can be represented analytically by equations (B.19) and (B.20).

Assume that a point $R(r_1, r_2, r_3)$ is a point of the line X_c , then if $r_1 = q_1$, the coordinates r_2 and r_3 are given by the following equation:

$$\begin{vmatrix} \alpha_{32} & \alpha_{33} \\ B & C \end{vmatrix} \begin{vmatrix} r_2 \\ r_3 \end{vmatrix} = \begin{vmatrix} -\alpha_{31} \\ -A \end{vmatrix} \quad (\text{B.24})$$

Solving (B.24) for r_2 and r_3 the direction cosines of X_c are obtained as following:

$$\alpha_{11} = \frac{r_1}{(r_1^2 + r_2^2 + r_3^2)^{1/2}} \quad (\text{B.25})$$

$$\alpha_{12} = \frac{r_2}{(r_1^2 + r_2^2 + r_3^2)^{1/2}} \quad (\text{B.26})$$

$$\alpha_{13} = \frac{r_3}{(r_1^2 + r_2^2 + r_3^2)^{1/2}} \quad (\text{B.27})$$

Direction Cosines of \underline{Y}_c

The direction cosines of \underline{Y}_c are calculated by utilizing the vector product of the vectors \underline{Z}_c and \underline{X}_c because

$$\underline{Z}_c \times \underline{X}_c = \underline{Y}_c \quad (\text{B.28})$$

Using equations (B.13) and (B.15), the vector product of \underline{Z}_c and \underline{X}_c can be written in the following determinant formulation:

$$\underline{Z}_c \times \underline{X}_c = \begin{vmatrix} \underline{i} & \underline{j} & \underline{k} \\ \alpha_{31} & \alpha_{32} & \alpha_{33} \\ \alpha_{11} & \alpha_{12} & \alpha_{13} \end{vmatrix} \quad (\text{B.29})$$

or

$$\begin{aligned} \underline{Y}_c = & (\alpha_{32} \cdot \alpha_{13} - \alpha_{33} \cdot \alpha_{12}) \underline{i} \\ & - (\alpha_{31} \cdot \alpha_{13} - \alpha_{33} \cdot \alpha_{11}) \underline{j} \\ & + (\alpha_{31} \cdot \alpha_{12} - \alpha_{32} \cdot \alpha_{11}) \underline{k} \end{aligned} \quad (\text{B.30})$$

From equation (B.14) and (B.30) we obtain the following:

$$\alpha_{21} = \alpha_{32} \cdot \alpha_{13} - \alpha_{33} \cdot \alpha_{12} \quad (\text{B.31})$$

$$\alpha_{22} = \alpha_{33} \cdot \alpha_{11} - \alpha_{31} \cdot \alpha_{13} \quad (\text{B.32})$$

$$\alpha_{23} = \alpha_{31} \cdot \alpha_{12} - \alpha_{32} \cdot \alpha_{11} \quad (\text{B.33})$$

The above are the components of the vector representing the \underline{Y}_c axis. The direction cosines \underline{Y}_c are calculated by using these components.

Angular Momentum of the System

The angular momentum of the system athlete + hammer about its center of mass was calculated with the following equations:

$$\underline{L}_x = \sum_{i=1}^{13} [\underline{L}'_{xi} + \underline{L}''_{xi}] \quad (\text{B.34})$$

$$\underline{L}_y = \sum_{i=1}^{13} [\underline{L}'_{yi} + \underline{L}''_{yi}] \quad (\text{B.35})$$

$$\underline{L}_z = \sum_{i=1}^{13} [\underline{L}'_{zi} + \underline{L}''_{zi}] \quad (\text{B.36})$$

where: $\underline{L}_x, \underline{L}_y, \underline{L}_z$ are vectors representing the angular momentum of the system about its center of mass;
 $\underline{L}'_{xi}, \underline{L}'_{yi}, \underline{L}'_{zi}$ are vectors representing the angular momentum of the i th segment about the center of mass of the system, considering the segment as a point mass;
 $\underline{L}''_{xi}, \underline{L}''_{yi}, \underline{L}''_{zi}$ are the vectors representing the angular momentum of the i th segment about its center of mass.

$\underline{L}'_{xi}, \underline{L}'_{yi}, \underline{L}'_{zi}$ are calculated as follows. Let $\underline{r}_1, \underline{r}_2$ be the position vectors of the center of mass of the segment with respect to the center of mass of the system in two successive frames (j th and $(j+1)$ th frame) The components of the two vectors are the coordinates of the points C and C' (figure B.1) measured from the center of mass of the system at the $(j+1)$ th frame. A vector in the direction of the

angular momentum is given by the following equation:

$$\underline{N} = \underline{r}_1 \times \underline{r}_2 \quad (\text{B.37})$$

Let C_x, C_y, C_z and C_x', C_y', C_z' be the components of the two vectors, then

$$\underline{N} = a_1 \underline{i} + a_2 \underline{j} + a_3 \underline{k} \quad (\text{B.38})$$

$$\begin{aligned} \text{where: } a_1 &= C_y \cdot C_z' - C_z \cdot C_y' \\ a_2 &= C_z \cdot C_x' - C_x \cdot C_z' \\ a_3 &= C_x \cdot C_y' - C_y \cdot C_x' \end{aligned}$$

The magnitude of this vector is

$$N = (a_1^2 + a_2^2 + a_3^2)^{1/2} \quad (\text{B.39})$$

The direction cosines of the vector are $\beta_1, \beta_2, \beta_3$ where $\beta_1 = a_1 / N, \dots$ etc. The magnitude of the angular momentum vector is:

$$L = m \cdot N / \Delta t \quad (\text{B.40})$$

where m is the mass of the segment and Δt the time interval between the two frames.

Finally the angular momentum of the segment about the center of mass of the system is:

$$L_x' = L \cdot \beta_1 \quad (\text{B.41})$$

$$L_y' = L \cdot \beta_2 \quad (\text{B.42})$$

$$L_z' = L \cdot \beta_3 \quad (\text{B.43})$$

The magnitudes of the vectors \underline{L}''_x , \underline{L}''_y , \underline{L}''_z are calculated due to the following equations:

$$L''_{xi} = I'_{xi} \cdot \omega_{xi} - I'_{xyi} \cdot \omega_{yi} - I'_{xzi} \cdot \omega_{zi} \quad (\text{B.44})$$

$$L''_{yi} = I'_{yi} \cdot \omega_{yi} - I'_{xyi} \cdot \omega_{xi} - I'_{yzi} \cdot \omega_{zi} \quad (\text{B.45})$$

$$L''_{zi} = I'_{zi} \cdot \omega_{zi} - I'_{yzi} \cdot \omega_{yi} - I'_{xzi} \cdot \omega_{xi} \quad (\text{B.46})$$

where: I'_{xi} , I'_{yi} , I'_{zi} and I'_{xyi} , I'_{xzi} , I'_{yzi} are the moments and products of inertia of the i th segment about the center of mass of the segment; ω_{xi} , ω_{yi} , ω_{zi} are the angular velocities of the segment about a system of axes with origin at the center of mass of the segment and parallel to the space fixed axes.

I'_{xi} , I'_{yi} , I'_{zi} , I'_{xyi} , I'_{xzi} , I'_{yzi} are calculated as it is shown in equations (B.7) to (B.12).

Angular Velocity of the Segmental Principal Axes

Referring to figure B.1, the i th segment moves from the j th frame and from its position $C(X_c, Y_c, Z_c)$ to the $(j+1)$ th frame and to the position $C'(X_c', Y_c', Z_c')$. The direction cosines of the axes X_c, Y_c, Z_c and the axes X_c', Y_c', Z_c' are calculated as in part 3 of this appendix. Let a_{11} , a_{12} , a_{13} be the direction cosines of the X_c axis, a_{21} , a_{22} , a_{23} the direction cosines of the Y_c axis, a_{31} , a_{32} , a_{33} the

direction cosines of the Z_c axis, $\beta_{11}, \beta_{12}, \beta_{13}$ the direction cosine of $X_{c'}$, $\beta_{21}, \beta_{22}, \beta_{23}$ the direction cosines of the $Y_{c'}$ axis and $\beta_{31}, \beta_{32}, \beta_{33}$ the direction cosines of the $Z_{c'}$ axis. The angles θ_1 of the X_c axis with the $X_{c'}$ axis, θ_2 of the Y_c axis with the $Y_{c'}$ axis and θ_3 of the Z_c axis with the $Z_{c'}$ axis can be found by using the dot product of the vectors representing the axes and they are as follows:

$$\theta_1 = \arccos(a_{11}\beta_{11} + a_{12}\beta_{12} + a_{13}\beta_{13}) \quad (B.47)$$

$$\theta_2 = \arccos(a_{21}\beta_{21} + a_{22}\beta_{22} + a_{23}\beta_{23}) \quad (B.48)$$

$$\theta_3 = \arccos(a_{31}\beta_{31} + a_{32}\beta_{32} + a_{33}\beta_{33}) \quad (B.49)$$

The magnitudes of the angular velocities of the axes are:

$$\omega_1 = \theta_1/\Delta t \quad (B.50)$$

$$\omega_2 = \theta_2/\Delta t \quad (B.51)$$

$$\omega_3 = \theta_3/\Delta t \quad (B.52)$$

where: Δt is the time between the J th and $(J+1)$ th frame.

The above angular velocities can be represented by three vectors each of them normal to the planes formed by the axes X_c and $X_{c'}$, Y_c and $Y_{c'}$, Z_c and $Z_{c'}$ respectively, after the they have been translated to a common origin. Let \underline{w}_1 , \underline{w}_2 and \underline{w}_3 be the three vectors, then

$$\underline{w}_1 = \underline{Xc} \times \underline{Xc}' \quad (\text{B.53})$$

$$\underline{w}_2 = \underline{Yc} \times \underline{Yc}' \quad (\text{B.54})$$

$$\underline{w}_3 = \underline{Zc} \times \underline{Zc}' \quad (\text{B.55})$$

(Note: \underline{w}_1 , \underline{w}_2 , \underline{w}_3 are not necessarily orthogonal vectors.)

By using the directions of the axes and the equations (B.53) to (B.55) we obtain:

$$\begin{aligned} \underline{w}_1 = & (a_{12} \cdot \beta_{13} - a_{13} \cdot \beta_{12}) \underline{i} \\ & - (a_{11} \cdot \beta_{13} - a_{13} \cdot \beta_{11}) \underline{j} \\ & + (a_{11} \cdot \beta_{12} - a_{12} \cdot \beta_{11}) \underline{k} \end{aligned} \quad (\text{B.56})$$

$$\begin{aligned} \underline{w}_2 = & (a_{22} \cdot \beta_{23} - a_{23} \cdot \beta_{22}) \underline{i} \\ & - (a_{21} \cdot \beta_{23} - a_{23} \cdot \beta_{21}) \underline{j} \\ & + (a_{21} \cdot \beta_{22} - a_{22} \cdot \beta_{21}) \underline{k} \end{aligned} \quad (\text{B.57})$$

$$\begin{aligned} \underline{w}_3 = & (a_{32} \cdot \beta_{33} - a_{33} \cdot \beta_{32}) \underline{i} \\ & - (a_{31} \cdot \beta_{33} - a_{33} \cdot \beta_{31}) \underline{j} \\ & + (a_{11} \cdot \beta_{12} - a_{12} \cdot \beta_{11}) \underline{k} \end{aligned} \quad (\text{B.58})$$

Let γ_{11} , γ_{12} , γ_{13} represent the components of \underline{w}_1 , γ_{21} , γ_{22} , γ_{23} represent the components of \underline{w}_2 and γ_{31} , γ_{32} , γ_{33} represent the components of \underline{w}_3 . The direction cosines of these vectors will be:

$$\delta_{11} = \gamma_{11} / (\gamma_{11}^2 + \gamma_{12}^2 + \gamma_{13}^2)^{1/2}$$

similar for δ_{12} , δ_{13} , δ_{21} , ..., etc.

The total angular velocity vector of the segment about its center of mass is:

$$\underline{w} = \underline{w}_1 + \underline{w}_2 + \underline{w}_3 \quad (\text{B.59})$$

The components of the velocity vector in the X, Y and Z axis are:

$$\omega_x = \omega_1 \cdot \delta_{11} + \omega_2 \cdot \delta_{21} + \omega_3 \cdot \delta_{31} \quad (\text{B.60})$$

$$\omega_y = \omega_1 \cdot \delta_{12} + \omega_2 \cdot \delta_{22} + \omega_3 \cdot \delta_{32} \quad (\text{B.61})$$

$$\omega_z = \omega_1 \cdot \delta_{13} + \omega_2 \cdot \delta_{23} + \omega_3 \cdot \delta_{33} \quad (\text{B.62})$$

Instantaneous Angular Velocity of the System

After the moments of inertia, the products of inertia and the angular momentum of the system have been calculated, the angular velocity of the system about its center of mass, can be calculated by solving the following system of equations for Ω_x , Ω_y and Ω_z .

$$L_x = I_x \cdot \Omega_x - I_{xy} \cdot \Omega_y - I_{xz} \cdot \Omega_z \quad (\text{B.63})$$

$$L_y = I_y \cdot \Omega_y - I_{xy} \cdot \Omega_x - I_{yz} \cdot \Omega_z \quad (\text{B.64})$$

$$L_z = I_z \cdot \Omega_z - I_{yz} \cdot \Omega_y - I_{xz} \cdot \Omega_x \quad (\text{B.65})$$

where: L_x , L_y , L_z are the angular momentum of the system;
 I_x , I_y , I_z and I_{xy} , I_{xz} , I_{yz} are the moments and products of inertia of the system about its center of mass;
 Ω_x , Ω_y , Ω_z the requested angular velocities.

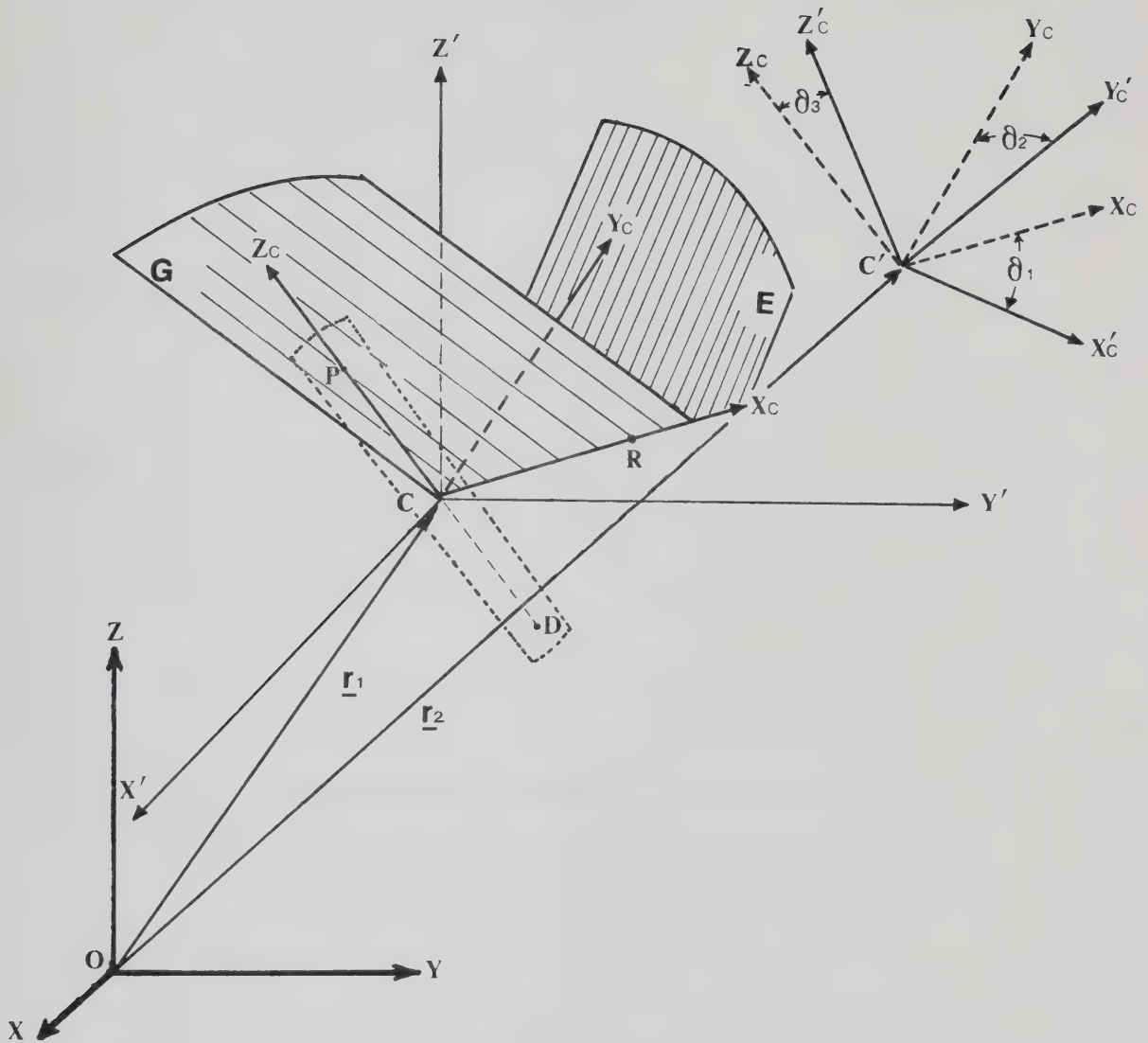


Figure B.1 Representation of the i th segment in space at the j th and $(j+1)$ th frame.

$O(X, Y, Z)$ = Orthogonal system of axes parallel to the space fixed system of axes and having origin at the center of mass of the system;

$C(X', Y', Z')$ = Orthogonal system of axes parallel to $O(X, Y, Z)$ with origin at the center of mass of the segment (point C) at the j th frame;

$C(X_c, Y_c, Z_c)$ = System of the principal axes of the segment at the j th frame;

$C'(X_c', Y_c', Z_c')$ = System of the principal axes of the segment at the $(j+1)$ th frame;

P and D = The proximal and distal point of the segment.

APPENDIX C

Radius and Center of Curvature

This appendix deals with the derivation of the equations for the calculation of the radius and center of curvature of the orbit of a point P which moves along a space curve (Γ), as in Figure C.1. The method is based on vector analysis (Spiegel, 1959). The kinematics of the point are calculated numerically from the time-displacement data of the point.

Radius of Curvature.

Let P be a point moving along curve (Γ). The position vector of P with respect to the origin O is:

$$\underline{r} = x\underline{i} + y\underline{j} + z\underline{k} \quad (\text{C.1})$$

where: x, y, z are the coordinates of P;

$\underline{i}, \underline{j}, \underline{k}$ are the rectangular unit vectors of the reference frame.

A tangent vector to (Γ) at point P is:

$$\frac{d\underline{r}}{dt} = x'\underline{i} + y'\underline{j} + z'\underline{k} \quad (\text{C.2})$$

where: x', y', z' denote the derivatives of x, y, z with respect to time t .

The arc length s is related to \underline{r} by the following equation:

$$\left| \frac{d\underline{r}}{dt} \right| = \frac{ds}{dt} = (x'^2 + y'^2 + z'^2)^{1/2} \quad (\text{C.3})$$

A unit vector tangent to (Γ) is:

$$\underline{T} = \frac{d\underline{r}/dt}{|d\underline{r}/dt|} = \frac{x'\underline{i} + y'\underline{j} + z'\underline{k}}{(x'^2 + y'^2 + z'^2)^{1/2}} \quad (C.4)$$

The first of the Frenet-Serret formulas is:

$$\frac{d\underline{T}}{ds} = \kappa \underline{N} \quad (C.5)$$

where: $d\underline{T}/ds$ is the derivative of \underline{T} with respect to s ;
 κ is the curvature;
 \underline{N} is the unit vector in the direction of $d\underline{T}/ds$. It is normal to the curve (Γ) at point P .

Since \underline{N} is a unit vector,

$$\kappa = \left| \frac{d\underline{T}}{ds} \right| \quad (C.6)$$

Now, let us calculate $d\underline{T}/ds$. From vector calculus, we obtain:

$$\frac{d\underline{T}}{ds} = \frac{d\underline{T}/dt}{ds/dt} \quad (C.7)$$

Using equation (C.4) to calculate $d\underline{T}/dt$, we obtain:

$$\frac{d\underline{T}}{dt} = \frac{d}{dt} \left[\frac{x'}{w} \right] \underline{i} + \frac{d}{dt} \left[\frac{y'}{w} \right] \underline{j} + \frac{d}{dt} \left[\frac{z'}{w} \right] \underline{k} \quad (C.8)$$

$$\text{Where: } w = (x'^2 + y'^2 + z'^2)^{1/2} \quad (C.9)$$

However,

$$\frac{d}{dt} \left[\frac{x'}{w} \right] = \frac{x''w - x'(x'x'' + y'y'' + z'z'')/w}{w^2} \quad (C.10)$$

or:

$$\frac{d}{dt} \left[\frac{x'}{w} \right] = \frac{x''(x'^2 + y'^2 + z'^2) - x'(x'x'' + y'y'' + z'z'')}{(x'^2 + y'^2 + z'^2)^{3/2}} \quad (C.11)$$

In the same way:

$$\frac{d}{dt} \left[\frac{y'}{w} \right] = \frac{y''(x'^2 + y'^2 + z'^2) - y'(x'x'' + y'y'' + z'z'')}{(x'^2 + y'^2 + z'^2)^{3/2}} \quad (C.12)$$

$$\frac{d}{dt} \left[\frac{z'}{w} \right] = \frac{z''(x'^2 + y'^2 + z'^2) - z'(x'x'' + y'y'' + z'z'')}{(x'^2 + y'^2 + z'^2)^{3/2}} \quad (C.13)$$

Let u and v be defined as follows:

$$v = w^2 = x'^2 + y'^2 + z'^2 \quad (C.14)$$

$$u = x'x'' + y'y'' + z'z'' \quad (C.15)$$

Using equations (C.7), (C.8), (C.11), (C.12), (C.13), (C.14) and (C.15), we obtain the following expression of $d\underline{T}/ds$:

$$\frac{d\underline{T}}{ds} = \frac{(x''v - x'u)\underline{i} + (y''v - y'u)\underline{j} + (z''v - z'u)\underline{k}}{v^2} \quad (C.16)$$

From equations (C.6) and (C.16),

$$\kappa = \frac{[(x''v - x'u)^2 + (y''v - y'u)^2 + (z''v - z'u)^2]^{1/2}}{v^2} \quad (C.17)$$

The radius of curvature is defined by:

$$\rho = \frac{1}{\kappa} \quad (\text{C.18})$$

From equations (C.17) and (C.18), we obtain:

$$\rho = \frac{v^2}{[(x''v - x'u)^2 + (y''v - y'u)^2 + (z''v - z'u)^2]^{1/2}} \quad (\text{C.19})$$

Center of Curvature.

Let $C(C_x, C_y, C_z)$ be the center of curvature and $P(x, y, z)$ be the point of the curve which has radius $\rho = 1/\kappa$, as calculated above. Then:

$$\underline{PC} = \rho \underline{N} \quad (\text{C.20})$$

From equation (C.5),

$$\underline{N} = \frac{1}{\kappa} \cdot \frac{d\underline{T}}{ds} \quad (\text{C.21})$$

Substituting equation (C.16) into equation (C.21), the following expression is obtained for \underline{N} :

$$\underline{N} = \frac{(x''v - x'u)\underline{i} + (y''v - y'u)\underline{j} + (z''v - z'u)\underline{k}}{\kappa v^2} \quad (\text{C.22})$$

Substituting equation (C.22) into equation (C.20), we obtain:

$$\underline{PC} = \frac{(x''v - x'u)\underline{i} + (y''v - y'u)\underline{j} + (z''v - z'u)\underline{k}}{(\kappa v)^2} \text{ But:} \quad (C.23)$$

$$\underline{PC} = (C_x - x)\underline{i} + (C_y - y)\underline{j} + (C_z - z)\underline{k} \quad (C.24)$$

Combining (C.23) and (C.24):

$$C_x - x = \frac{x''v - x'u}{(\kappa v)^2} \quad (C.25)$$

$$C_y - y = \frac{y''v - y'u}{(\kappa v)^2} \quad (C.26)$$

$$C_z - z = \frac{z''v - z'u}{(\kappa v)^2} \quad (C.27)$$

The coordinates of the center of curvature are given by solving equations (C.25), (C.26) and (C.27):

$$C_x = x + \frac{x''v - x'u}{(\kappa v)^2} \quad (C.28)$$

$$C_y = y + \frac{y''v - y'u}{(\kappa v)^2} \quad (C.29)$$

$$C_z = z + \frac{z''v - z'u}{(\kappa v)^2} \quad (C.30)$$

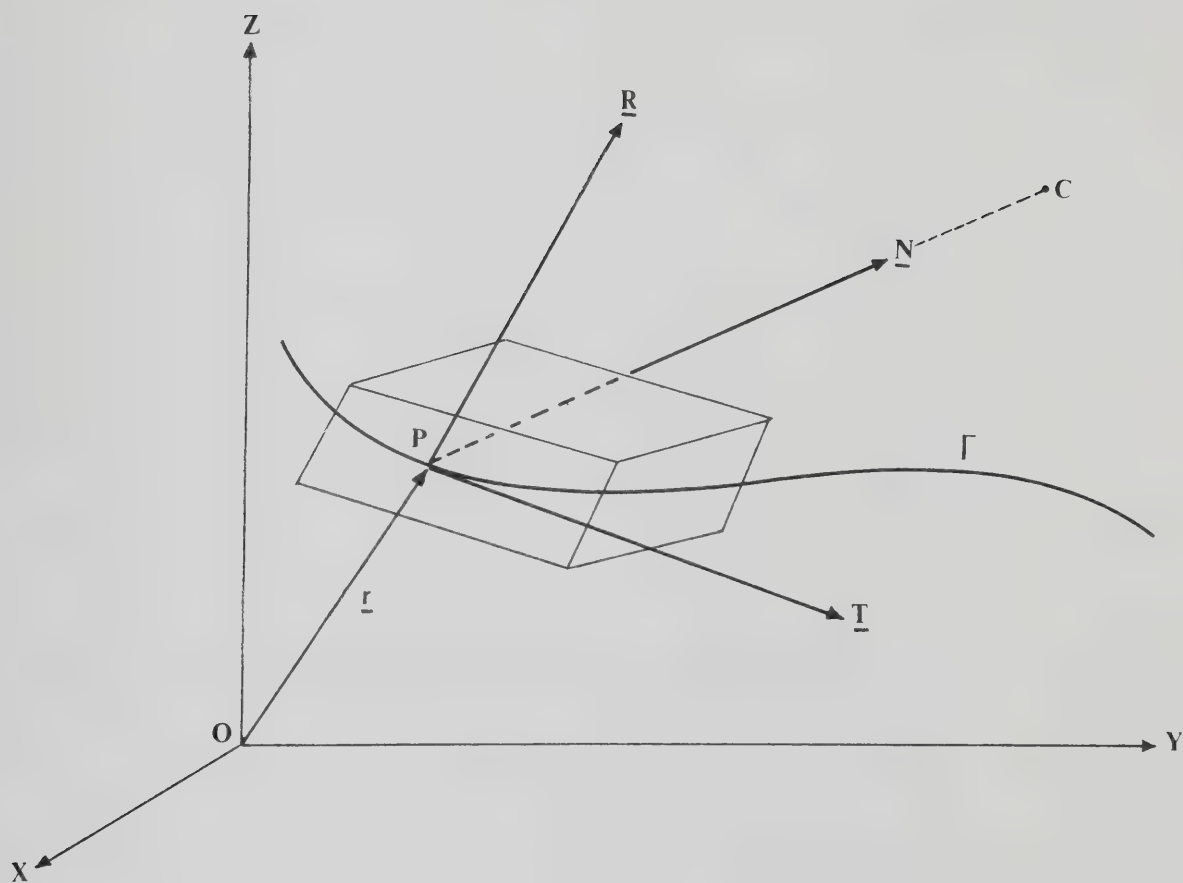


Figure C.1 Representation of the curve Γ in the space.

\underline{N} = Normal unit vector to the curve;
 \underline{T} = Tangent unit vector;
 \underline{R} = Binormal unit vector;
 \underline{C} = Center of curvature.

APPENDIX D

C.P. Coordinates and Calibration Coefficients

=====

DIGITIZED COORDINATES OF THE CONTROL POINTS

=====

C.P.	CAMERA #2(slave)		CAMERA #1(master)	
	U	V	U	V
1	-1.02	0.17	4.30	0.21
2	-1.02	-0.38	4.30	-0.42
3	0.02	-0.53	0.06	-0.64
4	6.00	0.24	10.77	0.11
5	7.31	0.11	6.71	-0.05
6	6.01	-0.31	10.75	-0.54
7	7.31	-0.48	6.70	-0.67
8	0.02	1.60	0.08	1.60
9	7.32	1.66	6.71	1.58
10	9.93	1.64	9.09	1.57
11	-1.01	1.67	4.32	1.70
12	6.01	1.73	10.78	1.72
13	8.51	1.72	13.17	1.71
14	-1.60	5.09	6.40	5.33
15	-1.02	5.12	4.35	5.35
16	0.00	5.19	0.12	5.37
17	0.50	5.23	-2.29	5.38
18	5.42	5.13	12.90	5.35
19	6.01	5.13	10.82	5.35
20	7.32	5.20	6.77	5.41
21	8.12	5.26	4.60	5.40
22	-3.89	10.76	-3.33	11.13
23	-0.02	10.79	0.17	11.21
24	7.32	10.85	6.83	11.27
25	11.19	10.89	10.32	11.29
26	-4.77	10.51	1.08	10.97
27	-1.03	10.53	4.42	11.00
28	6.01	10.53	10.88	11.10
29	9.67	10.54	14.35	11.10
30	-0.03	14.94	0.21	15.53
31	7.32	14.93	6.86	15.60
32	-1.04	14.55	4.47	15.20
33	6.01	14.47	10.92	15.30

*** (measurements in digitizing units)

=====

=====

CALIBRATION COEFFICIENTS FOR TWO CAMERAS (330.P.)
REFINEMENT WITH MODEL #4 (KARARA)

=====

CAMERA #2(slave)

CAMERA #1(master)

P[1, 1] =	0.727964815	P[2, 1] =	-2.973285640
P[1, 2] =	5.005433327	P[2, 2] =	4.473462036
P[1, 3] =	-0.005677486	P[2, 3] =	0.049626023
P[1, 4] =	0.009346074	P[2, 4] =	0.093457246
P[1, 5] =	-0.095659062	P[2, 5] =	-0.109783363
P[1, 6] =	0.037760662	P[2, 6] =	-0.031392528
P[1, 7] =	5.145819255	P[2, 7] =	5.356062744
P[1, 8] =	0.042616315	P[2, 8] =	0.015643203
P[1, 9] =	-0.027527678	P[2, 9] =	-0.021970396
P[1,10] =	0.002238655	P[2,10] =	-0.006858224
P[1,11] =	0.000237219	P[2,11] =	-0.000572463
P[1,12] =	-0.000107308	P[2,12] =	-0.000053501
P[1,13] =	0.000001758	P[2,13] =	0.000000387
P[1,14] =	-0.000000011	P[2,14] =	-0.000000001
P[1,15] =	-0.000004135	P[2,15] =	-0.000004783
P[1,16] =	-0.000192219	P[2,16] =	-0.000038812

=====

REFINEMENT WITH MODEL #4 (KARARA)

	Xm	Xs	dx	Yp	Ys	1Y	ym	Zs	dZ
1	-146.500	-146.500	0.09	0.00	0.00	0.00	0.00	0.29	0.29
2	-146.500	-146.500	0.30	0.00	-0.00	0.00	0.50	-0.24	-0.24
3	-146.500	-146.500	0.08	0.00	-0.00	0.00	0.50	-0.00	-0.00
4	-146.500	-146.500	0.33	0.00	0.00	0.00	0.50	0.00	0.00
5	-146.500	-146.500	0.33	0.00	0.00	0.00	0.50	0.00	0.00
6	-146.500	-146.500	0.22	0.00	0.00	0.00	0.50	0.00	0.00
7	-146.500	-146.500	0.35	0.00	0.00	0.00	0.50	0.00	0.00
8	-146.500	-146.500	0.24	0.00	0.00	0.00	0.50	0.00	0.00
9	-146.500	-146.500	0.29	0.00	0.00	0.00	0.50	0.00	0.00
10	-146.500	-146.500	0.18	0.00	0.00	0.00	0.50	0.00	0.00
11	-146.500	-146.500	0.04	0.00	0.00	0.00	0.50	0.00	0.00
12	-146.500	-146.500	0.03	0.00	0.00	0.00	0.50	0.00	0.00
13	-146.500	-146.500	0.03	0.00	0.00	0.00	0.50	0.00	0.00
14	-146.500	-146.500	0.03	0.00	0.00	0.00	0.50	0.00	0.00
15	-146.500	-146.500	0.03	0.00	0.00	0.00	0.50	0.00	0.00
16	-146.500	-146.500	0.03	0.00	0.00	0.00	0.50	0.00	0.00
17	-146.500	-146.500	0.13	0.00	0.00	0.00	0.50	0.00	0.00
18	-146.500	-146.500	0.15	0.00	0.00	0.00	0.50	0.00	0.00
19	-146.500	-146.500	0.03	0.00	0.00	0.00	0.50	0.00	0.00
20	-146.500	-146.500	0.03	0.00	0.00	0.00	0.50	0.00	0.00
21	-146.500	-146.500	0.03	0.00	0.00	0.00	0.50	0.00	0.00
22	-146.500	-146.500	0.03	0.00	0.00	0.00	0.50	0.00	0.00
23	-146.500	-146.500	0.03	0.00	0.00	0.00	0.50	0.00	0.00
24	-146.500	-146.500	0.03	0.00	0.00	0.00	0.50	0.00	0.00
25	-146.500	-146.500	0.03	0.00	0.00	0.00	0.50	0.00	0.00
26	-146.500	-146.500	0.03	0.00	0.00	0.00	0.50	0.00	0.00
27	-146.500	-146.500	0.03	0.00	0.00	0.00	0.50	0.00	0.00
28	-146.500	-146.500	0.03	0.00	0.00	0.00	0.50	0.00	0.00
29	-146.500	-146.500	0.03	0.00	0.00	0.00	0.50	0.00	0.00
30	-146.500	-146.500	0.03	0.00	0.00	0.00	0.50	0.00	0.00
31	-146.500	-146.500	0.03	0.00	0.00	0.00	0.50	0.00	0.00
32	-146.500	-146.500	0.03	0.00	0.00	0.00	0.50	0.00	0.00
33	-146.500	-146.500	0.03	0.00	0.00	0.00	0.50	0.00	0.00
TOTAL	RMS		0.24			0.19			0.26
**	(measurements in cm.)								

=====

CALIBRATION COEFFICIENTS FOR TWO CAMERAS (27C.P.)
REFINEMENT WITH MODEL #4 (KARARA)

=====

CAMERA #2(slave)	CAMERA #1(master)
P[1, 1] = 0.728934932	P[2, 1] = -2.983975904
P[1, 2] = 4.986331717	P[2, 2] = 4.478170555
P[1, 3] = -0.011472292	P[2, 3] = 0.042490899
P[1, 4] = 0.011252642	P[2, 4] = 0.093224276
P[1, 5] = -0.093985903	P[2, 5] = -0.118584067
P[1, 6] = 0.028714357	P[2, 6] = -0.023109697
P[1, 7] = 5.130577101	P[2, 7] = 5.320859985
P[1, 8] = 0.034397477	P[2, 8] = 0.050121048
P[1, 9] = -0.026818994	P[2, 9] = -0.023960787
P[1,10] = -0.000637546	P[2,10] = -0.005898541
P[1,11] = -0.001838658	P[2,11] = -0.002306823
P[1,12] = 0.000231334	P[2,12] = -0.000218194
P[1,13] = -0.000008231	P[2,13] = 0.000001984
P[1,14] = 0.000000066	P[2,14] = -0.000000006
P[1,15] = 0.000042320	P[2,15] = -0.000203016
P[1,16] = -0.000247851	P[2,16] = 0.000001601

=====

B30425